Live-cell imaging of the early stages of colony development in *Fusarium oxysporum in vitro* and *ex vivo* during infection of a human corneal model

A thesis submitted to The University of Manchester for the degree of

Doctor of Philosophy

in the Faculty of Biology, Medicine and Health

2016

Smija Mariam Kurian

The School of Biological Sciences

Institute of Inflammation and Repair

LIST OF CONTENTS

CHAPTER 2: MATERIALS AND METHODS

CHAPTER 3: OPTIMISATION OF THE CULTURE CONDITIONS FOR ANALYSING CAT FUSION *IN VITRO* IN *F. OXYSPORUM*

CHAPTER 4: LIVE-CELL IMAGING OF CAT FUSION *IN VITRO*

CHAPTER 5: ROLE OF CALCIUM SIGNALLING DURING CAT FUSION

CHAPTER 6: STUDY ON *FUSARIUM* KERATITIS USING *EX VIVO* HUMAN CORNEA AS INFECTION MODEL

Word Count: 48,763

LIST OF TABLES

LIST OF ABBREVIATIONS

3D   three dimensional

AGE   agarose gel electrophoresis

BAPTA   1,2-bis(2-aminophenoxy)ethane-n,n,n′,n′ -tetraacetic acid

cAMP   cyclic adenosine monophosphate

CAT   conidial anastomosis tube

CCD   charge-coupled device

cDFFDA   carboxylic acid diacetate (carboxy- DFFDA)

CFU   colony forming unit

CFW   calcofluor white

CGD   chronic granulomatous disease

CICR Ca^{2+} induced Ca^{2+} release

Con A   concanavalin A

CRZ1   calcineurin-responsive zinc finger 1

CTAB   cetyl trimethylammonium bromide

DMEM   dulbecco's modified eagle medium

DMSO   dimethyl sulphoxide

DNA   deoxy ribo nucleic acid

dpi   days post infection

EDTA   ethylenediaminetetraacetic acid

ENA1 gene   exitus natru 1 (exit sodium) gene

FCS   foetal calf serum

FFSC   *Fusarium fujikuroi* species complex

FITC   fluorescein isothiocyanate

FM4-64   *n*-(3-triethylammoniumpropyl)-4-(6-(4-(diethylamino) phenyl) hexatrienyl) pyridinium dibromide

Fol   *Fusarium oxysporum* f.sp. *lycopersici*

FOSC   *Fusarium oxysporum* species complex

FRET	forster resonance energy transfer
Fso	*Fusarium* soft protein
FSSC	*Fusarium solani* species complex
GFP	green fluorescent protein
GPDH	glyceraldehyde 3-phosphate dehydrogenase
GT	germ tube
HACS	high affinity Ca^{2+} uptake system
HGU	hyphal growth unit
HGT	horizontal gene transfer
HCT	horizontal chromosome transfer
HIV	human immunodeficiency virus
hpi	hours post inoculation
LACS	low affinity Ca^{2+} uptake system
LASAF	leica application suite advanced fluorescence
LB	medium luria bertani medium
LS	lineage specific
MIC	minimum inhibitory concentration
MIP-2	macrophage inflammatory protein-2
min	minutes
mRNA	messenger ribonucleic acid
NADPH	nicotinamide adenine dinucleotide phosphate
NETs	neutrophil extracellular traps
PAMPs	pathogen associated molecular patterns
PBS	phosphate buffered saline
PCR	polymerase chain reaction
PDA	potato dextrose agar
PDB	potato dextrose broth
PMNs	polymorphonuclear neutrophils

PRRs   pattern recognition receptors

qPCR   quantitative polymerase chain reaction

RFP   red fluorescent protein

RNA   ribo nucleic acid

ROS   reactive oxygen species

RU360 $C_2H_{26}Cl_3N_8O_5Ru_2$ (oxo-bridged dinuclear ruthenium amine complex)

SIX3   secreted in xylem 3

SLO   scanning laser ophthalmoscopy

STM   spore tip mucilage

TLRs   toll-like receptors

WGA   wheat germagglutinin

ABSTRACT

The University of Manchester

Name: Smija Mariam Kurian

Degree title: Doctor of Philosophy

Research title: Live-cell imaging of the early stages of colony development in *Fusarium oxysporum in vitro* and *ex vivo* during infection of a human corneal model

Date: May 2016

Abstract: *Fusarium oxysporum* is a major fungal plant pathogen and emerging human pathogen. It has been hypothesised that conidial anastomosis tube (CAT) fusion may facilitate horizontal gene/chromosome transfer that could result in the acquisition of new genetic traits in fungi lacking sexual reproduction. However, we know little about the mechanistic basis of CAT fusion in fungi lacking sexual stages such as *F. oxysporum*.

In the first part of my research the optimal culture conditions were determined for subsequent studies of CAT fusion in this fungus. CAT fusion was optimal in 1% potato dextrose broth supplemented with one of a diverse range of chemicals inoculated with microconidia of 1 x 10^6 spores/ml at 22-25 °C and pH 5.5-6.3. Cell adhesion facilitated by the chemical supplement was required for CAT fusion. ~ 40% CAT fusion was routinely observed with these conditions at 12 h post incubation.

In the second part of my research live-cell imaging was used to characterize the process of CAT fusion and differentiate between CATs and germ tubes. In particular, the composition of the CAT cell wall surface was shown to be different from that of germ tubes. Nuclei, mitochondria, vacuoles and lipid droplets were also shown to move between germlings following CAT fusion.

In the third part of my research quantitative analysis of the influence of various Ca^{2+} modulators on CAT fusion was done and evidence obtained showed that Ca^{2+} signalling is important during CAT fusion and involves the uptake of Ca^{2+} from the external environment by the Cch1 Ca^{2+} channel, and the involvement of the primary intracellular Ca^{2+} receptor, calmodulin, and the mitochondrial Ca^{2+} uniporter.

In the final part of my thesis, the morphogenesis of the fungus was analysed during infection of an *ex vivo* human corneal model. The stages of infection that were characterised were: spore adhesion; bipolar germination; hyphal extension, branching, fusion and penetration into the corneal tissue; and sporulation involving the formation of microconidia and intercalary chlamydospores within the host tissue. Image analysis techniques were developed for the quantification and analysis of branching angles, total hyphal length, number of hyphal branches and hyphal growth units within the infected *ex vivo* corneal tissue. Using the fusion mutant, Δ*fso*, CAT fusion was shown not to be required for infection.

LAY ABSTRACT

Fusarium oxysporum is a fungus that is a major plant pathogen and an emerging animal pathogen. In humans, it is a major cause of corneal infections called keratitis. It has been hypothesized that this fungus and others like it that lack a sexual stage in their life cycles, are able to transfer their genes and/or chromosomes through connections that they make by fusing with cells of other fungal colonies that are genetically different. Some of these genes/chromosomes provide factors that can make fungal pathogens more virulent. The main focus of my research has been to understand this process of cell fusion both with the fungus growing in culture and in donated human corneas. The latter served as a useful infection model. In my project the conditions and techniques for studying the development and cell fusion of the fungus in culture and the human cornea were optimised and these processes characterized in detail using time-lapse, live-cell imaging under the microscope.

DECLARATION

I confirm that no portion of the work referred to in the thesis has been submitted in support of an application for another degree or qualification of this or any other university or other institute of learning.

COPYRIGHT STATEMENT

i. The author of this thesis (including any appendices and/or schedules to this thesis) owns certain copyright or related rights in it (the "Copyright") and s/he has given The University of Manchester certain rights to use such Copyright, including for administrative purposes.

ii. Copies of this thesis, either in full or in extracts and whether in hard or electronic copy, may be made only in accordance with the Copyright, Designs and Patents Act 1988 (as amended) and regulations issued under it or, where appropriate, in accordance with licensing agreements which the University has from time to time. This page must form part of any such copies made.

iii. The ownership of certain Copyright, patents, designs, trade marks and other intellectual property (the "Intellectual Property") and any reproductions of copyright works in the thesis, for example graphs and tables ("Reproductions"), which may be described in this thesis, may not be owned by the author and may be owned by third parties. Such Intellectual Property and Reproductions cannot and must not be made available for use without the prior written permission of the owner(s) of the relevant Intellectual Property and/or Reproductions.

iv. Further information on the conditions under which disclosure, publication and commercialisation of this thesis, the Copyright and any Intellectual Property University IP Policy (see http://documents.manchester.ac.uk/display.aspx?DocID=24420), in any relevant Thesis restriction declarations deposited in the University Library, The University Library's regulations (see http://www.library.manchester.ac.uk/about/regulations/) and in The University's policy on Presentation of Theses.

"In the beginning was the Word, and the Word was with God, and the Word was God. He was with God in the beginning. Through him all things were made; without him nothing was made that has been made. In him was life, and that life was the light of all mankind. The light shines in the darkness, and the darkness has not overcome it."

John 1:1-5
The Holy Bible

I would like to dedicate my thesis to all my teachers (from Amma, V'mummy and Fr. K.D. Joseph to Ali and Nick) who shared their knowledge and wisdom with great love and wit! ☺

ACKNOWLEDGEMENTS

THE AUTHOR

Name: Smija Mariam Kurian

Education qualifications: B.Sc. Botany and Biotechnology, M.Sc. Biotechnology

Work experience: Research technician at Fungal Cell Biology Group, University of Edinburgh from August 2010 to December 2011

Chapter 1: Introduction and Aims of the PhD project

1.1 The genus *Fusarium*

Species within the genus *Fusarium* are soil-borne filamentous fungi that exhibit saprotrophic, endophytic and parasitic lifestyles. The genus *Fusarium* belongs to the order Hypocreales of Ascomycetes (Fig. 1.1) and was first described by Johan F. Link in 1809 for fungi with banana-shaped conidia (Fourie *et al.,* 2011).

Kingdom: Fungi
Subkingdom: Dikarya
Phylum: Ascomycota
Subphylum: Pezizomycotina
Class: Sordariomycetes
Order: Hypocreales
Family: Nectriaceae
Genus: *Fusarium*

Fig. 1.1 (A) Taxonomic classification of *Fusarium* species.

Fusarium spp. form a range of different types of spores (macroconidia, chlamydospores, microconidia and ascospores) which have the following characteristics. Macroconidia are produced are 3-7 celled canoe-shaped spores formed by holoblastic conidiation from phialides (Gullino *et al*., 2012). Chlamydospores are thick-walled, lipid-rich vegetative cells, which are adapted to survive extreme environmental conditions (Couteaudier and Alabouvette, 1990). Microconidia are 1- or 2-celled spores formed by holoblastic conidiation from phialides. Microconidia are formed by only certain species of *Fusarium.* Ascospores are produced within asci inside fruitbodies (called perithecia) by species with a sexual stage in their life cycle such as *Fusarium graminearum* (Gullino *et al*., 2012).

Fusarium spp. primarily non-pathogenic, saprotrophic fungi found in soil close to asymptomatic crop plants. Some *Fusarium* spp. can also exist as endophytes without causing symptoms in the host plant. Many species of *Fusarium* are major plant pathogens affecting many economically important crop plants (Gullino *et al*., 2012). *Fusarium spp.* cause vascular wilts, cortical rot, head blight, leaf spot, root rot, fruit rot, die back, and cankers in plants (Gullino *et al*., 2012). For example *F. graminearum* is a major wheat pathogen. Two *Fusarium* species, *F. graminearum* and *Fusarium*

oxysporum are among the first five major fungal plant pathogens (Dean *et al*., 2012). Certain *Fusarium spp.* are also emerging human pathogens (Boutati and Anaissie, 1997; see section 1.5).

Fusarium spp. also produces mycotoxins such as zearalenone and fumonisins (Bennett and Kilch, 2003). Ingestion of food with these mycotoxins can lead to mycotoxicosis in animals and humans (Nucci and Anaissie, 2007). Some of the strains of *F. oxysporum* have also been used as biocontrol agents providing antifungal activity against other *Fusarium* species by existing as root endophytes of plants (Alabouvette *et al.,* 2009; Michielse *et al*., 2009).

1.1.1 *Fusarium oxysporum species complex*

Fusarium oxysporum is a species complex which has a broad host range yet it is a highly host specific pathogen with numerous sub-species termed *formae speciales* (Correll *et al*., 1987). Different *formae speciales* are termed on the basis of the different plant species they infect and are further divided into races based on their crop cultivar specificities (i.e. pathogenicity towards specific host cultivars) (Fourie *et al.,* 2011). *F. oxysporum* species are also grouped into vegetative compatibility groups (VCGs) based on their ability to form stable heterokaryons. Members of any particular VCG may include both pathogenic and non-pathogenic strains which possess diverse pathogenic lineages. A single race may be associated with multiple VCGs (Kistler *et al*., 1998; Fourie *et al*., 2011). *Fusarium* wilt of banana (or Panama disease) is currently one of the most significant plant diseases and is causing devastating losses to banana plantations around the globe. It is caused by *F. oxysporum* f.sp. *cubense*, a fast disseminating pathogenic *formae speciales* of *F. oxysporum* (Ploetz, 2015). *F. oxysporum* is the third most frequently isolated species of *Fusarium* in human infections (section 1.5.1).

F. oxysporum f. sp. *lycopersici* is primarily a pathogen of tomato plants causing wilt of infected plants (Di Pietro, 2003). Germination of soil-borne spores is followed by adhesion to root surfaces of plants. After spore germination, an interconnected hyphal network is formed over the root surface by means of vegetative hyphal fusion. Systemic infection of the whole plant occurs upon successful infection of the root and this leads to water blockage through xylem vessels causing wilting disease symptoms. *F.oxysporum* produces three types of spores; macroconidia, microconidia and chlamydospores and lacks a sexual stage in its life cycle. Three races have been

described and these have evolved in the field by acquiring point mutations in avirulence genes (Mechielse and Rep, 2009).

The genome of this species was first sequenced in 2007 (Ma *et al*., 2010). It has 15 chromosomes of which 11 are core chromosomes and 4 are lineage specific chromosomes (LS) (chromosomes 3, 6, 14, 15 and parts of chromosome 1 and 2). The house keeping genes are exclusively present on the core chromosomes and there is a high level of synteny among the core chromosomes of *F. oxysporum*, *F. graminearum*, *F. verticilloides* and *F. solani*. Of these species, only *F. oxysporum* and *F. solani* have LS chromosomes which carry genes specific for host-pathogen interactions such as genes encoding effector proteins. 50% of the genes on the LS chromosomes lack any homologues in the other two species of *Fusarium* and these regions have a distinct codon usage. Approximately 93% of proteins encoded by genes on LS chromosomes have close homologues in other ascomycete fungi. Thus the LS chromosomes of *F. oxysporum* has a diverse phylogenetic evolution compared to the core chromosomes and it has been hypothesized that the LS chromosomes have been acquired by horizontal gene/chromosome transfer (HGT/HCT) from an ancestral ascomycete fungal species (Sanders, 2006; Ma *et al*., 2010; Mehrabi *et al*., 2011).

1.2 Conidial anastomosis tube fusion

1.2.1 Tropic growth responses in filamentous fungi

Polarised hyphal tip growth of hyphae is an essential feature of filamentous fungi (Riquelme, 2013). Tropic growth responses exhibited by filamentous fungi involve the re-orientation of tip growth in response to different environmental stimuli (Brand and Gow, 2009; Brand and Gow, 2012). These hyphal tropisms include: chemotropism in response to chemical stimulation (e.g. Gooday, 1974; Turra and Di Pietro, 2015), thigmotropism in response to topography sensing or touch (e.g. Read *et al*., 1996; Collins and Read, 1997), phototropism in response to light (e.g. Linden *et al*., 1997), gravitropism in response to gravitational forces (e.g. Tomita-Yokotani and Shinozaki, 2003), sexual tropism mediated by pheromones (e.g. Bolker and Kahmann, 1993). The nature of these positive or negative hyphal tropic responses depends on the organism and the stimuli involved.

In *F. oxysporum*, the positive chemotropic growth of germ tubes towards roots of its tomato host was recently shown to be mediated by the catalytic activity of class III

peroxidases secreted by the roots (Turra *et al*., 2015). Screening and identification of mutants defective in this positive chemotropic response to these peroxidases revealed the involvement of the fungal cell integrity mitogen-activated protein kinase (MAPK) cascade and a functional homologue of the sex pheromone α receptor of *Saccharomyces cerevisiae* (Turra *et al*., 2015).

1.2.2 Conidial Anastomosis Tube (CAT) fusion in fungi

Fusion between conidial anastomosis tubes (CATs) formed by many filamentous fungi is an example of a positive chemotropic growth and response (Roca *et al.*, 2003; Read *et al*., 2012). CATs are short, thin protrusions that arise from conidia or germ tubes (GTs). They home towards each other and fuse to form conidial germling networks during the initial stages of colony development in filamentous fungi (Fig. 1.2). Cytoplasm and organelles move through fused CATs as has been shown in *Colletotrichum lindemuthianum* and *Neurospora crassa* (Roca *et al*., 2003, 2004, 2005b and 2010). Amongst other roles, CAT fusion helps in efficient colony establishment by distributing water and nutrients throughout the developing colony from the natural external environment in which they are normally heterogeneously distributed (Roca *et al*., 2005b).

CAT fusion has been shown to occur in 73 different species of filamentous fungi (Roca *et al.,* 2005b) and has been reported to develop both in culture and in host-pathogen systems (Ishikawa *et al*., 2012; Ruiz-Roldan *et al.*, 2010). The culture conditions which induce CAT fusion *in vitro* are different in different fungi. In *N. crassa*, CAT fusion occurs in Vogel's minimal media within 4 to 6 h of inoculation (Roca *et al*., 2005) whereas it occurs in water in *C. lindemuthianum* after incubation for 72 h in the dark (Ishikawa *et al.,* 2010; Roca *et al*., 2003).
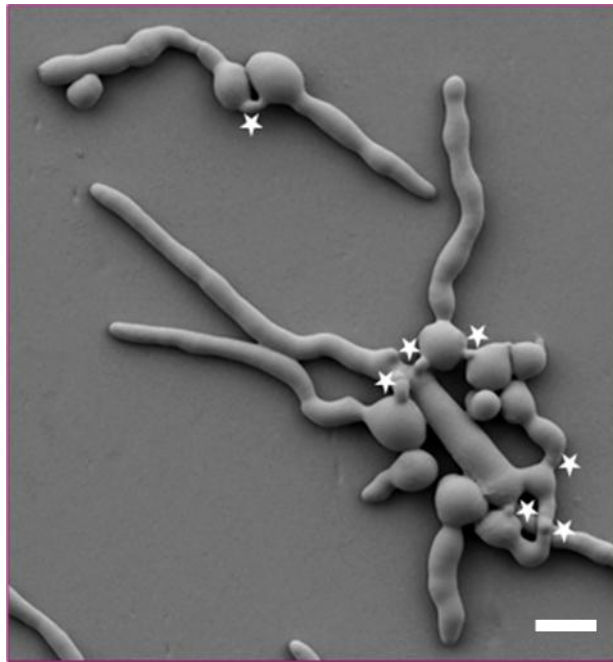
Fig. 1.2 CAT fusion between germlings of *N. crassa*. Scale bar = 10 µm. Reproduced from Roca *et al*. (2005).

CAT fusion in *N. crassa* is being used as an experimental model for studies on positive chemotropic responses in filamentous fungi that involve self-signalling between genetically identical cells (Read *et al*., 2012). It involves two individual germlings interacting and their CATs growing towards each other in response to an unidentified self-signalling signal and this leads to fusion between the two individual germlings which can then function as a single entity (Roca *et al*., 2005; Goryachev *et al*. 2012). CATs are usually non-branched and fusions have been shown to occur between two CATs arising from two conidia, two germ tubes or between a conidium and a germ tube (Roca *et al*., 2005). The process of CAT fusion has been shown to be physiologically distinct and under separate genetic control to that of germ tubes (Roca *et al*, 2005b). The stages of CAT fusion in *N. crassa* have been described as 1) CAT induction marked by the emergence of CATs as small cell protrusions, 2) CAT homing and 3) CAT fusion (Roca *et al*., 2005; Read *et al*., 2009, 2012). CAT fusion and the underlying signalling mechanisms have been extensively studied in the model organism *N. crassa* in which over 50 mutants defective at different stages of CAT fusion have been characterised (Read *et al*., 2012; Fu *et al*., 2014; Weichert and Fleissner, 2015;) and considerable insights into the mechanism of self-signalling involved leading up to CAT fusion has been obtained (Read *et al*., 2012; Herzog *et al*., 2015).

The role of MAP kinase pathway in CAT fusion during colony initiation and hyphal fusion in established colonies has been analysed in detail in *N. crassa* (Fu *et al*., 2014; Jonkers *et al*., 2014; Leeder *et al*., 2013; Roca *et al*., 2005; Pandey *et al*., 2004). An oscillatory recruitment of MAK-2 and SO (soft) proteins to CAT tips, a process termed the 'ping-pong mechanism', has been shown to occur during CAT initiation, homing and fusion between genetically identical germlings (Figs. 1.3 and 1.4; Fleissner *et al*., 2009; Read *et al*., 2009, 2012; Herzog *et al*., 2015).
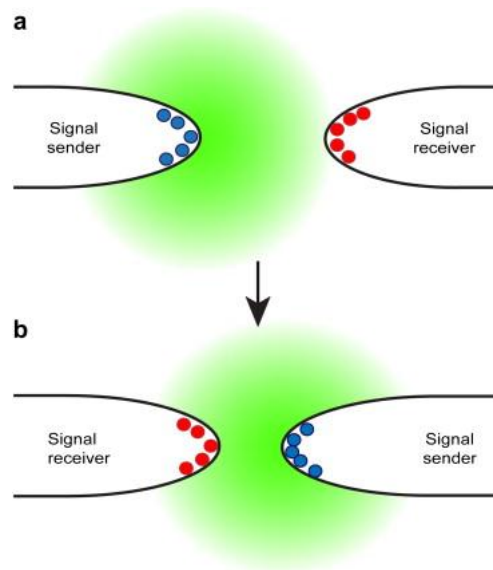
Fig. 1.3 Cartoon summarizing the proposed ping–pong exchange of pulses of the unknown chemoattractant. **(a)** In the first half-period of the signalling, SO protein (blue) is involved in releasing a chemoattractant signal (green cloud) from the left CAT tip, while MAK-2 (red) in the right CAT tip acts in the receiving signal transduction pathway to orientate tip growth towards the chemoattractant source. **(b)** In the second half period the roles reverse: in the right tip MAK-2 feedback inhibits itself and recruits SO to the apex which releases the next chemoattractant pulse. In the meantime SO has been replaced by MAK-2 in the left tip which is now ready to receive the 'response'. This sequence of pulsatile signalling repeats until just after both tips come into contact with each other (reproduced from Read *et al*., 2009; 2012).
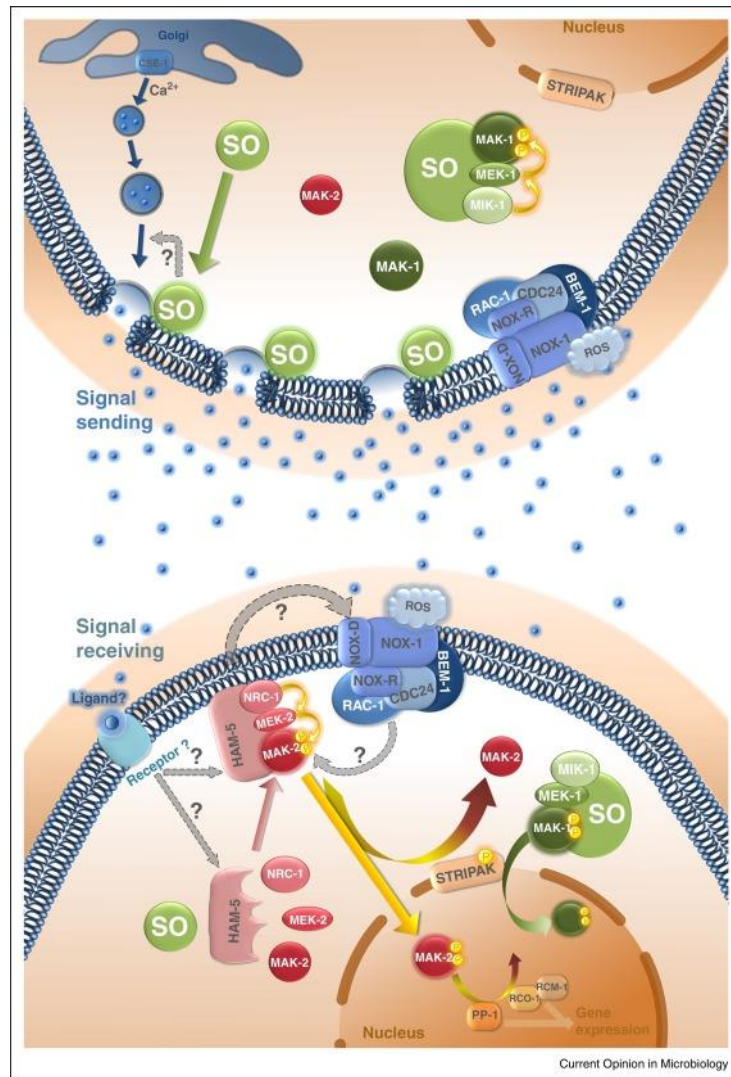
Fig. 1.4 The most recent working model of the self-signaling events resulting in germling fusion between two fusion partners. The two fusion partners coordinately switch between signal sending (top) and receiving (bottom). The 'signal sender' releases a ligand by exocytosis in a Ca^{2+}-dependent and SO-dependent manner which binds to a so far unknown receptor in the signal receiving cell. This in turn leads to the activation of a MAK-2 MAP kinase cascade which results in the following: the production of reactive oxygen species (ROS) either upstream or down-stream of MAK-2, regulation of the activity of the transcription factors PP-1 and RCO-1/RCM-1 (after their translocation into the nucleus) and phosphorylation of MOB-3/phocein of the STRIPAK complex. The phosphorylation of STRIPAK complex results in the accumulation in the nucleus of MAK-1, the MAP kinase in the cell integrity pathway. The signaling is terminated by a negative feedback loop, which is followed by the next signal release from the signal sending partner (reproduced from Herzog *et al.*, 2015).

The screening and analysis of *N. crassa* mutants, combined with live-cell imaging of fluorescently labelled proteins involved in cell fusion, has led to the most recent

working model of the self-signalling mechanism presented in Figure 1.4. During the oscillatory recruitment exhibited by MAK-2 and SO to CAT tips growing chemotropically towards each other, one cell acts as the 'signal sender' and the other as the 'signal receiver' (Fig. 1.3). A Ca^{2+}- and SO-dependent exocytosis of the chemoattractant has been hypothesized to occur from the signal sender cell. The nature of the secreted self-signalling extracellular ligand is not known but a peptide is considered to be a likely candidate (Read *et al*., 2012). Furthermore, it is also thought probable that this ligand acts as both a CAT inducer and a CAT chemoattractant (Read *et al*., 2009).

1.2.3 CAT fusion in *Fusarium oxysporum*

In 1973, Mesterhazy reported observing anastomosis between macroconidia of *F. oxysporum*. f. sp. *medicaginis* and between macroconidia of *F. graminearum*. He termed this form of cell fusion as 'appresorium-type fusion' (Mesterhazy, 1973). Microconidia of *F. oxysporum* f. sp. *lycopersici* have also been shown to undergo CAT fusion in culture and also on the surfaces of plant roots (Ruiz-Roldan *et al*., 2010). After the fusion of germlings on solid agar medium by *F. oxysporum,* nuclei have been observed to migrate from one germling to the other and this migration was followed by the degradation of the nucleus in the host cell (Ruiz-Roldan *et al*., 2010).

1.2.4 The FSO protein and its role in hyphal fusion

Soft (SO) is a protein of unknown function, which is characterised by having a WW domain. Proteins having this domain have been implicated in protein-protein interactions (Fleissner *et al*., 2005). The *so* gene is conserved in all filamentous ascomycete species and a *so* knockout mutant in *N. crassa* was found to be defective in CAT fusion (Fleissner *et al*., 2005, 2009; Read *et al*., 2012; Weichert and Fleissner, 2015). As indicated in the last section, SO exhibits oscillatory recruitment to CAT tips undergoing chemotropism towards each other and it is believed that exocytosis of the chemoattractant is SO-dependent (Figs. 1.3 and 1.4). PRO40 in the *Sordaria macrospora* is homologous to SO in *N. crassa* and is required for fruiting body formation. PRO40 has been shown to co-localize with HEX1, which is the main protein of the septal pore plugs called Woronin bodies (Engh *et al*., 2007). Vegetative hyphal fusion has been shown not to be required for plant infection as the *F. oxysporum* SO mutant (Δ*fso* mutant) cannot undergo hyphal fusion but can still infect tomato plants.

Nevertheless, hyphal fusion has been shown to be essential for efficient colonisation of the root surface and thus probably plays a significant role in the establishment of infection by *F. oxysporum* (Prados Rosales and Di Pietro, 2008).

1.2.5 Horizontal gene/chromosome transfer and the significance of CAT fusion in facilitating it

Fusarium oxysporum is a fungus with no sexual stage reported in its life cycle (Kistler, 1997). This fungus, however, has many *formae speciales* which have evolved from a common ancestor (Di Pietro *et al*., 2003). Analysis of the sequenced genome of *F. oxysporum* reported the existence of supernumerary chromosomes, thought to be acquired by horizontal gene transfer (HGT) events in the course of evolution from another fungal species (Ma *et al*., 2010). Such studies also revealed the flexible nature of the *F. oxysporum* genome which is prone to gene transfer events leading to genetic variation within the species (Kistler *et al*., 2013). Horizontal gene/chromosome transfer is an alternative to the common method of vertical chromosome transfer and meiotic recombination in eukaryotes (Soanes and Richards, 2014). The former can allow the formation of recombinant strains by means of the parasexual cycle involving heterokaryon formation and mitotic recombination, as was originally described in *Aspergillus nidulans* (Pontecorvo, 1956). Although evidence for such events is increasing as a result of comparative genetic studies and genome sequencing, the mechanism that facilitates heterokaryon formation in nature is little understood (Kistler, 1997; Ma *et al.,* 2010; Mehrabi *et al*., 2011; Soanes and Richards, 2014; Vlaardingerbroek *et al*., 2016).

When vegetative hyphal fusion occurs between mature colonies of incompatible strains or species, this commonly leads to cell death and physical isolation of the fused cells preventing intermixing of nuclei and other cell components between the two colonies (Glass *et al*., 2000; Glass and Dementhon, 2006; Ishikawa *et al*., 2012). Molnar *et al*. (1990) described parasexual recombination between vegetatively incompatible strains of *F. oxysporum* using complementing auxotrophs. Although it was assumed that hyphal anastomosis had occurred in these experiments, it was not directly shown by microscopy. Ma *et al*. (2010) reported the transfer of mobile accessory chromosomes carrying pathogenicity factors between a non-pathogenic and pathogenic strain of *F. oxysporum*. Very recently, genetic evidence for the transfer between co-incubated strains of *F. oxysporum* of core chromosomes, in addition to accessory chromosomes,

has been obtained (Vlaardingerbroek *et al*., 2016). However a detailed description of the cytology of the process which facilitates is lacking. The heterokaryon incompatibility response has been shown to be suppressed following CAT fusion between conidial germlings of two incompatible strains in the plant pathogen *C. lindemuthianum.* In contrast, cell death resulted from the fusion of hyphae between mature colonies of incompatible strains of this fungus. It was hypothesised that CAT fusion may facilitate HGT (Ishikawa *et al.*, 2012) that could result in the transfer of supernumerary and/or core chromosomes resulting in the acquisition of new genetic traits, including virulence factors, in fungi lacking sexual reproduction. Hence it is important to study the mechanistic basis of CAT fusion in fungi such as *F. oxysporum* that lack a sexual stage in their life cycles.

1.3 Spore germination and infection of plant roots by *F. oxysporum*

In general terms, spore germination can be regarded as involving the emergence of a germ tube and/or a CAT. The formation of germ tube is the first step in the development of a fungal colony. The three stages of spore germination leading to germ tube formation have traditionally been described as involving: the activation of the resting spore; isotropic growth of the spore and finally; polarized outgrowth of the germ tube (d'Enfert, 1997) although there is no reported evidence for isotropic growth of spores occurring in many fungi including *Fusarium* spp. During spore germination, changes in various processes have been shown to occur, including changes in trehalose metabolism, gene expression (RNA and protein synthesis), cell wall biogenesis and the cell cycle. Oxygen, a carbon source and water are also very important requirements for spore germination (d'Enfert, 1997). The establishment of a polarised actin cytoskeleton, the supply of secretory vesicles to emerging germ tube tips are some of the other physiological changes accompanying germination resulting in germ tube or CAT formation (Czymmek *et al.*, 2005; Roca *et al*., 2010; Berepiki *et al*., 2010; Lichius *et al*., 2011; Berepiki and Read, 2013).

The stages of infection resulting from conidial germination by *F. oxysporum* on plant roots have been described as involving: germination of spores induced by root exudates; adhesion; direct penetration of the root; extracellular and intracellular invasion of the root cortex; and finally colonisation of the plant vascular tissue (Rodriguez-Galvez and Mendgen, 1995; Di Pietro *et al*., 2001; Di Pietro *et al*, 2003). Mutants of *fmk1*, a gene encoding MAP kinase 1 of *F. oxysporum,* has been shown to be defective in

pathogenicity of tomato plant roots probably as a result of a combination of factors such as: reduced adhesion of germinating conidia to the host surface; reduced hyphal penetration of roots; reduced surface hydrophobicity of conidia and hyphae; a reduction in the transcript levels of pectate lyase, a cell wall degrading enzyme; and defects in the invasion of the host that produce the disease symptoms (Di Pietro *et al*., 2001).

Flavonoids present in root exudates have been shown to stimulate germination of macroconidia and chlamydospores of *F. solani*. cAMP dependent protein kinase (PKA) was found to be involved in the signalling of this process (Ruan *et al*., 1995). However, phenolic compounds from root exudates have also been shown to have an inhibitory effect on germination of microconidia of *F. oxysporum* (Steinkellner *et al.*, 2007). In addition, as indicated earlier (section 1.2.1), the chemotropic growth of germ tubes of *F. oxysporum* is mediated by the catalytic activity of class III peroxidases secreted by the roots (Turra *et al*., 2015).

1.4 Calcium signalling

1.4.1 Calcium as a second messenger in cells

Calcium is a universal secondary messenger molecule in eukaryotes. As a signal molecule, Ca^{2+} is central to regulating many cellular processes (Bootman *et al*., 2001) in response to environmental and developmental cues (Sanders *et al.*, 2002). In general, cells adapt to environmental changes by triggering specific signalling pathways using second messengers such as Ca^{2+} (Bootman *et al*., 2001).

Cells maintain a cytosolic free calcium concentration ($[Ca^{2+}]_c$) of ~100 nM in there resting state and a usually a very large gradient (~20,000 fold in mammalian cells) in free Ca^{2+} concentration between the extracellular environment and the cytoplasm. This gradient is maintained by sequestration of Ca^{2+} in different cell organelles such as vesicles, endoplasmic reticulum (ER) and mitochondria, by pumping Ca^{2+} out of the cell, and by Ca^{2+} buffering in the cytoplasm (Bootman *et al*., 2001; Clapham, 2007).

The Ca^{2+} signalling system is composed of elementary and global Ca^{2+} signals. Elementary signals directly control cell processes through their localised and specific action and also serve as building blocks of global Ca^{2+} signals. The openings of Ca^{2+} channels in membranes are responsible for the introduction of elementary signals. Waves and spikes constitute global Ca^{2+} signals leading to larger physiological responses that have been well characterised in mammalian cells (Bootman *et al*., 2001).

Ca^{2+} waves and spikes are introduced and maintained by the co-ordinated action of many components of the Ca^{2+} signalling machinery (Berridge *et al.*, 2003). Ca^{2+} receptors, transducers, Ca^{2+} permeable channels, Ca^{2+} pumps and exchangers, Ca^{2+} buffers, Ca^{2+} effectors and Ca^{2+}-sensitive enzymes are the major components of the 'Ca^{2+} signalling toolkit' (Sanders *et al.*, 2002; Berridge *et al.*, 2003).

One of the key regulators of Ca^{2+} signalling in animal and plant cells has been identified as inositol 1,4,5-triphosphate (IP_3) (Sanders *et al.*, 2002; Berridge, 2005). In mammalian cells, activation of specific receptors on the plasma membrane leads to the activation of the enzyme phospholipase C, which in turn hydrolyses inositol 4,5-bisphosphate to IP_3 and diacylglycerol. IP_3 then diffuses through the cytoplasm and binds to its receptors on the ER which opens Ca^{2+} channels in the ER membrane. Thus a Ca^{2+} influx from the ER into the cytoplasm occurs. Its ability to rapidly diffuse, its short lifetime and its spatially restricted action are some of the features that make IP_3 an efficient regulator of Ca^{2+} signalling (Bootman *et al.*, 2001). Ca^{2+} by itself can activate Ca^{2+} channels and this is termed Ca^{2+}-induced Ca^{2+} release (CICR).

A major adaptor protein, and the main intracellular Ca^{2+} receptor, in cells is calmodulin. Calmodulin undergoes a change in its conformation when bound to Ca^{2+} thereby allowing it to activate a wide range of other proteins involved in regulating many different cell processes (Clapham, 2007). A key regulatory protein in cells that is activated by Ca^{2+} bound to calmodulin is the protein phosphatase, calcineurin (Rusnak and Mertz, 2000). Calcineurin is an intracellular phosphatase which exists in an autoinhibited state during normal cellular processes. Calcineurin has two subunits; a catalytic A subunit and regulatory B subunit. The autoinhibitory domain is displaced when Ca^{2+} - calmodulin complex binds to subunit A of calcineurin in response to a range of exnvironmental stimuli (Steinbach *et al.*, 2007; Rispail *et al.*, 2009). This in turn regulates downstream processes through dephosphorylation and subsequent nuclear localization of transpcription factors such as Crz1 (Calcineurin-Responsive Zinc Finger 1) (Hernandez-Ortiz *et al.*, 2013; Thewes, 2014; Liu *et al.*, 2015), one of a number of fungal proteins that is in turn activated by active calcineurin.

An important feature of Ca^{2+} signals are their pulsatile nature. The long term maintenance of a high cytoplasmic concentration of Ca^{2+} is toxic to the cell and hence Ca^{2+} signals are transient but highly effective in inducing specific functions (Bootman *et al.*, 2001; Kim *et al.*, 2012).

1.4.2 Role of calcium signalling in growth and development of filamentous fungi

In filamentous fungi, evidence has been obtained for Ca^{2+} signalling being involved in the regulation of secretion, hyphal tip growth, hyphal branching, sporulation, dimorphism, cytoskeletal organization, differentiation of infection structures and circadian rythms (Borkovich *et al*., 2004; Nelson *et al*., 2004; Bencina *et al*., 2009; Fig. 1.5).

Comparative genomic analyses of many different filamentous fungi, including *F. graminearum*, have shown that many components of the Ca^{2+} signalling machinery in animals and plants are conserved in fungi (Zelter *et al*., 2004; Bencina *et al*., 2009; Rispail *et al*., 2009). However, certain significant components have been shown not to be conserved (e.g. IP_3 receptors) (Galagan *et al*., 2003; Zelter *et al*., 2004).
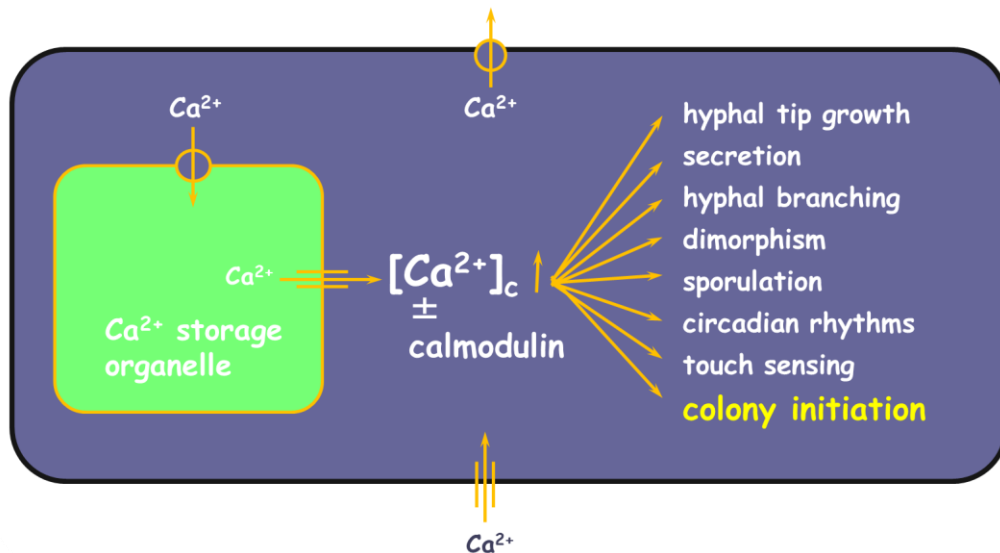
Fig. 1.5 Simple summary of the Ca^{2+} signalling machinery in filamentous fungi (provided by N.D. Read). Cells (represented by blue box with black border) maintain an $[Ca^{2+}]_c$ resting level of ~100 nM. An appropriate stimulus will trigger the transient opening of Ca^{2+} channels in the plasma membrane or in the membrane of a Ca^{2+} storage organelle (represented in green with a yellow border) thereby leading to an influx of Ca^{2+} ions into the cytoplasm. This will transiently increase the $[Ca^{2+}]_c$ concentration to a level at which it becomes an intracellular signal that can activate various Ca^{2+}-dependent proteins. The increased $[Ca^{2+}]_c$ is brought back down to the resting level by sequestration of Ca^{2+} within organelles and/or by its transport to the extracellular region by the action of Ca^{2+} antiporters and Ca^{2+} pumps. Cytoplasmic Ca^{2+} buffering also plays a role in reducing the increased $[Ca^{2+}]_c$ concentration. Whilst the $[Ca^{2+}]_c$

concentration is transiently elevated, the Ca^{2+} interacts with calmodulin and other Ca^{2+} binding proteins that regulate numerous physiological processes.

Polarised hyphal growth has been reported to be regulated by maintaining a Ca^{2+} gradient in the tip growing region (Silverman-Gavrila and Lew, 2003). However recent results have indicated that hyphae of *F. oxysporum* can grow in the absence of a tip-focussed Ca^{2+} gradient (Kim *et al*., 2012). This indicates that there is not an obligatory link between the presence of a tip-focused Ca^{2+} gradient and tip growth in filamentous fungi as there is in tip growing plant cells such as pollen tubes and root hairs (e.g. Hepler, 2005).

The oscillatory recruitment of the proteins MAK-2 and SO to CAT tips during CAT fusion has been predicted from mathematical modelling to involve the pulsatile secretion of a self-signalling chemotropic ligand (Goryachev *et al*., 2012) (Figs. 1.3 and 1.4). This pulsatile secretion and the merging of the plasma membranes of fusing CATs have been hypothesised to be regulated by Ca^{2+} signalling (Herzog *et al*., 2015). FIG1 was found to localize to plasma membrane during cell fusion in yeast and mutants of Fig1, a predicted low affinity Ca^{2+} channel, has been found to be defective in membrane fusion in yeasts (Aguilar *et al*., 2007). Extracellular Ca^{2+} has been shown to be required for CAT fusion in *N. crassa* and a Ca^{2+} sensor mutant, *Δcse-1*, exhibited a defective fusion phenotype. Deletion mutants of PIK-1 and NFH-2, two possible interacting partners of CSE-1, also showed similar phenotypic defects in cell fusion to that of the *Δcse-1* mutant (Palma-Guerrero *et al*., 2013). Ca^{2+} signalling has been proposed to regulate the interaction between these three proteins leading to exocytosis of the chemoattractant and/or receptor during hyphal fusion (Palma-Guerrero *et al*., 2013; Weichert and Fleissner, 2015). In addition, deletion of the gene encoding the Ca^{2+}-binding protein HAM-10 has been found to exhibit fusion defects (Fu *et al*., 2011) and the calmodulin-binding protein HAM-3, has also been shown to be required for cell fusion (Simonin *et al*., 2010).

However, our understanding of the roles of Ca^{2+} signalling during growth and development in filamentous fungi has been limited particularly because of the problems with imaging $[Ca^{2+}]_c$ dynamics in living fungal cells at the single-cell level (Kim *et al*., 2012). These problems have been associated with the difficulty of successfully impaling small turgid cells with Ca^{2+}-sensitive microelectrodes without killing the cells; poor uptake of Ca^{2+}-sensitive dyes into cells; sequestration of dyes by organelles; or low

expression of genetically encoded, Ca^{2+}-sensitive fluorescent probes (Nelson *et al*., 2004; Hickey *et al*., 2005).

Kim *et al*. (2012, 2015) were the first to report the successful imaging of subcellular $[Ca^{2+}]$ dynamics in living filamentous fungi. This was achieved by imaging the genetically encoded FRET (Forster Resonance Energy Transfer)-based Ca^{2+} probe, cameleon, in *Magnoporthe oryzae*, *F. oxysporum* and *F. graminearum.* This important technological achievement has provided a very powerful tool for understanding the role of Ca^{2+} signalling in fungi in the future.

Besides the use of mutants and the direct imaging/measurement of $[Ca^{2+}]_c$ dynamics in living cells, pharmacological agents have been extensively employed to study Ca^{2+} signalling in filamentous fungi (e.g. Nelson *et al.*, 2004; Goncalves *et al*., 2014) using the many drugs that act as modulators of Ca^{2+} signalling in animal cells (e.g. BAPTA, verapamil, calmidazolium, thapsigargin and ruthenium red – see section 5.1).

1.5 Human infections by *Fusarium* species

Fusarium is a significant opportunistic fungal pathogen of humans and other animals. Any infection caused by a *Fusarium* species in animals is termed 'fusariosis' (Nucci *et al*., 2015; Esnakula *et al*., 2013). Immunocompromised patients with neutropenia and T-cell deficiency have been reported to be at the highest risk of fusariosis (Nucci and Anaissie, 2007). In immunocompetent hosts, *Fusarium* species can cause localized infections (e.g. keratitis and onychomycosis) or post trauma skin infections resulting from burns or wounds. In immunocompromised hosts, however, *Fusarium* species can cause serious disseminated infections that can be life-threatening (Gupta *et al*., 2000; Nucci and Anaissie 2007; Muhammed *et al*., 2013; Nucci *et al*., 2015). The susceptibility of immunocompromised patients to fusariosis is due to damage of the patient's innate immune system leading to reduced numbers of neutrophils and macrophages which otherwise provide protection against mould infections (Campo *et al*., 2010; Esnakula *et al*., 2013). Manifestations of systemic fusariosis include the formation of erythematous painful papules, lesions or nodules affecting most of the organs including heart, kidney and brain, the most frequently in the skin (Nucci and Aniassie 2002; Nucci and Anaissie, 2007).

The most common *Fusarium* species isolated from human infections is *F. solani* followed by *F. oxysporum* and *F. verticillioides* (Nucci and Anaissie, 2007; Esnakula *et*

al., 2013; Guarro 2013; Muhammed *et al*., 2013; Nucci *et al*., 2015). Factors contributing to the increased risk of fusariosis include increasing antifungal resistance within different *Fusarium* species complexes and the increased use of corticosteroids to treat diseases, which results in suppression of the host immune system (Pujol *et al*., 1997; Campo *et al*., 2010; Low and Rotstein, 2011; Guarro, 2013; Nucci *et al*., 2015; Kadri *et al*., 2015; Stempel *et al*., 2015).

Identification of the *Fusarium* species being involved in infection can result from a combination of one or more of the following techniques: histological analysis of tissue biopsy samples, culturing the fungus from infected tissue, the serum galactomannan assay, and the *β*-1,3-glucan assay. A definite identification at the species level requires molecular methods such as polymerase chain reaction (PCR) (Guarner and Brandt, 2011) or matrix-assisted laser desorption ionization-time-of-flight (MALDI-TOF) analysis (Marinach-Patrice *et al*., 2009).

To gain further insights into human infections caused by *Fusarium* species, all the published case reports of *Fusarium* infections in humans from 2011-2015 were reviewed. Sixty five case reports of human fusariosis were identified from pubmed searches (www.pubmed.com) and an additional 10 were identified by Google searches. Thus 75 case reports were reviewed overall and these contained a total 98 cases of human fusariosis. Sections 1.5.1 to 1.5.3 provide a summary of this review.

1.5.1 *Fusarium* species causing fusariosis

Table 1.1 shows the number of cases corresponding to the different species of *Fusarium* that have been reported to cause human infection This data has been grouped into the different species complexes to which each of the species belong. Figure 1.6 shows the percentage of cases belonging to each of the different species complex. The *F. solani* species complex was found to be the most prominent species responsible for human infections (32.7%). This was followed by *F. verticilloides* species complex (11.2%) and *F. oxysporum* species complex respectively (5.1%). Earlier reviews of cases of fusariosis in humans from 1966-2001 (Nucci and Anaissie, 2002), 2002-2005 (Nucci and Anaissie, 2007), 2000-2009 (Muhammed *et al*., 2013) and 2005-2011 (Nucci *et al*., 2013) reported similar findings. *F. solani* was the most frequent isolate from human infections comprising 50% of all cases reported while *F. oxysporum* and *F. verticilloides* were reported in 20% of cases each. Dalyan Cilo *et al*., (2015) did a study of all the reported fusariosis cases over a 20-year period in a hospital in Turkey from

which they identified *F. verticilloides* species complex to be the most commonly reported (~50%) followed by *F. solani* species complex, *F. dimerium* species complex and *F. oxysporum* species complex, respectively.

Table 1.1 Number of reported fusariosis cases (2011-2015) associated with different species of *Fusarium.*

Species	No. of cases	Species complex (where relevant)
F. andiyazi	1	*Fusarium fujikuroi* species complex
F. chlamydosporum	1	-
F. equisetti	2	-
F. heterosporum	1	-
F. falciforme	3	*Fusarium solani* species complex
F. monoliforme	1	*Fusarium fujikuroi* species complex
F. oxysporum	4	*Fusarium oxysporum* species complex
F. proliferatum	4	*Fusarium fujikuroi* species complex
F. petroliphilum	1	*Fusarium solani* species complex
F. vasinfectum	1	*Fusarium oxysporum* species complex
F. verticilloides	4	*Fusarium fujikuroi* species complex
F. solani	42	*Fusarium solani* species complex
F. temperatum	1	*Fusarium fujikuroi* species complex
Unnamed *Fusarium* spp.	32	-
Total	98	
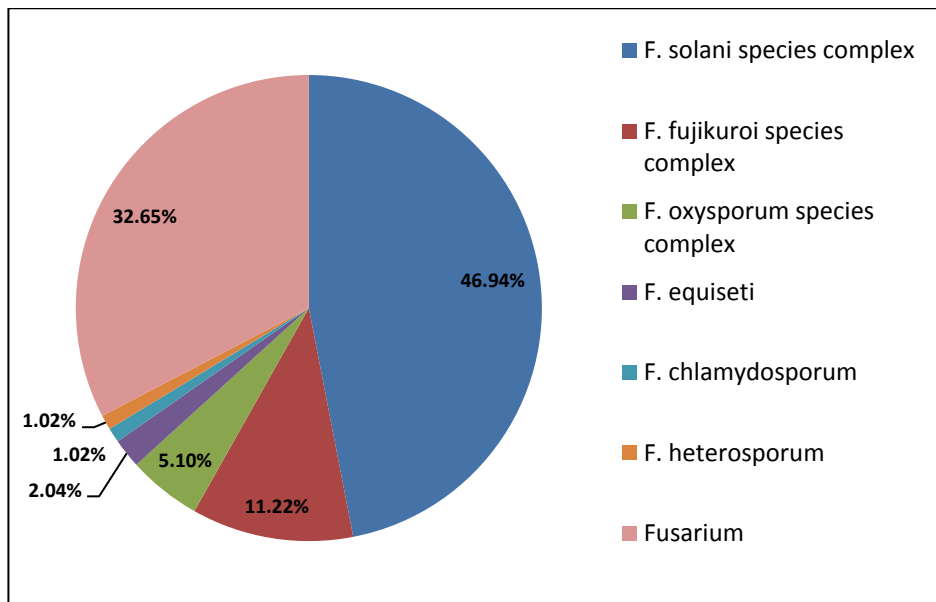
Fig. 1.6 Percentage of reported fusariosis cases involving different *Fusarium* species / species complexes (2011-2015)

1.5.2 Human organs affected by different types of fusariosis

Data collected about the different clinical manifestations of fusariosis in human hosts were used to identify the most common and the organs affected. Skin was the most commonly affected organ in the case reports (39.8%) followed by eyes (29.6%), which is in accordance with earlier reviews (Nucci and Anaissie, 2007; Muhammed *et al*., 2011). 21.4 % of cases reported infection of the lungs, airways or the nasal cavity. Nucci *et al*., (2015) reviewed 357 case reports from 1966-2014 and identified 42% of cases caused by *Fusarium* species that were associated with pneumonia in both immunocompromised and immunocompetent hosts. 86% of these cases were infections of both the lungs of patients. Other prominent *Fusarium* infections were of nails (6.1%), the heart (5.1%), kidneys (5.1%) and the brain (4.08%).
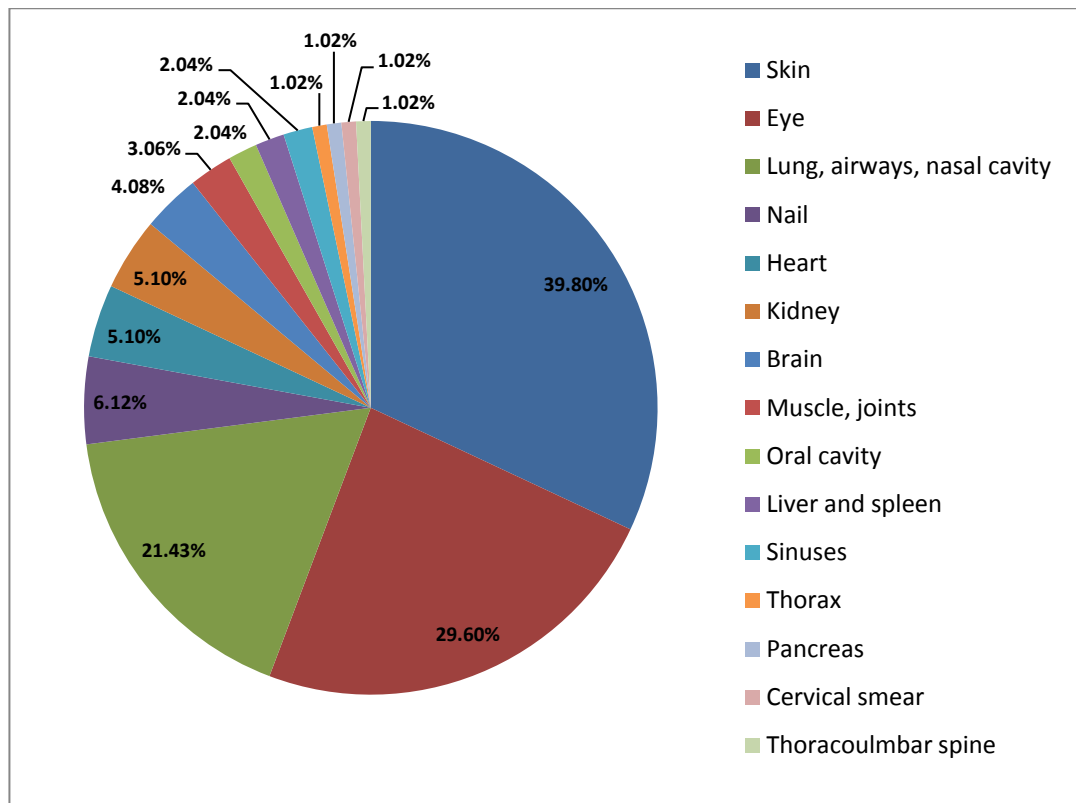
Fig. 1.7 Percentage of reported fusariosis cases associated with different organs (2011-2015).

1.5.3 Underlying medical conditions and mortality in immunocompromised hosts with fusariosis infections

60% of reported fusariosis cases in immunocompromised hosts were in leukemia patients (Fig. 1.8). 90% of these were disseminated infections. Hence it can be concluded that there is a higher probability of *Fusarium* infections becoming systemic in immunocompromised hosts especially those with hematologic malignancy, and this is in agreement with previous reports (Wu *et al*., 2004; Nucci and Anaissie, 2007). Fusariosis that occurred post organ transplantation comprised 21% of cases and 4% of cases had aplastic anaemia infections (Fig. 1.8). One case of fusariosis each was reported for patients with Hurler's syndrome, chronic granulomatous disease (CGD) (Okura *et al*., 2015), HIV, asthma, end stage renal disease, autoimmune disease, multiple organ injury and neuroblastoma (Fig. 1.8).

36% of all reported cases of fusariosis resulted in the death of the patients while 53% of the reported patient recovery (Fig. 1.9). 4% of cases involving eye infections required eye enucleation (removal).
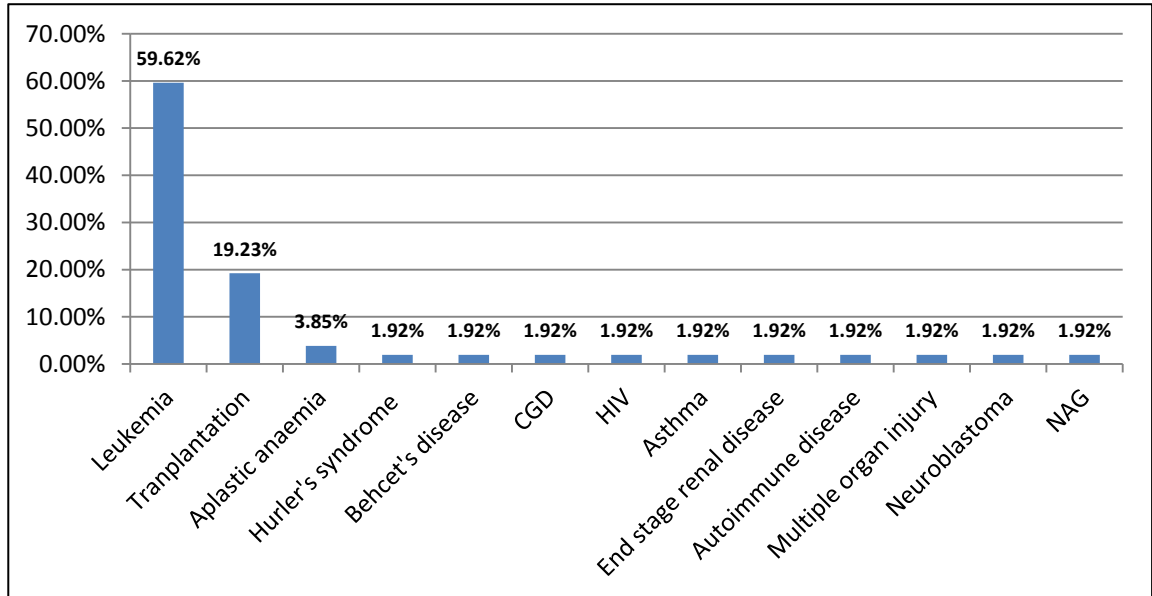
Fig. 1.8 Percentage of underlying medical condition in fusariosis cases in immunocompromised hosts (2011-2015). CGD: chronic granulomatous disease. HIV: human immunodeficiency virus infected patients. NAG: inadequate information provided.

1.6 Keratitis caused by different fungi

Human corneal infections by fungi (or mycotic keratitis) are increasingly being reported from around the world and comprise 50% of all cases of keratitis infections (Neilsen *et al*., 2015; Ruhnke *et al*., 2015; Taj-Aldeen *et al*., 2015; Khwakhali *et al*., 2015; GAFFI, www.gaffi.org, 2016). Many cases often result in complete loss of vision requiring penetrating keratoplasty (corneal transplantation to remove scar tissue) or enucleation of the eye to prevent further dissemination of the infection to other organs (Gungel *et al*., 2011; Edelstein *et al*., 2012). It has been estimated that over 1 million people lose their vision in at least one eye due to fungal keratitis every year (GAFFI, www.gaffi.org, 2016). An increase in the number of cases of corneal transplantation due to cataracts or other infections poses an increased risk for acquiring fungal infections. People in tropical regions of the world with a humid climate experience an increased risk of acquiring mycotic keratitis as is evident from 44%-47% of global fungal keratitis cases being reported from India (Vemuganti *et al*., 2002; Kredics *et al*., 2015). 63% of all keratitis infections in India are caused by fungi, which is in contrast to the comparatively higher number of bacterial keratitis cases in Europe (Basak *et al*., 2005; Sreenivasan, 2007). The major fungal genera causing keratitis are *Fusarium*,

Aspergillus, *Candida* and *Curvularia* (Karthikeyan *et al*., 2011; Kredics *et al*., 2015; He *et al*., 2016).

1.7 Keratitis caused by *Fusarium* species

Fusarium species are a leading cause of mycotic keratitis, especially in contact lens-related outbreaks (Chang *et al*., 2006; Khor *et al*. 2006; Gorscak *et al*., 2007; Epstein, 2007; O' Donnell *et al*., 2007; Ng *et al*., 2008; Karthikeyan *et al*., 2011; Mela *et al*., 2015; He *et al*., 2016). The risks of developing keratitis by *Fusarium* are primarily from trauma (Siatiri *et al*., 2011; Lai *et al*., 2014), contact with infected plant material (Mochizuki *et al*., 2012; Jiang *et al*., 2013), unhygienic use of contact lens or lens solutions (Chang *et al*., 2006; Khor *et al*., 2006; Gaujoux *et al*., 2008; Behrens-Baumann *et al*., 2012; Mela *et al*., 2015) and contamination during surgical intervention (Gungel *et al*., 2011; Byun and Kim, 2011).

In my review of the literature of reported fusariosis cases during the period 2011-2015 (sections 1.5.1-1.5.3), of the 29 cases reported involving eye infections (~30% of all cases), 15 (45%) of them were described as keratitis and 3 (10%) were cases in which keratitis progressed to endophthalmitis (internal inflammation of the coats of the eye) (Fig. 1.9). 87% of all eye infections reported were in immunocompetent hosts. All the 18 cases with *Fusarium*-associated keratitis were in immunocompetent hosts caused by localized trauma to the eye. The most common *Fusarium* species complexes/species isolated from the eyes of patients with keratitis were the *F. solani* complex followed by the *F. fujikuroi* species complex (Fig. 1.11). One case each was reported *F. oxysporum* species complex, *F. equisetti* and *F. temperatum*. Species level identification was not done for 7 of the cases (Fig. 1.11).
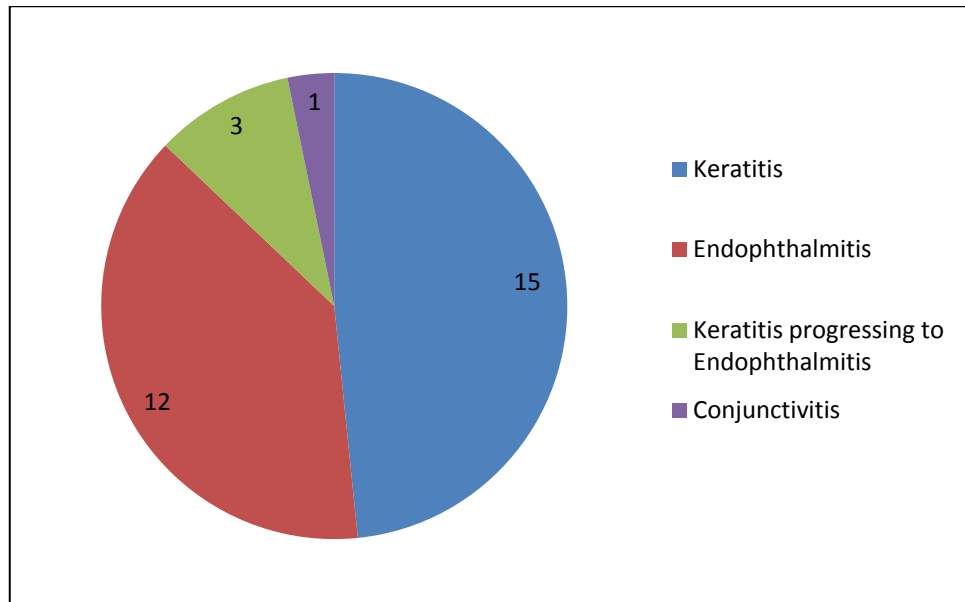
Fig. 1.9 Reported fusariosis cases involving eye infections (2011-2015)
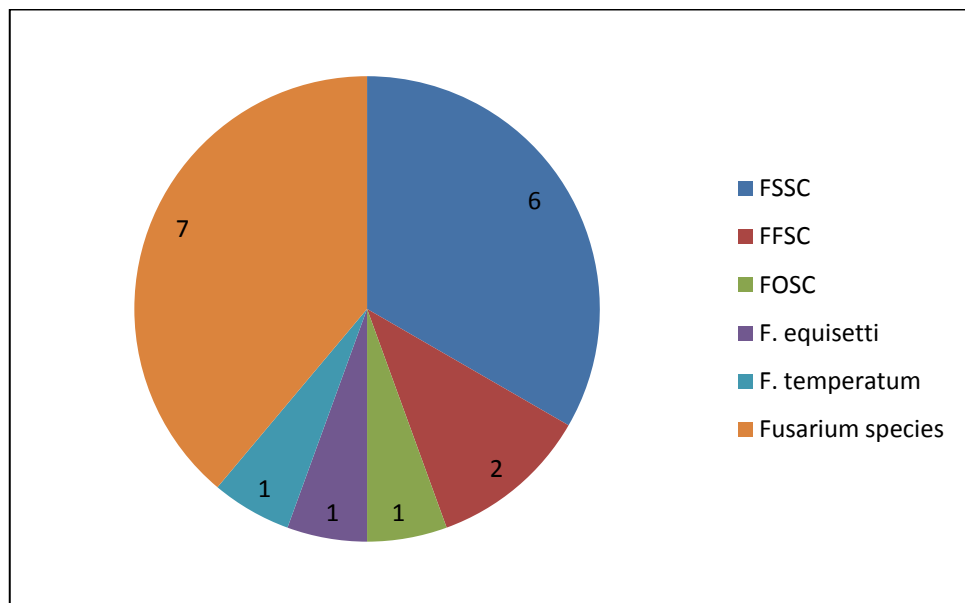
Fig. 1.10 Causative *Fusarium* species complexes in reported fusariosis cases involving eye infections (2011-2015)

1.8 Structure of the human cornea

The cornea is the first layer of human eye that refracts light from the external environment to the retina. A tear film protects the surface of the cornea *in vivo*. The human cornea is a transparent avascular structure with 5 different types of tissue layers and is approximately 500 μm thick (Delmonte and Kim, 2011). The first (outermost) layer is the epithelium which forms the primary defence layer for protection from

external agents. The epithelium can be of 4-6 cells thick and is continuously replaced every 6 to 7 days *in vivo*. Of the 4-6 cell layers of epithelium, the outermost region is composed of squamous epithelial cells the innermost layer is composed of tightly packed columnar cells termed the basal epithelial layer. Below the basal epithelium is the Bowman's membrane which is a non-cellular layer. Beneath this is a thick layer of stroma. Stroma is composed of approximately 200 layers of collagen fibres arranged at right angles to the adjacent layer. Keratocytes are distributed throughout this layer. The corneal keratocytes are specialized fibroblasts that play a role in keeping the cornea transparent, healing its wounds, and synthesizing its components (Delmonte and Kim, 2011). Below the stroma is the Descemet's membrane under which there is a thin layer of endothelium (Fig. 1.6).
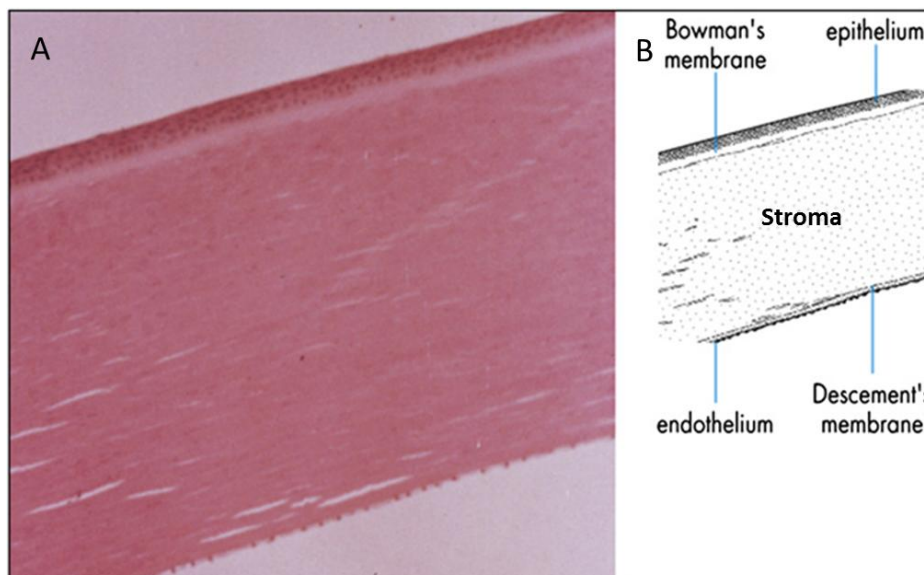
Fig. 1.11 (A) Light micrograph showing a stained longitudinal cross section of human corneal tissue. **(B)** Diagrammatic representation of the different layers of corneal tissue. Reproduced from Farjo *et al*. (2008).

1.9 Infection models that have been used to study *Fusarium* keratitis

Detailed studies on fungal keratitis require good infection models. Monolayer cell cultures lack the properties of the 3D tissue structure which makes it impossible to derive realistic conclusions about such aspects as the penetration of tissues by fungal hyphae during infection. Studies with murine models however have revealed significant insights about *Fusarium* infections (Legrand *et al*., 1991; Mayayo *et al*., 1999; Ortoneda *et al*., 2004; Schafer *et al*., 2014a) but have several limitations. High resolution live-cell imaging *in vivo*, although achievable to some extent in whole mouse models (e.g. two-

photon microscopy) (Weighert *et al*., 2013; Park *et al*., 2015), requires highly advanced microscope systems with a complex experimental set up (Carriles *et al*., 2009). Measurement of fungal burden in infected mice using PCR and histopathology data with different inoculum concentrations is the most commonly employed method (Schafer *et al*., 2014a). There have been discrepancies in the results from murine models compared to the results obtained from human infections (Nucci and Anaissie, 2007; Nucci *et al*., 2013). The structure of the cornea differs between animals with different visual abilities. The Bowman's membrane and arrangement of stromal layers including its thickness are two features which vary in different mammals and in different primates (Hayes *et al*., 2007). This justifies the use of *ex vivo* human corneas as the best for studying fungal keratitis of humans. It not only has all the benefits of being the original host tissue but also it is easier to culture due to its smaller size (~11 mm in diameter) than using murine models. It can also be analysed using histopathology (Hua *et al*., 2010) and molecular (He *et al*., 2016) methods.

1.10 Importance of fungal morphology data for the identification of fungi causing keratitis

Morphological features from histopathological tissue sections and cultures have been largely used for identifying fungal infections especially at an earlier stage (Guarner and Brandt, 2011; Ostrosky-Zeichner, 2012). *Fusarium* species are the most important causative species isolated from mycotic keratitis, especially tropical countries (GAFFI, www.gaffi.org; Vemuganti *et al*., 2002; Kredics *et al*., 2015; He *et al*., 2016). The genus *Fusarium* is comprised of candidate species which have evolved to exhibit host specificity at the sub-species level (Mechielse and Rep, 2009; Ma *et al*., 2010). They are also one of the most drug resistant groups of organisms exhibiting high minimum inhibitory concentration (MIC) values against most commonly used antifungal drugs (Rueben *et al*., 1989; Rotowa *et al*., 1990; Pujol *et al*., 1997).

 Fusarium solani, *F. oxysporum* and *F. verticilloides*, the three major human pathogenic species in genus *Fusarium* are all species complexes each composed of several sub-species exhibiting morphological similarities but with significant genetic variability (Nucci and Anaissie, 2007; Ma *et al*., 2010; Esnakula *et al*., 2013; Muhammed *et al*., 2013; Coleman, 2016). The four major pathogenic species of *Fusarium*: *F. graminearum, F. verticilloides, F. oxysporum* and *F. solani* has 4, 11, 15 and 17 chromosomes respectively (Ma *et al*., 2010; Coleman, 2009; Coleman, 2016). This

poses a major difficulty for the identification of *Fusarium* at the species-level, or even distinguishing *Fusarium* from other filamentous fungi such as *Aspergillus* from histopathology data alone (Guarner and Brandt, 2011). Variation in antifungal resistance by different sub-species of the species-complex of *Fusarium* is another significant factor which indicates the importance of identifying the correct causative sub-species in order to prescribe appropriate antifungal drug at a correct dosage of the drugs for patients suffering from fusariosis (Zhang *et al*., 2007; Ersal *et al*., 2015; Dalyan Cilo *et al*., 2015; Kredics *et al*., 2015; Al-Hatmi *et al*., 2016).

Improvement in the identification of fungal species from clinical specimens will be assisted by having a better understanding of the specific morphological features and quantitative parameters associated with different sub-species of the fungal pathogen. Histological techniques used for identifying fungal infections include: histochemical staining (use of dyes that selectively stain the fungal elements allowing better contrast relative to the surrounding tissue); immunohistochemistry (use of antibodies that bind to fungal antigens); and *in situ* hybridisation (use of probes to specific DNA binding sequences in fungal nuclei) (Guarner and Brandt, 2011). The haematoxylin-eosin, Periodic Acid Schiff (PAS) and Grocott's methenamine silver-stain are commonly used in histological studies of fusariosis (Avellino silva *et al*., 2015; Garcia *et al*., 2015).

A lack of expert knowledge in the identification of appropriate features of fungi from histopathology and culture data is a major problem in the diagnosis of fungal infections (Ostrosky-Zeichner, 2012; Kozel and Wickes, 2014; www.gaffi.org). Individual 2D images obtained using standard histological methods lack a third dimension and hence are inadequate in order to provide a visualization of a fungus invading a host tissue. An improved visualization of morphological structures associated with infection not only serves to identify key factors to facilitate the identification of the fungal species involved but also allows one to study the pathology of the infection process. This major shortcoming is beginning to be overcome in the clinic by the availability of new diagnostic tools that allow real time imaging of *in vivo* infection from a patient's eye. For this purpose, a type of confocal microscopy called scanning laser ophthalmoscopy (SLO) has been developed for diagnostic *in vivo* imaging of the human cornea or retina (Sharp *et al*., 2004).

Morphological features that have been described from direct observation of histological sections in case reports of *Fusarium* infections include: hyaline septate hyphae (King *et*

al., 2011; Edelstein *et al*., 2012; Silva *et al*., 2013), hyaline non-septate hyphae (Al Hatmi *et al*., 2014), acute angled branches (Liu *et al*., 2011; Morel *et al*., 2013), right angled branches (Mochizuki *et al*., 2012; Pereira *et al*., 2013; Son *et al*., 2015), intercalary chlamydospores (Woolf *et al*., 2012; Esnakula *et al*., 2013), giant cells infiltrated with hyphal elements (Keskar *et al*., 2014; Wu *et al*., 2014), intercellular fungal hyphae (Keskar *et al*., 2014), yeast like structures along with hyphal elements (Avellino-Silva *et al*., 2015), and transepidermal growth and penetration of vascular vessels by hyphal elements (Do *et al*., 2011; Pereira *et al*., 2013; Nakai *et al*., 2014).

1.11 Host immune responses during fungal keratitis

Fungi invade human corneal tissue by overcoming the non-specific primary defences, particularly eye blinking and tear production (Karthikeyan *et al*., 2011; Wu *et al*., 2015). Neutrophils, mononuclear leukocytes (e.g. macrophages and monocytes), and dendritic cells of the innate immune system play an important role in the defence response against fungal invasion (Romani, 2004; Hu *et al*., 2014; Kadri *et al*., 2015). These defence responses are activated through recognition of Pathogen Associated Molecular Patterns (PAMPs) by specific Pattern Recognition Receptors (PRRs) such as the Toll-like receptors (TLR) on the surfaces of epithelial cells (Romani 2004; Jin *et al*., 2007). Surfactant D proteins, which are specific pattern recognition receptors secreted by lung alveolar cells, are also present in lacrymal gland, tears and corneal epithelial cells. The expression of surfactant D proteins was shown to be significantly higher in corneal epithelium, stroma and endothelium of *F. solani* infected rat corneas which implicates a role for this collectin family of receptors in the defence mechanism against *Fusarium* keratitis (Che *et al*., 2012). In an expression analysis of receptors and interleukins in corneal ulcers from 110 patients with keratitis caused by *F. solani* or *Aspergillus flavus*, Dectin 1, TLR2, TLR4, TLR9, NOD-like receptor protein (NLRP), interleukin 1β (IL-1β), IL-8, IL-17, interferon γ and tumour necrosis factor α were found to be elevated with no significant difference observed between the responses to the two fungal species (Karthikeyan *et al*., 2011).

Fungal pathogenesis resulting in fungal infection causes inflammatory responses in the corneal tissue marked by the infiltration of inflammatory cells such as macrophages and polymorphonuclear neutrophils (PMNs) (Zhong *et al*., 2009). Kathikeyan *et al*. (2011) reported 95% of neutrophils and 5% of mononuclear cells (epithelial cells and monocytes) to be present among the infiltrating cells in the corneal ulcers of patients

41

with keratitis caused by *F. solani* and *A. flavus*. This process has been shown to be mediated by chemokines and cytokines. Macrophage inflammatory protein-2 (MIP-2) and Interleukin 1β (IL-1β) are two major inflammatory cytokines highly expressed during fungal keratitis in mice infections (Zhong *et al.,* 2009). Activation of macrophages by latex beads prior to infection with *F. solani* in murine models was shown to enhance the inflammatory response in the cornea as determined by the expression of inflammatory cytokines and lymphocytes in corneal tissue following infection (Hu *et al*., 2014). Reactive oxygen species (ROS) derived from NADPH oxidases are also known to play a role in immune responses by causing the migration of professional phagocytes, such as neutrophils and macrophages, to sites of fungal invasion (Hogan and Wheeler, 2014).

Neutrophils kill the fungal cells by their phagocytic action which helps to control the fungal infection at an earlier stage. The phagocytosed fungal spores or hyphae are lysed by the release of hydrolytic enzymes and by the accumulation of ROS by NADPH oxidases. Apart from phagocytosis, neutrophils can also kill invading fungi by degranulation and the formation of neutrophil extracellular traps (NETs). Degranulation is a process in which antimicrobial compounds are released, which helps in the degradation of the pathogens to make them more readily phagocytosed. NETs are formed by the secretion of neutrophil nuclear DNA into the extracellular matrix by dying neutrophils. These NETs entrap invading pathogens preventing their further movement (Cunha *et al*., 2014; Hogan and Wheeler, 2014). Granulocyte transfusions have been successfully used to treat cases of invasive fusariosis in neutropenic patients by increasing their neutrophil counts which emphasises the role that neutrophils play in the defence against *Fusarium* infections (Kadri *et al*., 2015).

1.12 Aims of the research carried out in my PhD

1.12.1 Overall aims

Using *Fusarium oxysporum* f.sp. *lycopersici* as an experimental system (see section 1.2), the main aims of my research were to:

1. Optimise the conditions to analyse the cell biology of conidial anastomosis tube fusion (CAT) fusion.
2. Analyse the cell biology of CAT fusion using advanced live-cell imaging and image analysis techniques.
3. Provide evidence for a role of Ca^{2+} signalling in CAT fusion.
4. Analyse *Fusarium* keratitis by using live-cell imaging and an *ex vivo* human corneal model.

1.12.2 Aims of the research described in Chapter 3

The cell biology of CAT fusion has only been extensively studied in the experimental model and saprotropic fungus, *Neurospora crassa* (see section 1.2). However, CAT fusion has not been analysed in depth in either a human or plant fungal pathogen. *F. oxysporum* is both a major plant pathogen and a human pathogen. In order to determine the optimal *in vitro* culture conditions for subsequent live-cell imaging and quantitative analysis of CAT fusion in *F. oxysporum* f. sp. *lycopersici*, the aims of the research described in chapter 3 were to:

1. Determine the optimal liquid media conditions for CAT fusion
2. Determine the optimal temperature for CAT fusion
3. Determine the optimal cell density for CAT fusion
4. Determine the optimal pH for CAT fusion
5. Determine whether stress conditions (oxidative stress) will induce CAT fusion
6. Determine whether human serum will induce CAT fusion

1.12.3 Aims of the research described in Chapter 4

Evidence for CAT fusion facilitating HGT in fungi lacking a sexual stage in their life cycles has been obtained from studies on the major plant pathogen *Colletotrichum lindemuthianum*. Cell fusion has been proposed to facilitate HGT in *F. oxysporum*

which is another asexual homothallic fungus (see section 1.2.5). However, a detailed cytological analysis of CAT fusion, and the transport of organelles, between fused germlings, is lacking. The aims of the research described in chapter 4 were to:

1. Characterise the stages of development from spore germination leading to CAT fusion by using bright field and confocal live-cell imaging.
2. Provide a detailed morphological characterisation and comparison of CATs and germ tubes.
3. Image the dynamics of labelled organelles transported between germlings via sites of CAT fusion
4. Determine the requirement of the microtubule and F-actin cytoskeleton for CAT fusion

1.12.4 Aims of the research described in Chapter 5

Preliminary evidence has been obtained for Ca^{2+} signalling playing roles during CAT fusion in *N. crassa* (see section 1.4.2). In order to obtain evidence for Ca^{2+} signalling being involved in regulating CAT fusion in *F. oxysporum*, the aim of the research described in chapter 5 was to:

Provide a quantitative analysis of the influence of a range of Ca^{2+} modulators on microconidial germination and CAT fusion

1.12.5 Aims of the research described in Chapter 6

Mycotic keratitis is a leading cause of blindness around the world and *Fusarium* species, including *F. oxysporum*, have been identified as a leading cause of keratitis (see section 1.7). However our understanding of the dynamic process of keratitis infection caused by any fungus is lacking and has not been studied using advanced live-cell imaging and image analysis techniques. The aims of the research described in chapter 6 were to:

1. Characterise the dynamic morphogenetic changes during infection by *F. oxysporum* using an *ex vivo* human corneal model and confocal live-cell imaging
2. Identify useful measurable traits from the live-cell imaging for the quantitative characterisation of infection and develop optimised methods for their measurement by using image processing and analysis software

3. Determine the occurrence of, and requirement for, hyphal fusion during human corneal infection

4. To assess the applicability of using my image analysis methods for analysing clinical image data obtained from the eye of a patient suffering from fungal keratitis caused by *F. solani* using a diagnostic confocal scanning laser opthalmoscope used in reflectance mode.

Chapter 2: Materials and Methods

2.1 Chemicals

All chemicals were obtained from Sigma Aldrich unless otherwise specified.

2.2 Strains of *Fusarium oxysporum* f.sp. *lycoperisici* used

The *F. oxysporum* f. sp. lycopersici (*Fol*) wild-type strain 4287 (FGSC strain 9935; Manchester Fungal Infection strain *Fol-1*) was used. This strain expressing pgpdAsGFP targeted to the cytoplasm (strain *Fol-2*) (Di Pietro *et al*., 2001), or this strain expressing H1-GFP (strain *Fol-3*) or H1-mCherry (strain *Fol-4*) (Ruiz-Roldan *et al*., 2010) to label nuclei, or the *Δfso* mutant (Prados Rosales and Di Pietro, 2008) of this strain, were also used. These five strains are stored in the Manchester Fungal Infection Group strain collection and were originally provided by Prof Antonio Di Pietro (University of Cordoba, Spain).

2.3 Preparation of *F. oxysporum* stock cultures

Stock cultures of the different *F. oxysporum* strains were prepared as spore suspensions each with a concentration of 1×10^7 spores and stored in a final volume of 30% glycerol at $-80\ ^0C$.

2.4 Culture conditions for harvesting microconidia

For the production of microconidia for harvesting, 100% PDB was inoculated with a microconidial suspension from the specified *F. oxysporum* stock culture and was grown at 28 °C in a shaking incubator with 170 rpm or 225 rpm. Microconidia were harvested from these cultures after 5-10 days of incubation by filtering the cultures through 2 layers of sterile Miracloth (Calbiochem). This was followed by centrifuging the samples in centrifugation tubes (Nalgene Oak Ridge tubes 50 ml PolyProp, Sigma Aldrich) at 10,000 rpm for 10 min at 25 °C, removing the supernatant and washing the pellet twice with sterile distilled water at 10,000 rpm for 10 min at 25 °C. Spore suspensions of defined concentrations were produced from the pelleted spores after cell counting using a haemocytometer (Fuchs Rosenthal chamber slide).

2.5 Culture media

To prepare the liquid minimal medium, the following ingredients were dissolved in 1 L of tap water: 1 g KH_2PO_4; 0.5 g $MgSO_4.7H_2O$; 0.5 g KCl; 2 g $NaNO_3$; 20 g glucose and 200 g sucrose

Potato dextrose broth (PDB) was prepared from 1 kg of commercially available baking potatoes that had been peeled, chopped into small cubes and boiled in 1.5 L of water for 1 h before filtering the broth through layers of cheese cloth placed in a funnel. The potato broth was diluted to a final volume of 5 L to which 2% glucose was added. This represented 100% PDB which was diluted accordingly for different experiments.

Potato dextrose agar (PDA) was prepared from commercially available PDA according to the manufacturers' instructions (Fluka).

2.6 CAT fusion and spore germination assays

CAT fusion assays were set up in 8 well borosilicate slide culture chambers (Nalge Nunc, Rochester, NY). 300 μl of a spore (i.e. microconidial) suspension was added to each well and incubated at 25 °C for 12 h in continuous light. The concentration of the spore suspension was $1x10^6$ spores per ml unless otherwise specified. A 1% dilution of 100% PDB with 25 mM $NaNO_3$ was used as the liquid growth medium for CAT fusion and spore germination assays unless otherwise specified. Any spore in which the oval symmetry had been broken due to the emergence of a tube-like protrusion was counted as germinated. The percentage of spores undergoing CAT fusion was determined by counting the spores or spore germlings that participated in CAT fusion. For example, a CAT fusion formed between two spores or between a spore and a germling or between two germlings was scored as 2 in each case. Thus:

% CAT fusion = [spores/germlings undergoing CAT fusion/total number of spores/germlings] x 100

Spores that formed germ tubes alone and were not involved in cell fusion were counted separately and were then added to the number of CAT fusions between spores alone to give the total number of germinated spores. This is because spore germination can be considered as involving the formation of a germ tube and/or a CAT (see section 1.3).

Thus:

% germination = [(spores forming germ tubes alone + spores undergoing CAT fusion)/Total number of cells] x 100

CAT fusion and spore germination were quantified from a minimum of 350 cells counted from microscopic images (see section 2.17.1). All experiments were repeated more than three times unless otherwise stated.

2.7 Microconidial adhesion assays

Adhesion was scored from short movies of 1 min with an image captured every second. The germlings which stopped exhibiting Brownian movement and were attached to the base of the chamber slide were scored as adhered whilst the ones which continued to move were scored as non-adhered (see Movie 3.3).

2.8 Pharmacological treatments

A range of pharmacological treatments and stress inducing agents were applied to assess their influence on CAT fusion and spore germination. The drugs and chemicals used for this purpose are shown in Table 2.1. CAT fusion and spore germination were quantified as described in Section 2.6. Stocks of the drugs were prepared by dissolving them in water or 100% DMSO as indicated in Table 2.1. An appropriate volume of each dissolved inhibitor was added to the growth medium at the beginning of each experiment to provide the desired final concentration. Unless otherwise stated, the final concentration of DMSO did not exceed 4% because higher concentrations were found to inhibit microconidial germination.

Table 2.1 Pharmacological agents and stress inducing agents used

Pharmacological drug/stress inducing agent	Solvent	Source
BAPTA	Water	Invitrogen Life Technologies
Verapamil	Water	Sigma Aldrich
FK506	DMSO	InvivoGen
Calmidazolium	DMSO	Acros Organics
RU360	Water	Calbiochem
Thapsigargin	DMSO	Sigma Aldrich
Benomyl	DMSO	Sigma Aldrich
Latrunculin A	DMSO	Tocris
Human serum (AB type)	Water	MP Biomedic
30% H_2O_2	Water	Sigma Aldrich

2.9 pH measurements

The pH of the standard growth medium (1% PDB supplemented with 25 mM $NaNO_3$) used for the spore germination and CAT fusion assays (section 2.6) was naturally at pH 5.5 and did not need adjusting. However, for experiments in which the influence of the external pH on spore germination and CAT fusion was analysed, the growth medium was adjusted with an Orion 710A+ pH meter (Thermoscientific) using 10M KOH, 5M NaOH and 16% HCl. The buffers used for adjusting the pH of media to the desired pH value for experiments with buffered pH media are shown in Table 2.2. 10 ml of the appropriate filter-sterilized buffer was mixed with 90 ml of autoclaved media (1% PDB or 1% PDB supplemented with 25 mM $NaNO_3$) to prepare a final 100 mM concentration of the buffer in the medium. Prior to using the buffered media for experiments, their pH was double-checked in small volumes separated from the buffered media to be used.

A pH glass microelectrode (Orion 9810BN, Fischer Scientific UK Ltd) was used in experiments to determine the influence of different medium supplements added to 1% PDB in the 8-well, slide culture chambers (section 2.6) in which spore germination and

CAT fusion were analysed. The initial pH and final pH after 12 h of incubation were measured in each experiment. Data was collected from three different experiments. Datasets were also generated from experiments in the absence of fungal cells, which were used as controls. These datasets were used to normalise the values obtained with the spore germlings present to generate the mean values of the change in media pH over the 12 h of incubation. The buffers and buffered media were stored at 4˚C.

Table 2.2 Buffers used for adjusting the pH of growth media

Buffer used	pH
1 M Glycine-HCl (pH adjusted to 3.5 with concentrated HCl)	3.5
1 M Glycolic acid (pH adjusted to 5 with 10 M NaOH)	5.0
1 M MES (pH adjusted to 6.5 with 10 M NaOH)	6.5
1 M Tris-HCl (pH adjusted to 7.5 with concentrated HCl)	7.2
1 M Tris-HCl (pH adjusted to 8.3 with concentrated HCl)	8.0

2.10 Extraction of genomic DNA

Mycelia were harvested from 3-5 day old wild type cultures by filtering them through one layer of miracloth. The mycelia were dried well within the miracloth by sandwiching them between paper towels. The mycelia were then collected in a fast prep tube each containing 2 ball bearings (only a quarter of a fast prep tube was filled with mycelia) and kept frozen in liquid nitrogen. The mycelia in the tubes were ground using a tissue lyser (Qiagen Tissue Lyser II). The homogenised suspension without the ball bearings was pipetted into an Eppendorf tube and 1 ml of freshly prepared CTAB extraction buffer (Table 2.3) was added and vortexed well. 4 µl of β-mercaptoethanol was added to the tube, vortexed and filled with a mixture of chloroform and isoamyl alcohol (24:1). This was again mixed well by vortexing. The tube was kept at 65 ^{0}C for 30 min followed by 15 min at room temperature. This was followed by centrifugation at 14,000 rpm for 10 min. The supernatant was collected from the Eppendorf tube and pipetted into a new Eppendorf tube containing 1 ml of 100% ethanol. This was left in the -20 ^{0}C freezer for 15 min followed by centrifugation at 14,000 rpm for 10 min at 4 ^{0}C. The supernatant was discarded and 1 ml of 75% ethanol added. This was

centrifuged at 14000 rpm for 10 min. The supernatant was discarded and the pellet was left to dry in a fume hood. This was followed by addition of 100 µl of distilled water and 4 µl of RNase. This was incubated on a thermoblock at 37 ^{0}C for 60 min. 2 µl of the extracted DNA was run on a gel for qualitative verification.

Table 2.3 Components of the CTAB extraction buffer (10 ml final volume)

3 ml of centrimethyl ammonium bromide (CTAB) (10% dissolved in distilled water)
2.8 ml of 5 M NaCl
0.4 ml of 0.5 M EDTA (pH 8.0)
1 ml of 1 M Tris-Cl (pH 8.0)
0.3 g of polyvinyl pyrrolidine (PVP)
0.02 ml of β- mercaptoethanol
2.48 ml H$_2$O

2.11 Corneal infection assays

Human corneas were received from the eye bank (Manchester Eye Bank, Central Manchester Hospitals), immersed in 100 ml of Dulbecco's Modified Eagle Medium (DMEM, Sigma), after their expiry period of 28 days for transplantation. The corneas were transferred to fresh DMEM media supplemented with 10% foetal calf serum (FCS, Sigma) containing the antibiotics streptomycin (Sigma) and ampicillin (Sigma) (both at 1µg/ml). The corneas were cultured for a specified period in a 34 °C incubator supplied with 0.5% CO$_2$. Sterile 6-well Corning Costar cell culture plates (Sigma), with 3 ml of media in each well, were used for culturing the cornea. Media was replaced every 24 h during culturing.

Corneas were infected with the desired concentration of spore suspension prepared in the same, but fresh, culture medium used for corneas. 5×10^5, 1×10^6 and 1×10^7 spores/ml were used as inocula for the different infection assays. Four 5 µl drops of spore suspension were added (using 10 µl pipette tips) to the centre region of the cornea. This was to allow an even distribution of spores over the surface of the cornea. Corneas were transferred to 2-well glass slides (Thermoscientific) with 1 ml of culture media prior to microscopy.

The *F. oxysporum* wild type strain 4287 (FGSC), H1 GFP strain, cytoplasmic GFP expressing strain and the *Δfso* mutant strain (section 2.2) were used in these assays. In experiments in which the GFP expressing strain was not used, calcofluor white (Sigma) and FM4-64 (Molecular Probes) were added at the same time as the spore inoculum on top of the corneas and incubated at 34 °C for 10 min prior to visualizing the fungal infection of the human tissue.

An artificial anterior chamber (Moria) was used for wounding the cornea by scratching it with a surgical needle. The scratching wound was comprised of 4 lines of scratches crossing each other (Fig 2.1) and each scratch was ~ 3 mm long. Th scratches were found to be 18-32 μm deep based on measurements from 3 z-stacks of confocal images of corneas (section 2.16.2; and Fig. 6.16). Hydrocortisone (Sigma) was added to culture media at a concentration of 1 μg/ml in experiments to test the effect of immunosuppression on infection.
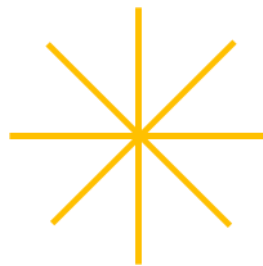
Fig. 2.1 Diagrammatic representation of the scratches made on the top of the cornea.

2.12 Homogenisation of human corneal tissue

The liquid culture media surrounding the corneal tissue was collected in 2 ml Eppendorf tubes to determine the number of colony forming units (CFUs) (see section 2.13). The surface of the corneal tissue was then washed by pipetting 1 ml of phosphate buffered saline (PBS, Life Technologies) over it and draining excess fluid to remove any non-adhered spores on the surface. The weight of each sample of corneal tissue was measured on a fine balance by placing it in a sterile plastic bag using sterile tweezers. The corneal tissue was then cut into small pieces using sterile scissors and tweezers. These corneal tissue pieces were collected in a 2 ml Eppendorf tube and immediately flash frozen in liquid nitrogen. 400 μl of PBS was added to each of the tubes and the frozen tissue was well ground using a hand held tissue homogeniser (Bennett Scientific Ltd). 1.2 ml of PBS was added to each tube after homogenisation to make up the final

volume of the homogenised suspension to 2 ml. The homogenised tissue was then stored at -20 ˚C for DNA extraction (next section).

2.13 DNA Extraction from human corneal tissue

100 μl of the frozen homogenised tissue that had been allowed to return to room temperature was used for DNA extraction. DNeasy Blood and Tissue Kit (Qiagen) was used for DNA extraction from the corneal tissues according to the manufacturer's instructions.

2.14 Determination of the colony forming unit counts

The number of CFUs of the wild type and Δ*fso* mutant strain of *F. oxysporum* were determined from: (a) *in vitro* cultures; (b) tissue homogenates of infected *ex vivo* human corneas used for qPCR; and (c) the medium surrounding the infected corneal cultures. (a), (b) and (c) were analysed 2 days post infection (dpi). Dilutions of 1 in 10, 1 in 100 and 1 in 1000 were prepared. 10 μl of each dilution was then inoculated on PDA plates (see section 2.5). The plates were incubated at 28°C and colony counts were made at intervals of 24 h from 24 h post inoculation up to 72 h post inoculation. Colony counts were done from two technical replicates and three experimental replicates for each dilution after 24, 48 and 72 h for the cultures from the tissue homogenates and from the surrounding media.

2.15 Determination of microconidial production and the viability of *F. oxysporum* strains

Microconidia harvested from cultures of the wild type and *Δfso* mutant strains of *F. oxysporum* grown in 100% PDB were freshly inoculated into 20 ml of fresh 100% PDB. A second culture of *F. oxysporum* was inoculated in 20 ml of DMEM media supplemented with 10% FCS and antibiotics (i.e. the same medium used for corneal infection assays; see section 2.11). 1×10^5 spores/ml were used as the spore concentration for inoculating both media. The PDB cultures were grown at 28°C in a shaking incubator (180 rpm) whereas the DMEM cultures were incubated at 34°C in a static CO_2 incubator. Microconidia were harvested at 48 h post inoculation and spore counts determined from each culture using a haemocytometer (see section 2.4). 1 in 10,

1 in 100 and 1 in 1000 dilutions of microconidia harvested from DMEM cultures were made and 10 µl of each of these were inoculated onto PDA media plates to determine the CFUs (see last section). The plates were incubated at 28°C and CFUs were determined at intervals of 24 h from 24 h post inoculation up to 72 h post inoculation.

The viability of microconidia of the wild type and Δ*fso* mutant strains of *F. oxysporum* were determined by inoculating 10 µl microconidial suspension at a concentration of 1 x 10^4 spores/ml onto PDA plates. The plates were incubated at 28 °C and CFUs were determined at intervals of 24 h from 24 h post inoculation up to 72 h post inoculation.

2.16 Fungal burden analysis using qPCR

The fungal burdens of the wild type and Δ*fso* mutant on the infected corneas were determined using quantitative RT-PCR. A concentration of 1 x10^7 spores/ml was used as inocula for initiating the infection and DNA was extracted from homogenised tissue at 48 hpi. Oligonucleotides used as primers for the specific identification of each strain are listed in Supplementary Table 1. The fungal burden was determined from ΔC_t values of each infected cornea after normalizing the C_t (threshold cycle) values with an internal control specific for the human tissue (which was glyceraldehyde 3-phosphate dehydrogenase). The qPCR data were analysed according to a modified nucleotide quantitation method as described and cited in O'Hanlon *et al*. (2011). The delta Ct values were calculated and adjusted with a correction factor calculated from the deviance (of spore viability counts) from the expected. The fungal burden was expressed as $\log_{10}$ of the transformed reciprocal value of the measured C_t to reflect the fact that a low C_t value reflects a high fungal burden.

A modified mathematical model (incorporating an adjustment for fungal inoculum) for the relative quantification of *six3* gene for the *F. oxysporum* wild type and glyceraldehyde 3-phosphate (GAPDH) gene for human tissue was adopted for each corneal infection sample using the formula:

$$\text{RATIO} = (E_{\text{target}})^{\Delta Ct(\text{fungal } six3 - \text{human GAPDH})}$$

where E = efficiency of amplification of target gene' based on efficiency calculations using the Ct slope method (Schmittgen and Livak, 2008). The same method was repeated for the Δ*fso* mutant with a different gene, the hph cassette marker (adapted

from an unpublished lab protocol for determining fungal burden from murine infections, Bignell, E., pers. comm.).

Table 2.4. Primers used for qPCR

Name	Sequence (5' – 3')	Sequence amplified (no, name)	Purpose	References if any
SIX3 FW	GCTGGGCTACCTGTGGAAGATG	*six3* (Secreted in xylem)	Specific identification of *F. oxysporum* f. sp. *lycopersici* wild type by qPCR	Lievens *et al*., 2009
SIX3 REV	CTAGCATAACCCAGAGGTTCGGTG	*six3* (Secreted in xylem)	Specific identification of *F. oxysporum* f. sp. *lycopersici* wild type by qPCR	Lievens *et al*., 2009
HpH FW	CTCGTCCGAGGGCAAAGGAATAG	Hygromycin cassette	Specific identification of *F. oxysporum* f. sp. *lycopersici* Δ *fso* mutant	

			by qPCR	
HpH REV	GGCACTCTTTGCTGCTTGGAC	Hygromyc in cassette	Specific identifica tion of *F. oxysporu m* f. sp. *lycopersi ci* Δ *fso* mutant by qPCR	
GAPDH FW	GAGTCAACGGATTTGGTCGT	Glyceralde hyde 3-phosphate	Specific identifica tion of human corneal tissue gene by qPCR	Joseph *et al*., 2014
GAPDH REV	TTGATTTTGGAGGGATCTCG	Glyceralde hyde 3-phosphate	Specific identifica tion of human corneal tissue gene by qPCR	Joseph *et al*., 2014

2.17 Microscopy

2.17.1 Live-cell imaging of spore germination and CAT fusion *in vitro*

Live-cell imaging of spore germination and CAT fusion was performed in 8-well cell culture chambers as described in section 2.6 was done in 8-well slides. Brightfield light microscopy and differential interference contrast (DIC) microscopy were performed using a Nikon Eclipse TE 2000E inverted microscope with a 60x/1.20 NA water immersion plan apo objective. A Hammamatsu Orca-ER CCD camera and Metamorph software (Universal imaging) was used for image acquisition. Further image analysis was done using Image J software (rsbweb.nih.gov/ij). Confocal microscopy was performed using a Leica TCS SP8 inverted microscope. LASAF software was used for image processing. The fluorescent dyes used for labelling organelles are listed in Table 2.5 and the excitation and emission peaks used for each fluorescent probe are shown in Table 2.6.

Table 2.5 Fluorescent dyes used for confocal live-cell imaging

Stain	Organelle labelled	Working concentrations	Source
Concanavalin A	cell wall	10 µg/ml, 17 µg/ml, 27 µg/ml	Sigma
Wheat germ aggluttinin	cell wall	10 µg/ml	Molecular Probes
Calcoflour white	cell wall	83 ng/ml	Sigma
cDFFDA	vacuoles	6.45 µg/ml	Sigma
Mitotracker Red	mitochondria	0.36 ng/ml	Molecular Probes
Nile red	lipid bodies	1 µg/ml	Sigma
DAPI	nuclei	0.083 ng/ml	Sigma

2.17.2 Live-cell imaging of infected *ex vivo* human cornea

Brightfield microscopy and differential interference contrast (DIC) microscopy were performed using a Nikon Eclipse TE 2000E inverted microscope with a 60x /1.20 NA water immersion plan apo objective. A Hammamatsu Orca-ER CCD camera and Metamorph software (Universal imaging) were used for image acquisition. 20 or more images were captured from each experimental treatment for CAT fusion and spore

germination assays (see section 2.6). All experiments were repeated more than three times unless and otherwise stated.

Table 2.6 Excitation and emission wavelengths used for confocal live-cell imaging with different fluorescent probes

Fluorescent probe	Excitation wavelength (nm)	Emission wavelength (nm)
GFP	488	508-551
mCherry	569	609-681
Alexafluor conjugate of Concanavalin A (Con A)	488	512-596
Alexafluor conjugate of Wheat germ agglutinin (WGA)	488	510-569
Calcofluor white (CFW)	405	424-476
cDFFDA	488	505-558
Mitotracker Red	581	622-689
Nile red	520	571-637
DAPI	405	432-462

An inverted Leica TCS SP8 Laser Scanning Confocal (Leica microsystems, www.leicamicrosystems.com) microscope was used for live-cell imaging. A 63x oil immersion objective (1.4 N.A.) and a 40x dry objective (1.10 N.A.) were used for live-cell imaging of *ex vivo* human corneal infections. 4-D imaging (XYZT) combined with the tile scan and automatic merging option was often used with the high (40x and 63x) magnification objectives to allow large fields of view to be captured at high spatial resolution. The following settings were used for collecting all the z-stacks for all quantitative measurements from *ex vivo* human cornea: 63x 1.4 NA oil immersion objective; z-stack thickness = 100 μm; number of optical sections = 201; optical section thickness = 0.50 μm; zoom factor = 1x; frame resolution = 512 x 512 pixels; scan speed = 600Hz; and pixel size = 0.891 μm.

2.18 Image analysis

Image analysis was done using the following software packages: LASAF (Leica microsystems, www.leicamicrosystems.com), Imaris (Bitplane, www.bitplane.com) and Image J (freeware from National Institutes of Health, rsbweb.nih.gov/ij).

All datasets collected for quantitative analysis were of images generated with the same settings on the confocal software (see sections 2.16.1 and 2.16.2). The depth of penetration of the corneal tissue by *Fusarium* hyphae was measured using the measurement tool in the 'Surpass module' of Imaris software. 100 μm thick z-stacks composed of 0.5 μm serial sections were analysed. Images to measure the depth of penetration were only captured from the central region of the convex cornea. The outer surface of the epithelium labelled with FM4-64 stain was used as the initial point (i.e. 0 μm) for depth measurements. This avoided the inclusion of any aerial hyphae over the surface of the cornea. An oblique slicer was placed within the stack in Imaris Surpass and the depth of penetration determined by successively moving through the different optical sections of the z-stack. The last optical section containing the hyphal profiles was taken as the end point of hyphal penetration. The depth measurements were made by using the 'Measurement tool' in Imaris (Fig. 2.2).

3D reconstructions of the volumetric data of each image stack were made using the Surpass module of Imaris (Fig. 2.3). 3D iso-surface volumes were created from single channel z-stacks of GFP labelled fungal hyphae after applying background subtraction with a filter width of 46.2 μm. All the z-stacks were processed using the same parameter settings. This was followed by the creation of iso-surface volumes using the 'iso-surface creation wizard' of Imaris Surpass. Volume data of each iso-surface were automatically calculated by the software and displayed at the end of the creation step.

Hyphal filaments were reconstructed in 3D using the 'Filament tracer' module in Imaris (Fig. 2.4). A combination of 'autopath' and 'autodepth' modes in the filament creation wizard was used. The diameter of the hyphae was set to 2 μm and filaments were created in a cylindrical form. The measurements of the hyphal branching angles (Fig. 2.5), total length of hyphae including branch lengths, and the number of hyphal tips, were exported as Excel files from Imaris. The hyphal growh units (HGU) were calculated using the following equation (Trinci, 1978):

Hyphal growth unit = Total length of hyphae/number of hyphal tips
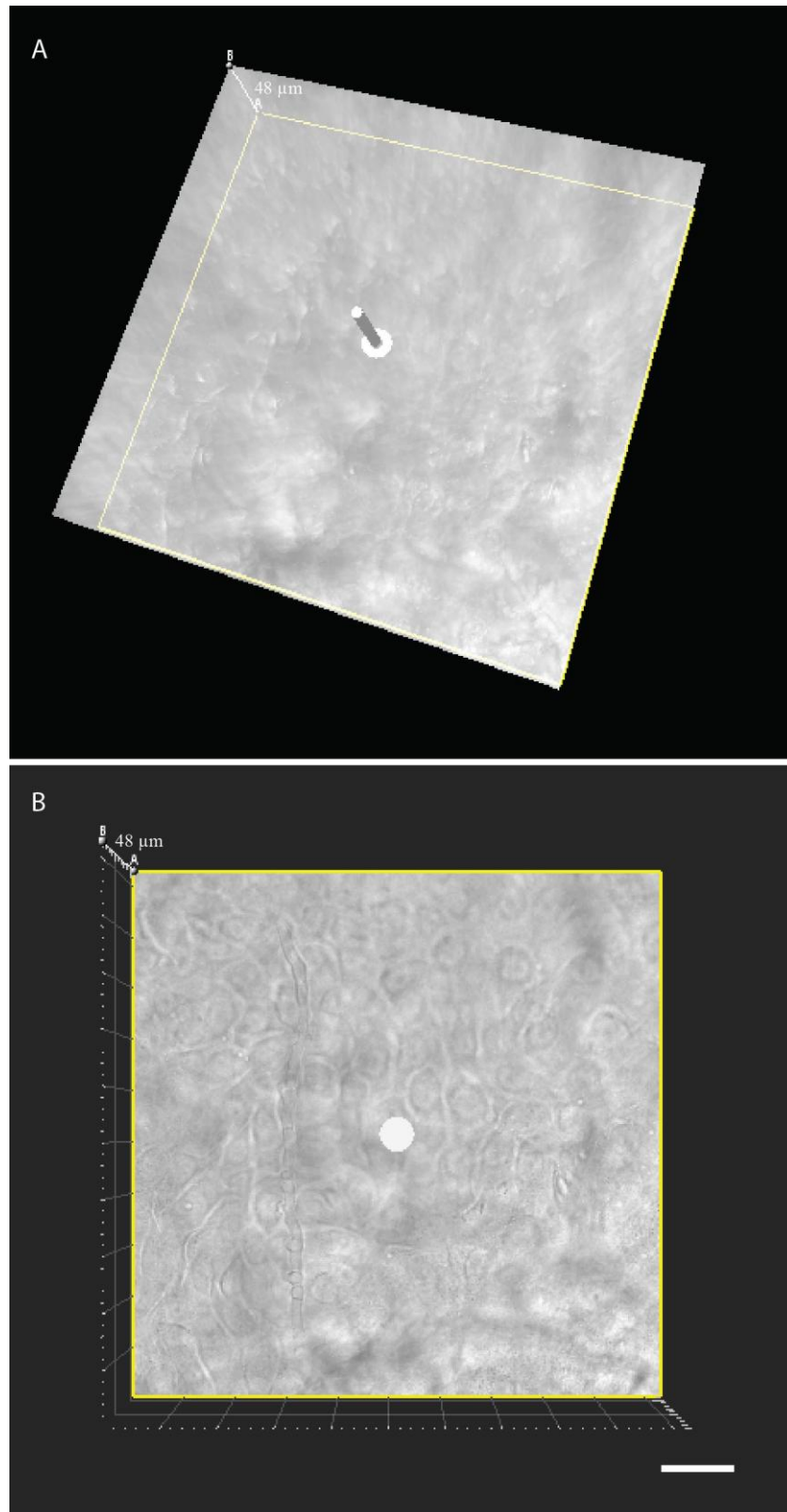
Fig. 2.2 Measurement of depth of penetration using the Imaris. **(A)** 3D volume of the z-stack with the oblique slicer inserted which allows one serial section within the stack to be rotated and imaged at any desired angle. **(B)** Visualisation from above of the same single section shown using the oblique slicer in (A). The top left hand corner of the frame in both images shows that the measured depth of the optical section is 48 μm. Scale bar = 30 μm.
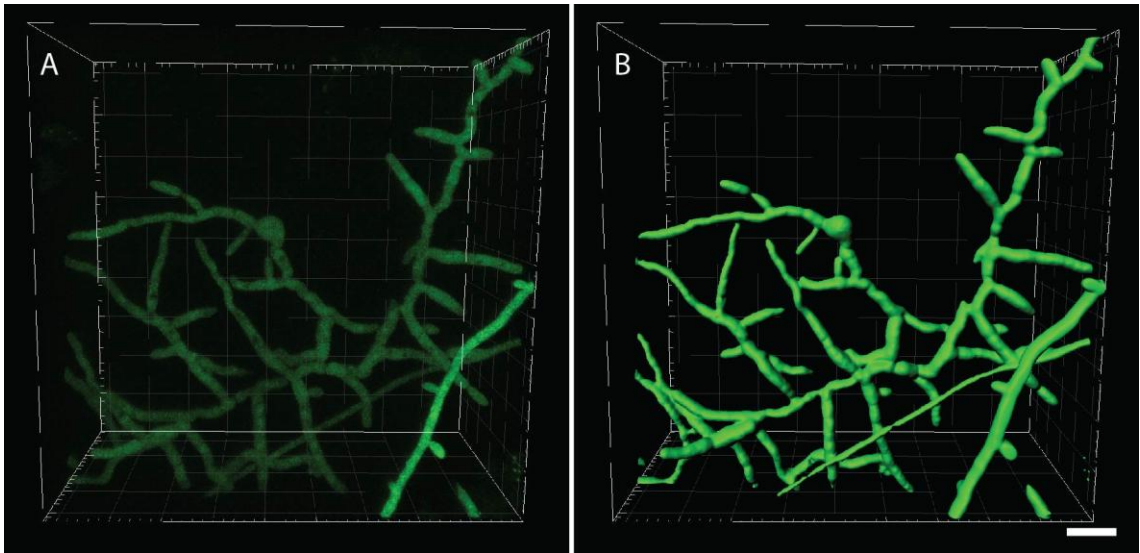
Fig. 2.3 Measurement of fungal volume in Imaris using the Surpass module. **(A)** 3D view of an z-stack. **(B)** Iso-surface volume (3D surface rendering of volume data) of the z-stack shown in (A) Scale bar = 20 μm.
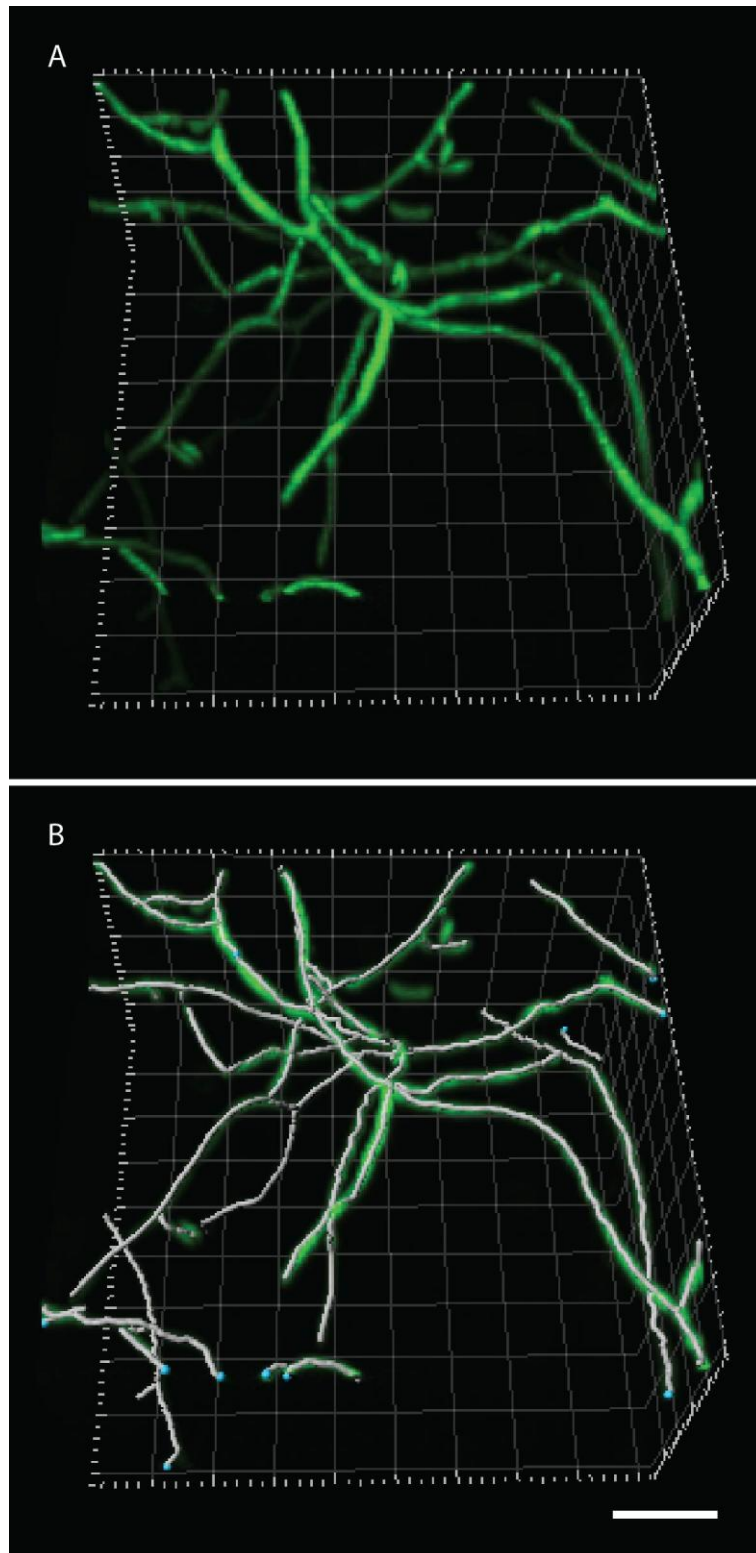
Fig. 2.4 Creation of hyphal filaments in Imaris for branch measurements. (**A**) 3D view of an z-stack. (**B**) Grey lines showing the filaments traced using the Filament tracer module in Imaris. Scale bar = 30 μm.
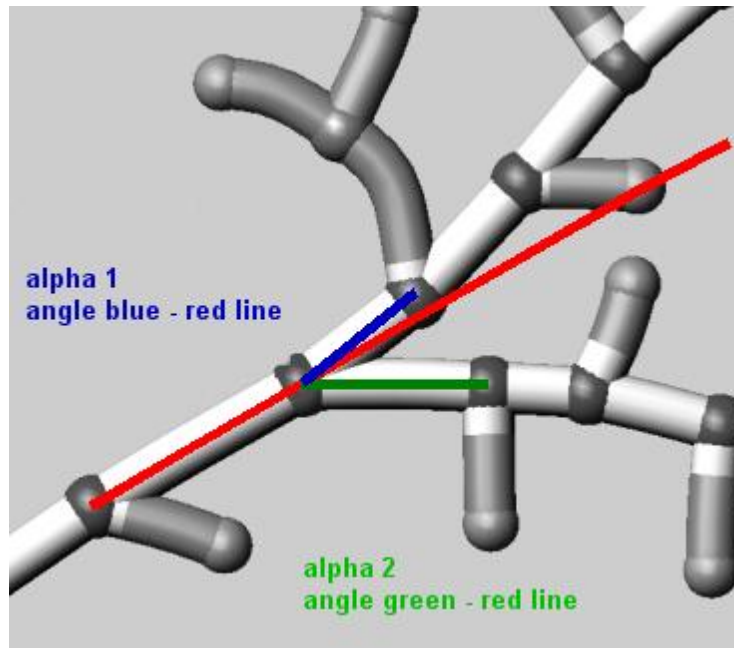
Fig. 2.5 Branch angle (α) measurements provided by Imaris from filaments created using the Filament tracer module in Imaris. Reproduced from Imaris Reference Manual (www.bitplane.com).

2.19 Statistical analyses

Graphs were plotted in Sigmaplot (Systat Software Inc, www.**sigmaplot**.co.uk) and statistical analyses of data were performed in Graphpad Prism (GraphPad Software, Inc, http://www.graphpad.com/). Error bars indicate standard deviations (SD). The significance of data were determined by determining the *p* values obtained from unpaired t-test, paired t-test, one-way ANOVA and two-way ANOVA where specified. The significance of the *p* values were determined as: **** = $p < 0.0001$, *** = $p < 0.0001$, ** = $p < 0.01$, and * = $p < 0.05$.

The statistical significance of variances between fungal burdens was calculated using a nonparametric Mann-Whitney t-test (adapted from an unpublished lab protocol for determining fungal burden from murine infections, Bignell, E., pers. comm.).

Chapter 3: Optimisation of the culture conditions for analysing CAT fusion *in vitro* in *Fusarium oxysporum*

3.1 Introduction

The conditions which induce CAT fusion *in vitro* have been shown to vary greatly in different fungi. The plant/human pathogen *Fusarium oxysporum* was previously reported to undergo fusion between microconidial germlings *in vitro* in 2% potato dextrose broth (PDB) supplemented with 20 mM glutamic acid and 0.8% agarose (Ruiz-Roldan *et al*., 2010). In the saprotrophic fungus *Neurospora crassa*, CAT fusion has been shown to be initiated rapidly, within 4 h of inoculation, in liquid Vogel's growth medium (Roca *et al*., 2005). In contrast, CAT fusion in the plant pathogen *Colletotrichum lindemuthianum* is inhibited by growth medium and only occurs in water after 72 h of inoculation (Ishikawa *et al*., 2010; Roca *et al*., 2003). A detailed analysis of the optimal conditions for promoting CAT fusion *in vitro* in *F. oxysporum f. sp. lycopersici,* the fungus used as the experimental system for my PhD research, has not been previously undertaken.

3.3   Results

3.3.1 CAT fusion was induced following cell adhesion in 1% PDB supplemented with specific nutrients/chemicals

Inoculating a rich medium (100% PDB) or a minimal liquid medium (section 2.5) failed to induce CAT fusion in *F. oxysporum* (Fig. 3.2). In contrast, CAT fusion occurred in a dilute 1% PDB supplemented with one of a number of different chemicals. In 1% PDB medium alone, the microconidia underwent adhesion-independent germination. The spores and germlings exhibited Brownian movement in the liquid medium and did not adhere to the borosilicate glass substratum of the slide culture chambers (Fig. 3.1A; Movie 3.1). However, when the 1% PDB was supplemented with one of a wide range of chemicals ($NaNO_3$, $CaCl_2$, NaCl, $MgCl_2$, KCl or monosodium salt of glutamic acid), adhesion of the germlings to the glass substrate occurred. The number of adhered microconidia and microconidial germlings increased with time from 2 to 12 h following inoculation (Figs. 3.1B and 3.3; Movies 3.2 and 3.3). After ~ 8 h of incubation spore germination was completed and ~ 80% of the spores had germinated (Fig. 3.4). After 12 h ~ 85% germlings were adhered (Fig. 3.3). In 1% PDB supplemented with $NaNO_3$ a

few microconidia started to form germ tubes before adhesion took place but most germ tubes were formed after it had occurred. Germ tube formation was initiated within 2 h post inoculation and then CAT fusion started to occurred after ~ 8 h when 80% of the microconidia had germinated (Fig. 3.4). Microconidia only produced single germ tubes (Figs. 3.1A, 3.1B). Interestingly, CAT fusion did not occur in 1% PDB in the presence NH_4NO_3 or $(NH_4)_2SO_4$ even though adhesion and 80-90% germination had occurred in each supplemented medium (Fig. 3.2). The adhesion of germlings incubated in 1% PDB supplemented with $NaNO_3$ was found to be very tenacious after incubation for 12 h because they could not be removed by adding water droplets using a pipette (Movie 3.8).
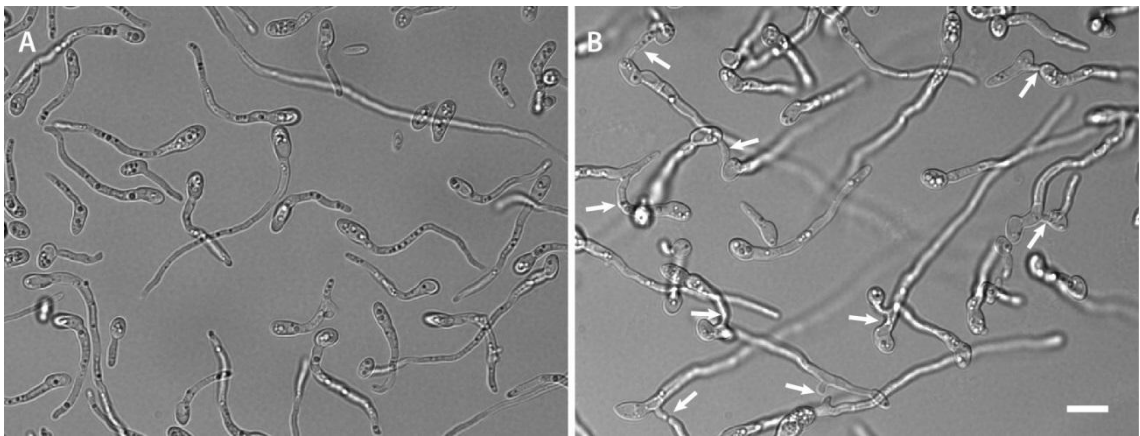
Fig. 3.1 (A) CAT fusion is not undergone by microconidial germlings in 1% PDB alone (also see Movie 3.2). **(B)** CAT fusion (arrows) occurs in 1% PDB supplemented with 25 mM $NaNO_3$ (also see Movie 3.3). Both samples were imaged 12 h post inoculation. Scale bar = 10 μm.

The amount of CAT fusion that occurred in 1% PDB supplemented with different nutrients/chemicals was different depending on the nutrient/chemical used (Fig. 3.2). 1% PDB medium supplemented with 25 mM $NaNO_3$ was selected as the medium that was routinely used for further studies of CAT fusion *in vitro* that are described in chapters 3-5. ~ 40% of CAT fusion was reproducibly obtained in this medium after 12 h of inoculation (Fig. 3.2). From the results presented in this section it was concluded that germ tube formation precedes CAT formation and that microconidial adhesion is a prerequisite for CAT formation and CAT homing leading to CAT fusion.
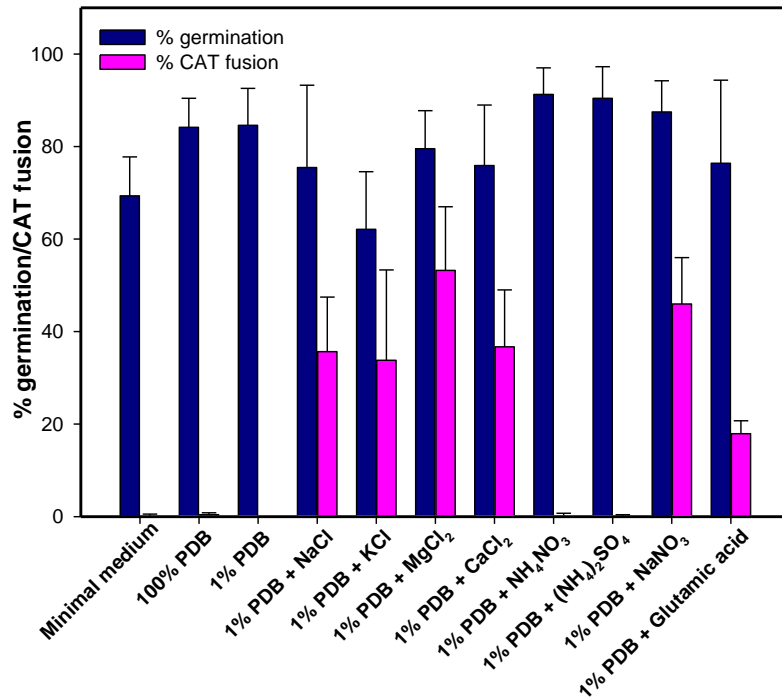
Fig. 3.2 Germination and CAT fusion of microconidia and macroconidial germlings in different media. CAT fusion was only induced in 1% PDB supplemented with various chemicals/nutrients ($NaNO_3$, $CaCl_2$, NaCl, $MgCl_2$, KCl or monosodium salt of glutamic acid).
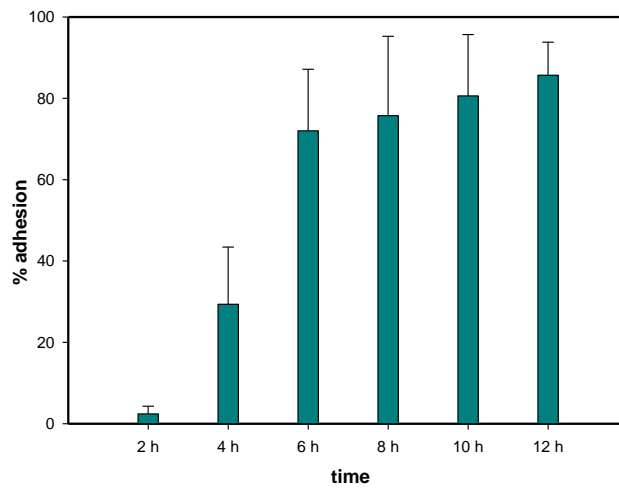
Fig. 3.3 Histogram showng the time-dependent adhesion of microconidia and microconidial germlings in 1% PDB + 25 mM $NaNO_3$.
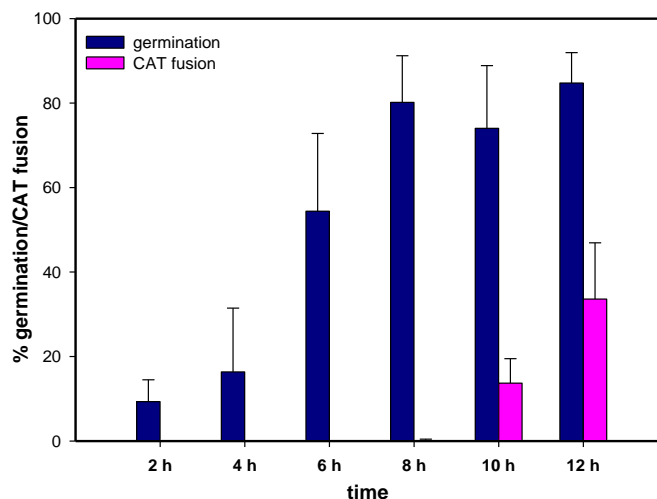
Fig. 3.4 Histogram showing the time-dependent microconidial germination and CAT fusion in 1% PDB + 25 mM NaNO$_3$.

To examine cell adhesion in more detail an experiment was performed in which microconidia were incubated in 1% PDB for 7.5 h in the slide culture chamber. At this time point most of microconidia had germinated to form germ tubes but none of the germlings had adhered to the underlying glass substratum. Two 20 µl drops of 50 µg/ml NaNO$_3$ were then added to these germlings growing in liquid growth medium to give a final concentration of ~ 25 mM NaNO$_3$ in the slide culture chamber well. Live-cell imaging showed that this addition of NaNO$_3$ resulted in the germlings becoming immediately immobilised as they adhered to the glass (Movie 3.5). Furthermore, when these germlings were incubated for an additional 4.5 h (to make the total time of incubation 12 h), significant CAT fusion had occurred between the adhered germlings. This provides further evidence that CAT fusion is dependent on cell adhesion (also see section 3.3.1)

3.3.2 Influence of incubation temperature on microconidial germination and CAT fusion

The influence of three different incubation temperatures (22°C, 25°C and 35°C) on microconidial germination and CAT fusion was assessed. Germ tube formation was only significantly inhibited at 35°C whilst CAT fusion occurred to a similar extent at each of the three temperatures tested (Fig. 3.5). As a result, all quantification of microconidial germination and CAT fusion *in vitro* were routinely performed at 25°C (section 2.6)
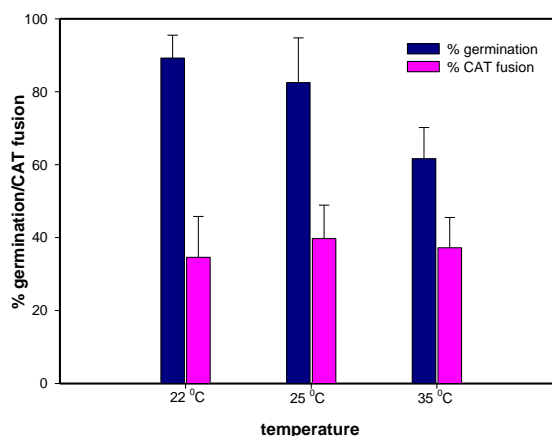
Fig. 3.5 Influence of temperature on microconidial germination and CAT fusion. With the exception of a ~15% reduction in germination at 35 °C, the three temperatures tested had no significant influence on the percentage of spore germination or CAT fusion.

3.3.3 Influence of microconidial density on germination and CAT fusion

Three different microconidial densities, 1×10^5, 1×10^6 and 5×10^6 spores per ml, in 8-well slide culture chambers were assessed for their influence on spore germination and CAT fusion. A spore density of 1×10^5 per ml was found to be optimal for spore germination and 1×10^6 spores/ml was found optimal for CAT fusion (Fig. 3.6). Since a much greater focus of my PhD research was on CAT fusion, all experiments involving the quantification of microconidial germination and CAT fusion *in vitro* were routinely performed at 25°C with 1×10^6 spores/ml (section 2.6).
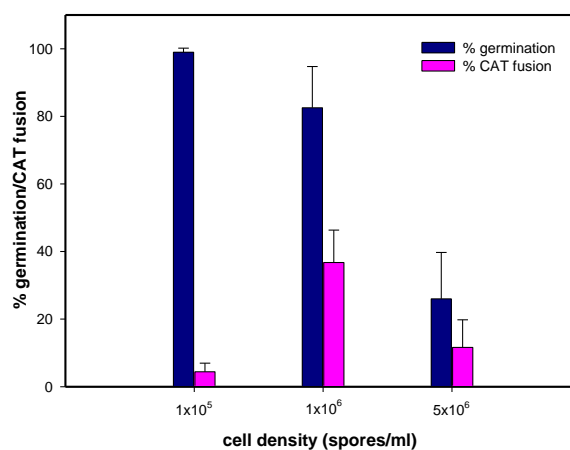
Fig. 3.6 Effect of microconidial density on germination and CAT fusion. 1 x 10^6 spores/ml provided the optimal spore for CAT fusion.

3.3.4 Influence of medium pH on microconidial germination and CAT fusion

CAT fusion was found to occur in unbuffered pH adjusted media (1% PDB + 25 mM NaNO$_3$) at a significant and similar level between pH 5 and 9 but was greatly or completely inhibited at acidic pH values of 4 or below (Fig. 3.7). Microconidial germination occurred at a similar level over a wider pH range (pH 4-7) and was greatly or completely inhibited at more acidic pH values (Fig. 3.7). The influence on spore germination and CAT fusion by buffering the media was also tested at the following pH values: 3.5, 5.1, 6.4, 7.5 and 8.3 (see section 2.9). The results from these experiments were similar results to those obtained with unbuffered media (Fig. 3.8). As a result, all experiments involving the quantification of germination and CAT fusion were routinely performed in unbuffered medium (1% PDB + 25 mM NaNO$_3$). The initial pH of this medium is ~ pH 5.5 (Fig. 3.7).

Another question that was addressed was whether the pH of the medium in which microconidia was inoculated changed after 12 h of incubation. In addition, a comparison was made of the initial and final pH values of the standard medium (1% PDB + 25 mM NaNO$_3$) with unbuffered 1% PDB with the different chemical supplements that was tested previously to determine whether they induced CAT fusion (Fig. 3.2). This experiment showed that there were significant differences in the pH values of some of the media at the beginning and end of the 12 h period of incubation (Fig. 3.9). As controls, the same experiment was repeated in the absence of fungal cells (Fig. 3.10). From the data presented in Figs. 3.9 and 3.10 it was possible to plot the data to show how much the pH changed in each of the different media tested either in the presence of fungal cells or not after 12 h of incubation (Fig. 3.11). These results showed that after incubation in the presence of the fungal cells for 12 h, the pH values of the media were all increased except those supplemented with NH$_4$NO$_3$ or (NH$_4$)$_2$SO$_4$ which became more acidic. Interestingly, the standard medium (1% PDB + 25 mM NaNO$_3$) routinely used in my experiments increased the pH the most of all the media tested (from pH 5.5 to 6.5) but still left the medium slightly acidic after 12 h (Fig. 3.9). The final pH values of media supplemented with NH$_4$NO$_3$ or (NH$_4$)$_2$SO$_4$, respectively, were both below pH 4 after 12 h incubation (Fig. 3.9). This correlated with the absence of

CAT fusion previously observed in these media (Fig. 3.2) and in the standard medium (1% PDB + 25 mM NaNO$_3$) in which the pH had been adjusted below pH 4 (Fig. 3.8).
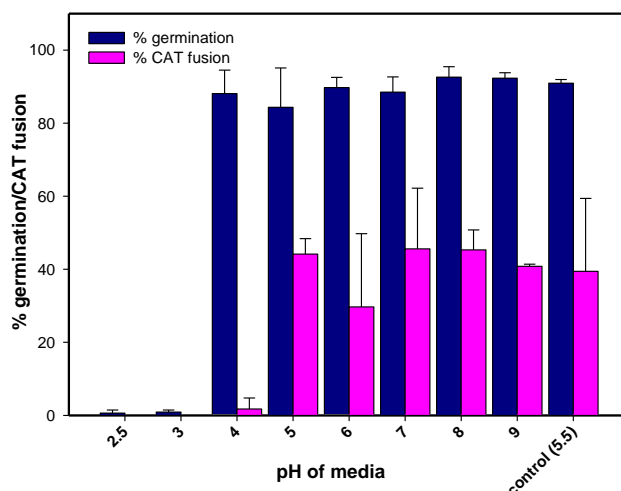
Fig. 3.7 Influence of pH on microconidial germination and CAT fusion at 12 h post inoculation in unbuffered media (1% PDB + 25 mM NaNO$_3$) that had had their pH adjusted to different pH values. The control represents the medium in which the pH has not been adjusted.
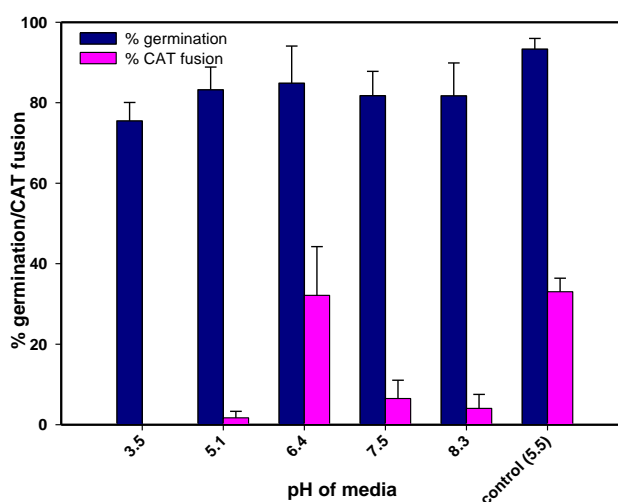
Fig. 3.8 Influence of pH on microconidial germination and CAT fusion at 12 h post inoculation in buffered media (1% PDB + 25 mM NaNO$_3$). The control represents the medium in which the pH has not been adjusted.
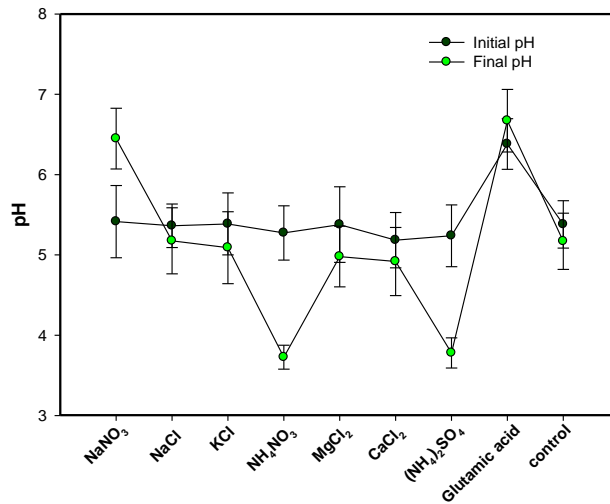
Fig. 3.9 Initial and final pH of unbuffered 1% PDB media with different supplements that promote CAT fusion. These media were each inoculated with 1×10^6 spores/ml and incubated for 12 h. The control is medium lacking any supplements.
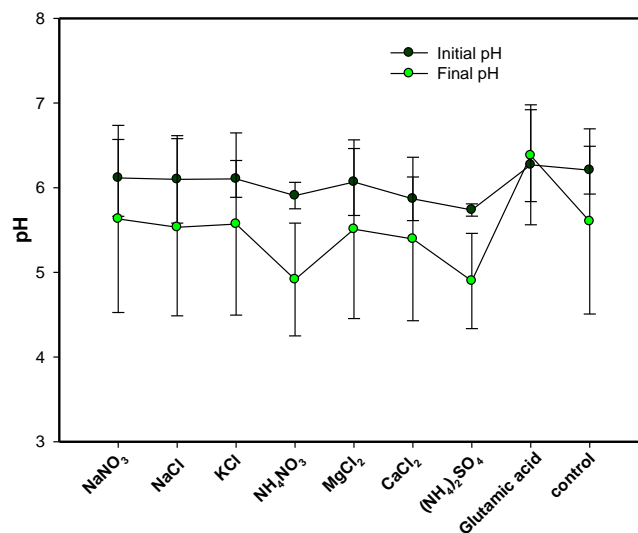
Fig. 3.10 Initial and final pH of buffered 1% PDB media with different supplements that were incubated in the absence of fungal cells for 12 h. The control is medium lacking any supplements.
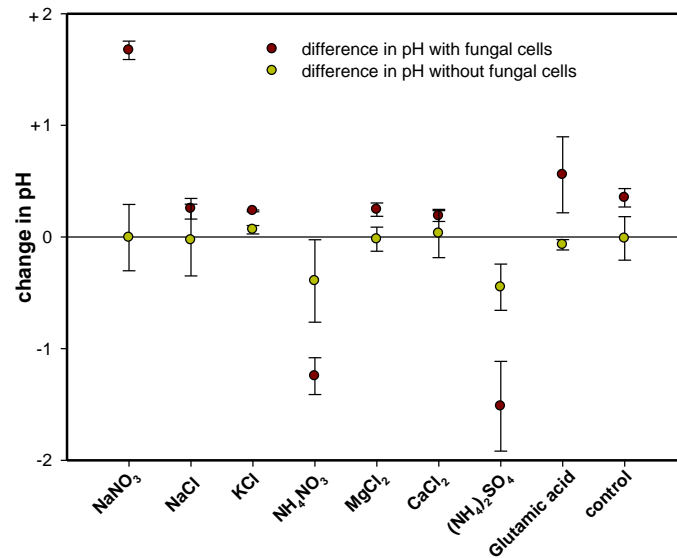
Fig. 3.11 Change in pH values of media with different nutrients after 12 h of incubation in the presence and absence of fungal cells. The results shown in this Figure are plotted from data shown in Figs. 3.9 and 3.10. The control is medium lacking any supplement.

3.3.5 Influence of oxidative stress and human serum on CAT fusion

To test whether CAT fusion is a general stress response to adverse conditions, the influence of oxidative stress on CAT fusion was tested. In addition, the influence of human serum on CAT fusion was also tested because of its potential relevance to infection of the human host by *F. oxysporum*.

Oxidative stress was applied by supplementing 1% PDB with H_2O_2. A very low concentration (0.001%) of H_2O_2 in 1% PDB was found to not influence the level of germ tube formation but it failed to induce spore adhesion or CAT fusion (Fig. 3.11). Increasing the amount of H_2O_2 in the PDB to 0.003% reduced germ tube formation by ~ 50% and 0.005% H_2O_2 reduced germ tube formation by ~ 75%. However, none of these concentrations of H_2O_2 induced spore adhesion or CAT fusion (Fig. 3.12; Movie 3.6).
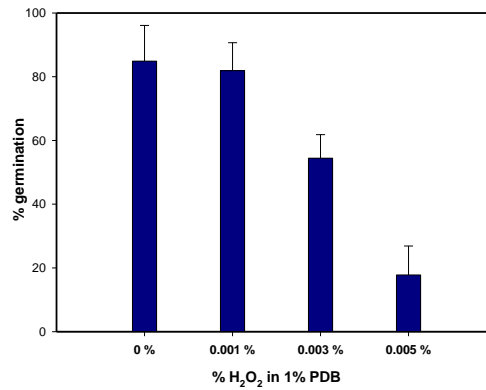
Fig. 3.12 Oxidative stress applied by supplementing 1% PDB with different concentrations of H$_2$O$_2$ inhibited germination (germ tube formation) but did not induce spore adhesion or CAT fusion.
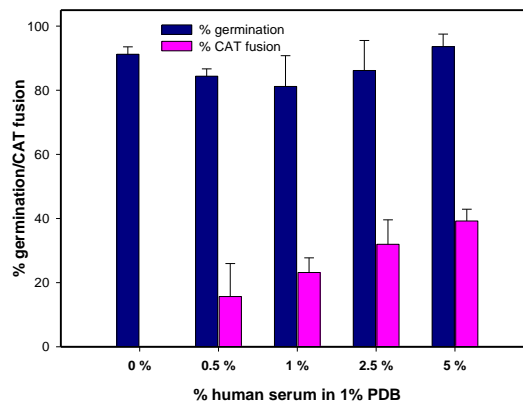
Fig. 3.14 1% PDB supplemented with human serum induced CAT fusion in a dose dependent manner.

In contrast to the negative result obtained with oxidative stress, 1% PDB supplemented with 0.5-5.0% human serum (AB type) did induce CAT fusion in a dose dependent manner (Fig. 3.14, Movie 3.8).

3.4 Discussion

As a result of the research described in this chapter, an optimal set of conditions for promoting CAT fusion *in vitro* in *F. oxysporum f. sp. Lycopersici* was also determined. From these studies, the standard growth medium and culture conditions selected for routine quantitative analyses and live-cell imaging of spore germination and CAT fusion in 8-well slide culture chambers were: unbuffered 1% PDB supplemented with 25 mM NaNO$_3$ that was inoculated with 1 x 10^6 spores/ml and incubated at 25°C for 12 h in continuous light (section 2.6). This medium and culture conditions reproducibly resulted

in ~ 40% of the germlings undergoing CAT fusion. In addition, there was a significant period between the initiation of microconidial germination (after 1-2 h) and CAT fusion (after 8 h). This contrasts markedly with *N. crassa* in which macroconidial germination and CAT fusion were initiated at approximately the same time (after 3-4 h, Roca *et al.*, 2005b).

In the experiments described in this chapter I also made some important observations relating to: spore and germling adhesion; the dependence of CAT fusion on cell adhesion to the substratum; the time course of spore germination and CAT fusion; the influence of the medium pH on spore germination and CAT fusion; CAT fusion not being a stress response; and the induction of CAT fusion by human serum. These observations are discussed in more detail in the sections 3.4.1-3.4.3 below.

3.4.1 Spore and germling adhesion

Microconidia and microconidial germlings were found not to undergo adhesion to the borosilicate glass substratum of the slide culture chamber when incubated in 1% PDB alone. However, when 1% PDB was supplemented with one of a diverse range of chemicals ($NaNO_3$, $CaCl_2$, NaCl, $MgCl_2$, KCl, the monosodium salt of glutamic acid), cell adhesion occurred. Time-courses generated from live-cell imaging showed that non-adhered microconidia or microconidial germlings of *F. oxysporum* exhibited Brownian movement in liquid media and were readily distinguished from adhered microconidia and microconidial germlings that were immobilised on the substratum surface (Movies 3.1 and 3.2), as has also been reported for non-adhered and adhered conidia of *Phyllosticta ampelicida* (Kuo and Hoch, 1996). After 6 h period of incubation only a minority of ungerminated spores had adhered. A time course between 6 and 10.5 h showed more and more spores undergoing adhesion, germination to form single germ tubes and finally CAT fusion (Movie 3.2). A few of the spores already had a short germ tube prior to adhesion. However, all of the germlings in 1% PDB supplemented with $NaNO_3$ had adhered by 12 h of incubation (Movie 3.3). Washing the glass substratum with drops of water did not detach adhered spores or germlings confirming their firm attachment to the glass. When drops of 50 µg/ml $NaNO_3$ were added to non-adhered germlings that had been previously incubated for 7.5 h in 1% PDB alone, all of the germlings immediately underwent adhesion (Movie 3.5). These results suggest that the surface properties of the microconidia and germlings at 7.5 h are different from freshly harvested microconidia because the latter did not adhere to the glass as soon as they

were used to inoculate 1% PDB supplemented with $NaNO_3$. It thus seems that competency of the spores/germlings to interact with $NaNO_3$ to facilitate cell adhesion gradually increases with time and by 7.5 h they are full competent to adhere. How $NaNO_3$ (and also the diverse range of other chemicals) induce cell adhesion in 1% PDB, is unclear. In the case of $NaNO_3$, adhesion cannot result from this chemical having a nutritional role in bringing about adhesion because it occurs so rapidly. Perhaps $NaNO_3$ and the other chemicals play a critical role in influencing the charge properties of the surfaces of some of the spores and all of the germlings causing them to become instantly adhesive to the glass substratum.

Production of an extracellular matrix outside the fungal cell wall has been found to be important for the adhesion of spores and spore germlings in many plant pathogenic fungi (e.g. Kwon and Epstein, 1993; Apoga *et al.*, 2001; Tucker and Talbot, 2001). Macroconidia of *F. solani,* in the presence of PDB, are induced to produce mucilage at their tips (the so-called 'spore tip mucilage' or STM) allowing them to adhere to a polystyrene surface. This STM was found to contain glycoproteins and α-mannans/α-glucans, and adhesion by the STM was blocked by adding the α-mannan/α-glucan binding lectin, concanavalin A (ConA) (Kwon and Epstein, 1993). It was found that STM was not associated with microconidia by staining with fluorescently labelled ConA, although α-mannans was localized on the surfaces of microconidia and germ tubes (Fig. 4.3). Similar results have also been shown by Schoffelmeer *et al.* (1999). The outer layer of fungal cell walls in general commonly contain an outer layer rich in α-mannans and these are often components of glycoproteins that play roles in fungal cell adhesion (Bowman and Free, 2006; Latgé, 2007; Osherov & Yarden, 2010). However, it is unlikely that α-mannans play a role in the adhesion of *F. oxysporum* germlings because it was found that the addition of 27 μg/ml Con A did not inhibit their adhesion in 1% PDB supplemented with $NaNO_3$ (data not shown).

Hydrophobic interactions between the cell and substratum surface have been shown to play roles in fungal cell adhesion. Notably, hydrophobin proteins present on the surface of the cell wall, such as MPG1 and SC3, have been found to have a role in cell adhesion to hydrophobic surfaces (Talbot *et al.,* 1993; Wosten *et al.*, 1994). However, similar evidence for hydrophobin proteins playing a role in cell adhesion in *Fusarium spp* is not known.

Evidence has been obtained that intracellular MAP kinase signalling may play a role in cell adhesion in *F. oxysporum* because a mutant defective in the *F. oxysporum* MAP kinase 1 gene, *fmk1* was shown to exhibit impaired microconidial germling attachment to tomato root surfaces (Di Pietro *et al*., 2001).

Overall, it is clear that the mechanistic basis of adhesion by microconidial germlings of *Fusarium spp.* is poorly understood and requires further study.

3.4.2 Influence of external conditions on germ tube formation and CAT fusion *in vitro*

Spore germination *in vitro* is influenced by a variety of environmental factors, including the presence of other spores, An appropriate combination of external conditions are important for the successful colonisation of a host by a fungal pathogen *in vivo*. External conditions also influence CAT fusion and in this chapter it has been shown that some of the optimal external conditions for CAT fusion are not optimal for germ tube formation. The influence of the following range of external factors were investigated *in vitro* in order to optimise the culture conditions for quantitative analyses and live-cell imaging of spore germination and CAT fusion for the experiments described in chapters 3-5: nutrients; substratum adhesion; temperature; spore density; pH; oxidative stress; and human serum.

Microconidia were found to germinate well in either 100% PDB or minimal medium but CAT fusion was absent. Previously, conidial germling fusion in *F. oxysporum* had been reported to undergo fusion in much more dilute PDB (2%) supplemented with 20 mM glutamic acid and 0.8 % agarose (Ruiz-Roldan *et al*., 2010). Diluted PDB (1%) supplemented with one of a range of supplements, including glutamic acid (see discussion in previous section) was hence used and found that CAT fusion reproducibly occurred at ~ 40%. Previously, it has been reported that CAT fusion was inhibited in 100% PDB in *N. crassa* and evidence was obtained that tryptophan played a role in this inhibition (Fischer-Harman *et al*., 2012).

Of particular interest for my analyses of CAT fusion, was the strong evidence that was obtained for microconidial germling adhesion to a substratum (borosilicate glass) being a requirement for CAT fusion to occur. CAT fusion on the glass surface was only observed between germlings in 1% PDB supplemented with $NaNO_3$, $CaCl_2$, NaCl, $MgCl_2$, KCl or glutamic acid. However, CAT fusion was not observed when 1% PDB

was supplemented with NH_4NO_3 or $(NH_4)_2SO_4$, even though the germlings adhered to the glass. A likely reason for this is that the media containing either of these ammonium salts were too acidic, each having an initial pH of ~ 4.0 (Fig. 3.9), which is not conducive for CAT fusion (Fig. 3.7). No previous studies have provided evidence for cell adhesion being a requirement for CAT fusion in any other fungal species, including *N. crassa*.

The influence of three different incubation temperatures (22°C, 25°C and 35°C) on microconidial germination and CAT fusion was assessed. Germ tube formation was only significantly inhibited at 35°C whilst CAT fusion occurred at a similar level at all three temperatures. Different optimal temperatures for different physiological or developmental processes have been previously reported for *Fusarium spp*. For example, Gupta *et al*. (2010) found that while 28°C was best for colony growth, optimal sporulation occurred at 34°C in *F. oxysporum* f. sp. *psidii* and *F. solani*. A high temperature of 35°C was found to inhibit the growth of *F. graminearum* and *F. culmorum* on synthetic and corn meal agar media at high water potential (Cook and Christen, 1976; Popovski and Celar 2013). Landa *et al.* (2001) reported that *Fusarium* wilt of chickpea was most severe at 25°C compared to 20°C and 30°C.

It was found that the inoculum density of microconidia influenced the percentage of spore germination and CAT fusion. A high microconidial density of 5×10^6 spores per ml had an inhibitory effect on germ tube formation and CAT fusion. The autoinhibition of spore germination in *F. oxysporum* at high spore densities has been previously reported (Garret and Robinson, 1969; Woltz and Jones, 1971) and the germination self-inhibitor was identified as nonanoic acid (Garret and Robinson, 1969). Autoinhibition of spore germination has been described in a number of fungal species in which a range of different germination self-inhibitors have been identified (Ugalde *et al*., 2014). It was found that 1×10^6 microconidia per ml was optimal for CAT fusion in *F. oxysporum*. This is the same as the macroconidial density which has been reported to be optimal for CAT fusion in *N. crassa* (Roca *et al*., 2005). In the latter study, evidence was presented that CAT formation may exhibit a form of quorum-sensing behaviour (i.e. involving a mechanism in which cells monitor their population density by releasing signaling molecules into the environment). The CAT inducer in *N. crassa*, however, has not yet been identified (Read *et al.,* 2012). However, the reduced cell fusion that was observed at a low concentration of microconidia (1×10^5 spores/ml) is also likely to be due to the increased spatial distance between spores/germlings producing CATs. The analysis of

15 different time-courses of CAT induction, homing and fusion, in which 1 x 10^6 microconidia had been used, showed that the maximum distance between germlings that underwent positive CAT tropisms towards was ~ 8 μm (section 4.3.1). In *N. crassa*, the greatest distance that CAT homing was found to be initiated was when germlings were less than ~15 μm (Fleiβner *et al*., 2009).

My results showed that microconidial germination in unbuffered media occurred at a similar level between pH 4 and 7 whilst CAT fusion occurred at a similar level between pH 5 and 9. Both processes were greatly or completely inhibited at acidic pH values of 4 or below. It was also shown in each of the unbuffered growth media in which CAT fusion was induced that the pH increased by up to 1 pH unit but still remained acidic over the 12 h incubation period. When buffered media was used, CAT fusion was maximal at pH 5.5 (control) and 6.3 whilst spore germination occurred at a high level from pH 3.5-8.3. In *N. crassa,* CAT fusion was found to be optimal in buffered media at pH 5 and 6 (Fischer-Harman *et al*., 2012), which was similar to my results obtained with buffered media. The external pH has been previously shown to influence spore germination, hyphal growth and sporulation in *Fusarium spp*. but the optimal pH values for these processes vary depending on the process and the species or species isolate of *Fusarium* analysed (Gupta *et al*., 2010; Joshi *et al*., 2013; Peng *et al*., 1999; Wheeler *et al*., 1991). Peng *et al*. (1999) found that chlamydospore germination by *Fusarium oxysporum* f. sp. *cubense* was highest at pH 8, which correlated with the soil pH at which infection resulting from chlamydospore germination was most severe. In *Fusarium oxysporum* f. sp. *psidii* and *F. solani*, maximal mycelial growth was reported to occur at pH 5.5 whilst pH 6.5 was found to be most optimal for sporulation (Gupta *et al*., 2010).

In fungi, a conserved regulatory pathway governs the pH-dependent expression of secreted proteins and adaptation to alkaline stress. This environmental adaptation mechanism operates via PacC/Rim101 transcription factors (Penalva *et al*., 2008). *Fusarium oxysporum* has a PacC orthologue, which negatively and positively regulates specific genes under acidic and alkaline conditions, respectively (Caracuel *et al*., 2003b). To my knowledge, it is not known whether PacC influences the pH-dependence of CAT fusion in *F. oxysporum.*

It was hypothesized that CAT fusion might be a response to stress conditions and tested this by incubating macroconidia in 1% PDB and exposing them to oxidative stress (by

the addition of 0.001-0.005% H_2O_2). CAT fusion was not induced under oxidative stress condition although germ tube formation was not prevented. Thus it was concluded that CAT fusion could not be induced by oxidative stress under these conditions. With regard to oxidative stress, it was found that 0.003% H_2O_2 (0.9 mM) or higher inhibited germination. This concurred with a previous report that that 1.6 mM H_2O_2 inhibited microconidial germination in *F. oxysporum* (Nagygyorgy *et al*. (2014).

Because of its potential relevance to infection of the human host by *F. oxysporum*, the influence of human serum was also tested on CAT fusion by incubating microconidia in 1% PDB supplemented with different concentrations of human serum. I observed that there was a dose-dependent increase in CAT fusion reaching ~ 40% CAT fusion in the presence of 5% human serum. Human serum is a complex mixture of a variety of components (Table 3.1) of which one or more may be responsible for inducing CAT fusion, including promoting germling adhesion prior to CAT fusion. Which of these components are important for inducing CAT fusion in *F. oxysporum* will require future analysis.

Table 3.1. Constituents of human serum (reproduced from www.mpbio.com)

glucose	97 mg/dl
sodium	144 mg/l
potassium	4.2 mg/l
chloride	119 mg/l
calcium	10.4 mg/dl
phosphorus	3.4 mg/dl
albumin	3.6 g/dl
total Bilirubin	0.4 mg/dl
cholesterol	178 mg/dl
triglycerides	97 mg/dl

3.5 Summary

- The optimal growth medium and culture conditions selected for routine quantitative analyses and live-cell imaging of spore germination and CAT fusion in 8-well slide culture chambers were: unbuffered 1% PDB supplemented with 25 mM $NaNO_3$ that was inoculated with 1×10^6 spores/ml and incubated at $25^{\circ}C$ for 12 h in continuous light

- Microconidial or microconidial adhesion is absent in 1% PDB but cell adhesion is promoted in 1% PDB supplemented with one of a diverse range of chemicals ($NaNO_3$, $CaCl_2$, NaCl, $MgCl_2$, KCl, the monosodium salt of glutamic acid, NH_4NO_3 or $(NH_4)_2SO_4$)

- CAT fusion only occurs following cell adhesion in 1% PDB supplemented with the all of the chemicals above unless the pH of the medium was < pH 4 (in the case of the NH_4NO_3 or $(NH_4)_2SO_4$ supplements), which was too acidic for CAT fusion to occur.

- CAT fusion was unaffected by temperature in the range of $22\text{-}35^{\circ}C$ whilst spore germination was partially inhibited at $35^{\circ}C$.

- CAT fusion was optimal at pH 5.5-6.4, but spore germination was little affected from pH 3.5-8.3, in buffered media

- CAT fusion was not induced by oxidative stress.

- Human serum induced CAT fusion when it was used to supplement 1% PDB.

Chapter 4: Live-cell imaging of CAT fusion *in vitro* in *Fusarium oxysporum*

4.1 Introduction

A detailed understanding of the cellular and subcellular dynamics of CAT fusion requires analysing this process by live-cell imaging. A detailed cytological analysis of CAT fusion, involving extensive live-cell imaging, has been done in *Neurospora crassa* in which it has been shown to involve three different stages: CAT formation, homing and fusion (Roca *et al*., 2005b; Read *et al*., 2012). CAT fusion in *N. crassa* has also been shown to create cytoplasmic continuity between fused germlings, which facilitates the movement of nuclei between them (Roca *et al*., 2005a). Surprisingly, this migration of nuclei in *N. crassa* was found to occur in the absence of the microtubule cytoskeleton. Furthermore, microtubules were shown not to be required for CAT induction, homing or fusion. In contrast, however, the F-actin cytoskeleton was found to play important roles in all three of these processes. Germ tube formation, on the other hand, was dependent on both microtubules and F-actin (Roca *et al*., 2010).

Comparative genome analysis following the sequencing of the *F. oxysporum* genome revealed the presence of supernumerary chromosomes which were hypothesised to be acquired by means of horizontal gene/chromosome transfer (HGT/HCT) events during evolution. These supernumerary chromosomes were shown to possess pathogenicity traits that were transferred between different strains of *F. oxysporum* (Ma *et al*., 2010). Recently, core chromosomes of *F. oxysporum* were also shown to be transferred between different sub-species of *F. oxysporum* (Vlaardingerbroek *et al*., 2016).

In the plant pathogen *Colletotrichum lindemuthianum*, CAT fusion was shown to facilitate the movement of nuclei between vegetatively incompatible strains. The results from this study indicated that vegetative incompatibility was supressed at early stages of colony initiation when CAT fusion occurred but was not suppressed in mature colonies in which heterokaryotic cells formed by cell fusion died (Ishikawa *et al*., 2012). CAT fusion has been hypothesised to facilitate HGT/HCT in plant pathogens (Sanders, 2006; Mehrabi *et al*., 2011; Ishikawa *et al*., 2012), including in *F. oxysporum* (Vlaardingerbroek *et al*., 2016). In a study by Ruiz-Roldan *et al*. (2010), CAT fusion was shown to facilitate the migration of nuclei between vegetatively compatible

germlings of the same wild type strain of *F. oxysporum* in which nuclei of the 'donor' germling were labelled with a different fluorescent marker to that of the 'host' germling. This migration was shown to be followed by degradation of the resident nucleus within the host germling cell that had received the nucleus from the donor germling cell.

A detailed cytological analysis of the process of CAT fusion by live-cell imaging is lacking in *F. oxysporum*. The results from this analysis will be critically important in order to determine whether this process plays a key role in facilitating HGT/HCT in this important pathogen.

4.3 Results

4.4 4.3.1 Stages of development from spore germination leading to CAT fusion by live-cell imaging

The three basic stages of CAT fusion (CAT formation, homing and fusion) described in *N. crassa* (Roca *et al*, 2005) were also observed in *F. oxysporum* in the liquid growth medium (1% PDB supplemented with 25 mM NaNO$_3$). The three stages are illustrated in Fig. 4.1 and Movie 4.1. In this time course, at the 0 min time point, a small projection from the side of the tip of the lower germ tube and a smaller projection from the tip of the upper germ tube can be seen to have formed. The two incipient CATs grew towards each other (0 to 53 min), the tips of the CATs attached (53 min) and finally the intervening cell walls of the two CATs degraded providing cytoplasmic continuity between the two germlings (54.0-54.5 min). In Movie 4.1, it is possible to see that refractile structures (later identified as lipid droplets – see section 4.12) move through the fused CATs from one germling to the other. The time for the whole process of CAT fusion to occur from the initial appearance of the CAT projections to the completion of fusion was determined from the analysis of 15 movies and varied between 42 min and 168 min (Table 4.1). A scatterplot was generated to determine if the distance between germlings correlated with the time taken for completion of CAT fusion; this scatterplot clearly showed that there was no correlation between these two parameters (Fig 4.2). Unequal growth was observed between the two CATs in nine of these time courses resulting in one CAT grew longer than the other. In six examples the two CATs were of approximately equal length. The initial distance between the spores/germlings that ultimately fused varied between 0 μm, when the fusing cells were immediately adjacent to each other, and ~ 8 μm (Table 4.1, Fig 4.2). In three instances, it was observed that

germlings initially touching each other became displaced as one or both CATs grew between the cells resulting in the germlings being pushed apart. Although it was not possible to visualise in this time-course, cytoplasmic continuity between the two germlings was probably achieved at some point during this germling displacement process (Movie 4.2).
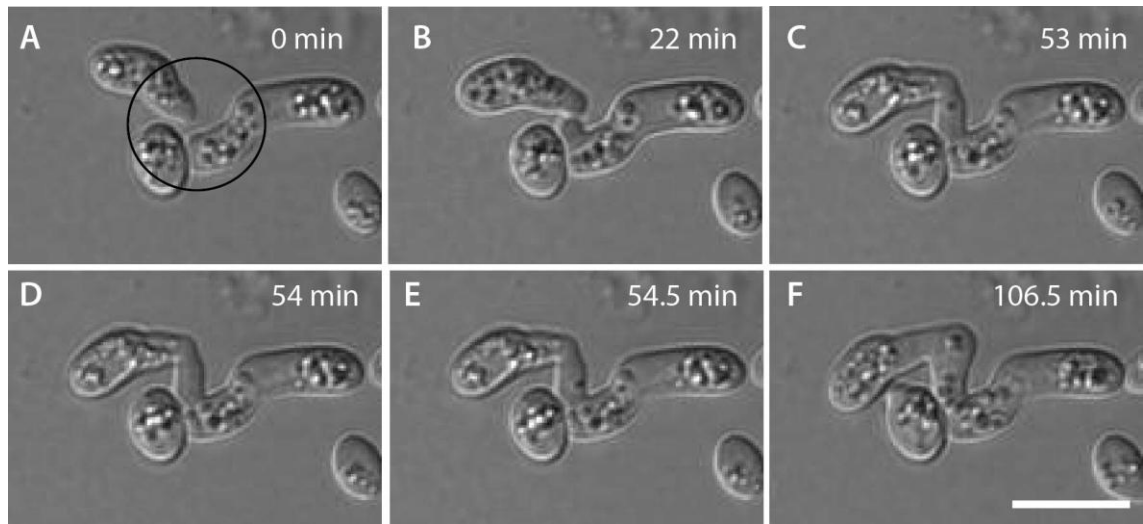
Fig. 4.1 Three stages of CAT fusion in *F. oxysporum*: CAT formation, CAT homing and CAT fusion. **(A)** CAT formation indicated by the formation of cell projections (circle) from the tip and side of two germ tubes (at 0 min). **(B)** CAT homing where the two cell projections (CATs) grow towards each other (at 22 min). **(C-F)** CAT fusion where the CATs attach and the cell walls in between break down establishing a cytoplasmic connection between the two germlings (53 min to 106.5 min). Scale bar = 10 μm.

Table 4.1. Distances between germlings undergoing CAT fusion that were monitored in individual time courses through the whole process from CAT initiation to CAT fusion (this data is also represented as a scatterplot in Fig. 4.2).

No.	Distances between germlings (μm)	Time (min)
1	7.9	168
2	1.1	147
3	0	41
4	2.2	121
5	4.6	42
6	3.2	86
7	3.0	90.5
8	0	58.5
9	2.0	118.5
10	0	115
11	2.8	118.5
12	2.4	77.5
13	1.4	50
14	0.6	67
15	6.1	78
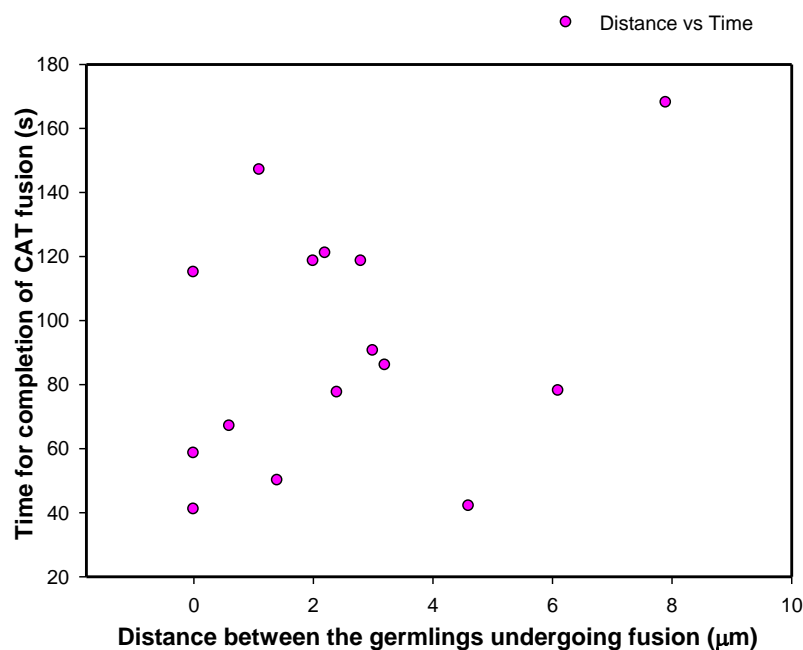
Fig 4.2 A scatterplot of the data presented in Table 4.1.

4.3.2 Morphological features of CAT fusion

CAT fusion can occur in a wide range of different ways and always involved the positive tropism of CATs towards each other (Figs. 4.1 and 4.3). The different types CAT fusion that occurred can be broadly described as between: two germ tubes; two

ungerminated spores; or between a germ tube and a non-germinated spore. Sometimes CAT fusion could be observed between cells that were immediately adjacent to each other (e.g. Movie 4.2). CAT fusion resulted from tip-to-tip fusion of CATs formed from growing germ tubes, tip-to-tip fusion between spores, tip-to-side fusion of CATs formed from a growing germ tube to a spore, and side-to-side fusion of CATs formed from adjacent germ tubes (Fig 4.3).

A morphological feature that allowed CATs to be distinguished from germ tubes in *N. crassa* were their difference in widths (Roca *et al*., 2005b). CATs were mostly thinner than germ tubes, the average width being 1.73 ± 0.52 µm (n = 100). The average width of germ tubes was 2.45 ± 0.45 µm (n = 100).
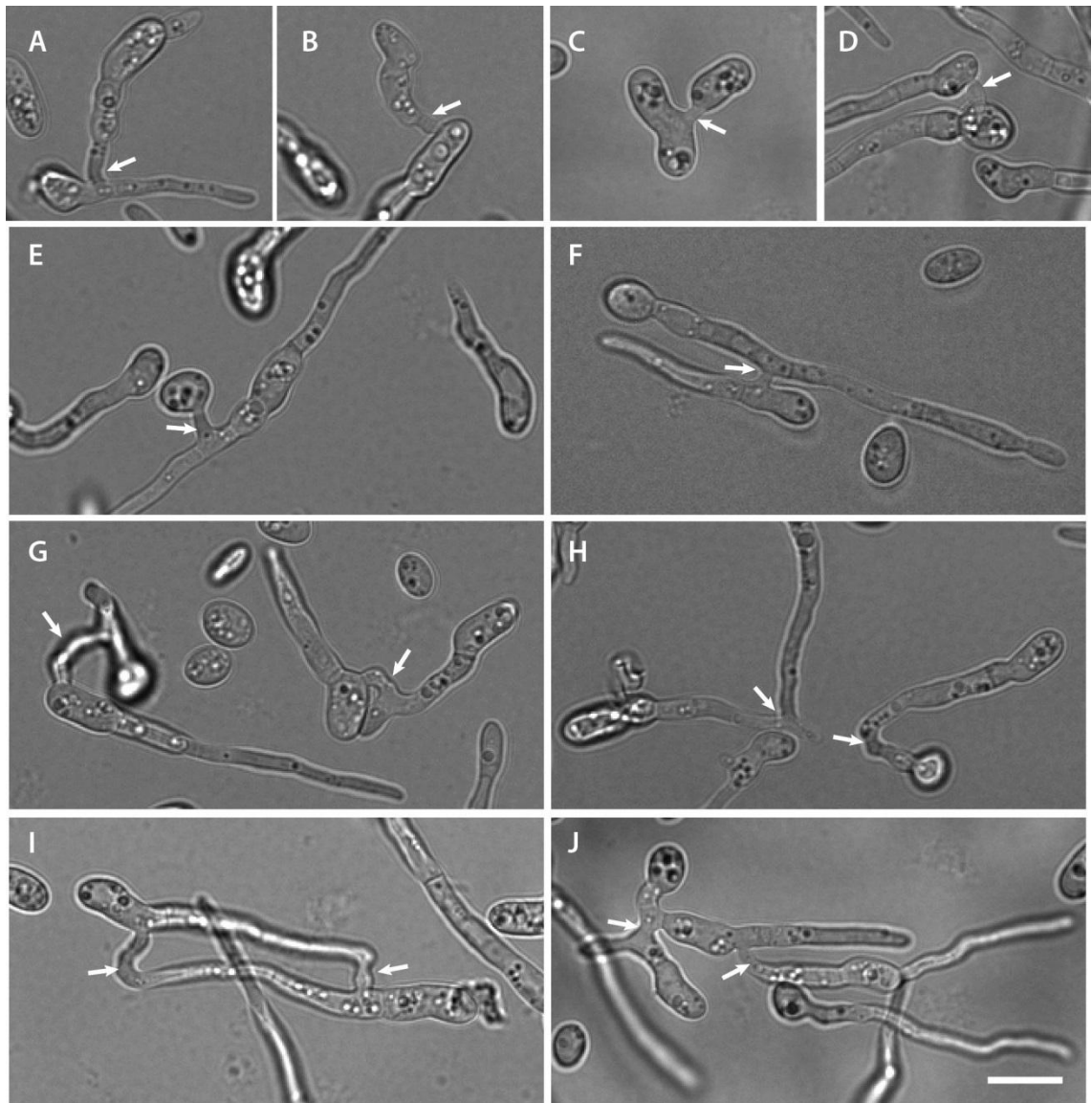
Fig. 4.3 Different types of CAT fusion observed between germlings. **(A, F, H and I)** CAT fusion between two germ tubes. **(C, D)** CAT fusion between two ungerminated spores. **(B, E, G)** CAT fusion between a germ tube and an ungerminated spore. CAT fusion resulted from tip-to-tip fusion of CATs formed from growing germ tubes (H), tip-to-side fusion of a CAT formed from a growing germ tube to a spore (A, B and I), and side-to-side fusion of CATs formed from adjacent germ tubes (F, G). Arrows point to region of CAT fusion. Scale bar = 10 μm.

4.3.3 Cell wall composition of CATs and germ tubes

Fluorescently tagged lectins were used to image and identify the cell wall components on the surfaces of germ tubes and CATs. An Alexa fluor 488 conjugate of concanavalin A (Con A), that binds to α-mannopyranosyl and α-glucopyranosyl residues of α-mannans and α-glucans (Schoffelmeer *et al*., 1997), exhibited significantly brighter staining of CAT cell walls, especially in CATs that were undergoing or had fused. In

contrast, the germ tube cell walls were only weakly stained with the fluorescently labelled ConA (Figs. 4.4A, 4.4A1, 4.5; Movie 4.3). Calcofluor white, which labels β-linked glucans such as chitin throughout cell walls and septa (Schoffelmeer *et al*., 1997), uniformly stained the cell walls of conidia, germ tubes and CATs (Figs. 4.4B, 4.4 B1). An Alexa fluor 488 conjugate of wheat germ agglutinin (WGA), which binds to sialic acid and N-acetyl glucosamine residues on the surfaces of cell walls (Schoffelmeer *et al*., 1997), did not stain the cell walls of CATs whilst spot-like stained regions were observed behind the growing tips of the germ tubes (Figs. 4.4C, 4.4C1).

Con A conjugated to Alex fluor 488 brightly stained the basal regions of conidiogenous cells from which microconidia are formed along the sides of hyphae (Fig. 4.6). Cell walls of ungerminated spores were uniformly stained with the Con A-Alexa fluor 488 conjugate (Figs. 4.4A, 4.4A1, 4.5 and 4.7), with the WGA-Alexa fluor 488 conjugate (Figs. 4.4C, 4.4C1, 4.6B 4.6B1) and with calcofluor white (Figs. 4.4B, 4.4B1).
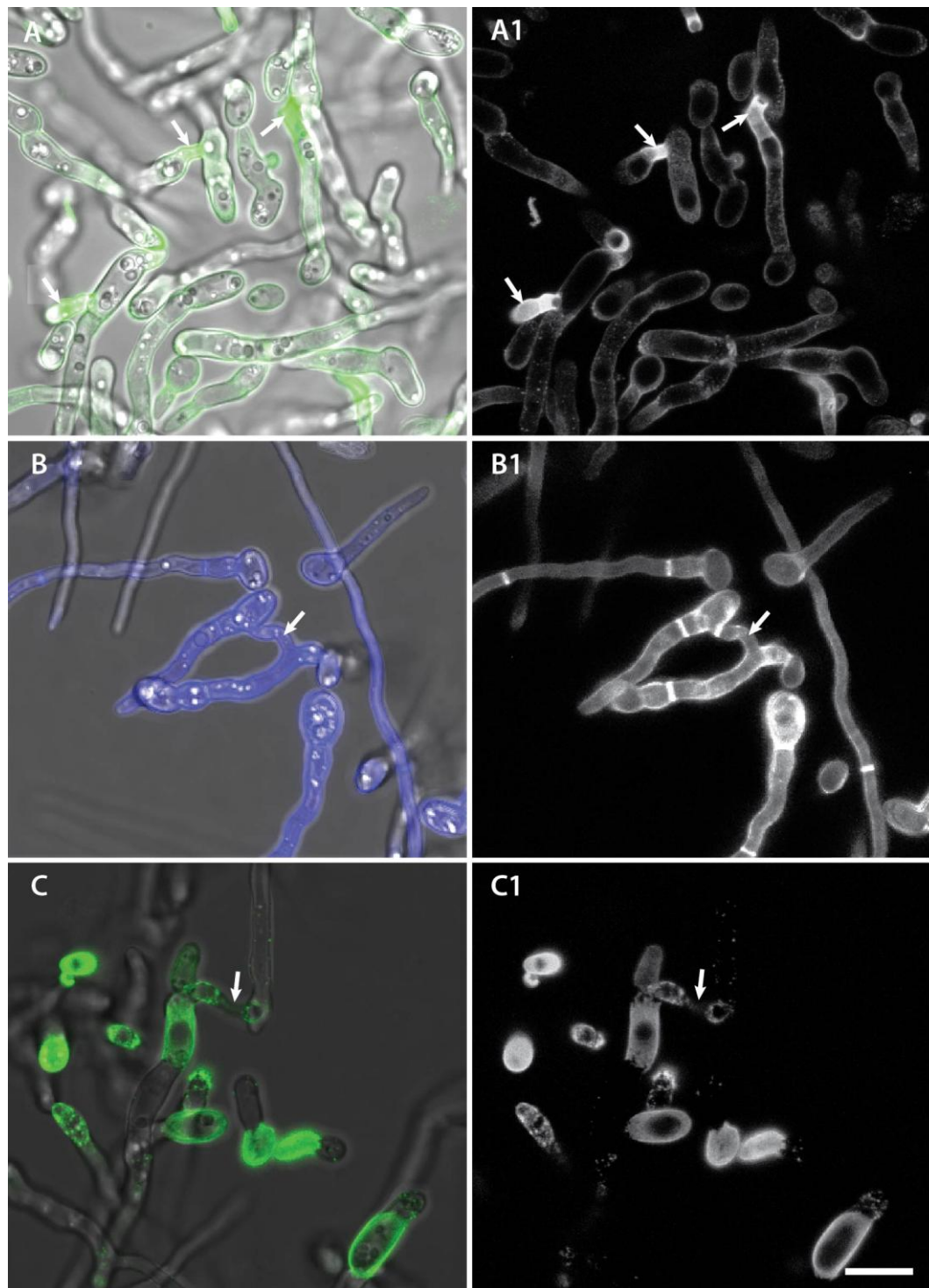
Fig. 4.4 The cell wall composition of CATs is different to that of germ tubes and spores. **(A, A1)** Staining with Con A conjugated to Alexa fluor 488 showed that the regions of CAT fusion exhibit brighter staining than that of germ tubes. **(B, B1)** Staining with calcofluor white showed no differential staining between CATs and germ tubes. **(C, C1)** Staining with wheat germ agglutinin tagged with Alexa fluor 488 showed strong staining of spore walls, spot-like staining of germ tubes behind their growing tips but no staining of CATs. A, B and C are overlay images of the fluorescence and brightfield channels whilst A1, B1 and C1 shows single channel images of fluorescence images alone. Arrows point to region of CAT fusion. Scale bar = 10 µm.
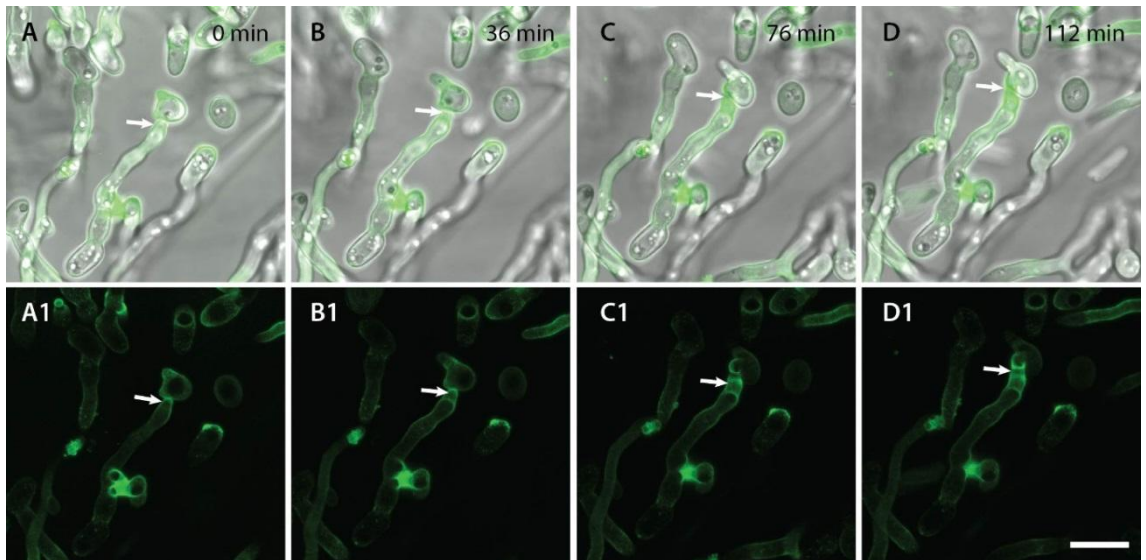
Fig. 4.5 Time course showing the bright staining of sites of CAT fusion with Con A conjugated to Alexa fluor 488. The CAT fusion event indicated by the arrow is occurring between a CAT from the tip of a germ tube and a CAT from an adjacent spore (see Movie 4.1). A-D are overlay images of brightfield and fluorescence channels whilst A1-D1 are the corresponding images of fluorescence channel alone. Scale bar = 10 μm.
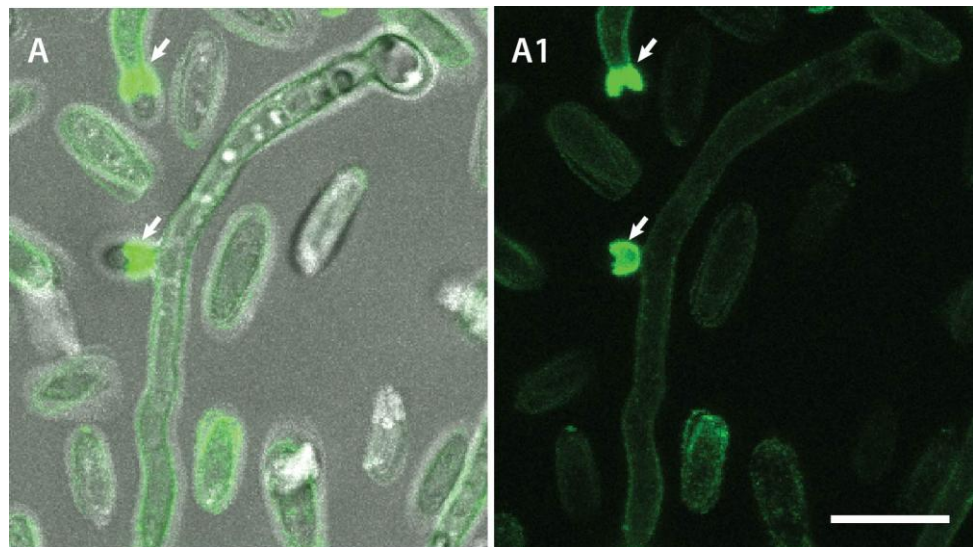
Fig. 4.6 (A, A1) Con A conjugated to Alexa fluor 488 brightly stains the basal regions of conidiogenous cells (indicated by arrows) from which microconidia are formed along the sides of hyphae. A is an overlay of the fluorescence and brightfield channels while A1 shows the fluorescence channel alone. Scale bar = 10 μm.
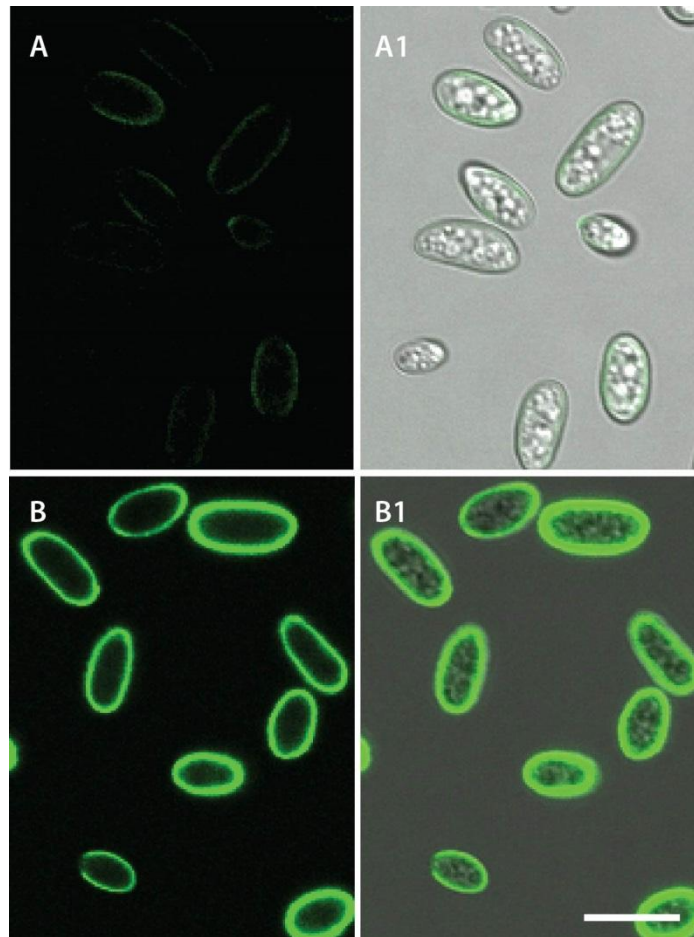
Fig. 4.7 (A, A1) Uniform staining of ungerminated, microconidial cell walls by Con A conjugated to Alexa fluor 488. (**B, B1)** Uniform staining of ungerminated, microconidial cell walls by wheat germ agglutinin conjugated to Alexa fluor 488. A and B show fluorescence channels alone whilst A1 and B1 shows overlay images of the brightfield and fluorescence channels. Scale bar = 10 μm.

4.3.4 Cytoplasmic connections are established by CAT fusion and facilitates the movement of organelles between germlings

Live-cell imaging provided conclusive evidence of cytoplasmic connections being formed by CAT fusion. Refractile organelles (later shown to be lipid droplets, Fig. 4.13 were observed moving between the two fused germlings as previously shown (Fig. 4.1, Movie 4.1) as well other organelles which are described below (Figs. 4.9, 4.11 and 4.12; Movies 4.5-4.7). We further analysed the achievement of cytoplasmic continuity by CAT fusion by mixing microconidia from a strain expressing cytoplasmic GFP with the unlabelled parental wild type strain from which it was derived. Live-cell imaging showed an immediate flow and mixing of cytoplasm between germlings once the intervening attached cell walls between fusing CAT had degraded (Fig. 4.8, Movie 4.4).

90
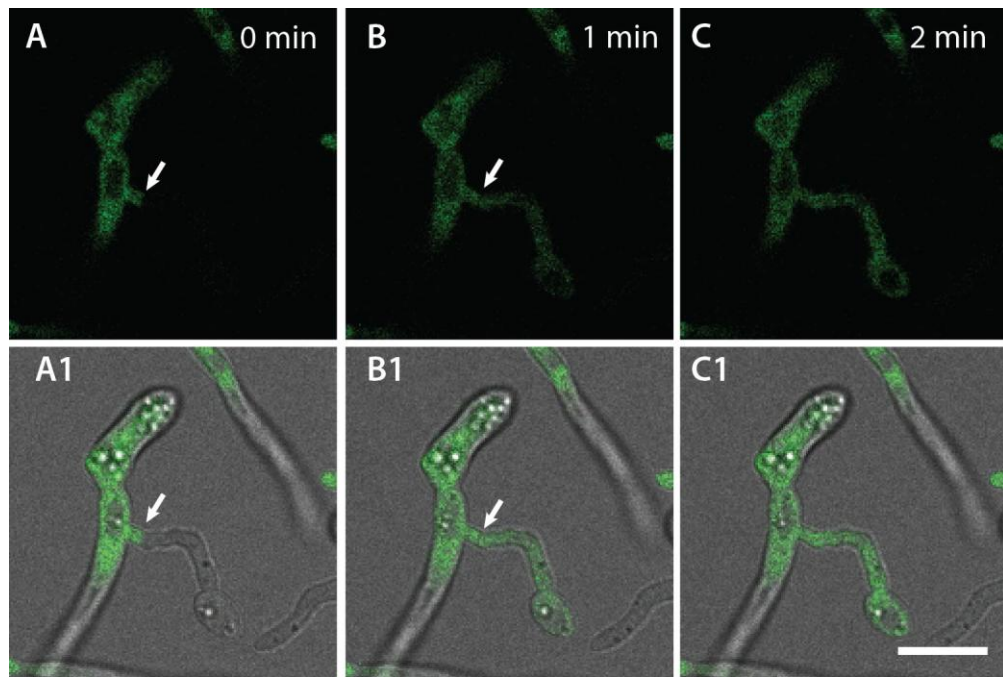
Fig. 4.8 Cytoplasmic flow and mixing is established following CAT fusion. **(A-C)** Time course showing final stages of CAT fusion between a cytoplasmic GFP expressing strain (left) and its parental wild type strain (right). When the attached intervening cell walls of the two CATs became degraded, GFP flowed from the left to the right hand germling indicating cytoplasmic mixing and continuity between the two germlings. A1, B1and C1 shows overlay images of brightfield and fluorescence channels while A, B and C shows GFP channel alone. Arrows point to region of fusion. Scale bar = 10 µm.

Strains in which the nuclei were labelled with H1-GFP (green) and H1-mCherry (red) were used to observe the movement of nuclei between and within fused germlings over a period of 30 min. These observations demonstrated that nuclei moved through fused CATs. A mitotic division was also commonly observed during this process (Fig. 4.9; Movie 4.5). The red nucleus had not degraded after the migration of the green nucleus into the 'host' cell of the red nucleus, as previously reported (Ruiz-Roldan *et al*., 2010; section 4.1). However, this may have been because the time course was only conducted over 30 min.

The H1-GFP and H1-mCherry expressing strains were imaged after co-incubation for 72 h. In these experiments, evidence of one red fluorescent nucleus undergoing degradation was often observed whilst sharing the cell compartment with an intact, healthy looking green fluorescent nucleus following CAT fusion (Figs. 4.10A1-4.10A3). This is consistent with the aforementioned observations of Ruiz-Roldan *et al*.

(2010) although it was not possible to capture the preceding process of nuclear migration from the 'donor' cell to a 'host' cell in a time course.

Another observation after incubating the red and green fluorescing strains for 72 h was the presence of red, green and yellow nuclei in some fields of view (Figs. 4.10B1-4.10B3). However, because of the extensive hyphal growth that had occurred after 72 h, it was not possible to convincingly confirm that any of the cell compartments that contained a yellow nucleus were uninucleate, which would be indicative of a second nucleus having undergone degradation. In addition, any obvious increase in the volume of the yellow nuclei compared with the green and red nuclei was not observed, which suggests that fusion had between green and red nuclei had not occurred.

Mitotracker Red, a mitochondrial stain (Hickey *et al*., 2004), was used for live-cell imaging of mitochondrial organization and dynamics during CAT fusion. Although difficult to clearly demonstrate, tubular mitochondria were observed to move between germlings through fused CATs (Fig. 4.11; Movie 4.6).

cDFFDA, a vacuolar stain (Hickey *et al*., 2004), was used for live-cell imaging of vacuolar organization and dynamics during CAT fusion. Round and elongated vacuoles of different and varying sizes and shapes were observed in germ tubes and CATs. The individual vacuoles and their morphologies were very dynamic when observed in time course movies. Small vacuoles pinching off from bigger ones can be observed to move through fused germlings in Fig. 4.12 and Movie 4.7.

A previously unidentified, spherical refractile organelle of varying size, < 2.4 μm in width, was observed in the microconidia, germ tubes and CATs of *F. oxysporum*. Microconidia and germlings were commonly full of these organelles, which were easily visualised by differential interference contrast or brightfield microscopy (e.g. Movies 3.2, 3.5, 3.6 and 4.1). The mitochondrial dye mitotracker red, the vacuolar dye cDFFDA, and the membrane selective dye FM4-64 (Fig. 4.14) all failed to stain these organelles. However, Nile red, a neutral lipid selective dye (Meadows, 2012), stained these round organelles very strongly which indicates that they are lipid droplets. These lipid droplets also moved between fused germlings through CATs (Movie 3.1; Fig. 4.13). However, the growing tips of germ tubes and CATs were devoid of these organelles as evident from live-cell imaging (Movie 4.1).
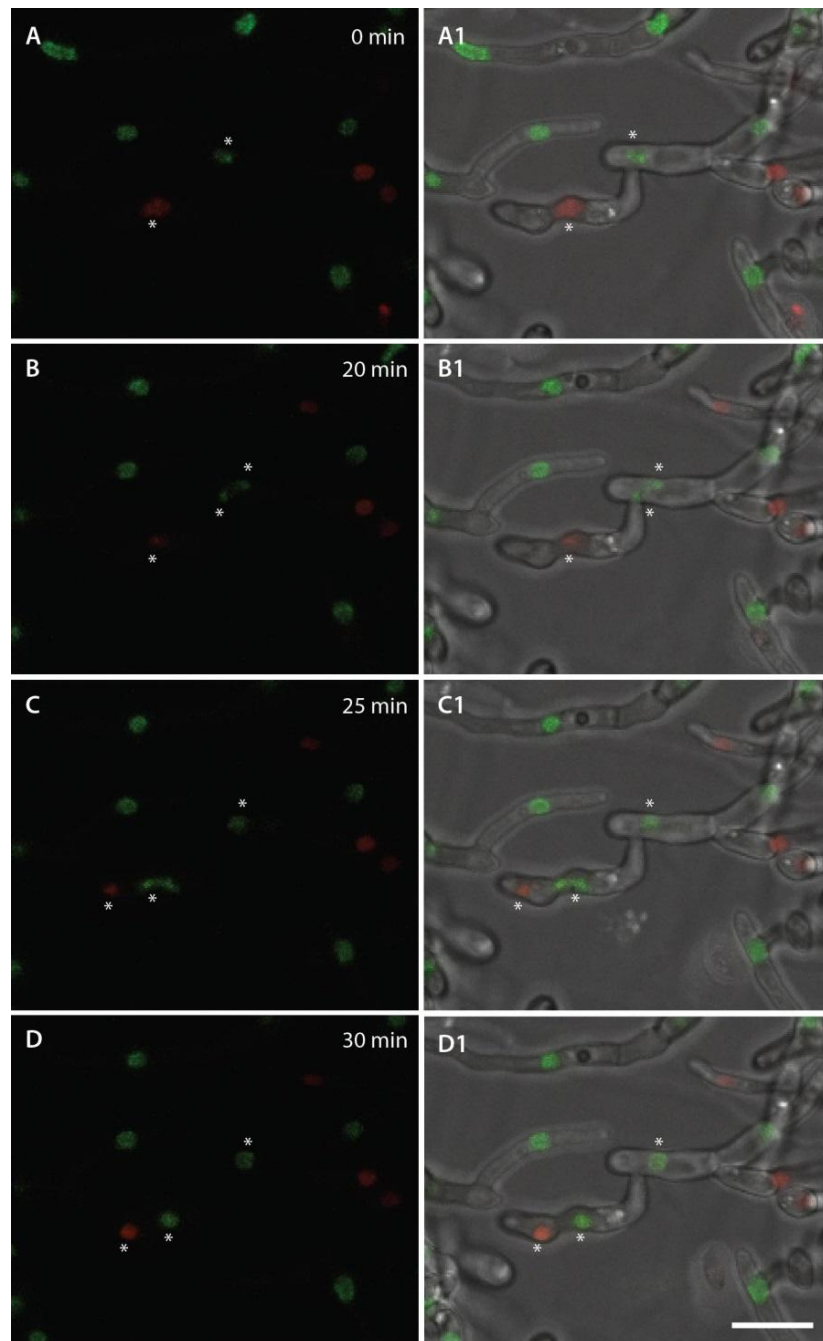
Fig. 4.9 CAT fusion facilitates the movement of nuclei between fused germlings (also see Movie 4.5). **(A-D)** Time course of nuclear division and migration observed during CAT fusion between H1-GFP (green) and H1 mCherry (red) nuclear labelled strains imaged in an overlay of only the green and red fluorescence channels. (A1-D1) Corresponding images from the same time course imaged in an overlay of the two fluorescence channel and the brightfield channel. Two nuclei, one in red and another in green are highlighted with asterisks. The green nucleus underwent a mitotic division at the 20 min time point. At 25 min, one of the green daughter nuclei migrated through the site of CAT fusion to the cell compartment containing a red nucleus (C and C1). At 30 min, the green nucleus regained its spherical form and shared the same cell compartment as the red nucleus. Scale bar = 10 μm.
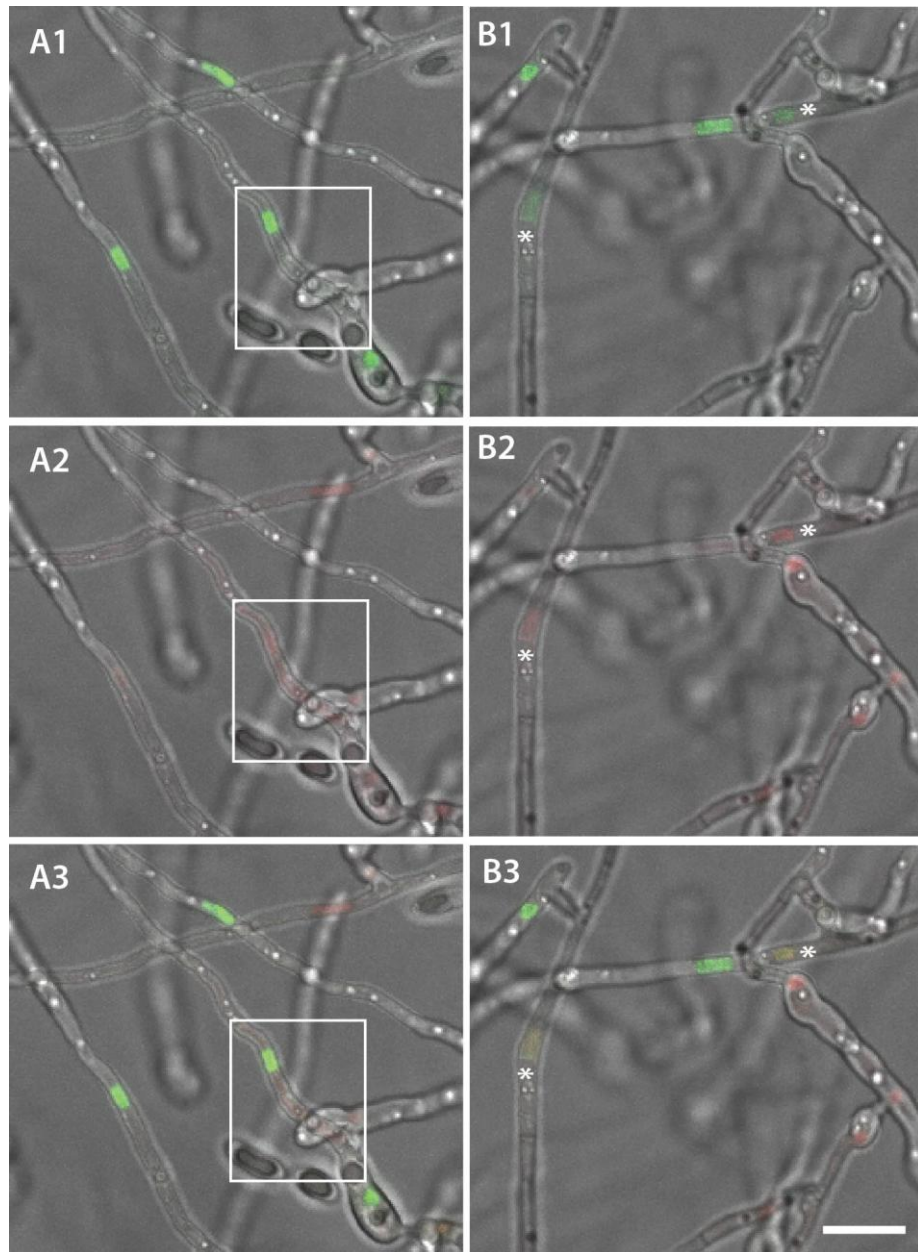
Fig. 4.10 Time courses showing the fate of nuclei following CAT fusion. **(A1-A3)** One nucleus within the box is intact and green (A2) whilst another nucleus in the same hypha and within the box has faint dispersed red fluorescence indicative of the nucleus having degraded (A2). In the overlay images it is quite clear that there is no colocalization of the green and the faint red nuclei (A3). **(B1-B3).** Two nuclei (asterisk) containing both H1-GFP (B1) and H1-GFP (B2) which in the overlay images appears yellow (B3). A1-A3 and B1-B3 are overlays of the green fluorescence, red fluorescence and brightfield channels. The H1-GFP and H1-mCherry strains were incubated for 72 h post inoculation in 1% PDB supplemented with 25 mM $NaNO_3$. Scale bar = 10 μm.
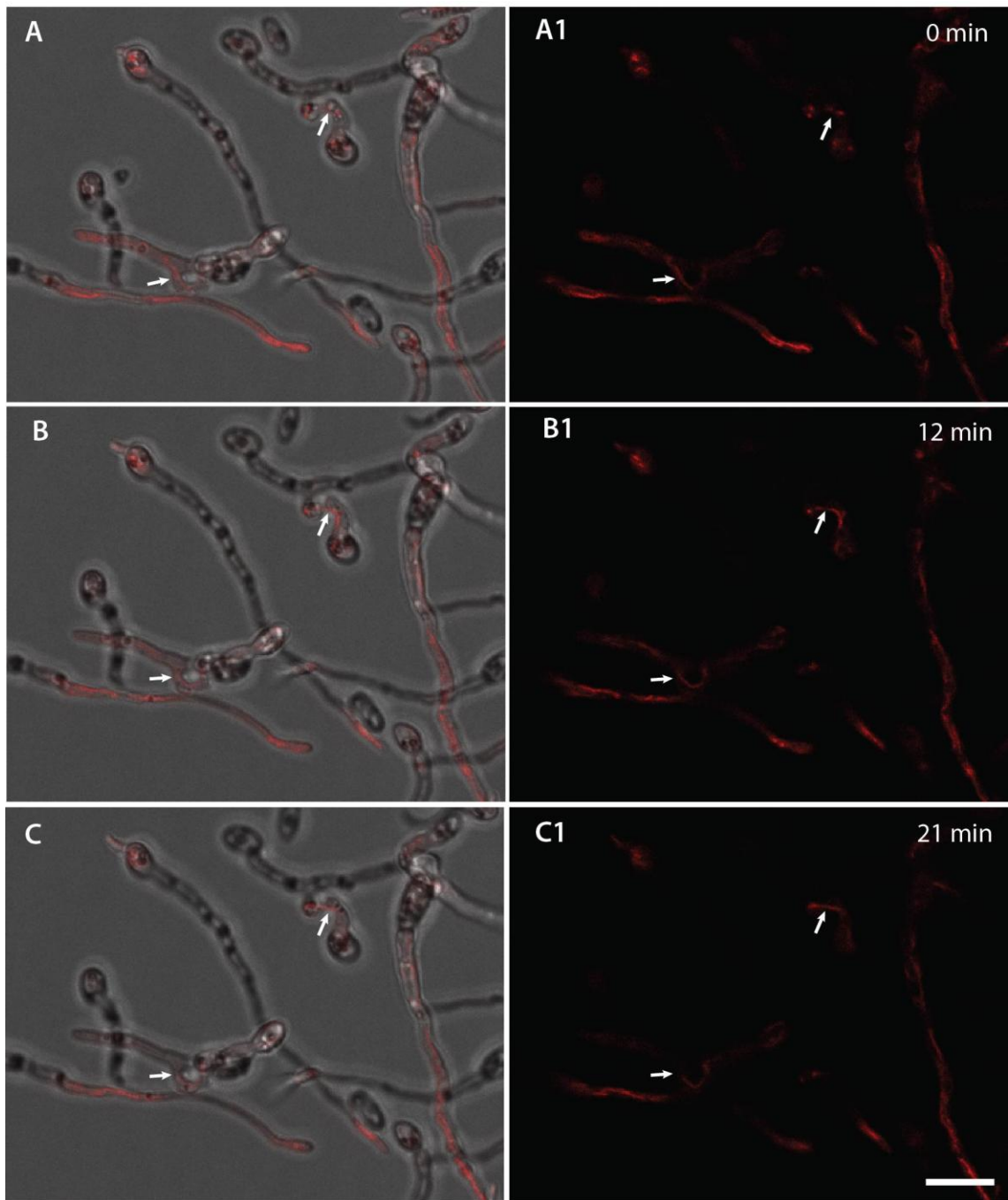
Fig. 4.11 CAT fusion facilitates the movement of mitochondria between fused germlings. (A-D). Time course showing the movement of mitochondria through sites of CAT fusion (indicated by arrows) between germlings. The mitochondria were stained with the mitotracker red stain. A-D are overlays of brightfield and red fluorescence channels whilst A1-D1 is the red fluorescence channel alone. Scale bar = 10 μm.
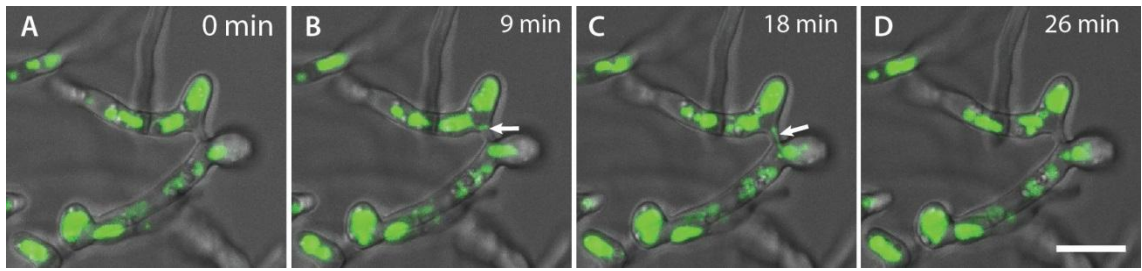
Fig. 4.12 CAT fusion facilitates the movement of vacuoles between fused germlings. **(A-D)** Time course showing the movement of vacuoles between two germlings through CATs that have fused. At 9 min (B), a small vacuolar compartment (arrow) can be seen pinching off from a bigger one before it becomes more elongated as it passed through the fused CAT connection between the two germlings. At 18 min (C), the small vacuole can be seen moving through the fused CAT connection into the second hyphal compartment (C). The movement of vacuole is complete at 26 min (D). The vacuoles were stained with the cDFFDA stain. Scale bar = 10 μm.
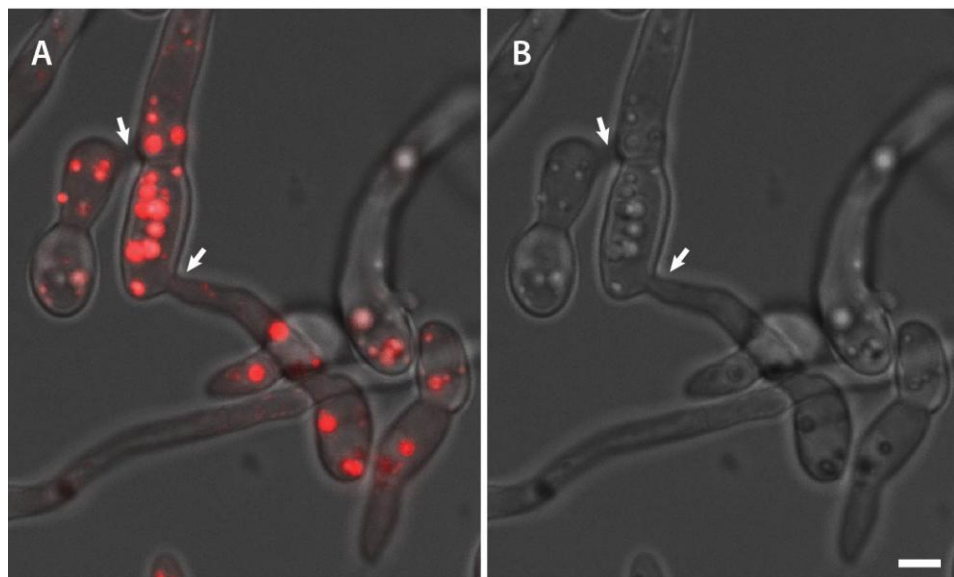
Fig. 4.13 The refractile organelles within microconidia and germlings are lipid droplets. **(A)** The lipid-specific dye Nile red stains these organelles as shown in an overlay image of the fluorescence and brightfield channels. Two CAT fusions (arrows) can be seen between three of the germlings in this image. (B) Refractile lipid droplets visualised in just the brightfield channel visualised in (A). Scale bar = 10 μm.
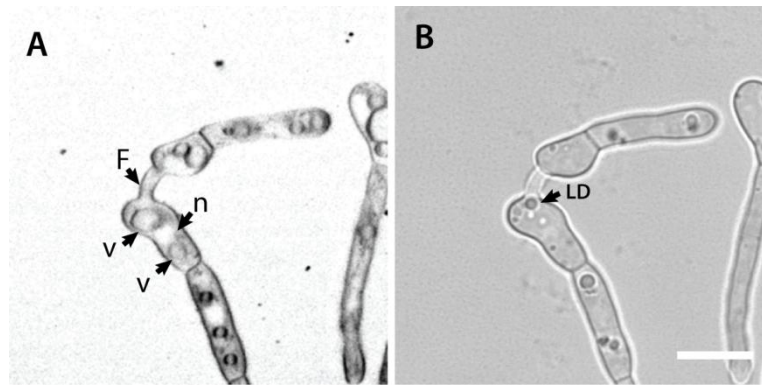
Fig. 4.14 Lipid droplets are distinct from vacuoles and nuclei. **(A)** Fluorescence image of two germlings that have undergone a CAT fusion (F) with each other and have been stained with membrane-selective fluorescent dye, FM4-64. **(B)** Negative image of fluorescence image in (A) in which the vacuolar membranes of vacuoles (v) have been labelled. **(C)** Brightfield image of the same germlings in A and B in which one of the refractile lipid droplets is highlighted (LD), is unstained in the fluorescence image shown in (A). Scale bar = 10 μm.

4.3.5 The F-actin and microtubule cytoskeleton are required for CAT fusion

Treatment with benomyl, which blocks the polymerisation of β-tubulin to form microtubules (Roca *et al*., 2010), inhibited CAT fusion in a dose dependent manner when continuously present in 1% PDB supplemented with $NaNO_3$ and incubated for 12 h. CAT fusion was completely inhibited with 10 μM benomyl at which concentration germination was only partially inhibited (Fig. 4.15). The germ tubes treated with 10 μM benomyl were very short (Fig. 4.17B) compared with the untreated control (Fig. 4.17A).

Latrunculin A, which inhibits the depolymerisation of F-actin microfilaments (Berepiki *et al*., 2010), inhibited both CAT fusion and germination in a dose dependent manner when continuously present in 1% PDB supplemented with $NaNO_3$ and incubated for 12 h. CAT fusion was completely inhibited with 5 μM latrunculin A and CAT fusion was more sensitive than germination to the drug (Fig. 4.16). With 5 μM latrunculin A the germ tubes that were produced often had swollen tips (compare Fig. 4.17C with 4.17A; Movie 4.9).

Adhesion of the germlings did not seem to be inhibited by treatment with either 10 μM benomyl (Movie 4.8) or 10 μM latrunculin A (Movie 4.9) but ungerminated spores in both treatments were mostly not adhered (Movies 4.8 and 4.9).
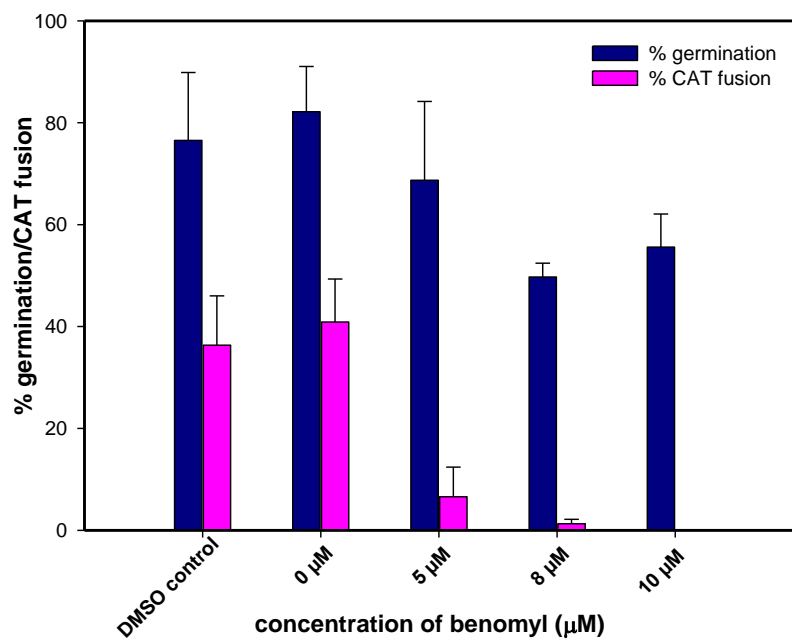
Fig. 4.14. Dose dependent inhibition of CAT fusion by the microtubule polymerisation drug, benomyl. Germ tube formation was only partially inhibited at high concentrations of benomyl.
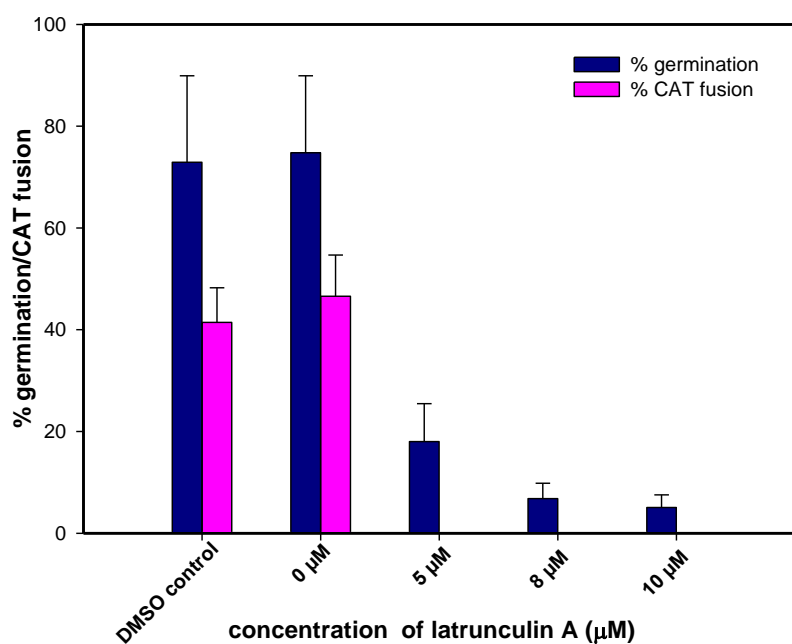
Fig. 4.15. Dose dependent inhibition of spore germination and CAT fusion by the F-actin depolymerising drug, latrunculin A.
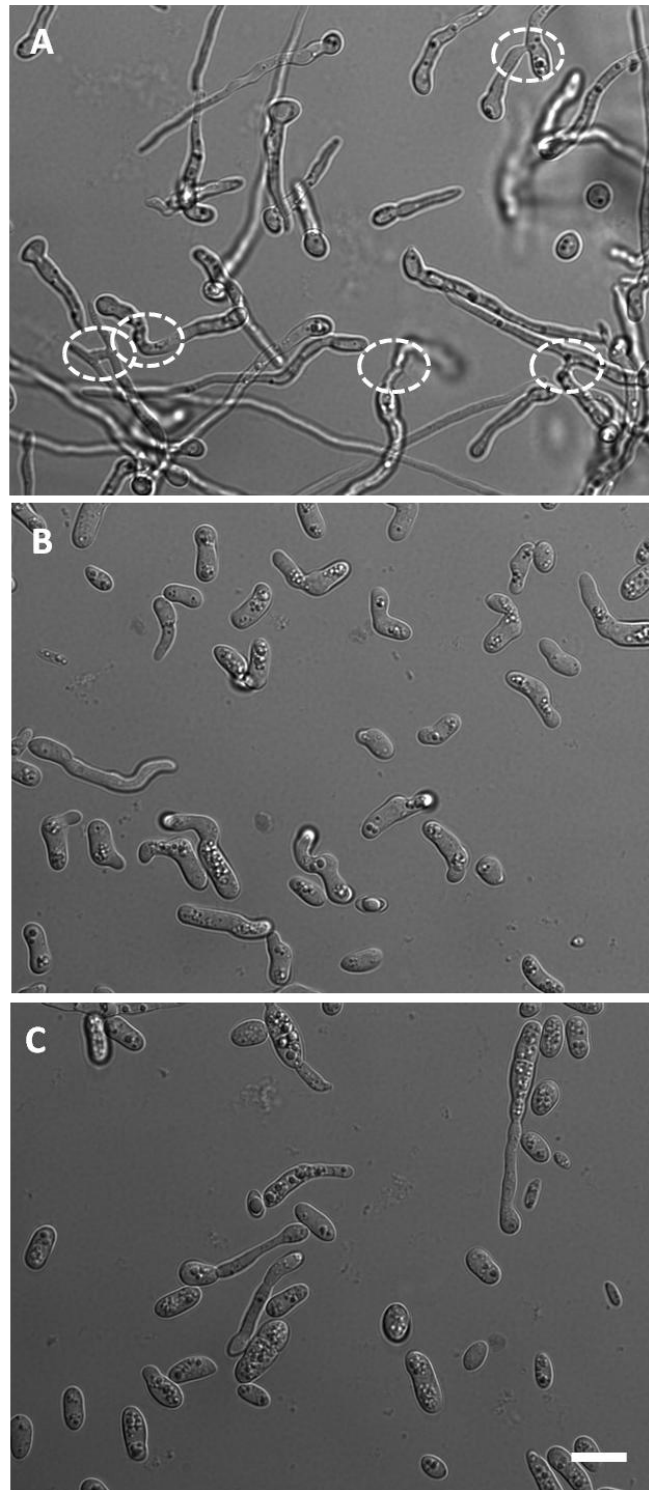
Fig 4.16 CAT fusion was inhibited by the microtubule polymerising inhibitor, benomyl and the F-actin depolymerising inhibitor, latrunculin A **(A)** Untreated germlings (control) showing CAT fusions highlighted within dotted circles. (B, C) Germlings treated with 10 μM benomyl and 10 μM latrunculin A, respectively, in which CAT fusion has been inhibited (also see movies 4.8 and 4.9). Bar scale = 10 μm.

4.4 Discussion

4.4.1 CATs are different from germ tubes

As a result of meticulous, time-lapse imaging the three basic stages of CAT fusion (i.e. CAT formation, homing and fusion) that were originally defined in *N. crassa* (Roca *et al*., 2005b; section 1.2.2; Fig. 1.2), also occur *Fusarium oxysporum.* The whole process from the identification of incipient CATs to CAT fusion that ultimately resulted in cytoplasmic continuity between the fused microconidial germlings varied between 41 and 168 min (n = 15). A rigorous quantification of the periods of time taken for the whole process of CAT fusion is not known to have taken place in *N. crassa* but looking at published images and movies of the process (e.g. Roca *et al*., 2005b; Read *et al*., 2012) it seems to usually occurs within ~ 45 min.

CATs can be distinguished physiologically from germ tubes by exhibiting positive tropisms towards each other, as previously reported in *N. crassa* (Roca *et al*., 2005b). It was found that the maximum initial distance when two CATs were formed and then grew chemotropically towards each other was ~ 8 μm compared with ~ 15 μm reported for *N. crassa* (Fleiβner *et al*., 2009). This distance will presumably relate to the distance that an appropriate concentration of the unidentified CAT inducer/chemoattractant can reach its 'partner spore/germling' to activate the unidentified receptor of the spore/germling that it is communicating with via the CAT fusion self-signalling mechanism (section 1.2.2). This could be influenced by many factors (e.g. the amount of the CAT inducer/chemoattractant ligand secreted from CAT tips; the number of ligand receptors present at CAT tips; or the amount of ligand digesting enzyme that might be secreted into the extracellular medium in order to generate CAT inducer/gradients between communicating cells).

It was found that the CATs of *F. oxysporum* can usually be distinguished morphologically from germ tubes by being thinner on average (average CAT width = 1.73 ± 0.52 μm; average germ tube width = 2.45 ± 0.45 μm). CATs were also found to be thinner than germ tubes in *N. crassa* but their average widths were found to vary between wild type strains (Roca *et al*., 2005b).

CATs were observed to arise either directly from microconidia or directly from a germ tube (either from the tip of the germ tube or as a subapical branch from it). CATs have also been shown to have these origins in *N. crassa* (Roca *et al*., 2005b). In addition,

CATs were sometimes not visible between fusing spores/germ tubes that were immediately adjacent to each other. The different types of CAT fusion were from tip-to-tip fusion of CATs formed from growing germ tubes, tip-to-tip fusion between two spores, tip-to-side fusion of a CAT formed from a growing germ tube to a spore, and side-to-side fusion of CATs formed from adjacent germ tubes. Again, similar types of CAT fusion have been reported for *N. crassa* (Roca *et al*., 2005b).

A newly discovered difference between CATs and germ tubes that was made is that their cell wall surface composition is different. This was demonstrated by using fluorescently labelled lectins that are selective for different sugars of polysaccharides on only cell wall surfaces because they are too large to penetrate into cells walls. It was possible to demonstrate that the CAT surface is much richer in α-mannans and α-glucans (revealed by fluorescently labelled ConA) than the germ tube or microconidial surface. These polysaccharides may be part of the cell surface itself, or possibly an extracellular matrix layer that is secreted over the surface of the CATs. It is possible that these α-mannans and/or α-glucans play a role in cell adhesion, as previously discussed in section 3.4.1. The other difference that was observed between CAT and germ tube surfaces, using fluorescently labelled WGA (which binds to sialic acid and N-acetyl glucosamine residues), was that the CATs lacked any exposed, visible chitin whilst germ tubes (and microconidia) did. Nevertheless, CAT cell walls still contained chitin (as revealed by calcofluor white staining) except it was absent from the CAT cell wall surface. Interestingly, small subapical concentrated patches of chitin exposed on the surfaces of germ tube cell walls were also observed. Previously, Schoffelmeer *et al*. (1997) have shown similar results with the staining of microconidia and germ tubes of *F. oxysporum* with fluorescently labelled Con A, WGA and with calcofluor white but they did not analyse the cell wall composition of CATs. An enriched staining by fluorescently labelled Con A was also observed at the base of sites of microconidiation along germ tubes.

Spore germination is accompanied by the synthesis of new wall material with the emergence of a germ tube (Allen, 1965). A major difference between in the cell surface composition was observed in relation to chitin because microconidia stained much more strongly with fluorescently labelled WGA than did germ tubes and they also lacked the spot-like staining of chitin observed on germ tubes. However, staining with calcofluor white, which generally stains chitin throughout the cell wall, was similar in both microconidia and germ tubes. Multiple patches of concentrated chitin have been

observed in ungerminated macroconidia *F. graminearum* using fluorescently labelled WGA (Harris, 2005).

4.4.2 Organelles move between germlings via CAT fusions

By performing time-lapse live-cell imaging of labelled organelles, it was possible to demonstrate the movement of nuclei, mitochondria, vacuoles and lipid droplets through the connections between germlings created by CAT fusion. Besides nuclear movement between fused germlings (Ruiz-Roldan *et al*., 2010), the movement of mitochondria, vacuoles and lipid droplets has not been previously shown by live-cell imaging in *F. oxysporum*. Nuclei have also been shown to move between fused germlings of vegetatively incompatible strains by live-cell imaging of *C. lindemuthianum* (Ishikawa *et al*., 2012).

The results that were obtained were consistent with 'host' cell nuclear degradation into the cell which the 'donor' nucleus had migrated into following fusion (Ruiz-Roldan *et al*., 2010) although it was not possible to image the whole of this process by time-lapse imaging. Examples of green, red and yellow nuclei were also observed in some fields of view of cultures in which H1-GFP and H1-RFP strains had been co-incubated for 72 h. However, it was not possible to obtain unequivocal evidence that the yellow nuclei were in uninucleate cell compartments because of the extensive hyphal growth that had occurred after 72 h. These yellow nuclei had probably resulted from green H1-GFP expressing nuclei and red H1-RFP expressing nuclei sharing the same cytoplasm and thus sharing their fluorescent fusion proteins. No evidence was obtained for the yellow nuclei to have resulted from the fusion of green and red nuclei because there was not an obvious increase in the volume of the yellow nuclei compared with the green and red nuclei.

Microtubules and F-actin microfilaments form a dynamic interconnected, interacting cytoskeletal networks throughout the cytoplasm of fungal cells and play a variety of roles including: forming spindles allowing chromosome segregation during nuclear division, nuclear positioning, providing tracks to transport secretory vesicles to hyphal tips for tip growth; and for the intracellular movement of organelles and protein complexes (Xiang and Oakley, 2010; Berepiki *et al*., 2011). However, interestingly Roca *et al*. (2010) were able to show that microtubules are not required for CAT fusion whilst F-actin is. This contrasted with my results in which showed that both

microtubules and F-actin are required for CAT fusion in *F. oxysporum*. The lack of a requirement for microtubules for CAT fusion was very surprising in *N. crassa*, particularly since nuclear transport is normally mediated by them in fungal hyphae (Roca *et al*., 2010). The precise roles that microtubules and F-actin play in CAT fusion, and particularly the movement of nuclei, mitochondria, vacuoles and lipid droplets between fused germings in *F. oxysporum* are not clear at this stage, and require future investigation. In addition, other proteins that associate with the cytoskeletal elements will undoubtedly play important roles in the directed transport of organelles through sites of CAT fusion from one germling to another. One of these proteins is ApsA, which is associated with microtubules and is known to regulate nuclear positioning and migration in fungi. Analysis of gene expression profiles during conidial germination of two *F. oxysporum* strains has shown high expression of ApsA (Deng *et al.* 2006). This might also be relevant during the period of CAT fusion during colony initiation. However, having put a lot of emphasis on cytoskeleton mediated organelle movement; it is also possible that some of the organelles that pass through sites of CAT fusion (e.g. lipid droplets) may move by Brownian movement independently of cytoskeletal elements.

Because of the wide range of roles that microtubules and F-actin have in fungal cells, it is not surprising that spore germination was inhibited by the drugs benomyl and latrunculin A as has been reported for other fungi (Xiang and Oakley, 2010; Berepiki *et al*., 2010).

4.5 Summary

- The three stages of CAT fusion (CAT formation, homing and fusion) were shown by time lapse, live-cell imaging of *F. oxysporum* cultured *in vitro*

- CAT fusion in *F. oxysporum* can occur in different ways during colony initiation: tip-to-tip, tip-to-side, and side-to-side between spores and/or germlings

- CATs in *F. oxysporum* can be distinguished from germ tubes by being thinner and by exhibiting positive tropisms towards each other prior to fusion

- The cell wall surface composition of CATs is different to that of germ tubes by being much richer in α-mannans and/or α-glucans lacking exposed chitin

- CAT fusion establishes cytoplasmic connections between fused germlings and facilitates the movement of nuclei, mitochondria, vacuoles and lipid droplets between these germlings

- Both microtubules and F-actin are required for CAT fusion to occur

Chapter 5: Role of calcium signalling during CAT fusion in *Fusarium oxysporum*

5.1 Introduction

Ca^{2+} signalling is known to play a major role in regulating many important morphologenetic and physiological processes in filamentous fungi. Preliminary evidence has been obtained for Ca^{2+} signalling playing roles during CAT fusion in *N. crassa* (see section 1.4.2) but there have been no studies on the role of Ca^{2+} signalling during CAT fusion is *Fusarium oxysporum*.

Three classes of transmembrane Ca^{2+} transporter proteins have been described in eukartyotic cells as regulatory components of signalling machinery; Ca^{2+} channels, pumps (Ca^{2+} ATPases) and Ca^{2+}/cation exchangers (Bencina *et al*., 2009). Ca^{2+} channels mediate the flow of free Ca^{2+} down a concentration gradient into the cytoplasm from the external medium or from internal organelle Ca^{2+} stores upon triggering by an extracellular or intracellular stimulus. Three types of Ca^{2+} channels have been described in mammalian cells based on their mode of activation: (i) voltage-gated channels; (ii) transient receptor potential (TRP) channels; and (iii) stretch-activated channels (Bencina *et al*., 2009). In fungi, there are two types of Ca^{2+} uptake systems involving the Ca^{2+} channel transport across the plasma membrane: the low affinity Ca^{2+} uptake system (LACS) and the high affinity Ca^{2+} uptake system (HACS). The LACS functions when there is a high availability of Ca^{2+} in the external medium whilst the HACS operates when the availability of external Ca^{2+} is low. The only known member of the LACS is Fig1 (Muller *et al*., 2001). The HACS comprises the L-type Ca^{2+} channel Cch1 and the regulatory proteins Mid1 and Ecm7 (Martin *et al*., 2011; Muller *et al*., 2011). Homologues of Cch1, Mid1 and Fig1 are present in filamentous fungi (Zelter *et al*., 2004) and they are believed to play similar roles in *Neurospora crassa* and *Giberella zeae* (the teleomorph of *Fusarium graminearum*) (Lew *et al*., 2008; Cavinder *et al*., 2011; Cavinder and Trail, 2012) as have been described in yeast. Yvc1 is an example of a TRP channel with homologues in yeast and filamentous fungi (Zelter *et al*., 2004; Bencina *et al*., 2009; Goncalves *et al*., 2014). It has been localized to the vacuolar membrane of yeast (Yoshimura *et al*., 2004). The genetically encoded fluorescent probe cameleon had been expressed in the wild type, *FoCCH1*, *FoMID1* and *FoYVC1* mutants of the *F. oxysporum* strain O-685 (which is different from the

tomato pathogenic *F. oxysporum* strain 4287 used in my study). The nature of the of the pulsatile increases in cytosolic free Ca^{2+} ($[Ca^{2+}]_c$) observed in growing hyphal tips (see section 1.4.2) was found to be different in the wild type and the three mutants although no causative relationship between the different Ca^{2+} signatures and their potential influence on hyphal tip growth was made (Kim *et al*., 2015).

Ca^{2+} modulatory pharmacological agents have played a major role in deducing the function of Ca^{2+} signalling machinery in eukaryotic cells. The following Ca^{2+} modulators have been used in the research described in this chapter:

1. **BAPTA** (or 2-[2-[2-[2-[bis(carboxymethyl)amino]phenoxy]-ethoxy]-N-carboxy-methyl)aniline]acetic acid; PubChem Compound; www.ncbi.nih.gov/pcccompound), which is a cell impermeant chelator of divalent cations with a higher selectivity for Ca^{2+} than other divalent cation chelators such as EGTA and EDTA. has been shown to remove extracellular Ca^{2+} and its role studied during growth and development in *F. graminearum* (Hallen and Trail, 2008; Cavinder *et al*., 2011; Cavinder and Trail., 2012).

2. **Verapamil** (or 2-(3,4-dimethoxyphenyl)-5-[2-(3,4-dimethoxyphenyl)ethyl-methylamino]-2-propan-2-ylpentanenitrile; PubChem Compound; www.ncbi.nih.gov/pcccompound), which inhibits the L-type Ca^{2+} channel Cch1 protein, which is a component of the high affinity calcium uptake system (HACS) in fungi (Martin *et al*., 2011; Muller *et al*., 2011).

3. **Calmidazolium** (or R24571 or 1-[bis(p-chlorophenyl)methyl]-3-[2,4-dichloro-β-(dichlorobenzyloxy)phenethyl]imid-azoliniumchloride; PubChem Compound; www.ncbi.nih.gov/pcccompound), is a highly selective inhibitor of calmodulin in mammalian cells (Gietzen *et al*., 1981), and is ~26 times more inhibitory than the commonly used calmodulin inhibitor, trifluoroperazine (TFP) (Gietzen *et al*., 1980).

4. **FK506** (or tacrolimus or 17-allyl- 1,14-dihydroxy-12-[2'-(4"-hydroxy-3"-methoxycyclohexyl)1-methylvinyl]-23,25-dimethoxy-13,19,21,27-tetramethyl-11,28-dioxa-4-azatricyclo[22.3.1.04,9]octacos-18-ene-2,3,10,16-tetraone; 17-allyl-1,14-di-hydroxy-12-[2-(4-hydroxy-3-methoxy-cyclohexyl)-1-methyl-vinyl]-23,25-dimethoxy-13,19,21,27-tetramethyl-11,28-dioxa-4-aza-tricyclo[22.3.1.04,9] octacos-18-ene-2,3,10,16-tetraone; PubChem Compound; www.ncbi.nih.gov/pcccompound), which is an inhibitor of calcineurin activity that is also used as immunosuppressant for treating patients. FK506 is a

macrolide that binds to FK506 binding proteins (FKBPs) that inhibit T-cell activation (Sikierka *et al*., 1989). FKBPs are found in the cytoplasm and exhibit peptidyl-prolyl isomerase (PPIase) activity that can catalyse cis-trans isomerisation of proline residues in proteins and peptides, including those involved in Ca^{2+} signalling (Sikierka *et al*., 1989; Steinbach *et al*., 2007).

5. **Thapsigargin** (or [(3S,3aR,4S,6S,6aR,7S,8S,9bS)-6-acetyloxy-4-butanoyloxy-3,3a-dihydroxy-3,6,9-trimethyl-8-[(Z)-2-methylbut-2-enoyl]oxy-2-oxo-4,5,6a,7,8,9b-hexahydroazuleno[4,5-b]furan-7-yl]   octanoate;   PubChem Compound; www.ncbi.nih.gov/pcccompound), which is an inhibitor of Ca^{2+} ATPase activity in the ER and prevents Ca^{2+} sequestration within the ER (Goncalves *et al*., 2014).

6. **Ruthenium 360** (or RU360 or azanide; formic acid; ruthenium(5+); trichloride; hydrate; PubChem Compound; www.ncbi.nih.gov/pcccompound), which is an inhibitor of the mitochondrial Ca^{2+} uniporter in cells (Kirichok *et al*., 2004) and has been shown to be active in *N. crassa* (Goncalves *et al*., 2014).

5.3 Results

5.3.1 Inhibitory effects of calcium modulators on microconidial germination and CAT fusion

The dose-dependent inhibitory effects of the Ca^{2+} modulators, BAPTA, verapamil, calmidazolium, thapsigargin, FK506 and RU360 on microconidial germination and CAT fusion were quantitatively analysed. The concentration ranges of inhibitors used all fell within those that have been previously reported to have inhibitory effects in fungi (Goncalves *et al*., 2014; Lamoth *et al*., 2015). Spore germination was analysed in both 1% PDB alone and in 1% PDB media supplemented with 25 mM $NaNO_3$. CAT fusion was only analysed in the latter medium because it does not occur in 1% PDB alone (see section 3.3.1).

5.3.1.1 BAPTA

Concentrations of 0.5-15 mM BAPTA were tested (Fig. 5.1). Germination in 1% PDB alone was unaffected by BAPTA concentrations up to 5 mM but showed a slight reduction (5-10%) with 10-15 mM verapamil. Germination in 1% PDB with $NaNO_3$ was not inhibited by BAPTA at concentrations up to 15 mM. CAT fusion was very

sensitive to BAPTA and was completely inhibited at concentrations of 5 mM or above. The IC_{50} value of BAPTA for CAT fusion was 0.2-0.75 mM (Fig 5.1).

5.3.1.2 Verapamil

Concentrations of 0.5-15 mM verapamil were tested (Fig 5.2). Germination in 1% PDB alone was completely inhibited by 5 mM verapamil. Germination in 1% PDB with $NaNO_3$ showed a similar dose dependent inhibition and was completely inhibited by 10 mM verapamil. CAT fusion was more sensitive to verapamil than germination and was completely inhibited by 5 mM of the drug. The IC_{50} value of verapamil on germination was 2-5 mM in both media whereas the IC_{50} value for CAT fusion was 0.2-0.75 mM (Fig. 5.2).
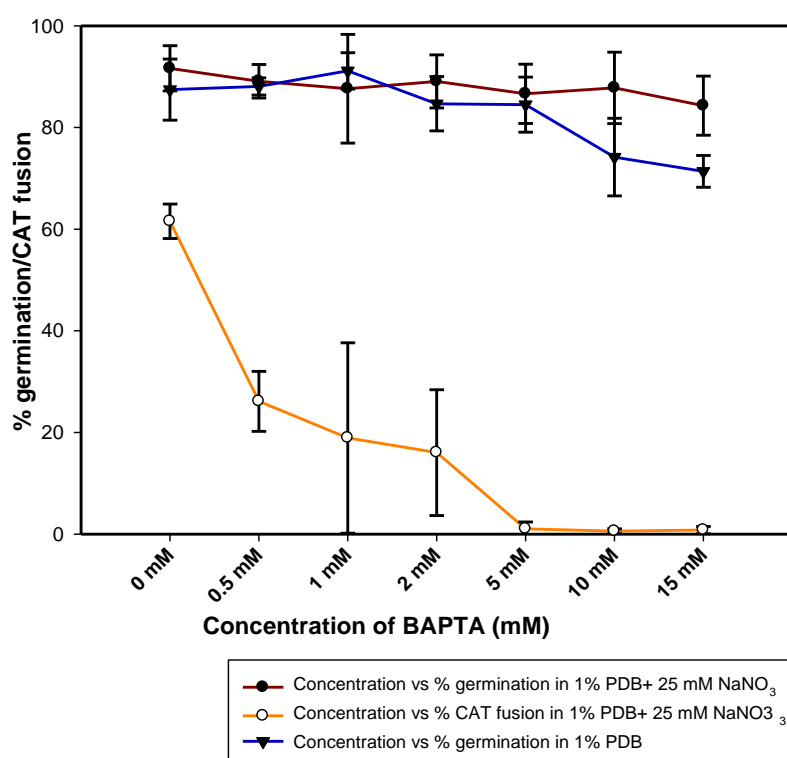
Figure 5.1 Effects of the Ca^{2+} chelator, BAPTA on microconidial germination and CAT fusion.
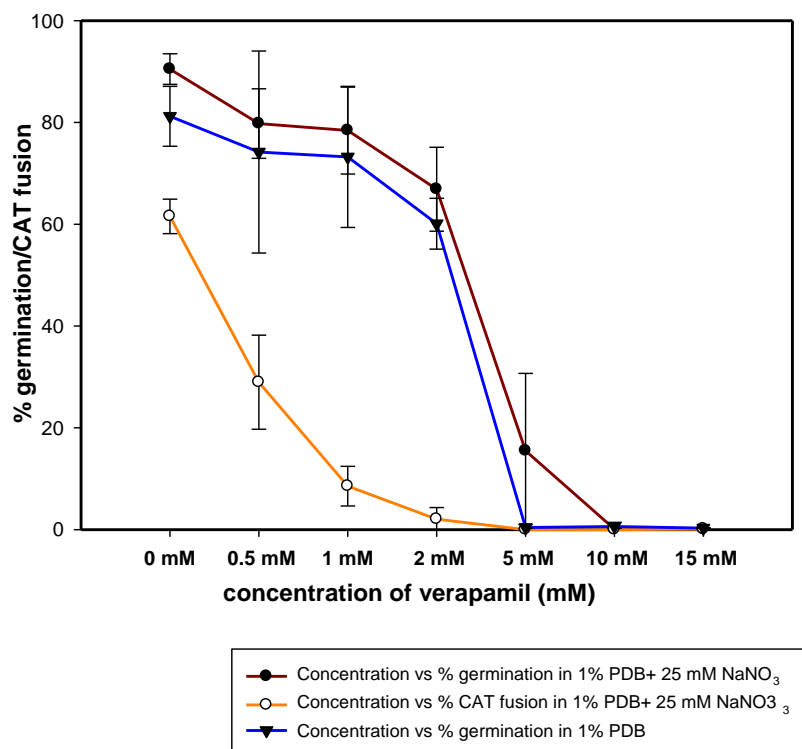
Figure 5.2 Effects of the L-type Ca^{2+} blocker, verapamil on microconidial germination and CAT fusion.

5.3.1.3 Calmidazolium

Concentrations of 0.5-20 μM calmidazolium were tested (Fig 5.3). Germination in 1% PDB alone and in 1% PDB with $NaNO_3$ was completely inhibited at 10 μM (Fig 5.3). CAT fusion was more sensitive than germination to calmidazolium and was completely inhibited by 5 μM. The IC_{50} value of calmidazolium on germination and CAT fusion was 2-5 μM in both media whereas the IC_{50} value for CAT fusion was 2-3 μM (Fig 5.3).
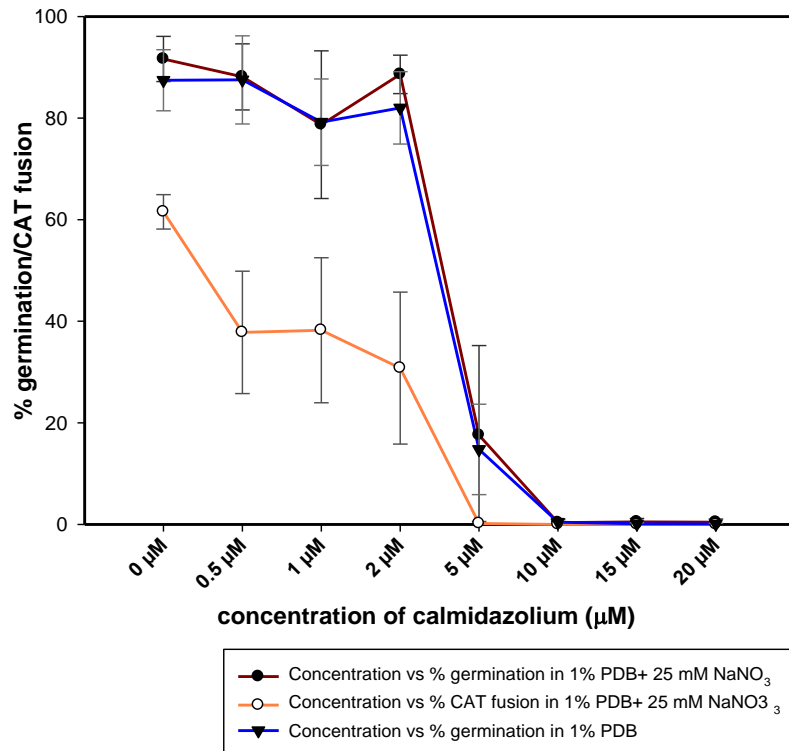
Figure 5.3 Effect of the calmodulin inhibitor, calmidazolium, on microconidial germination and CAT fusion.

5.3.1.4 FK506

Concentrations of 0.01-20 µM FK506 were tested. Neither germination nor CAT fusion were inhibited by even the highest concentration of FK506 used in either of the growth media (Fig 5.4).
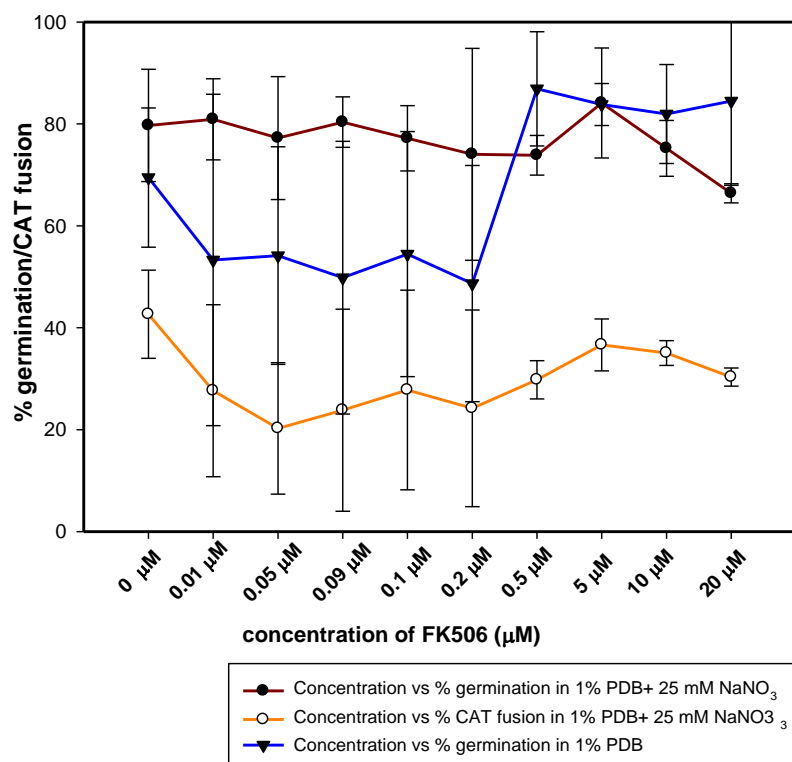
Figure 5.4 Lack of an inhibitory effect of the calcineurin inhibitor, FK506, on microconidial germination and CAT fusion.

5.3.1.5 Thapsigargin

Concentrations of 1-35 μM thapsigargin were tested (Fig 5.5). Germination in 1% PDB or 1% PDB with NaNO$_3$ was not significantly inhibited. CAT fusion, however, seemed to be significantly inhibited by thapsigargin in a dose dependent manner up to the highest concentration used (35 μM) (Fig 5.5). However, in these experiments the inhibitor was dissolved in DMSO and the concentration of DMSO increased as the concentration of thapsigargin increased. The 35 μM thapsigargin treatment contained 6% DMSO. When a control experiment was performed to determine the influence of 6% DMSO on CAT fusion it significantly inhibited CAT fusion (5.65 ± 1.58 % CAT fusion with 35 μM thapsigargin; 15.58% CAT fusion with 6% DMSO control; 31.41 ± 3.50 % CAT fusion in control media with no DMSO and thapsigargin). Taking the inhibitory effect of 6% DMSO into account, there was only a small (but significant) inhibition of CAT fusion following treatment with 35 μM thapsigargin. An IC$_{50}$ value for CAT fusion was not determined because of the inhibitory effects of DMSO.
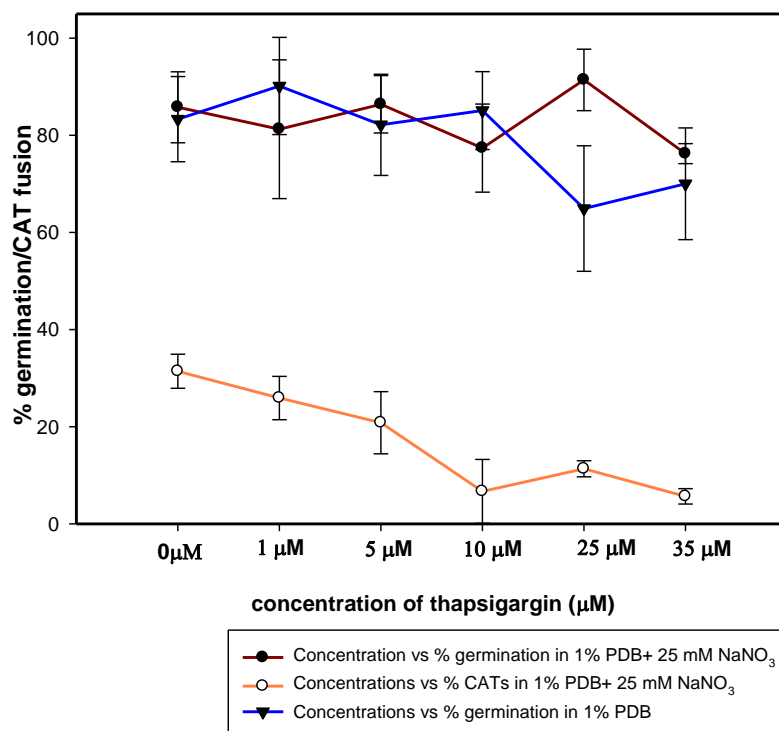
Figure 5.5 Effect of the ER Ca^{2+} ATPase inhibitor thapsigargin, on microconidial germination and CAT fusion.

5.3.1.6 RU360

Concentrations of 0.05-1 µM RU360 were tested (Fig 5.6). Germination in both 1% PDB and 1% PDB with $NaNO_3$ exhibited dose dependent inhibition with complete inhibition occurring with 1 µM RU360. CAT fusion also exhibited dose dependent inhibition and was completely inhibited by 0.5 µM RU360 (Fig 5.6). The IC_{50} value of RU360 on germination was 0.25-0.5 µM in both media whereas the IC_{50} value for CAT fusion was 0.15-0.25 µM
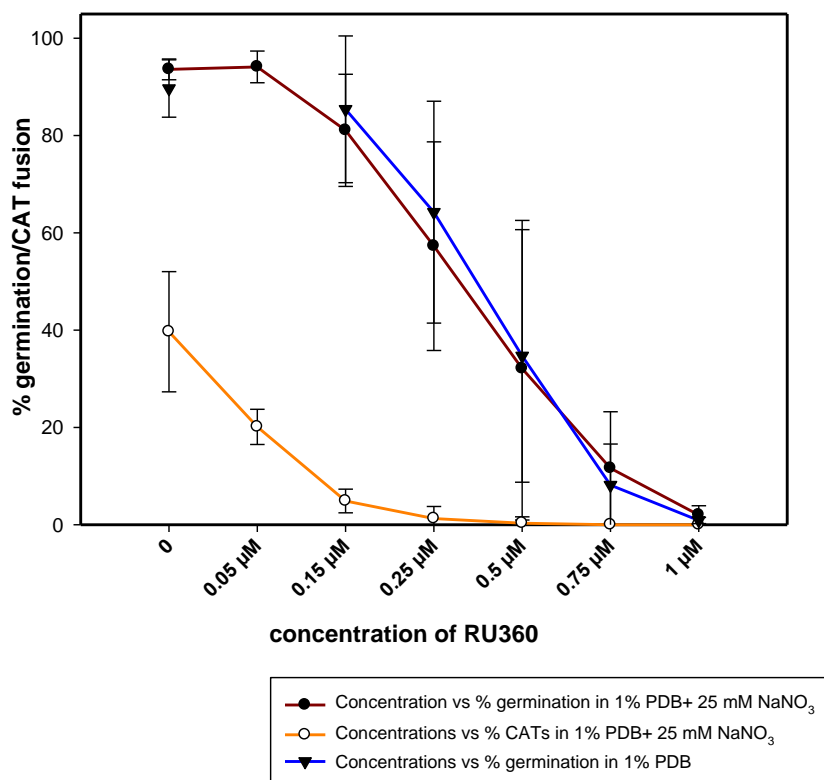
Figure 5.6 Effect of the mitochondrial Ca^{2+} uniporter inhibitor, RU360, on microconidial germination and CAT fusion.

5.4 Discussion

Results obtained using the Ca^{2+} chelator, BAPTA, showed that extracellular calcium is required for CAT fusion but not for germination as previously reported for CAT fusion in *N. crassa* (Hernandez-Ortez *et al*., in prep). Using the L-type Ca^{2+} channel blocker verapamil, or the calmodulin inhibitor calmidazolium, both germination and CAT fusion were inhibited but CAT fusion in each case was more sensitive to this inhibitor. Again similar results were obtained with verapamil and the calmodulin inhibitor, TFP, in *N. crassa* (Hernandez-Ortiz *et al*., in prep). It was also found that the mitochondrial Ca^{2+} uniporter, RU360, inhibited both spore germination and CAT fusion with CAT fusion being more sensitive to this drug. This has not been reported before in *N. crassa* although RU360 was previously found to alter Ca^{2+} signature of the transient increase of $[Ca^{2+}]_c$ in response to staurosporine-induced cell death in this species (Goncalves *et al*., 2014).

We did not obtain inhibition of spore germination or CAT fusion with the calcineurin inhibitor, FK506, and neither did the ER Ca^{2+} ATPase inhibitor thapsigargin provide convincing evidence of inhibiting these processes.

Overall, my results provide provides clear evidence of a significant role for Ca^{2+} signalling in CAT fusion that involves the uptake of Ca^{2+} from the external environment by the Cch1 Ca^{2+} channel, and the involvement of the primary intracellular Ca^{2+} receptor, calmodulin, and the mitochondrial Ca^{2+} uniporter.

5.5 Summary

- Pharmacological evidence was obtained for Ca^{2+} signalling being important during microconidial germination and CAT fusion
- This evidence indicated that the Ca^{2+} signalling during CAT fusion involves the uptake of Ca^{2+} from the external environment by the Cch1 Ca^{2+} channel, and the involvement of the primary intracellular Ca^{2+} receptor, calmodulin, and the mitochondrial Ca^{2+} uniporter.
- A similar involvement of these components of the Ca^{2+} signalling machinery (i.e. cch1, calmodulin and the mitochondrial Ca^{2+} uniporter), was found for spore germination but it did not have a requirement for extracellular Ca^{2+}.
- CAT fusion is more sensitive to Ca^{2+} modulators that positively inhibit it than spore germination.
- Convincing pharmacological evidence was not obtained for the involvement of calcineurin or ER Ca^{2+}ATPase activity during spore germination and CAT fusion

Chapter 6: Live-cell imaging and analysis of *Fusarium* keratitis using an *ex vivo human* cornea infection model

6.1 Introduction

Despite *Fusarium* being a leading cause of keratitis (see section 1.7), there have been very few studies on the cytology of the infection process (Hu *et al*., 2014; Hua *et al*., 2010; Schafer *et al*., 2014a; He *et al*., 2016). Most of the studies have used non-primate, mouse infection models (Ortoneda *et al*., 2004; Schafer *et al*., 2014a, Lee *et al*., 2016*)*. Such studies have characterised morphological features of the fungus such as the presence of chlamydospores and microconidia within the host tissue. Several studies have also reported the role of host immune cells during *Fusarium* keratitis (Karthikeyan *et al*., 2011; Che *et al*., 2012; Hu *et al*., 2014; Kadri *et al*., 2015). However, detailed cell biology studies involving live-cell imaging of the infection during *Fusarium* keratitis (or fungal keratitis in general) are lacking and will be important for diagnostic purposes (see section 1.10).

Scanning laser ophthalmoscopy (SLO) is a confocal microscope technique used for diagnostic *in vivo* imaging of the human cornea or retina. Different types of SLO devices have been developed (Sharp *et al*., 2004). A commonly used SLO system in eye hospitals is the Heidelberg Retina Tomograph (HRT) equipped with the Rostock Cornea Module (Heidelberg Engineering, www.heidelbergengineering.com). This instrument has been specifically developed for diagnostic *in vivo* imaging of human corneas (e.g Jullienne *et al*., 2015). It uses reflection-based confocal imaging with very fast laser scanning at long, near infrared wavelengths to prevent harmful effects to patients' eyes and image deeper within them. This type of confocal live-cell imaging contrasts with that imaging used for research purposes which normally involve exposing living tissue stained with, or expressing a genetically encoded, fluorescent probe. The latter type of confocal fluorescence microscope can achieve higher resolution and selective labelling of cells than SLO used in the reflection mode within a clinical setting, but is more harmful to the living tissue. An important advantage of using reflection-based confocal system is that tissue or cells can be imaged label-free.

6.3 Results

6.3.1 Morphological characterisation of infection of the *ex vivo* human cornea by live-cell imaging

Z-stacks of confocal optical sections were collected from uninfected corneal tissue to determine the normal morphology of the outermost layers of the *ex vivo* human cornea model. Fig. 6.1 shows the outer regions (epithelium and Bowman's membrane) of uninfected human cornea cultured for 6 days. The uppermost region of the epithelial layer is composed of squamous epithelial cells (Figs. 6.1A-6.1B) that overlays tightly packed columnar cells, which form the basal region of the epithelium (Fig. 6.1C). Beneath this is the Bowman's membrane (Fig. 6.1D) and stroma. The latter could not be visualized but was not readily distinguished from the tissues above because it was unstained and lacked sufficient contrast. Even deeper layers of cornea, Descemet's membrane and endothelium could not be imaged with the confocal microscope because of the reduced signal, reduced resolution and increased optical aberration at depth. The maximum depth that can be usually imaged in the cornea is ~ 100 μm. Thus live-cell confocal imaging was performed to characterise the initial stages of development of *F. oxysporum* germlings during infection of *ex vivo* human cornea down to this depth.
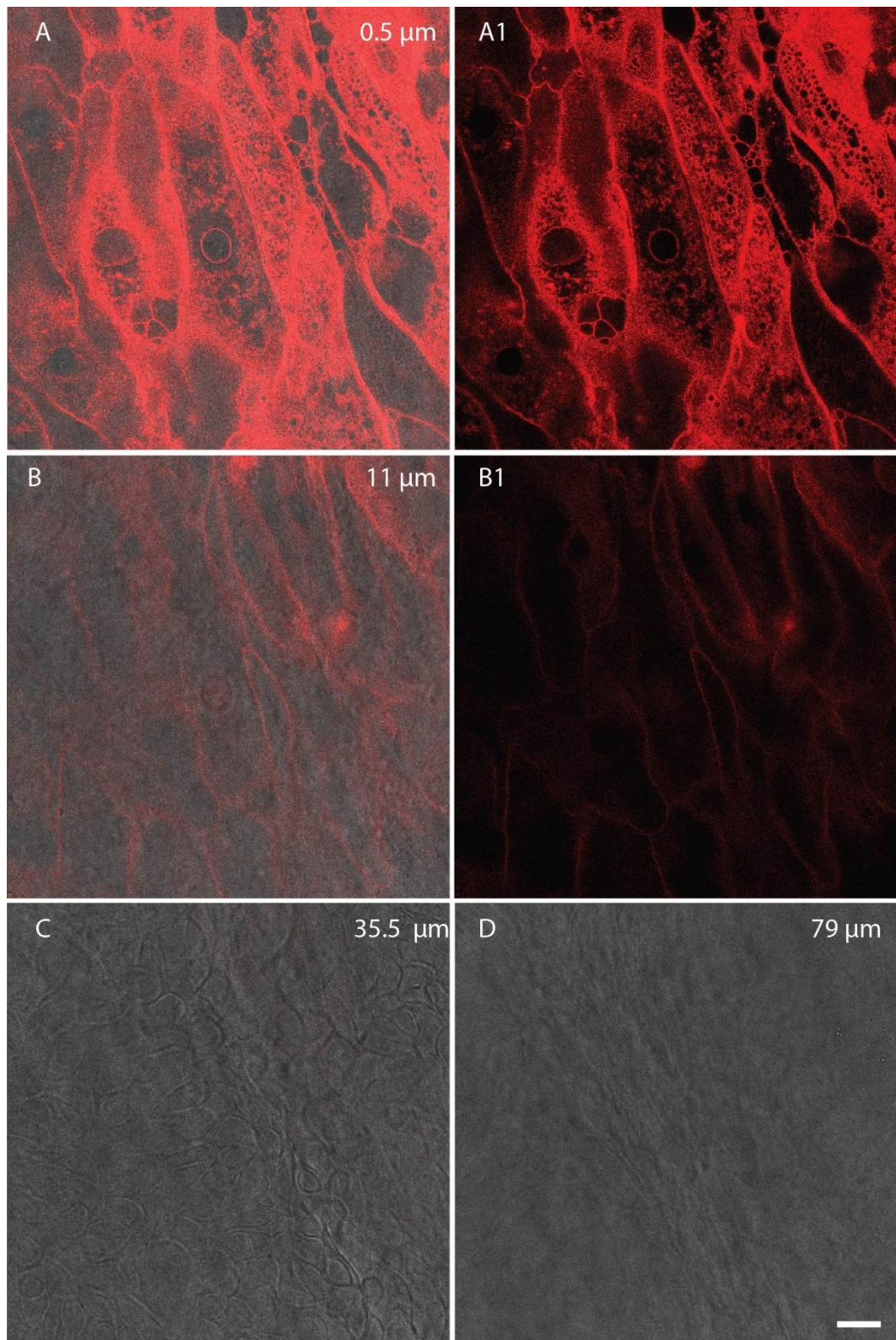
Fig. 6.1 Outer layers of the cornea. **(A, A1, B, B1)** Surface epithelium at different depths after staining with FM4-64. A and B are overlays of the brightfield and fluorescence channels; A1 and B1 are the fluorescence channel alone). **(C)** Brightfield image of the basal layer of the epithelium. **(D)** Brightfield image of the Bowman's membrane beneath the epithelium. The depth from the corneal surface is shown in the top right hand corner of (A-D). Scale bar = 20 μm.

The cytoplasmic GFP expressing wild type strain of *F. oxysporum* was used for live-cell imaging of the infection of the cornea. Microconidial germination on the corneal surface started to occur ~ 8 h post inoculation (hpi). Most microconidia that germinated produced two germ tubes and these emerged at opposite poles of the spores (Fig. 6.2). This bidirectional germination contrasts with the results obtained *in vitro* in which the microconidia only formed single germ tubes (section 3.3.1; Figs. 3.1A, 3.1B). The germ tubes then grew and branched to form a microcolony on the corneal surface (Fig. 6.3). Conidial anastomosis tube (CAT) fusion was observed on the corneal surface when high concentrations of microconidia were locally present on the corneal surface at the site of infection, particularly when using higher inoculum concentrations of 1 x 10^7 microconidia per ml (Fig. 6.4). This is different from the optimal concentration of 1x10^6 microconidia per ml for CAT fusion as described in chapter 3 (section 3.3.3), as the convex shaped cornea provides a larger surface area for the spread of germlings during inoculation compared to the smaller wells of 8 well slide culture chambers used for *in vitro* assays. Extensive hyphal branching and hyphal fusions occurred in developing colonies between 16 and 20 hpi (Fig. 6.5). Hyphal avoidance was observed between hyphal branches of the same colony derived from a single spore germination (Fig. 6.6). Penetration of epithelium occurred between 12 and 48 hpi after extensive surface colonisation (Fig. 6.7). Microconidia were formed both on the corneal surface (not shown) and within the epithelial tissue at depths of 45 μm between 24 and 48 hpi (Fig. 6.8) In clinical case reports of fusariosis, microconidiation has often been termed 'adventitious sporulation' (Thomas *et al*., 2011; Nucci *et al*., 2015; Lockwood and Crescencio, 2016). Figure 6.8 shows microconidia being formed from a conidiogenous cell at a depth of 45 μm. Figure 6.9 shows another example of microconidial formation within the corneal tissue that occurred over a period of 195 min. The formation of thick-walled intercalary chlamydospore was observed at depths of 21.5 μm within the corneal tissue (Fig. 6.10). Increased septation, and thus shorter hyphal compartments, were observed in hyphae that had penetrated to the basal region of the epithelium and Bowman's membrane compared with hyphae growing on or close to the upper epithelial tissue (Fig. 6.11). Thicker hyphae, interstitial chlamydospore formation and adventitious microconidiation were observed from hyphae which had penetrated into the corneal tissue as observed at the 48 hpi time point in Figs. 6.8, 6.9, 6.10 and 6.11. Hyphal fusion was only prominent on the surface of the epithelial tissue and was not clearly evident within the tissue. However, macroconidia, a defining morphological

feature of *Fusarium* species (section 1.1) were not observed on the surface or in the host tissue within 48 hpi.
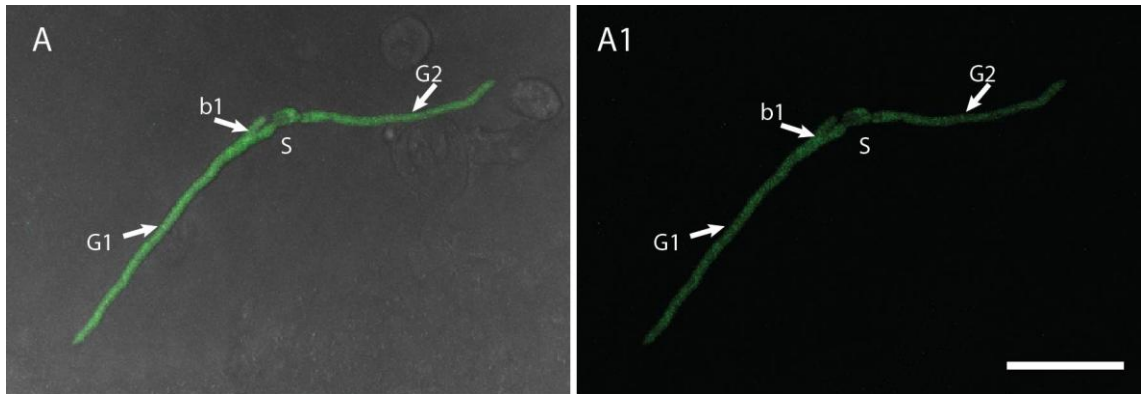
Fig. 6.2. Microconidium (S) that has produced two bidirectionally growing germ tubes (G1 and G2) from each pole on the surface of corneal tissue at 20 hpi. A small backwardly growing branch (b1) has also formed. Overlay of fluorescence and brightfield channels in (A) and fluorescence channel alone only in (A1). Scale bar = 40 µm.
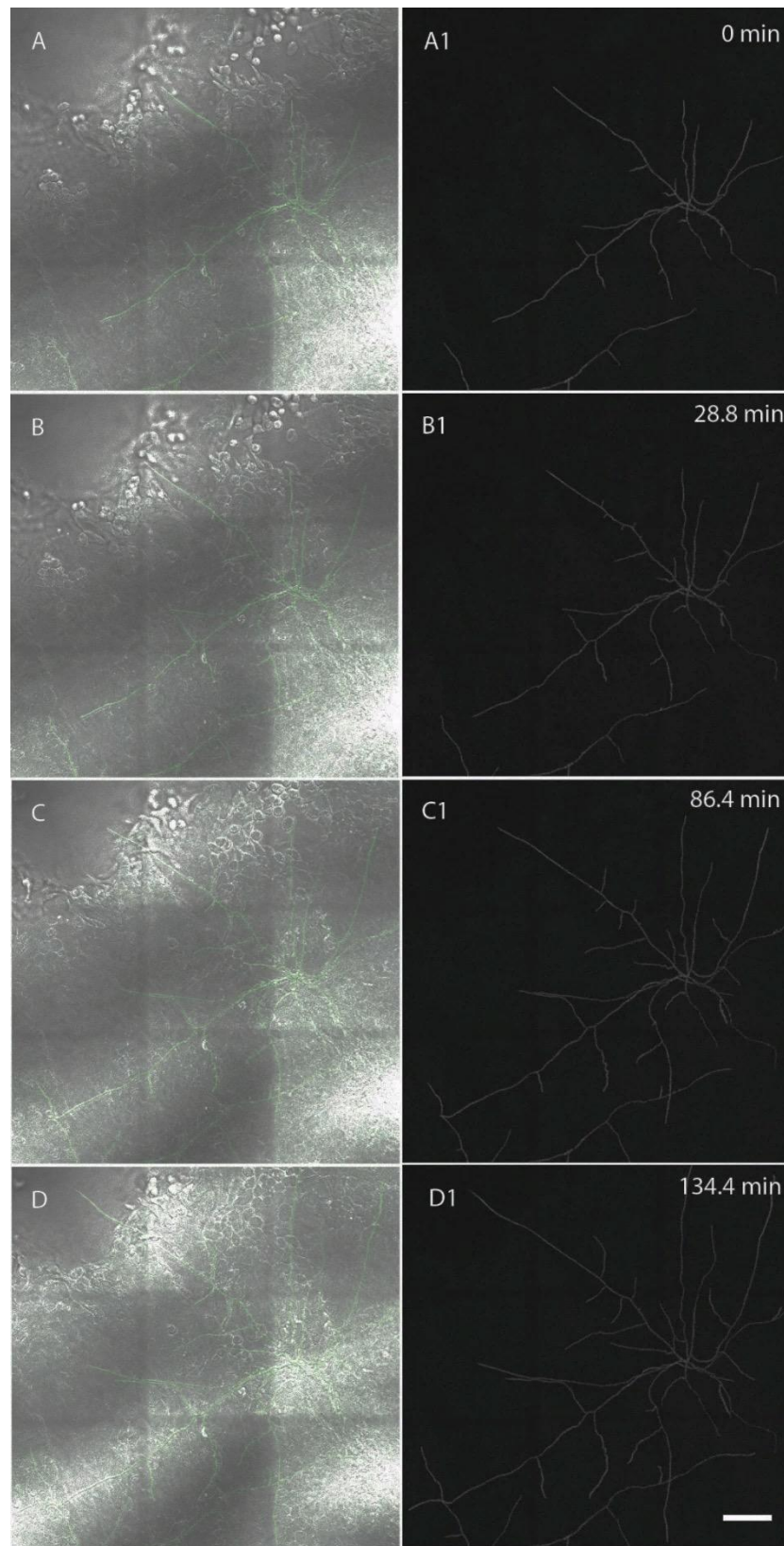
Fig. 6.3. Time-lapse imaging of the surface colonisation of the cornea by hyphae of the ecytoplasmic GFP expressing strain. Time lapse imaging initiated at 28 hpi. (A-D) show overlays of the fluorescence and brightfield channels whilst (A1-D1) show the fluorescence channel only. Note the artefactual dark lines distinguishing the 9 image fields that were

automatically stitched together using the LASAF software during imaging to visualize larger field of view (section 2.17). Scale bar = 100 μm (also see Movie 6.3).
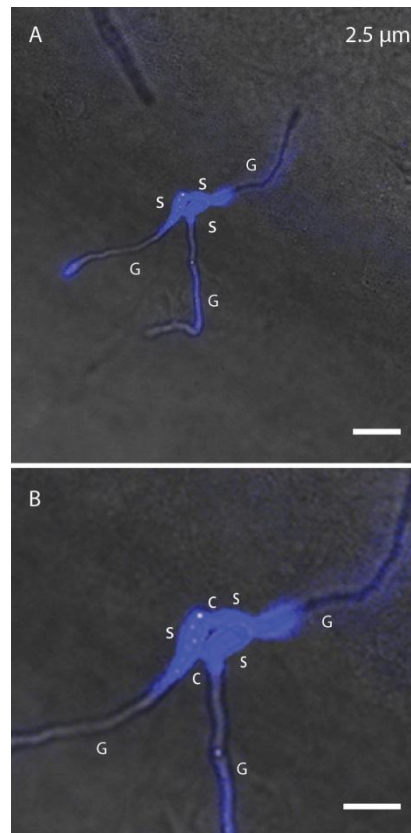
Fig. 6.4. Germlings of the wild type undergoing CAT fusion on the corneal surface at 16 hpi after staining with calcofluor white. **(A)** CAT fusion between three germlings. Scale bar = 20 μm. **(B)** Magnified view of CAT fusion between germlings shown in (A). Scale bar = 10 μm. Germlings stained with Calcofluor white with an overlay of the fluorescence and brightfield channels, S, spore, G, germ tube, C, CAT fusion.
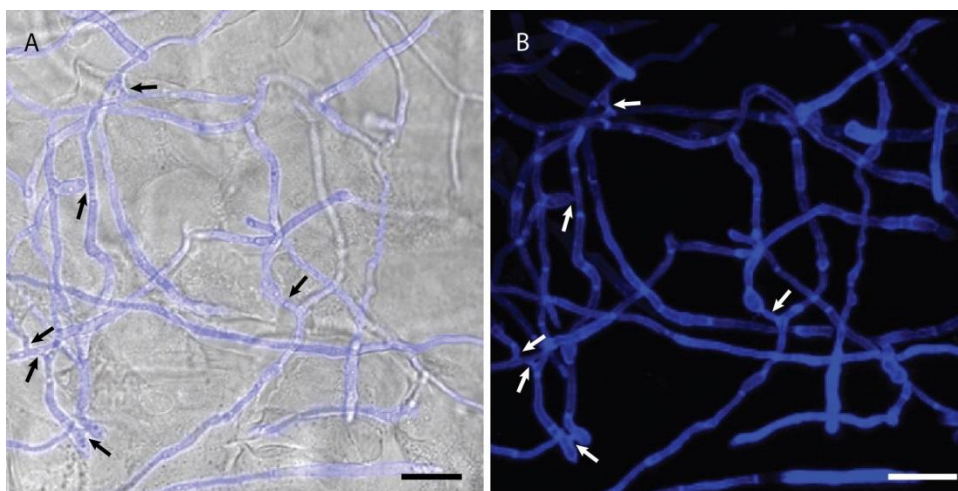
Fig. 6.5. Hyphal branching and hyphal fusions (arrows) of the wild type on the corneal surface after staining with calcofluor white at 48 hpi. **(A)** Overlay of both brightfield and fluorescence channels. (B) Fluorescence channel only. Scale bar = 20 μm.
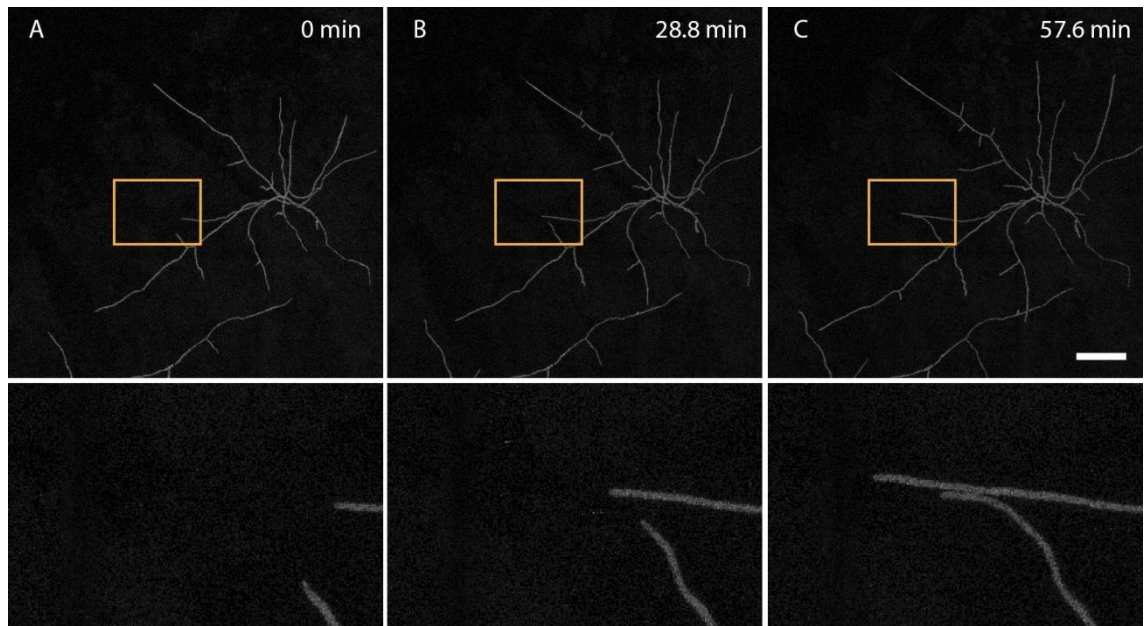
Fig. 6.6. Hyphal avoidance exhibited by hyphae from the same colony on the corneal surface at 28 hpi. **(A-C)** Time course of colony growth by the cytoplasmic GFP expressing strain growing on the corneal surface. Highlighted regions within the yellow boxes in the upper images are shown at higher magnification in the lower images. Scale bar = 70 μm.
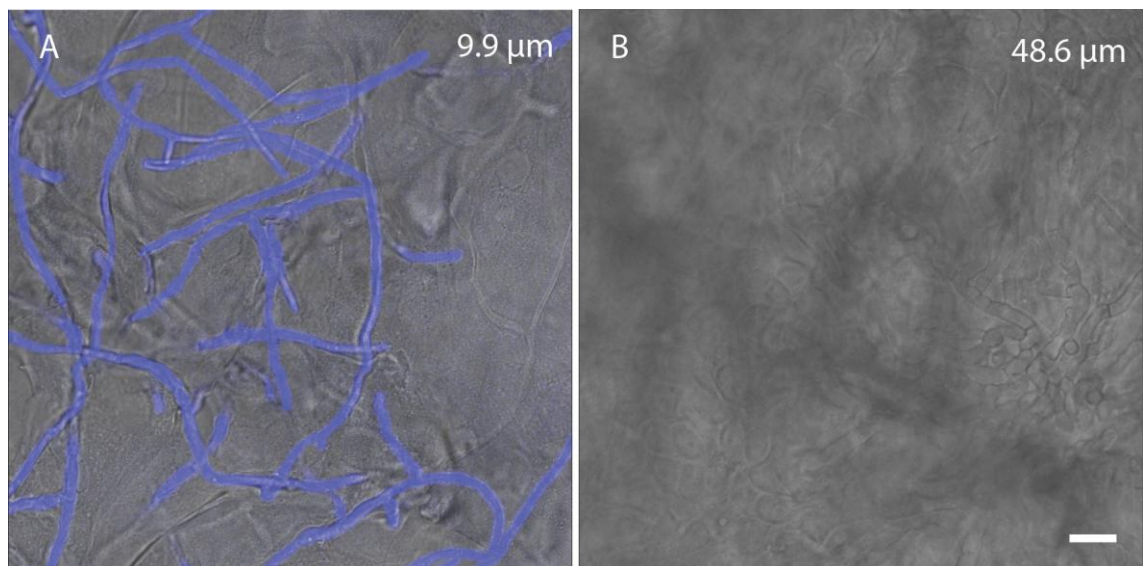
Fig. 6.7 Penetration of corneal epithelial tissue by wild type hyphae at 48 hpi. **(A)** Hyphal colonisation at a depth of 9.9 μm below the surface epithelial layer. Hyphae are stained in blue by calcofluor white staining. Overlay of fluorescence and brightfield channels. **(B)** Fungal

hyphae colonisation at a depth of 48.6 µm. Brightfield channel only shown because the calcofluor white dye did not penetrate to this depth. Scale bar = 15 µm.
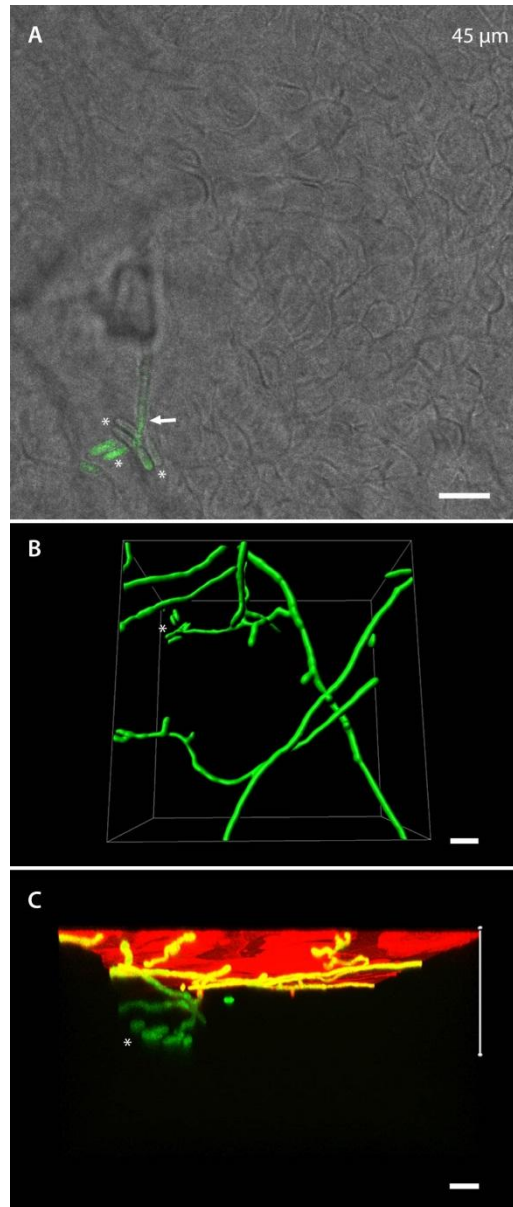
Fig. 6.8 Microconidiation of the GFP expressing strain within corneal tissue and imaged by 3D confocal microscopy. **(A)** Optical section 45 μm below the epithelial surface within a z-stack showing microconidia (in green, asterisks) formed by a conidiogenous hyphae (arrow). **(B)** Top view of the surface rendered z-stack (fluorescence channel alone) showing the formation of microconidia (asterisks). **(C)** Side view of 3D projection of z-stack of optical sections showing microconidiation (asterisks) occuring within the tissue. Top layer shown in red is the surface epithelial layer stained with FM4-64. The yellow hyphae show co-localization of the GFP and FM4-64 within the hyphae whilst the green hyphae are below the region of FM4-64 penetration into the tissue. Scale bar = 45 µm.
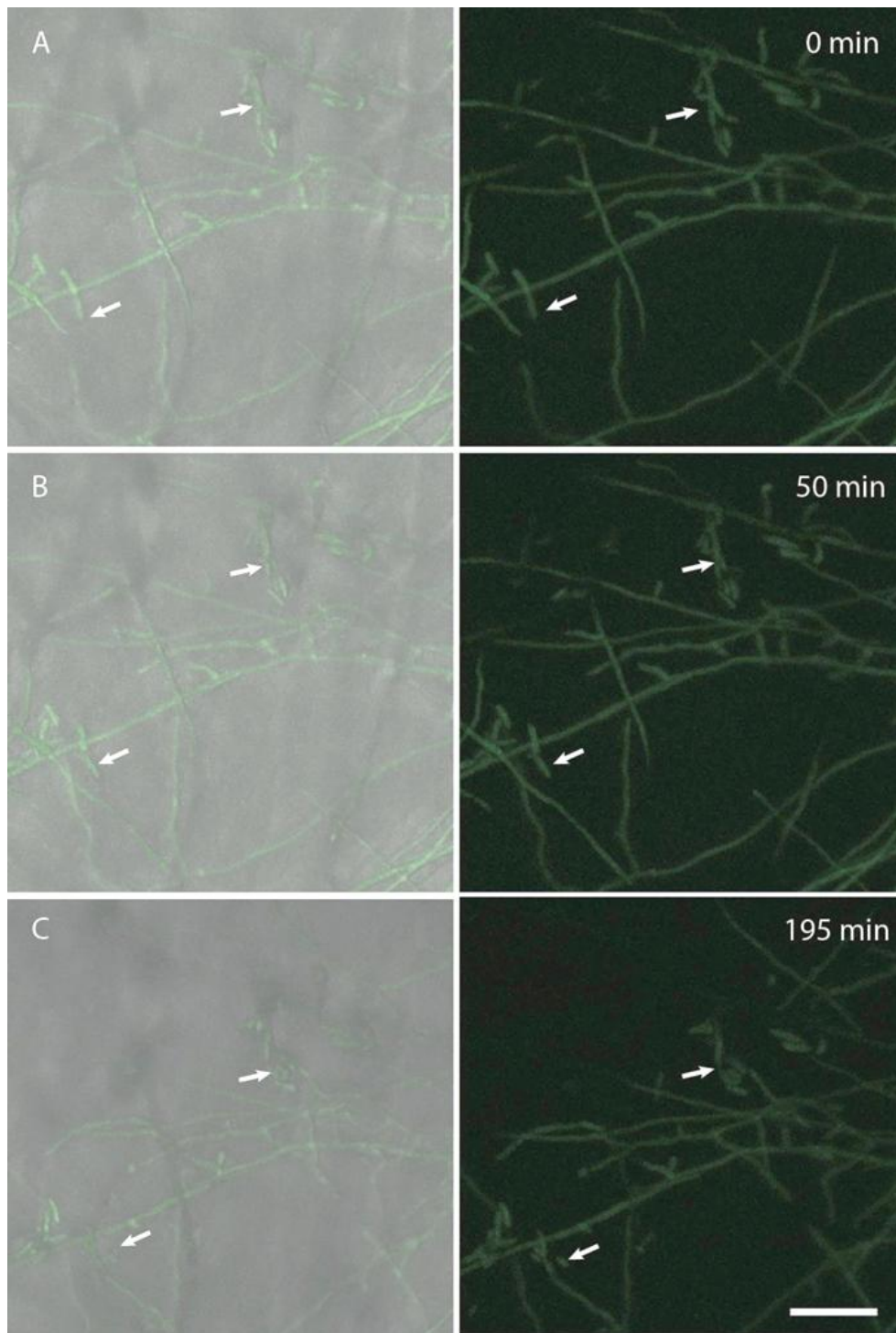
Fig. 6.9 Microconidiation by the GFP-expressing strain within corneal tissue. **(A-C)** Time course of microconidiation within a projection of a z-stack of optical sections from 1-34 μm below the epithelial surface. Arrows indicate sites of microconidiation. The images on the left are an overlay of the fluorescence and bright field channels whilst on the right the images are of the fluorescence channel alone. Scale bar = 40 μm.
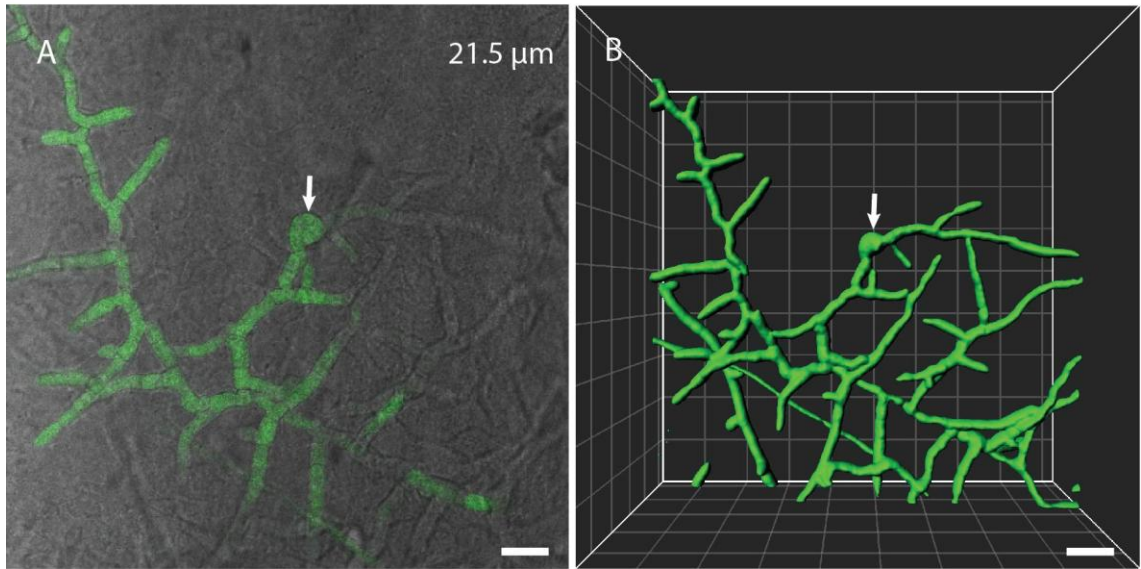
Fig. 6.10. Interstitial chlamydospore formation exhibited by the GFP expressing strain within corneal tissue. **(A)** A single optical section at a depth of 21.5 μm which shows the GFP-labelled branched hyphae with an interstitial chlamydospore (arrow). Overlay of the confocal fluorescence channel and widefield brightfield channels. Scale bar = 15 μm. **(B)** Side view of the surface rendered hyphae within a 3D projection of the same z-stack from which (A) is shown. Scale bar = 20 μm.
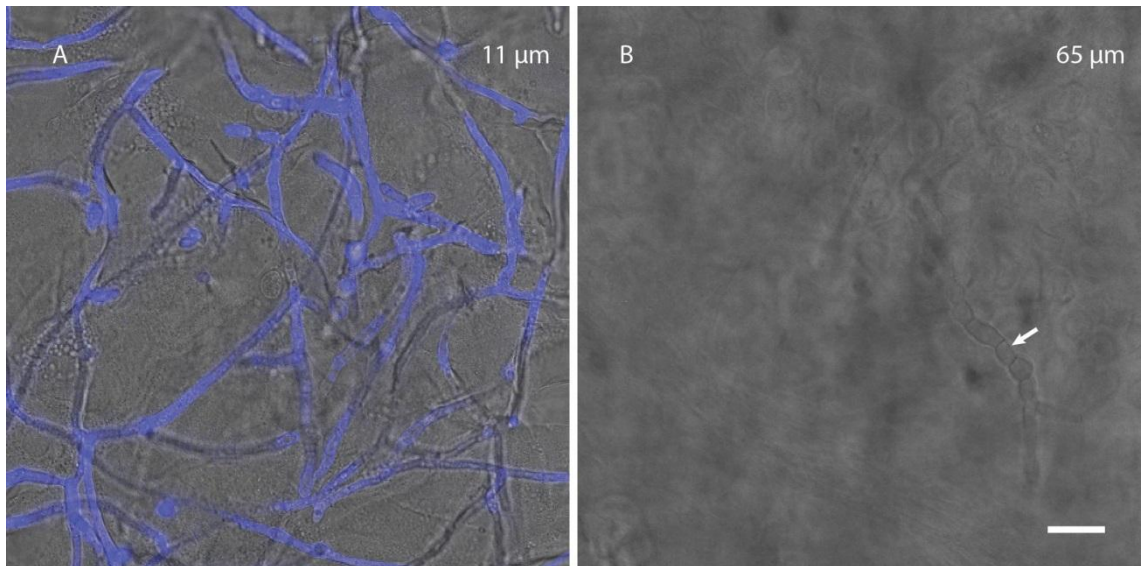
Fig. 6.11. Morphological differences observed between hyphae close to the corneal surface and deeper within the corneal tissue. **(A)** Calcofluor white stained hyphae in the upper region of the epithelial tissue at a depth of 11 μm depth from the corneal surface. Overlay of fluorescence and brightfield channels. **(B)** Hyphae growing just below the basal epithelial layer at a depth of 65 μm from the corneal surface. These hyphae have more septa, and thus shorter hyphal compartments, than those shown in (A). Brightfield channel only because the calcofluor dye does not penetrate this deep into the corneal tissue. Scale bar = 20 μm.

6.3.2 Quantitative traits measured from image data of *ex vivo* *Fusarium* infection

6.3.2.1   Depth of fungal penetration into the corneal tissue

The depth of penetration by fungal hyphae was determined as the depth from the uppermost surface of the epithelium labelled with fluorescent stain FM4-64 to the deepest point in the z-stack of images in which the fungal hyphae can be observed. Imaging was possible only up to a maximum depth of 100 μm because of fluorescence signal attenuation. The depth of penetration into human corneas by the wild type strain of *F. oxysporum* at different time points were compared. A significant increase in depth from 18.46 ± 6.5 at 16 hpi to 58 ± 16 at 48 hpi was observed (Fig. 6.12; $p < 0.0001$).
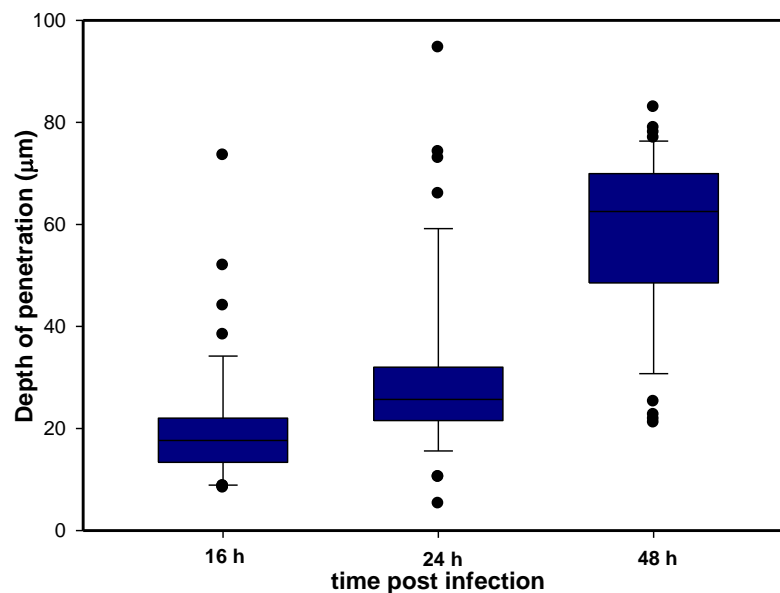
Fig. 6.12. Depth of penetration by hyphae of *ex vivo* human corneas at 16, 24 and 48 hpi. The depth of penetration at 16 hpi was 20.22 ± 12.10 μm whilst that at 24 hpi was 30.57 ± 18.20 μm. At 48 hpi, the depth of penetration was 58.30 ± 16.13 μm (n = 45 datasets from 3 different experimental repeats). The differences observed at 16, 24 and 48 hpi for depth of penetration was significant ($p < 0.0001$ from one-way ANOVA).

A difference was observed in the regeneration of the epithelial layers of the *ex vivo* cornea cultured for different numbers of days. Surface squamous epithelial cell layers were found to be regenerated when corneas were cultured for 6 days. The corneas cultured for 3 days only possessed the basal epithelial layer. The depth of penetration by fungal hyphae into corneas cultured for different days was analysed at 48 hpi from

infections of human corneas that had been previously cultured for 3 and 6 days (Fig. 6.13). The depth of penetration at 48 hpi of corneas culture for 3 days was 58.30 ± 16.13 μm and that of corneas cultured for 6 days was 49.85 ± 28.81 μm (n = 45 from 3 different experimental repeats). The difference in the mean depth of penetration at 48 hpi was not significantly different between the corneas cultured for the different periods of time ($p = 0.0897$ from an unpaired t-test). However, the use of corneas cultured for 3 days allowed the visualisation of infections in deeper regions of the cornea because of the absence of an outermost squamous epithelial region (see section 1.8; Figs. 6.1A-6.1B).

The dependence of the depth of penetration of tissues by using different spore (microconidium) inoculum concentrations was analysed. A comparison of the depth of penetration at 48 hpi using 1×10^5 spores/ml and 1×10^7 spores/ml as inocula is shown in Fig. 6.14. The depth of penetration was 38.98 ± 23.43 μm when the inoculum concentration was 1×10^5 spores/ml whilst it was 51.78 ± 32.14 μm when the higher concentration of 1×10^7 spores/ml was used (n = 30 datasets from 3 different experimental repeats). However these values were not significantly different ($p = 0.083$ from unpaired t-test).
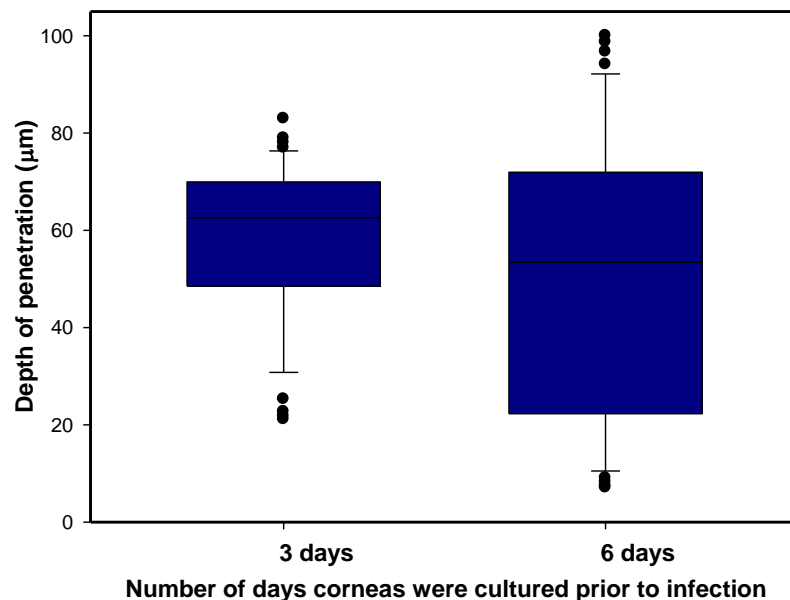
Fig. 6.13. Depth of penetration at 48 hpi by hyphae of corneas cultured for 3 and 6 days. Depth of penetration was 58.30 ± 16.13 μm (n = 45 from 3 different experimental repeats) when the corneas were cultured for 3 days alone whilst that of 6 days cultured cornea was 49.85 ± 28.81 μm (n = 45 from 3 different experimental repeat). There was no significant difference between the two groups in depth of penetration ($p = 0.089$ from an unpaired t-test).
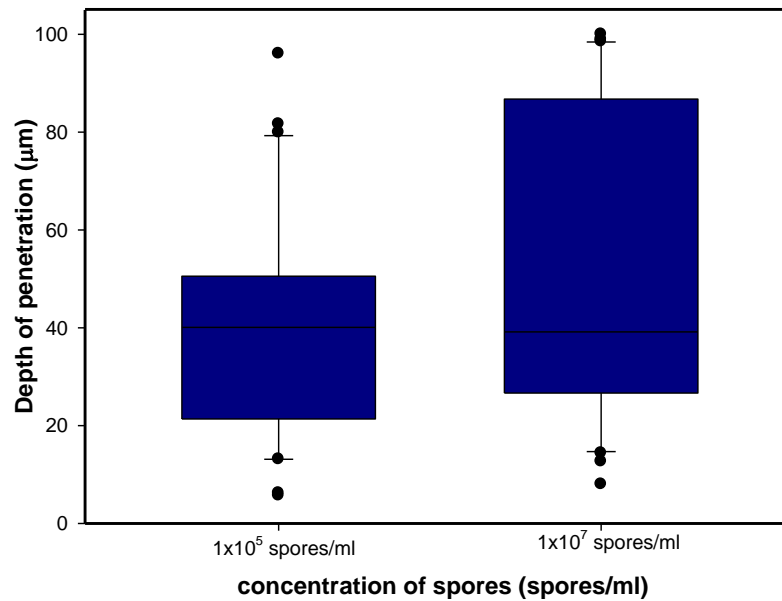
Fig. 6.14. Depth of penetration by hyphae of *ex vivo* human corneas at 48 hpi using different concentrations of microconidia as inocula to initiate the infection. The depth of penetration was 38.98 ± 23.43 µm when 1×10^5 spores/ml were used whilst the depth of penetration was 51.78 ± 32.14 µm when 1×10^7 spores/ml was used (n = 30 datasets from 3 different experimental repeats). There was no significant difference between the two concentrations with regard to the depth of penetration at 48 hpi ($p = 0.083$ from unpaired t-test).

The influences of scratching the corneal surface and immunosuppression with hydrocortisone on fungal infection were analysed. This was done by comparing the depth of penetration by hyphae at 48 hpi between untreated (no needle scratching and hydrocortisone) and treated (needle scratch and hydrocortisone) corneas. No significant difference in depth of penetration was observed between the treated and untreated groups ($p = 0.47$ from Two-way ANOVA).
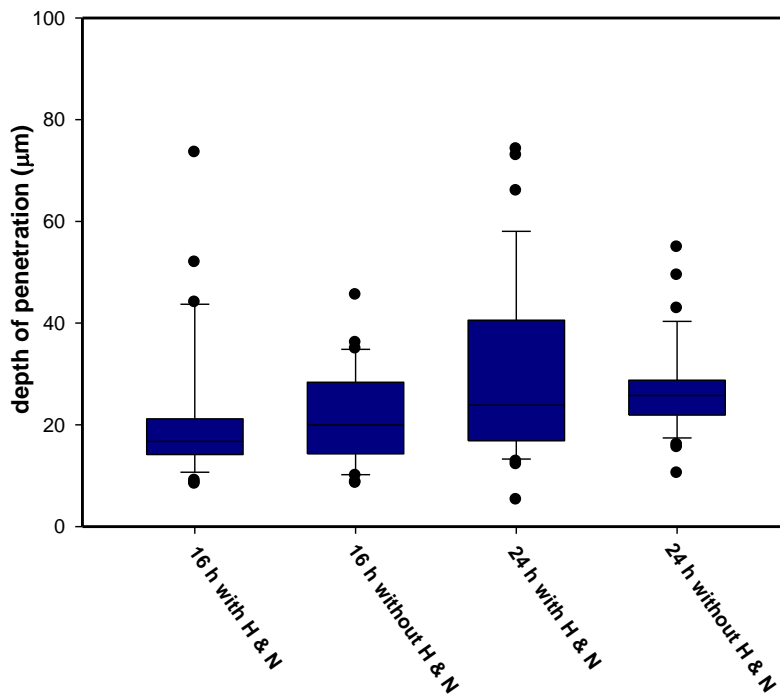
Fig. 6.15. Comparison of the depth of penetration by hyphae of corneas at 16 hpi and 24 hpi or after hydrocortisone (H) treatment and needle (N) scratching and without these treatments. The depth of penetration was 21.15 ± 13.47 µm at 16 hpi in the case of the treatment with hydrocortisone and needle scratching on the corneal surface whilst it was 21.60 ± 9.31 µm in the absence of both treatments. At 24 hpi, the depth of penetration was 30.05 ± 17.65 µm for hydrocortisone treated cornea with needle scratching and 26.52 ± 8.63 µm for untreated corneas. The *p* value were 0.21 and 0.88 for 16 and 24 hpi, respectively (n = 36 datasets from three different experimental repeats). There was no significant difference (*p* = 0.47 from Two-way ANOVA) between the datasets involving infection after treatment with hydrocortisone and needle scratching compared to the untreated corneas after culturing for 16 h and 24 h.

6.3.2.2 Fungal volume within infected corneal tissue

The total cell volume of the cytoplasmic GFP expressing strain of *F. oxysporum* within the infected corneal tissue at 48 hpi was determined by creating 'iso-surfaces' of the fungal hyphae with the Imaris software (see section 2.16). The volume of iso-surfaces created from the fungal fluorescent signal represented the volume occupied by the hyphal cytoplasm within the infected cornea (Fig. 6.16). Attempts to use calcofluor white, a fungal cell wall stain failed because the dye did not penetrate into the host tissue beyond ~ 40 µm (see Fig. 6.7). Fluorescence attenuation of the fluorescence signal from cytoplasmic GFP expressing strain also prevented the measurement of fungal volume because this was dependent on a strong enough fluorescence in order to create unbroken iso-surfaces of the fungal hyphae (Fig. 6.17). Hence this method could

not be used for measuring fungal cell volume in deeper regions of infection by this GFP expressing strain.
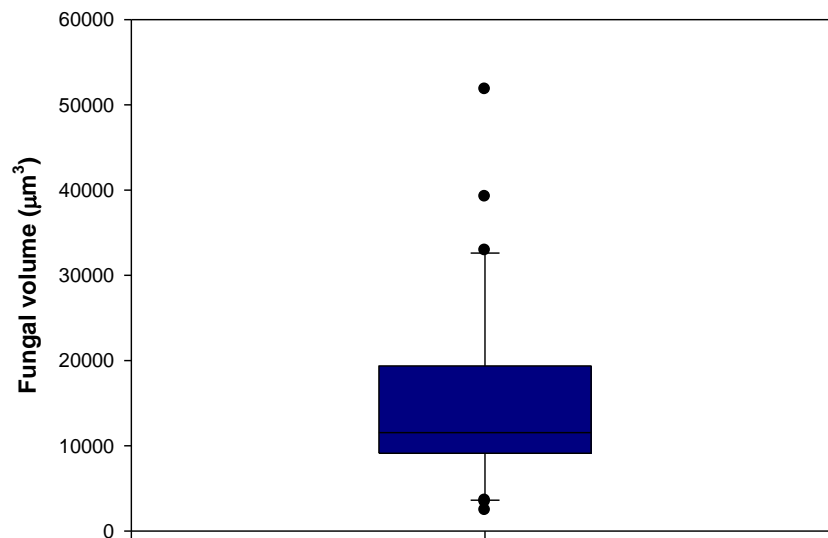
Fig. 6.16 Fungal volume of *F. oxysporum* cytoplasmic GFP strain infected corneal tissue at 48 hpi. The fungal volume was $15146.19 \pm 11113.16 \ \mu m^3$ at 48 hpi for this strain (n = 30 from three different experimental repeats).
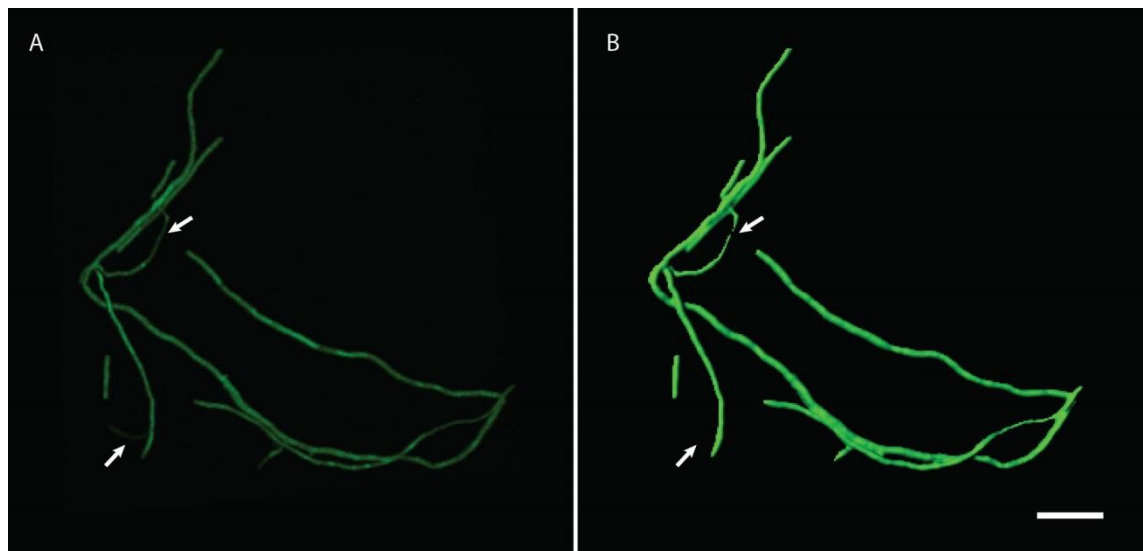
Fig 6.17 Problem with determining fungal volume from fluorescence images using Imaris. Fluorescence attenuation, leading to the detection of weak fluorescence signal, can affect the creation of unbroken iso-surfaces of fungal hyphae, as seen in the regions indicated by arrows. **(A)** 3D volume of a z-stack of hyphae expressing cytoplasmic GFP within an infected cornea. **(B)** Iso-surface of the stack shown in (A) created using the Surpass module of Imaris. Scale bar = 30 μm.

6.3.2.3 Branch angles and hyphal growth units of fungal hyphae within infected corneal tissue

Branching by *Fusarium* hyphae in corneal tissue at 48 hpi was analysed by measuring branch angles, total length of all branches per unit volume, total number of branches per unit volume and hyphal growth units (see section 2.16; Figs. 6.17 and 6.18).

The average hyphal branch angle was 37° but the branch angles varied considerably. The majority of hyphae (~ 77%) exhibited branching angles ≤ 90°. Some hyphae did not form any branches which were given a branch angle of 0° (Fig. 6.18).

A comparison of the hyphal growth units (see section 2.18) under *ex vivo* and *in vitro* conditions were determined. 1 x 10^5 spores/ml was used for the *ex vivo* infection while an inoculum concentration of 1 x 10^3 spores/ml was used for the *in vitro* conditions (Fig 6.18A). The reason for using different inoculum concentrations was because the convex structure of cornea led to an uneven distribution of spores, which became concentrated around its periphery region of the cornea whilst under *in vitro* condition on the flat surface of solid agar growth medium in a Petri dish plate the spores were uniformly distributed. An appropriate concentration of spores to inoculate corneas with to provide a similar average spore concentration per unit area on the corneal surface as on surface of the surface of the PDA medium was empirically determined. An inoculum concentration of 5 x 10^5 spores per ml was used to achieve the same spore density on the corneal surface (~ 1.43 x 10^5 spores per μm^2) as on the PDA surface inoculated with 1 x 10^3 spores per ml. The hyphal growth unit (HGU) (i.e. total length of hyphae/number of hyphal tips) is a standard method for measuring an aspect of fungal colony growth (Trinci, 1974). For the cytoplasmic GFP expressing strain at 48 hpi in the infected cornea it was determined to be 86.96 ± 61.46 µm whereas growing on and within PDA it was 43.14 ± 24 µm. The HGU value was significantly higher during the infection of the cornea ($p < 0.0001$) which indicates a lower branching frequency of the fungus in the *ex vivo* infected tissue compared with the *in vitro* PDA (Fig 6.18A and 6.16B; $p < 0.0001$).
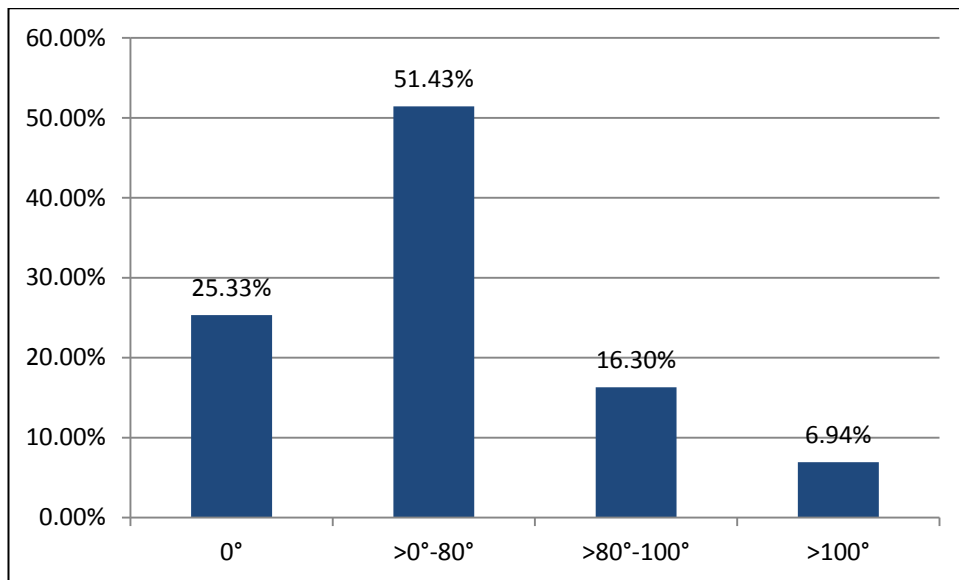
Fig. 6.18 The range of different hyphal branch angles exhibited by the cytoplasmic GFP expressing strain infecting corneal tissue at 48 hpi (n = 908 branches from 45 z-stacks and 3 different experimental repeats).
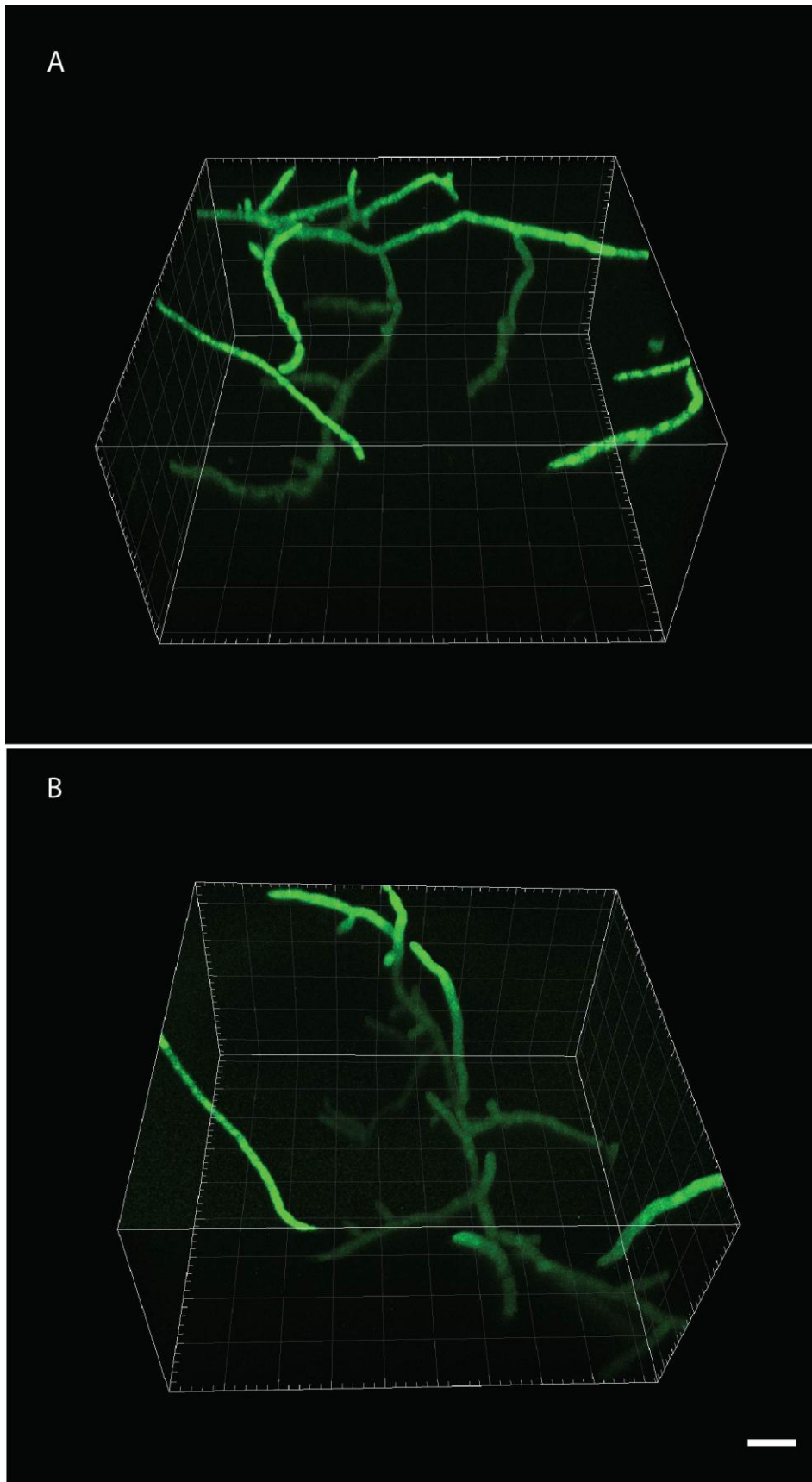
Fig. 6.19. Comparison of hyphal growth and branching by the cytoplasmic GFP expressing strain 48 hpi within *ex vivo* corneal tissue (A) and *in vitro* PDA (B). Scale bar = 20 μm.
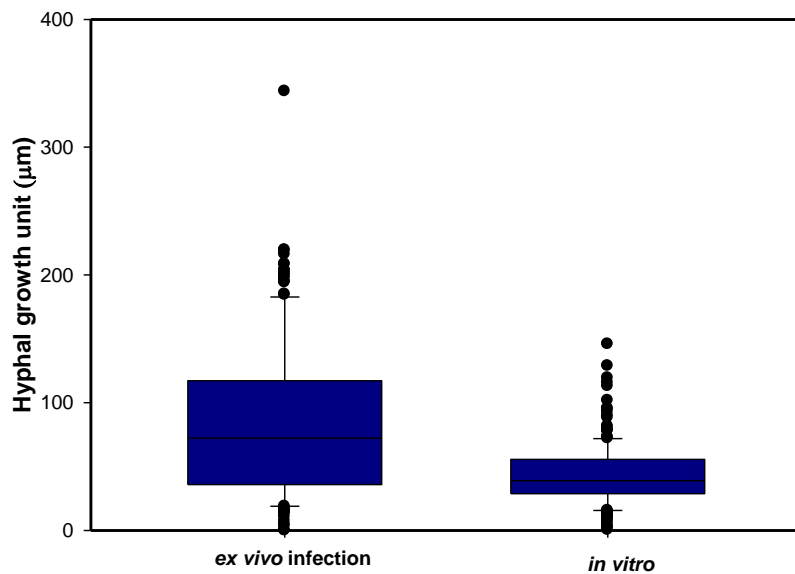
Fig. 6.20 Comparison of hyphal growth units of the cytoplasmic GFP expressing strain 48 hpi within *ex vivo* infected corneal tissue and *in vitro* PDA. The hyphal growth units were determined from 186 branches from three different experimental repeats under *ex vivo* conditions and 196 from three different experimental repeats under *in vitro* conditions.

6.3.3 Role of hyphal fusion during human infection

A comparison of the wild type strain of *F. oxysporum* and the Δ*fso* mutant which is defective in hyphal fusion (Prados Rosales and Di Pietro, 2008) was made to identify potential roles for hyphal fusion during human corneal infection. This was analysed in a variety of ways. At first, a verification of the Δ*fso* mutant being defective in CAT fusion was performed using the quantitative procedure described in section 2.7. The results from this experiment showed that the Δ*fso* mutant did not undergo CAT fusion but underwent the same level of microconidial germination as the wild type (Fig 6.20).
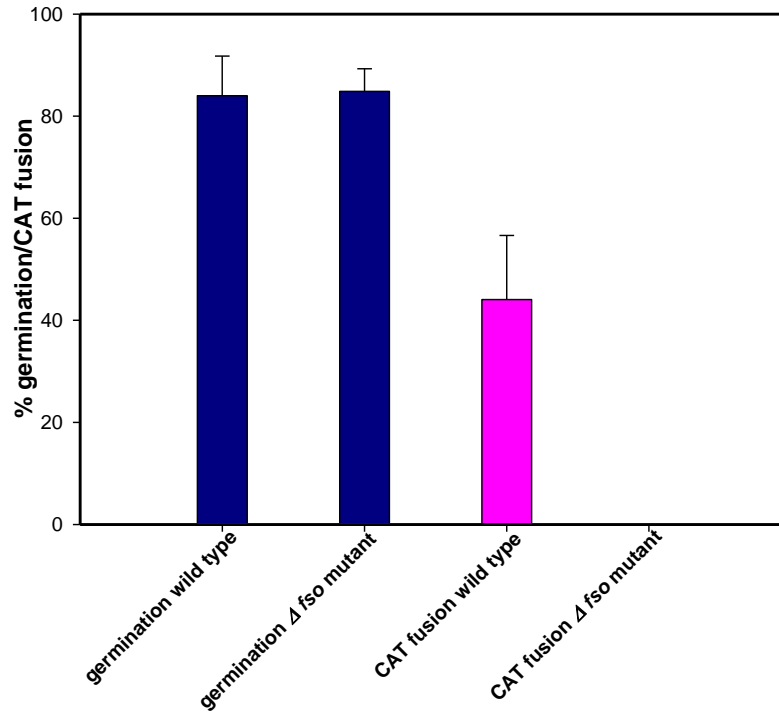
Fig. 6.21. Comparison of microconidial germination and CAT fusion in the wild type and the Δ*fso* mutant showing that CAT fusion does not occur in the mutant.

The *in vitro* microconidial production and viability of the two strains harvested from liquid growth media were determined by direct measurement of the number of spores produced using a haemocytometer and by counting the number of colony forming units (CFUs) involving the serial dilution and plating out of spores onto solid potato dextrose agar medium (see sections 2.14 and 2.15). Spore production by the two strains was compared by direct spore counts from 48 h grown cultures in two different media: (a) 100% PDB; (b) DMEM supplemented with 10% FCS and antibiotics (Fig. 6.20). There was no significant difference in spore production by the two strains on either medium (Fig. 6.20).
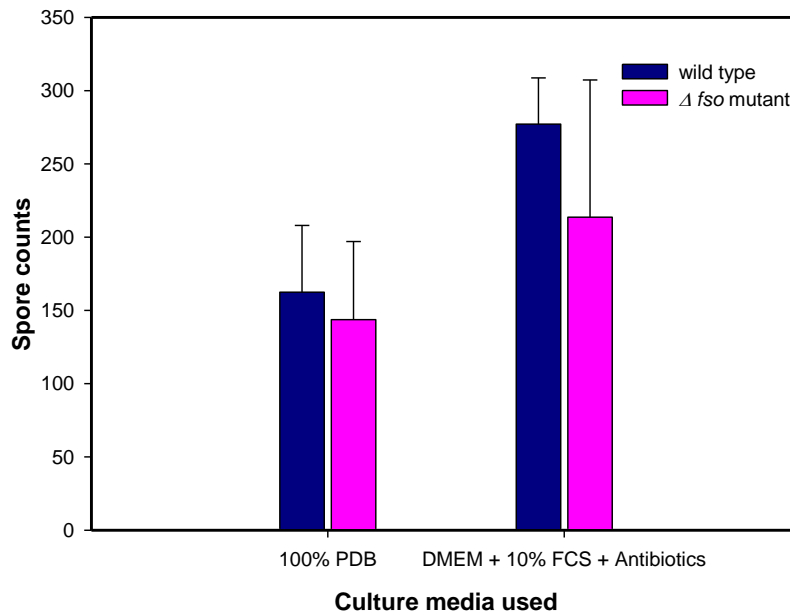
Fig. 6.22. Histogram showing direct measurement of the number of microconidia by the wild type and Δ *fso* mutant grown of liquid cultures in 100% PDB and DMEM + 10% FCS + antibiotics medium (see section 2.14) (n = 3). The spore count in 100% PDB media was 162.5 ± 45.47 per ml for the wild type and 143.67 ± 53.41 per ml for the *Δfso* mutant. The spore count in DMEM + 10% FCS + antibiotics media was 277.17 ± 31.51 per ml for the wild type and 213.67 ± 93.61 for the *Δfso* mutant. A *p* value of 0.27 was determined by a Two-way ANOVA analysis of these spore counts showing there was no significant difference in the number of spores produced by these two strains cultured in either media.

Figure 6.21 shows the CFUs measured from the wild type and Δ*fso* mutant strains harvested from 100% PDB grown cultures. There was no significant difference in the number of CFUs (and thus the spore viability) between these strains after PDA plates had been inoculated with an equal concentration of 1 x 10^4 spores/ml.
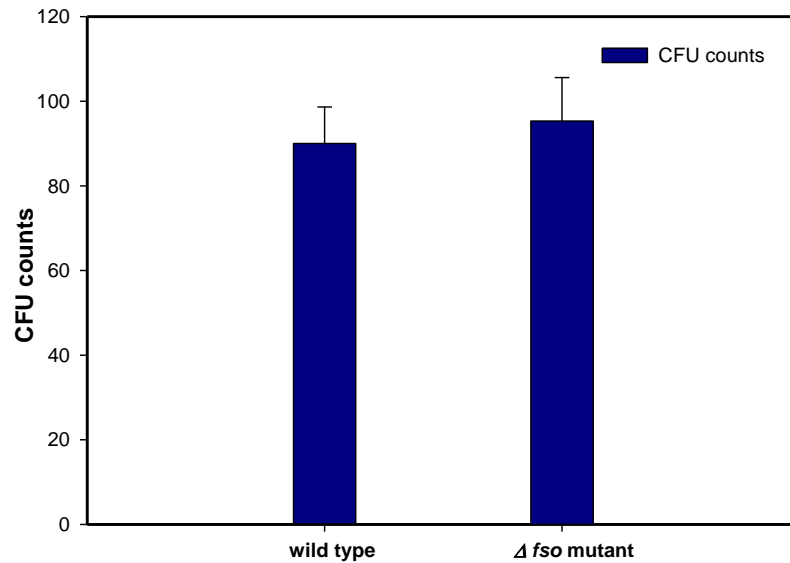
Fig. 6.23. Histogram showing CFUs from inocula of 1 x 10^4 spores/ml of the wild type and Δ *fso* mutant, respectively, to compare the spore viability (n = 3). The *p* value was determined to be 0.67 and hence there is no significant difference.

The depth of penetration by the wild type and the Δ*fso* mutant strains was compared from *ex vivo* corneal infections by using the z-stacks collected at 48 hpi (see sections 2.16.1 and 2.17). The Δ*fso* mutant exhibited a greater depth of penetration compared to that of the wild type ($p < 0.01$).

A comparison was also done of the fungal burden of the wild type and Δ*fso* mutant at 48 hpi by determining and comparing measurements of the CFU and by using qPCR from total corneal tissue homogenates at 48 hpi (Fig. 6.23 and 6.24). The wild type strain exhibited a significantly higher fungal burden than the Δ*fso* mutant when a 1 in 10 dilution of spores was used (***$p<0.001$; Figure 6.23). The higher dilutions did not give a significant difference between the two strains. The qPCR data gave a higher fungal burden for the Δ*fso* mutant compared to the wild type (Figure 6.24). However the differences observed were not statistically significant.
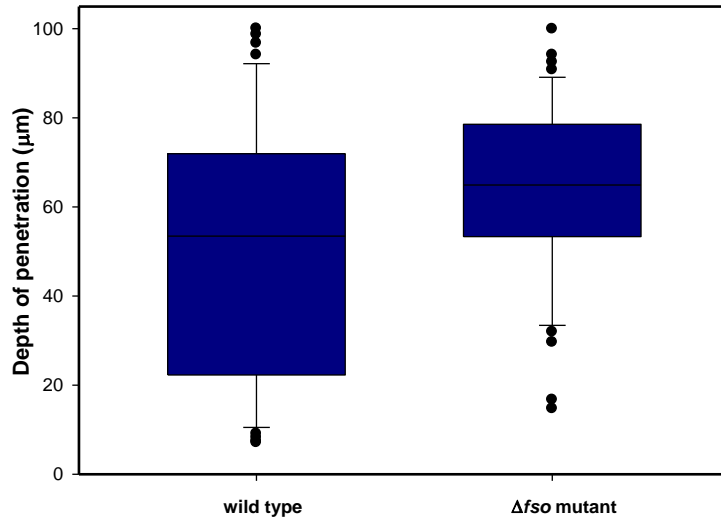
Fig. 6.24. Depth of penetration into the corneal tissue by the wild type and the Δ*fso* mutant at 48 hpi. The depth of penetration was 49.85 ± 28.81 μm for the wild type strain while that of the Δ*fso* mutant was 63.79 ± 19.58 μm (n = 45 from three different experimental repeats), was significantly greater ($p < 0.01$ from unpaired t-test).
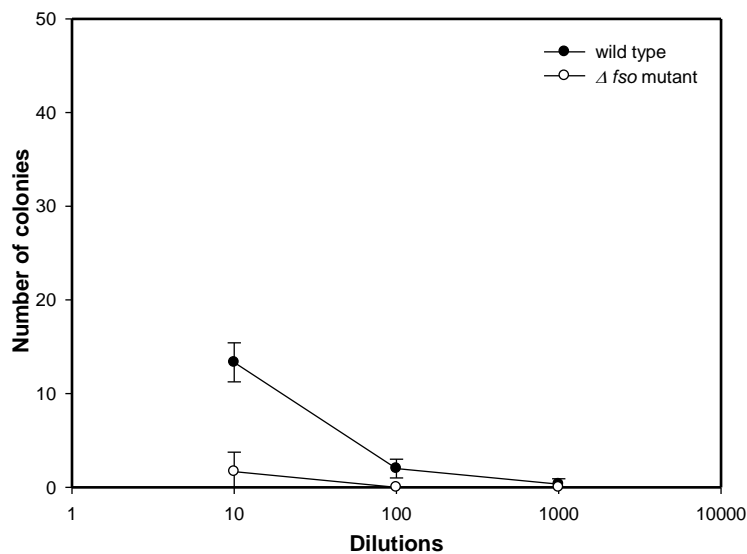
Fig. 6.25. Comparison of the fungal burden from CFUs produced from tissue homogenates of corneas infected with the wild type or the Δ*fso* mutant at 48 hpi. CFUs from serial dilutions of 1 in 10, 100 and 1000 from the tissue homogenates are shown (n = 2 technical replicates each from three different experiments). A p value of 0.003 from a Two-way ANOVA analysis of the 2 data from each dilution was determined. A significant difference between the wild type and the Δ*fso* mutant was only shown with a dilution of 1 in 10 alone ($p < 0.01$ from Two-way ANOVA).
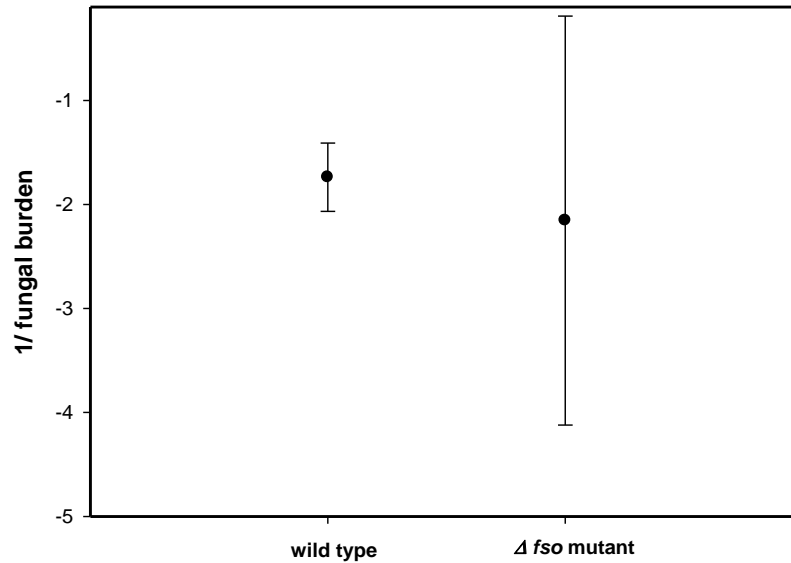
Fig. 6.26. Comparison of the fungal burden from tissue homogenates of corneas infected with the wild type or the *Δfso* mutant at 48 hpi determined from qPCR. The mean values of 1/fungal burden calculated from C_t values were -1.738 and -2.155 for the wild type and the *Δfso* mutant, respectively, which indicates that the wild type exhibited a higher fungal burden. However this was not statistically significantly different (p value was determined to be 0.7 from Mann-Whitney test).

6.3.4 Analysis of the hyphal growth unit in an *in vivo F. solani* infected cornea from a patient

A z-stack of image confocal images of a corneal infection by *F. solani* in a human patient obtained using a diagnostic confocal scanning laser ophthalmoscope in reflection mode (the HRT equipped with the Rostock Cornea Module - see section 6.1), and kindly provided by Dr. Jaya Chidambaram (London School of Hygiene and Tropical Medicine), was analysed using the image analysis techniques described in sections 2.18. The HGU was determined from a z-stack of 10 images collected 14 days after the initial report of infection in the patient. The HGU value was determined to be 27559.27 ± 3568 (Figures 6.26). This proof-of-concept experiment shows that, using image analysis techniques that have been developed to analyse data obtained using a research confocal microscope in fluorescence mode, it is possible to perform similar analyses from images of keratitis infection in a human patient obtained with a diagnostic opthalmoscope in reflection mode.
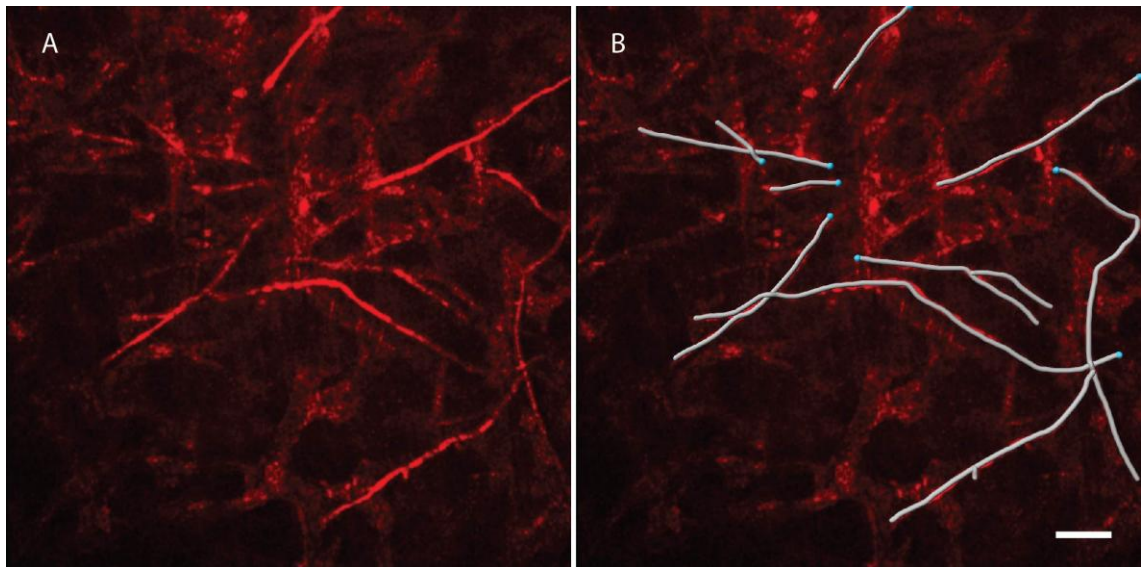
Fig. 6.27. Tracing hyphal filaments from *in vivo* infection data to determine the HGU. (A) shows the raw data whilst (B) shows the filaments superimposed above the hyphae using the filament tracer in the Imaris software. Scale bar = 60 µm.
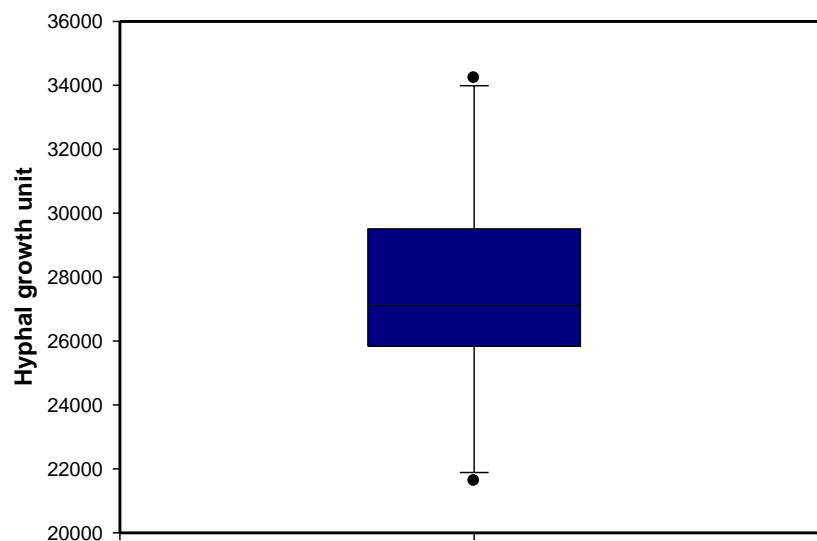
Fig. 6.28. Hyphal growth unit of an *in vivo* dataset from a patient's cornea infection with *F. solani* keratitis. The HGU was determined from a z-stack of 10 images to be 27559 ± 3568.

6.4 Discussion

In this chapter, the use of *ex vivo* human corneas as an excellent model has been demonstrated for live-cell imaging of the dynamics of fungal morphogenesis during infection by *Fusarium oxysporum* f.sp. *lycopersici*, which has previously been primarily analysed as a plant pathogen (see section 1.1.1). Quantification of useful morphological

traits has been done from this study using advanced image analysis techniques that were optimised for the *ex vivo* human corneal infection model. The occurrence and roles of hyphal fusion, which was previously studied *in vitro* (see chapters 3 and 4), were analysed during corneal infection. Finally, the applicability of using one of the image analysis techniques, that was developed in my study of the infection of the *ex vivo* human corneal model, was successfully tested on clinical image data obtained with confocal reflectance microscopy from the eye of a keratitis patient infected with *F. solani*.

6.4.1 Characterization of the morphogenetic stages of *F. oxysporum* during corneal infection

A schematic diagram of the developmental stages that were characterized in my study during infection of the *ex vivo* corneal model by *F. oxysporum* are shown in Figure 6.29.

To begin with microconidia underwent adhesion to the corneal surface, which could be distinguished from non-adhered spores by lacking Brownian movement, as described *in vitro* (section 3.3.1). This was followed by the germination, which with most microconidia was bipolar resulting in the formation of two germ tubes. This contrasted markedly with spores germinated *in vitro* in 1% PDB (with or without chemical supplements) which each formed just a single germ tube (section 3.3.1). What factor(s) in the host tissue and/or the DMEM medium induce the formation of a second germ tube from a microconidium is/are unclear at this stage. The bipolar germination on the corneal surface was initiated after ~ 8 hpi, which is significantly after the time (~ 2 h) that germination was first observed to occur *in vitro* (section 3.3.1). Again it is unclear what factor(s) is/are responsible for the delayed germination on the corneal host tissue.

Whilst the germ tubes/hyphae grew bidirectionally across the corneal surface they underwent subapical branching. The germ tubes and branches avoided each other (a negative tropism), which is well documented in filamentous fungi although the mechanism of intercellular signalling involved is unknown (Moore *et al.,* 2011). After ~ 16 hpi many of the germlings on the corneal surface underwent CAT fusion.
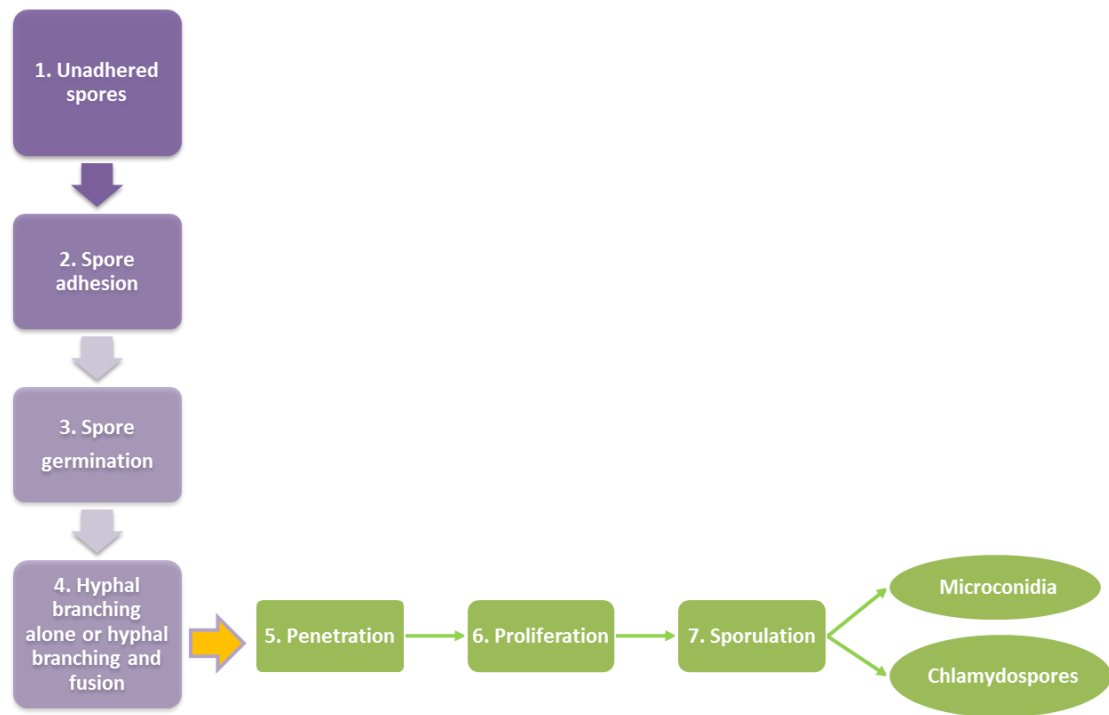
Fig. 6.29. Schematic diagram showing the developmental stages during infection of *ex vivo* human cornea by *F. oxysporum* f. sp. *lycopersici.* Purple boxes show stages occuring on the surface of the corneal tissue while green boxes show stages within the corneal tissue. Most microconidia underwent bipolar germination to form two germ tubes at opposite end of the microconidium. Hyphal growth on the surface included hyphal extension branching and fusion. After penetration into the epithelial tissue, the fungal colony continued to proliferate by further hyphal extension branching and fusion. Sporulation within the corneal tissue also occurred resulting in the formation of both microconidia and chlamydospores..

The hyphae started to invade the epithelial tissue between 12 and 48 h. It seemed that most of the invading hyphae were growing between the epithelial cells as it was not possible to convincingly show evidence of hyphae penetrating individual epithelial cells. Most of the epithelial tissue looked healthy during hyphal invasion so if host cell death was occurring then it was not very widespread.

It was possible to quantify the depth of hyphal penetration into corneal tissue at different time points from measurements obtained from z-stacks of confocal images. The average depth penetrated by hyphae at 48 hpi was found to be 58.30 ± 16.13 µm. The average thickness of human corneal tissue is ~ 500 µm and the epithelial layers accounts for the first 40-45 µm followed by the Bowman's membrane which is ~15 µm thick (Delmonte and Kim, 2011). Hence ~10% of corneal tissue in the z-direction from the corneal surface is colonised by the fungus at 48 hpi. The depth of penetration and

images collected indicated that the fungus had penetrated to the depth of the Bowman's membrane by this time. The invasive growth rate of the hyphae in the z-direction from 16 hpi to 24 hpi was 0.74 μm per h while it increases to 1.54 μm per h from 24 to 48 hpi. It was found that culturing the cornea in fresh medium for 6 days resulted in regeneration of the surface epithelium that was lacking after only 3 days in fresh medium. However, it was found that the depth of hyphal penetration was not influenced by the presence or absence of surface epithelial layer. Several other factors also did not influence the depth of penetration: the microconidial concentration of the inoculum used; scratching the corneal surface with a needle or immunosuppression by pre-treatment with hydrocortisone. The latter finding is supported by *Fusarium* keratitis being prominent in immunocompetent hosts (section 1.10).

Hyphal branch angles have been previously used as a parameter for describing hyphal growth within host tissue infected with *Fusarium* (section 1.10). Most case reports of fusariosis have reported acute angled branches and rarely right angled branches (Dutta *et al*., 2013; Keskar *et al*., 2014; Son *et al.,* 2015). It was found that ~ 50% of hyphal branches within the infected corneal tissue were acute angled. However, my results suggest that branch angles alone may not be a good parameter for the identification of *Fusarium* corneal infections as many near right-angled branches were also observed.

Hyphal growth units were compared between *ex vivo* infection of corneas and *in vitro* growth within PDA medium using measurements of the sum of hyphal lengths divided by number of hyphal tips, which is a standard method for measuring an aspect of hyphal growth in Petri dish culture (Trinci, 1974). My results clearly indicated that under *ex vivo* conditions there was more branching than under *in vitro* conditions because more hyphal tips were measured per unit hyphal length within the corneal tissue.

My results clearly demonstrated that hyphal fusion was not required for *ex vivo* human infection and it did not seem to play a role in increasing the rate of infection. This was based on my finding that the Δ*fso* mutant was not deficient in penetrating the corneal tissue but actually penetrated it more efficiently than the wild type. Furthermore, the fungal burden measured by qPCR from homogenised infected corneal tissue showed that the fungal burden was greater for infections with the Δ*fso* mutant than the wild type. However, this latter data was contradicted by the wild type producing higher colony forming units (CFUs) than the Δ*fso* mutant. The latter result could be due to the wild type producing more spores within and/or on the surface of corneal tissue than the

Δ*fso* mutant. No difference was observed between these two strains in terms of spore production or spore viability under *in vitro* culture conditions. However, spore production *in vitro* and *ex vivo* could be different because the fungus is exposed to different environmental conditions in these two situations. In addition, CFU counts alone have been previously reported as being unreliable for fungal burden measurements as discrepancies have been found between CFU and qPCR data (Gonzalez *et al*., 2013). Hence the interpretation of my contradictory fungal burden data needs to be treated with caution. Previously the *F. oxysporum* Δ*fso* mutant had been shown not to be essential for the infection of tomato roots although evidence was presented that it was defective in efficient colonisation of root surfaces (Prados Rosales and Di Pietro, 2008).

The fungus underwent sporulation within the host tissue forming two types of spores: microconidia and intercalary (insterstitial) chlamydospores. To my knowledge, microconidial formation has not been clearly described before in fusariosis cases involving keratitis. However, *Fusarium* keratitis cases in which *Fusarium* cells have been referred to as yeast-like structures (Nucci *et al*., 2015; Avellino Silva *et al*., 2015) probably refer to microconidia and the term 'adventitious sporulation' associated with keratitis likely refers to microconidiation. The process of adventitious sporulation in fusariosis has been reported to be significant for dissemination of the disease to other organs via the blood stream (Thomas *et al.,* 2011; Guarner and Brandt, 2011; Lockwood and Crescencio, 2016). Microconidial production within plant roots infected with *F. oxysporum* has not been previously reported (Czymmek *et al*., 2007; van der Does *et al*., 2008; Michielse and Rep, 2009).

Chlamydospores are thick-walled, non-deciduous asexual spores formed by fungi and can either be intercalary or formed at the end of a hyphal cell (Ainsworth, 1961). They are commonly formed under adverse environmental conditions (Cochrane and Cochrane 1970; Staib and Morschhauser, 2007). Many fusariosis case reports have shown the presence of thick walled intercalary chlamydospores in histology sections (Guarner and Brandt, 2011; Woolf *et* al., 2012; Guarro, 2013; Esnakula *et al*., 2013). Only intercalary chlamydospore formation was observed within infected tissue and never in culture under *in vitro* conditions. *Fusarium oxysporum* has been shown to form chlamydospores on the root surface and within the vascular tissue of plants (Czymmek *et al*., 2007; van der Does *et al*., 2008; Michielse and Rep, 2009). The factor(s) which induce chlamydospore formation within host tissues are unknown although bacterial

toxins in the soil have been shown to induce chlamydospore formation in *F. solani* (Venkataraman, 1952). The *fvs1* gene, which is involved in post transcriptional regulation and signal transduction, was found to increase chlamydospore production in *F. oxysporum* f. sp. *melonis* (Lida *et al*., 2014). Another transcriptional regulator, FoSTUA was also found to be a negative regulator of chlamydospore formation (Ohara and Tsuge 2004).

6.4.2 Relevance of my results to diagnostic clinical data collected by opthalmoscopy

As a proof-of-concept, it was shown that by using image analysis techniques that were developed to analyse data obtained using a research confocal microscope in a fluorescence mode, it was possible to perform similar analyses from images of keratitis infection in a human patient obtained with an diagnostic opthalmoscope in reflection mode. Such measurements of HGUs would be useful for quantitatively analysing the time course of any fungal corneal infection, and the influence of antifungal drug treatment, *in vivo* in the same patient at different points in time. The *in vivo* reflection image dataset obtained from the corneal infection of the patient's eye were not as good as the fluorescence image datasets from my *ex vivo* studies, particularly because the *in vivo* images were of lower resolution and suffered from background reflection from the surrounding tissue. However, it is clear that the quality of the images from the ophthalmoscopy would be sufficiently good for quantifying branch angles which together with the measurement of HGUs might be useful for the identification of *F. oxysporum in vivo*, especially if it was automated. Extending these image analysis methods to different filamentous fungi causing keratitis may also facilitate the identification of diagnostic morphological features at the genus, species or even sub-species level.

6.4.3 Advantages and disadvantages of the *ex vivo* human corneal infection model

The *ex vivo* human cornea proved to be an excellent material for live-cell imaging to study the dynamics of fungal keratitis as is evident from the time courses of high quality 3D image data sets collected in this study. The transparent structure of human cornea is optically very good and allowing confocal imaging much deeper into tissue (< 100 μm) than is normally achievable. In addition, the size of human corneas (~11 mm in diameter) is easier to handle than those of mice. Another advantage, of course, is the relevance of the human cornea model to human patients.

However, several limitations were identified using this *ex vivo* model system. It was not possible to image beyond a depth of 100 μm within the specimen using the 63x plan apo objective of the confocal microscope. Using a lower magnification objective allows imaging at greater depths and wider fields of view but it provides less resolution compared with higher magnification objective. Also, it was only possible to follow the infection of corneal tissue by live-cell imaging up to 72 hpi because after that time the corneal tissue was too heavily covered with fungal hyphae to image deep into the specimen. Also, after that time the corneal tissue started to degenerate by the shedding of its cells. However, this parameter of host tissue degeneration might be used as a useful parameter to measure in the future if it can be readily quantified. The *ex vivo* cornea fails to replicate the *in vivo* condition with regard to immune response from host. It is also not bathed in tear fluid from the lachrymal glands and it is not subjected to blinking. Furthermore, the corneal tissue by itself is an avascular structure. *In vivo*, the human cornea gets supplied with blood, with its cells and other components, by the blood vessels of the limbus and from aqueous humor. In the *ex vivo* condition, a blood supply, and immune responses to infection resulting from the blood supply, cannot be mimicked. Finally there is significant variation in the *ex vivo corneas* used from experiment to experiment because they are from different people, the majority of which are old.

6.5 Summary

- Confocal live-cell imaging of *Fusarium oxysporum* infecting an *ex vivo* human cornea model provides an excellent experimental system for studying the dynamics of *Fusarium* keratitis infection down to a depth of ~ 100 μm from the corneal surface but it also has its drawbacks.
- Stages in the development of *F. oxysporum* during the first 72 h of infection of corneal tissue were characterised and shown to involve: spore adhesion; bipolar germination; hyphal extension, branching, fusion and penetration into the corneal tissue; and sporulation involving the formation of microconidia and intercalary chlamydospores within the host tissue.
- Image analysis techniques were developed for the quantification and analysis of depth of penetration, branching angles, total hyphal length, number of hyphal branches and hyphal growth units within the infected *ex vivo* corneal tissue.

- Some of the image analysis techniques developed in the *ex vivo* corneal infection study were successfully applied to the analysis of an image dataset collected *in vivo* using ophthalmoscopy from a human patient with a *F. solani* keratitis infection.
- Hyphal fusion was found not to be required for corneal infection as the *Δfso* fusion mutant was not defective in the penetration and colonisation of the cornea.

Chapter 7: General discussion and future work

Fusarium oxysporum is a major fungal plant pathogen and emerging human pathogen. Conidial anastomosis tube (CAT) fusion is known to be formed by germlings of *Fusarium oxysporum* during plant root colonisation (Rosales and Di Pietro, 2009). CAT fusion facilitates efficient colonisation during early stages of colony development from germlings by enabling the formation of hyphal networks as shown in case of *Neurospora crassa* (Roca *et al*., 2005). It was hypothesised that conidial anastomosis tube (CAT) fusion may facilitate horizontal gene/chromosome transfer that could result in the acquisition of new genetic traits in fungi lacking sexual reproduction (Sanders, 2006; Mehrabi *et al*., 2011). However, we know little about the mechanistic basis of CAT fusion in fungi lacking sexual stages such as *F. oxysporum*.

In the research described in chapter 3, the optimal culture conditions were determined for subsequent studies of CAT fusion in *F. oxysporum*. My study concluded that CATs can be formed *in vitro* in specific liquid nutrient media conditions by *F. oxysporum* (see section 3.3.2 , Fig 3.1 and 3.2) at initial stages of colony development from spore or germ tube (GT) enabling hyphal network formation between germlings (see Fig 3.1). The fusion process was found to be dependent on adhesion and induced by the presence of right nutrient supplements (see section 3.3.1, Fig 3.1 and 3.3). CAT fusion was influenced by cell density and pH of the media while it did not vary at temperature conditions between 22 °C to 35 °C (see sections 3.3.3, 3.3.4 and 3.3.5). The optimal cell density for CAT fusion was $1x10^6$ spores/ml (see section 3.3.4, Fig 3.7) which in turn is determined by a minimum proximity required between germlings for the formation of CAT fusion. CAT fusion was found to occur between germlings separated by distance upto ~8 µm. CAT fusion was inhibited at highly acidic pH of 2.5 and 3 while a pH of 4 to 9 favoured CAT fusion (see section 3.3.5, Fig 3.8, 3.9 and 3.10). Stress inducing agent hydrogen peroxide failed to induce CAT fusion while CATs were formed in presence of human serum (see section 3.3.6). This could be more of an effect of the nutrients present in human serum rather than stress. CAT fusion exhibited differences from germ tube formation. Germ tube formation was independent of adhesion and was induced in presence of all nutrient supplements (see section 3.3.1). CAT formation is induced post germ tube formation at ~8 h post incubation at 25 °C (see Fig 3.3.2).

The liquid media method optimised in this study could be employed for such studies using live-cell imaging as it does not have any background fluorescence as in case of rich media condition (as mentioned in Shahi *et al.*, 2015).

Differentiation of adhesion dependent and adhesion independent germination exhibited by *F. oxysporum* has not been described previously. Search in literature identified a similar finding by Kwon and Epstein (1993) in *F. solani* and *C. gloeosporioides*. However, detailed studies involving the screening of mutants defective in different signalling pathways is required to get further insights into the different signalling mechanisms involved in these two different developmental pathways and the physiological significance of each. Further studies involving different substrates, including natural substrates, are required to determine the mechanistic basis of spore and germling adhesion in *F. oxysporum*.

Following key questions and possible experimental approach to answer them have been summarised to be addressed in future, following on from the results of my research described in chapter 3:

- What is the mechanistic basis of adhesion of germlings?
  Screening mutants of *F. oxysporum* that are defective in cell wall composition and exhibiting defects in key signalling pathways, for adhesion in the two different culture conditions described in this study, 1% PDB and 1% PDB supplemented with 25 mM NaNO$_3$ could be done to identify the mechanistic basis of adhesion.
- Are there any differences in the composition of cell wall between the germlings in adhesion inducing and non-inducing conditions?
  Electron microscopy of germlings post 12 h of incubation in 1% PDB and 1% PDB + 25 mM NaNO$_3$ could be done to visualize the composition of cell wall under both media conditions. Substances that selectively bind to different cell wall constituents could be analysed for inhibition of adhesion to identify their role in adhesion.
- Is there an extracellular matrix that is formed during hydration of spores in specific media conditions that facilitates adhesion?
  Fluorescent stains bound to extracellular matrix selective antibodies could be used to visualize the extracellular matrix.

- What are the signalling mechanisms governing CAT formation, homing and fusion?

  Screening of mutants defective in a wide range of different signalling pathways would be useful here. Over 50 mutants that are defective at different stages of the CAT fusion process in *N. crassa* and many of these are involved in signalling (e.g. Read et al., 2012). Undoubtedly many more signalling mutants involved in this process will be identified in the future.

- What is the role of pH in CAT fusion?

  Screening of mutants defective in pH signalling could help to further understand the role of pH during CAT fusion. Reducing the pH of media post germ tube formation and during CAT homing could identify if CAT homing and fusion is dependent on pH of media.

- Is CAT fusion an adaptation for withstanding and overcoming stress conditions?

  Analysing different stress conditions *in vitro* on germlings post CAT fusion and in conditions without CAT fusion could help to determine if CAT fusion helps in overcoming stress conditions.

In the second part of my research live-cell imaging was used to characterize the process of CAT fusion and differences between CATs and germ tubes. In particular, it was shown that the composition of the CAT cell wall surface is different from that of germ tubes. Concanavalin A, which binds to α-mannans on the cell wall exhibited selective brighter staining in the region of CAT fusion alone (4.3.2.3). The widths of CATs were thinner than GTs (see section 4.3.2.2) and the stages of CAT fusion were CAT induction, CAT homing and CAT fusion (see section 4.3.1). It was also shown that CAT fusion establishes cytoplasmic connections facilitating the movement of nuclei, mitochondria, vacuoles and lipid droplets between fused germlings (see section 4.3.3). CAT induction was also found to be dependent on the polymerisation of actin and microtubules (see section 4.3.4).

The observations made in my research of cytoplasmic connections and movement of organelles being facilitated by CAT fusion were between germlings of the same wild type strain. It would be very interesting to repeat the same experiments between two vegetatively incompatible strains of *F. oxysporum* or even between two different sub-species of *F. oxysporum* to test the hypothesis of CAT fusion facilitating horizontal gene/chromosome transfer (HGT/HCT). Evidence was reported to be gathered from

other studies for HGT/HCT events of both core and accessory chromosomes in *F. oxsyporum* (Ma *et al*., 2010; Vlaardingerbroek *et al*., 2016) but the cell biology of the process facilitating HGT/HCT is lacking. HGT/HCT might occur physically either by the fusion of nuclei sharing the same cytoplasm followed by loss of chromosomes during successive mitotic divisions or by the integration of nuclear constituents of a degrading nuclei by an intact or actively dividing nuclei sharing the same hyphal compartment followed by non-meiotic recombination (Sanders, 2006). The images acquired from my study have provided evidence for nuclear degradation and the coexistence of both parental nuclei sharing the same cytoplasm post CAT fusion (Fig.4.9).

We did not see an increase in size of nuclei as would be expected in case of increase in ploidy during stable heterokaryon formation (Bennett and Johnson 2003, Schoustra *et al*. 2007, Forche *et al*., 2008). Microconidia produced by hybrids formed by anastomosis in the study on parasexual genetic recombination by Molnar *et al*. (1990) were characterised as monokaryotic and exhibiting haploid-like sizes. Both the events post nuclear migration observed in this study could be significant as recently evidence has been gathered for the movement of core chromosomes followed by nuclear fusion and loss of chromosomes post-fusion between co-cultured *F. oxysporum* strains (Vlaardingerbroek *et al*., 2016) in addition to the accessory chromosomal regions (or LS chromosome; see section 1.1.2) explained previously in Ma *et al*. (2010). The transfer of LS chromosomes was shown to transfer pathogenicity factors between non-pathogenic and pathogenic strains (Ma *et al*., 2010). However, the cell biology of the process which facilitated these events was not shown in either case.

Brighter staining in the region of CAT fusion alone indicating a difference in the wall composition of CATs and germ tubes has not been identified before. Such enrichment of wall composition is indicative of a specialized role for CAT fusion during initial stages of colony development. Polymerisation of actin and microtubules was required for CAT formation as evident from the inhibition of CAT formation under conditions that inihibited the polymerisation of actin or microtubules (see section 4.3.5). This is different from *N. crassa* where CAT fusion but not germ tube formation is independent of the polymerisation of microtubules.

The following key questions and possible experimental approach to answer them have been summarised to be addressed in future, following on from the results of my research described in chapter 4:

- Is CAT fusion followed by non-meiotic recombination as hypothesised in case of HGT/HCT?

  Vegetatively incompatible strains of *F. oxysporum* expressing different fluorescent and antibiotic markers could be analysed *in vitro* by live-cell imaging for nuclear fusion events accompanied by increased size of nuclei during CAT fusion. Spores generated post CAT fusion could be sub-cultured on selective media plates with antibiotics corresponding to the antibiotic markers present in the strains. Recombinant strains expressing both the genetic markers from parental strains could be selected and sub-cultured on selective media for selecting stable recombinants or heterokaryons. Genetic composition of any stable heterokaryons generated could be verified by PCR and Southern blotting.

- Mutants that play a role in nuclear fusion (e.g. genes that have been identified having this role in the formation of diploid nuclei from the fusion of haploid nuclei in yeast; Rose, 1991) could be screened for heterokaryon formation following CAT fusion to confirm the role of nuclear fusion in generating heterokaryons by CAT fusion. Live-cell imaging of fluorescently labelled specific chromosomes or genes (e.g. virulence) and their tracking during fusion events could be done as has been described in the case of yeast cells (Fauth and Zink, 2001).

- What is the role of cytoskeletal structures in facilitating the movement of organelles through CAT fusion?

  Strains expressing Lifeact GFP and β-tubulin GFP in combination with fluorescent stains or genetically encoded markers selective for different organelles could be used to look into dynamics of cytoskeletal structures and their role in organelle movement within *Fusarium*.

In the third part of my research a quantitative analysis of the influence of various Ca^{2+} modulators on CAT fusion was done and evidence was obtained that Ca^{2+} signalling is important during CAT fusion and involves the uptake of Ca^{2+} from the external environment by the Cch1 Ca^{2+} channel, and the involvement of the primary intracellular Ca^{2+} receptor, calmodulin, and the mitochondrial Ca^{2+} uniporter (see sections 5.3.1.1, 5.3.1.3, 5.3.1.4 and 5.3.1.5). CATs were more sensitive to these chemical modulators of

Ca^{2+} signalling compared to germ tubes (see section 5.3.1). However, further experimentation by live-cell imaging is required to acquire further insights into the dynamic role played by Ca^{2+} signalling during CAT fusion.

The Ca^{2+} modulators used in this study were all originally developed for use with mammalian cells. As a result, their modes of action have mostly only been characterized in depth in mammalian cells. Hence caution must be taken in interpreting the results obtained using these pharmacological agents in this study on *F. oxysporum*, and also other studies on fungi, until their specificity/selectivity for their fungal targets have been verified.

Following key questions have been summarised to be addressed in future along with possible experimental approaches to answer them following on from the results of my research described in chapter 5:

- Can the Ca^{2+} signals generated during CAT fusion be visualized using live-cell imaging?

  Genetically encoded Ca^{2+} probes such as GCaMPs could be expressed to study the sub-cellular Ca^{2+} dynamics. The transformation of *F. oxysporum* with GCaMP5, one of the available variants of GCaMP probe was done during my PhD but the results obtained with it were not included in the thesis because they were inconclusive. The presence of the probe as an insert in the *F. oxysporum* genome was confirmed by PCR in 12 successful transformant colonies that were isolated but no further evidence for GCaMP5 expression was obtained for cells from any of the transformants. A shorter version of *Aspergillus gpdA* promoter was used to make the original GCaMP5 construct and this may have been a reason for not observing expression of the probe. In future, expression of GCaMP6, a brighter GCaMP variant, under the control of a completed *gpdA* promoter or a different promoter of *F. oxysporum* might be employed as has been successfully done with the *tef-1* promoter in *N. crassa* (Hernandez-Ortiz *et al*., in prep). Another way of possibly improving probe expression may be to express multiple copies of the GCaMP6 gene ectopically integrated within the *F. oxysporum* genome.

- How can pharmacological evidence gathered for role of components of Ca^{2+} signalling machinery during CAT fusion be verified?

Generation of knock out mutants of Ca^{2+} signalling in *F. oxysporum* is another way of gaining further insights into the involvement of Ca^{2+} signalling in CAT fusion. Ca^{2+} channels, calmodulin, ER Ca^{2+} ATPase and mitochondrial calcium uniporter were found to be involved in CAT fusion from pharmacological experimental evidence gathered in this study. Creation of *cch1* and *mcu1* knock outs in *F. oxysporum* followed by analysis of CAT fusion assays with the knock out mutants could verify the role of these components of Ca^{2+} signalling machinery during CAT fusion.

In the final part of my thesis, the early stages of colony development *ex vivo* during infection of a human corneal model were observed. The stages of development was characterised as adhesion, bi-directional germination, hyphal fusion (including CAT fusion), branching, penetration and sporulation (interstitial chlamydospore formation and microconidiation) (see section 6.3.1). The methods were optimised for studying *ex vivo* human corneal infection by live-cell imaging and image analysis methods for determination of quantitative features such as the depth of penetration, number of branches, branch length sum, branch angles and hyphal growth unit. Using the fusion mutant, Δ*fso*, it was shown that CAT fusion is not required for infection. CAT fusion was induced during *ex vivo* human corneal infection (see Fig 6.6.). However, it was found not to be essential for human infection as the Δ*fso* mutant, a hyphal fusion mutant was not affected in human corneal infection compared to the wild type strain of *F. oxysporum* (see section 6.3.3).

The following key questions have been summarised to be addressed in future along with possible experimental approaches to answer them following on from the results of my research described in chapter 6:

- Is hyphal penetration exhibited by *F. oxysporum* through the epithelial layers intracellular of intercellular?
  Performing Transmission Electron Microscopy (TEM) on fixed sections of cornea could help to identify closely the features of penetration through different tissue layers.
- Is invasion of corneal tissue by *F .oxysporum* nectrotrophic or hemibiotrophic?
  Use of cell death specific markers of mammalian host tissue during different stages of infection could help to identify if the surrounding tissue is killed by the fungus during invasion.

The *ex vivo* model for fungal infection could be extended to the following applications in future:

- To study *F. solani* and other fungal candidate species significant in keratitis (*A. flavus, C. albicans*) which could lead to better identification characters of these species *in vivo*.

- To investigate the morphological differences between two selected candidate sub-species of the same species during *ex vivo* infection (for e.g. *F. petroliphilum* and *F. falciforme* of *F. solani*). This could confirm if there are differences between different sub-species during infection.

- To investigate the suitability of this model system for studying the effect of antifungal treatments post infection.

- To investigate and improve the confocal imaging system (used in research) in reflection mode so that infected cornea from patient's eye could be imaged directly without the need for fluorescently labelled strains. This can help to characterise the morphological features of fungal keratitis from *in vivo* infection samples of cornea in laboratory set up. Also, this could help in bridging the gap between the current imaging techniques used for diagnosis.

- To perform mRNA sequencing to determine genes expressed by *F. oxysporum* during infection. A comparison of the expressed genes during infection could be made with the genes identified from plant infections of this strain (for e.g. expression of effectors during infection).

Bibiliography

Abbouda, A., Estrada, A. V., Rodriguez, A. E. & Alio, J. L. 2014. Anterior segment optical coherence tomography in evaluation of severe fungal keratitis infections treated by corneal crosslinking. *Eur J Ophthalmol,* 24**,** 320-4.

Abdel-Monaim, M. F., Abdel-Gaid, M. A. & Armanious, H. A. H. 2012. Effect of chemical inducers on root rot and wilt diseases, yield and quality of tomato. *International Journal of Agricultural Sciences,* 2**,** 211- 220.

Abou Shousha, M., Santos, A. R., Oechsler, R. A., Iovieno, A., Maestre-Mesa, J., Ruggeri, M., Echegaray, J. J., Dubovy, S. R., Perez, V. L., Miller, D., Alfonso, E. C. & Bajenaru, M. L. 2013. A novel rat contact lens model for *Fusarium* keratitis. *Mol Vis,* 19**,** 2596-605.

Aguilar, P. S., Engel, A. & Walter, P. 2007. The plasma membrane proteins Prm1 and Fig1 ascertain fidelity of membrane fusion during yeast mating. *Mol Biol Cell,* 18**,** 547-56.

Aimi, T., Yotsutani, Y. & Morinaga, T. 2002. Cytological Analysis of Anastomoses and Vegetative Incompatibility Reactions in *Helicobasidium monpa. Current Microbiology,* 44**,** 148-152.

Ainsworth, G. C. 1961. Dictionary of the Fungi. Commonwealth Mycological Institute.

Aizawa, H., Katadae, M., Maruya, M., Sameshima, M., Murakami-Murofushi, K. & Yahara, I. 1999. Hyperosmotic stress-induced reorganization of actin bundles in Dictyostelium cells over-expressing cofilin. *Genes Cells,* 4**,** 311-24.

Alabouvette, C., Olivain, C., Migheli, Q. & Steinberg, C. 2009. Microbiological control of soil-borne phytopathogenic fungi with special emphasis on wilt-inducing *Fusarium oxysporum. New Phytol,* 184**,** 529-44.

Al-Hatmi, A. M., Bonifaz, A., De Hoog, G. S., Vazquez-Maya, L., Garcia-Carmona, K., Meis, J. F. & Van Diepeningen, A. D. 2014. Keratitis by *Fusarium temperatum*, a novel opportunist. *BMC Infect Dis,* 14**,** 588.

Al-Hatmi, A. M., Meis, J. F. & De Hoog, G. S. 2016. *Fusarium*: Molecular Diversity and Intrinsic Drug Resistance. *PLoS Pathog*, 12, e1005464.

Ali, N., Adil, S. N. & Shaikh, M. U. 2014. Bloodstream and central line isolates from hematopoietic stem cell transplant recipients: data from a developing country. *Transpl Infect Dis,* 16**,** 98-105.

Aljohani, A. J., Edwards, G., Guerra, Y., Dubovy, S., Miller, D., Lee, R. K. & Bhattacharya, S. K. 2014. Human trabecular meshwork sphingolipid and ceramide profiles and potential latent fungal commensalism. *Invest Ophthalmol Vis Sci,* 55**,** 3413-22.

Allen, P. J. 1965. Metabolic aspects of spore germination. *Annu. Rev. Phytopathol.,* 3**,** 313- 342.

Alnawaiseh, M., Bohm, M. R., Idelevich, E. A., Becker, K., Grewe, S., Grenzebach, U. H. & Eter, N. 2014. [Successful treatment of *Fusarium*-associated keratitis with multiresistant pathogen and multimorbid patient]. *Ophthalmologe,* 111**,** 259-61.

Ananthi, S., Venkatesh Prajna, N., Lalitha, P., Valarnila, M. & Dharmalingam, K. 2013. Pathogen induced changes in the protein profile of human tears from *Fusarium*

keratitis patients. *PLoS One,* 8**,** e53018.

Antonissen, G., Martel, A., Pasmans, F., Ducatelle, R., Verbrugghe, E., Vandenbroucke, V., Li, S., Haesebrouck, F., Van Immerseel, F. & Croubels, S. 2014. The impact of *Fusarium* mycotoxins on human and animal host susceptibility to infectious diseases. *Toxins (Basel),* 6**,** 430-52.

Apoga, D., Barnard, J., Craighead, H. G. & Hoch, H. C. 2004. Quantification of substratum contact required for initiation of *Colletotrichum graminicola* appressoria. *Fungal Genet Biol,* 41**,** 1-12.

Apoga, D., Jansson, H. & Tunlid, A. 2001. Adhesion of conidia and germlings of the plant pathogenic fungus *Bipolaris sorokiniana* to solid surfaces. *Mycological Research,* 105**,** 1251 - 1260.

Araujo, J. M., De Araújo, J.V., Braga, F.R., Ferreira, S.R., Tavela, A.D.O 2013. Predatory activity of chlamydospores of the fungus *Pochonia chlamydosporia* on *Toxocara canis* eggs under laboratory conditions. *Rev. Bras. Parasitol. Vet.,* 22**,** 171-174.

Arboleda, A., Miller, D., Cabot, F., Taneja, M., Aguilar, M. C., Alawa, K., Amescua, G., Yoo, S. H. & Parel, J. M. 2014. Assessment of rose bengal versus riboflavin photodynamic therapy for inhibition of fungal keratitis isolates. *Am J Ophthalmol,* 158**,** 64-70 e2.

Atty, C., Alagiozian-Angelova, V. M. & Kowal-Vern, A. 2014. Black plaques and white nodules in a burn patient. *Fusarium* and Mucormycosis. *JAMA Dermatol,* 150**,** 1355-6.

Avelino-Silva, V. I., Ramos, J. F., Leal, F. E., Testagrossa, L. & Novis, Y. S. 2015. Disseminated *Fusarium* infection in autologous stem cell transplant recipient. *Braz J Infect Dis,* 19**,** 90-3.

Barhoom, S. & Sharon, A. 2004. cAMP regulation of "pathogenic" and "saprophytic" fungal spore germination. *Fungal Genet Biol,* 41**,** 317-26.

Behrens-Baumann, W., Seibold, M., Hofmuller, W., Walter, S., Haeberle, H., Wecke, T., Tammer, I. & Tintelnot, K. 2012. Benefit of polyhexamethylene biguanide in *Fusarium* keratitis. *Ophthalmic Res,* 48**,** 171-6.

Benčina, M., Bagar, T., Lah, L. & Kraševec, N. 2009. A comparative genomic analysis of calcium and proton signaling/homeostasis in *Aspergillus* species. *Fungal Genetics and Biology,* 46**,** S93-S104.

Bennett, J. W. & Klich, M. 2003. Mycotoxins. *Clin Microbiol Rev,* 16**,** 497-516.

Bennett, R. J., Johnson, A.D. 2003. Completion of a parasexual cycle in *Candida albicans* by induced chromosome loss in tetraploid strains. *The EMBO Journal,* 22**,** 2505-2515.

Berepiki, A., Lichius, A., Shoji, J. Y., Tilsner, J. & Read, N. D. 2010. F-actin dynamics in *Neurospora crassa. Eukaryot Cell,* 9**,** 547-57.

Berepiki, A. & Read, N. D. 2013. Septins are important for cell polarity, septation and asexual spore formation in *Neurospora crassa* and show different patterns of localisation at germ tube tips. *PLoS One,* 8**,** e63843.

Berridge, M. J., Bootman, M. D. & Roderick, H. L. 2003. Calcium signalling: dynamics, homeostasis and remodelling. *Nat Rev Mol Cell Biol,* 4**,** 517-29.

Bhaskaran, A., Hosseini-Moghaddam, S. M., Rotstein, C. & Husain, S. 2013. Mold

infections in lung transplant recipients. *Semin Respir Crit Care Med,* 34**,** 371-9.

Bolker, M., Kahmann, R. 1993. Sexual pheromones and mating responses in fungi. *The Plant Cell,* 5**,** 1451-1489.

Bootman, M. D., Collins, T. J., Peppiatt, C. M., Prothero, L. S., Mackenzie, L., De Smet, P., Travers, M., Tovey, S. C., Seo, J. T., Berridge, M. J., Ciccolini, F. & Lipp, P. 2001. Calcium signalling - an overview. *Seminars in Cell & Developmental Biology,* 12**,** 3-10.

Borkovich, K. A., Alex, L. A., Yarden, O., Freitag, M., Turner, G. E., Read, N. D., *et al.*, 2004. Lessons from the Genome Sequence of *Neurospora crassa*: Tracing the Path from Genomic Blueprint to Multicellular Organism. *Microbiology and Molecular Biology Reviews,* 68**,** 1-108.

Bouanani, N., Lamchahab, M., Quachouh, M., Soussi, M., Quessar, A. & Benchekroun, S. 2013. [Disseminated fusariosis during autologous stem cells transplant]. *J Mycol Med,* 23**,** 119-22.

Bowman, S.M. and Free, S.J. 2006. The structure and synthesis of the fungal cell wall. *BioEssays*, 28, 799-808.

Brand, A. & Gow, N. A. 2009. Mechanisms of hypha orientation of fungi. *Curr Opin Microbiol,* 12**,** 350-7.

Brown, A. J., Leach, M. D. & Nicholls, S. 2010. The relevance of heat shock regulation in fungal pathogens of humans. *Virulence,* 1**,** 330-2.

Buchta, V., Feuermannova, A., Vasa, M., Baskova, L., Kutova, R., Kubatova, A. & Vejsova, M. 2014. Outbreak of fungal endophthalmitis due to *Fusarium oxysporum* following cataract surgery. *Mycopathologia,* 177**,** 115-21.

Bullock, J. D., Elder, B. L., Warwar, R. E., Snyder, S. A. & Sizemore, I. E. 2014. Mechanism of drug failure in *Fusarium* keratitis, 2004-2006. *N Engl J Med,* 370**,** 88-9.

Byun, Y. S. & Kim, M. S. 2011. Superimposed fungal ulcer after fibrin glue sealant in infectious corneal ulcer. *Korean J Ophthalmol,* 25**,** 447-50.

Calcaterra, D., Karam, K. & Suzuki, Y. 2013. Computed tomography findings in a patient with fungal aortitis: acute aortic syndrome secondary to fusariosis. *Interact Cardiovasc Thorac Surg,* 17**,** 171-2.

Campo, M., Lewis, R. E. & Kontoyiannis, D. P. 2010. Invasive fusariosis in patients with hematologic malignancies at a cancer center: 1998-2009. *J Infect,* 60**,** 331-7.

Candoni, A., Caira, M., Cesaro, S., Busca, A., Giacchino, M., Fanci, R., *et al.*, 2014. Multicentre surveillance study on feasibility, safety and efficacy of antifungal combination therapy for proven or probable invasive fungal diseases in haematological patients: the SEIFEM real-life combo study. *Mycoses,* 57**,** 342-50.

Caracuel, Z., Casanova, C., Roncero, M. I., Di Pietro, A. & Ramos, J. 2003. pH response transcription factor PacC controls salt stress tolerance and expression of the P-Type Na$^+$ -ATPase Ena1 in *Fusarium oxysporum. Eukaryot Cell,* 2**,** 1246-52.

Caracuel, Z., Roncero, M. I., Espeso, E. A., Gonzalez-Verdejo, C. I., Garcia-Maceira, F. I. & Di Pietro, A. 2003. The pH signalling transcription factor PacC controls

virulence in the plant pathogen *Fusarium oxysporum*. *Mol Microbiol,* 48**,** 765-79.

Carriles, R., Schafer, D. N., Sheetz, K. E., Field, J. J., Cisek, R., Barzda, V., Sylvester, A. W. & Squier, J. A. 2009. Invited review article: Imaging techniques for harmonic and multiphoton absorption fluorescence microscopy. *Rev Sci Instrum,* 80**,** 081101.

Cavallini, G. M., Ducange, P., Volante, V. & Benatti, C. 2013. Successful treatment of *Fusarium* keratitis after photo refractive keratectomy. *Indian J Ophthalmol,* 61**,** 669-71.

Cavinder, B., Hamam, A., Lew, R. R. & Trail, F. 2011. Mid1, a mechanosensitive calcium ion channel, affects growth, development, and ascospore discharge in the filamentous fungus *Gibberella zeae*. *Eukaryot Cell,* 10**,** 832-41.

Cavinder, B. & Trail, F. 2012. Role of Fig1, a component of the low-affinity calcium uptake system, in growth and sexual development of filamentous fungi. *Eukaryot Cell,* 11**,** 978-88.

Chan, T. S., Gill, H., Hwang, Y. Y., Sim, J., Tse, A. C., Loong, F., Khong, P. L., Tse, E., Leung, A. Y., Chim, C. S., Lie, A. K. & Kwong, Y. L. 2014. Breakthrough invasive fungal diseases during echinocandin treatment in high-risk hospitalized hematologic patients. *Ann Hematol,* 93**,** 493-8.

Chang, D. C., Grant, G.B., O'donnell, K., Wannemuehler, K.A., Noble-Wang, J., Rao, C.Y., Jacobson, L.M., Crowell, C.S., Sneed, R.S., Lewis, F.M.T., Schaffzin, J.K., Kainer, M.A., Genese, C.A., Alfonso, E.C., Jones, D.B., Srinivasan, A., Fridkin, S.K., Park, B.J. 2006. Multistate outbreak of *Fusarium* keratitis associated with use of a contact lens solution. *JAMA,* 296**,** 953-963.

Chang, S. C., Macedo, D. P., Souza-Motta, C. M. & Oliveira, N. T. 2013. Use of molecular markers to compare *Fusarium verticillioides* pathogenic strains isolated from plants and humans. *Genet Mol Res,* 12**,** 2863-75.

Che, C. Y., Li, X. J., Jia, W. Y., Li, N., Xu, Q., Lin, J., Wang, Q., Jiang, N., Hu, L. T. & Zhao, G. Q. 2012. Early expression of surfactant proteins D in *Fusarium solani infected rat cornea. Int J Ophthalmol, 5, 297-300.*

Cheng, P., Meng, F. & Zhang, D. 2014. Fatal *Fusarium solani* infection after stem cell transplant for aplastic anemia. *Exp Clin Transplant,* 12**,** 384-7.

Choi, K. S., Yoon, S. C., Rim, T. H., Han, S. J., Kim, E. D. & Seo, K. Y. 2014. Effect of voriconazole and ultraviolet-A combination therapy compared to voriconazole single treatment on *Fusarium solani* fungal keratitis. *J Ocul Pharmacol Ther,* 30**,** 381-6.

Clapham, D. E. 2007. Calcium Signaling. *Cell,* 131**,** 1047-1058.

Cochrane, V. W., Cochrane, J.C. 1970. Chlamydospore development in the absence of protein synthesis in *Fusarium solani*. *Developmental Biology,* 23**,** 345-354.

Cochrane, V. W., Cochrane, J. C., Vogel, J. M. & Coles, R. S. 1963. Spore germination and carbon metabolism in *F. solani*. *J . Bacteriol.,* 86**,** 312 - 319.

Coleman, J. J. 2016. The *Fusarium solani* species complex: ubiquitous pathogens of agricultural importance. *Mol Plant Pathol,* 17**,** 146-58.

Coleman, J. J., Rounsley, S. D., Rodriguez-Carres, M., Kuo, A., Wasmann, C. C., Grimwood, J., *et al.,* 2009. The genome of *Nectria haematococca*: contribution

of supernumerary chromosomes to gene expansion. *PLoS Genet,* 5**,** e1000618.

Collado, C., Medina, L., Zorraquino, A., Baeza, T., Ferrer, C., Plazas, J. & Colom, M. F. 2013. Cutaneous fusariosis by a species of the *Fusarium dimerum* species complex in a patient with acute myeloblastic leukemia. *Rev Iberoam Micol,* 30**,** 119-21.

Collins, T. J., Read, N.D. 1997. Appressorium induction by topographical signals in six cereal rusts. *Physiological and Molecular Plant Pathology*, 51, 169-179.

Cook, R. J. & Christen, A. A. 1975. Growth of cereal root- rot fungi as affected by temperature - water potential interactions. *Phytopathology,* 66**,** 193 - 197.

Cornely, O. A., Cuenca-Estrella, M., Meis, J. F. & Ullmann, A. J. 2014. European Society of Clinical Microbiology and Infectious Diseases (ESCMID) Fungal Infection Study Group (EFISG) and European Confederation of Medical Mycology (ECMM) 2013 joint guidelines on diagnosis and management of rare and emerging fungal diseases. *Clin Microbiol Infect,* 20 Suppl 3**,** 1-4.

Correll, J. C., Klittich, C. J. R. & Leslie, J. F. 1987. Nitrate non utilizing mutants of *Fusarium oxysporum* and their use in vegetative compatibility tests. *Phytopathology,* 77**,** 1640-1646.

Couteaudier, Y., Alabouvette, C. 1990. Quantitative comparison of *Fusarium oxysporum* competitiveness in relation to carbon utilization. *FEMS Microbiology Ecology,* 74**,** 261-268.

Cunha, C., Kurzai, O., Loffler, J., Aversa, F., Romani, L. & Carvalho, A. 2014. Neutrophil responses to aspergillosis: new roles for old players. *Mycopathologia,* 178**,** 387-93.

Czymmek, K. J., Bourett, T. M., Shao, Y., Dezwaan, T. M., Sweigard, J. A. & Howard, R. J. 2005. Live-cell imaging of tubulin in the filamentous fungus *Magnaporthe grisea* treated with anti-microtubule and anti-microfilament agents. *Protoplasma,* 225**,** 23-32.

Czymmek, K. J., Fogg, M., Powell, D. H., Sweigard, J., Park, S. Y. & Kang, S. 2007. *In vivo* time-lapse documentation using confocal and multi-photon microscopy reveals the mechanisms of invasion into the Arabidopsis root vascular system by *Fusarium oxysporum. Fungal Genet Biol,* 44**,** 1011-23.

D'enfert, C. 1997. Fungal Spore Germination: Insights from the Molecular Genetics of *Aspergillus nidulans* and *Neurospora crassa. Fungal Genetics and Biology,* 21**,** 163–172.

Dean, R., Van Kan, J. A., Pretorius, Z. A., Hammond-Kosack, K. E., Di Pietro, A., Spanu, P. D., Rudd, J. J., *et al*., 2012. The Top 10 fungal pathogens in molecular plant pathology. *Mol Plant Pathol,* 13**,** 414-30.

Delmonte, D. W. & Kim, T. 2011. Anatomy and physiology of the cornea. *J Cataract Refract Surg,* 37**,** 588-98.

Deng, Y., Dong, H., Jin, Q., Dai, C., Fang, Y., Liang, S., Wang, K., Shao, J., Lou, Y., Shi, W., Vakalounakis, D. J. & Li, D. 2006. Analysis of expressed sequence tag data and gene expression profiles involved in conidial germination of *Fusarium oxysporum. Appl Environ Microbiol,* 72**,** 1667-71.

Di Pietro, A., García-Maceira, F. I., Méglecz, E. & Roncero, M. I. 2001. A MAP kinase of the vascular wilt fungus *Fusarium oxysporum* is essential for root penetration

and pathogenesis. *Mol Microbiol.,* 39**,** 1140-52.

Di Pietro, A., Madrid, M. P., Caracuel, Z., Delgado-Jarana, J. & Roncero, I. G. 2003. *Fusarium oxysporum*: exploring the molecular arsenal of a vascular wilt fungus. *Molecular Plant Pathology,* 4**,** 315-325.

Dony, A., Perpoint, T., Ducastelle, S. & Ferry, T. 2013. Disseminated fusariosis with immune reconstitution syndrome and cracking mycotic aortic aneurysm in a 55-year-old patient with acute myeloid leukaemia. *BMJ Case Rep,* 2013.

Duhard, E. 2014. [Paronychia]. *Presse Med,* 43**,** 1216-22.

Dutta, D., Cole, N., Kumar, N. & Willcox, M. D. 2013. Broad spectrum antimicrobial activity of melimine covalently bound to contact lenses. *Invest Ophthalmol Vis Sci,* 54**,** 175-82.

Dutta, P., Premkumar, A., Chakrabarti, A., Shah, V. N., Behera, A., De, D., Rudramurthy, S. M. & Bhansali, A. 2013. *Fusarium falciforme* infection of foot in a patient with type 2 diabetes mellitus: a case report and review of the literature. *Mycopathologia,* 176**,** 225-32.

Elmer, W. H. 2012. *Fusarium, Biology and Epidemiology,* St Paul, MN, American Phytopathology Society.

Engh, I., Wurtz, C., Witzel-Schlomp, K., Zhang, H. Y., Hoff, B., Nowrousian, M., Rottensteiner, H. & Kuck, U. 2007. The WW domain protein PRO40 is required for fungal fertility and associates with Woronin bodies. *Eukaryot Cell,* 6**,** 831-43.

Epstein, A. B. 2007. In the aftermath of the *Fusarium* keratitis outbreak: what have we learned? *Clinical Ophthalmology,* 1**,** 355-366.

Esnakula, A. K., Summers, I. & Naab, T. J. 2013. Fatal disseminated *Fusarium* infection in a human immunodeficiency virus positive patient. *Case Rep Infect Dis,* 2013**,** 379320.

Farjo, A., McDermott, M., Soong, H.K. 2008. Corneal anatomy, physiology, and wound healing. in: M. Yanoff, J.S. Duker (Eds.) Ophthalmology. 3rd ed. Mosby, St. Louis, MO, 203–208.

Fauth, C., Zink, D. 2001. Live-cell microscopy of single nuclear chromosomes and genome compartments: evaluation of labelling procedure and imaging conditions. *Cytometry,* 45, 214-224.

Fanci, R., Pini, G., Bartolesi, A. M. & Pecile, P. 2013. Refractory disseminated fusariosis by *Fusarium verticillioides* in a patient with acute myeloid leukaemia relapsed after allogeneic hematopoietic stem cell transplantation: a case report and literature review. *Rev Iberoam Micol,* 30**,** 51-3.

Fischer-Harman, V., Jackson, K. J., Muñoz, A., Shoji, J. Y. & Read, N. D. 2012. Evidence for tryptophan being a signal molecule that inhibits conidial anastomosis tube fusion during colony initiation in *Neurospora crassa. . Fungal Genet Biol.,* 49**,** 896-902.

Fitz-Aranda, J. A., Mendoza-De-Gives, P., Torres-Acosta, J.F.J., Lie´Bano-Herna´Ndez, E., Lo´Pez-Arellano,M.E., Sandoval-Castro, C.A., Quiroz-Romero, H. 2015. *Duddingtonia flagrans* chlamydospores in nutritional pellets: effect of storage time and conditions on the trapping ability against *Haemonchus contortus* larvae. *Journal of Helminthology,* 89**,** 3–18.

Fleissner, A., Sarkar, S., Jacobson, D. J., Roca, M. G., Read, N. D. & Glass, N. L. 2005. The so locus is required for vegetative cell fusion and post fertilization events in *Neurospora crassa. Eukaryot Cell,* 4**,** 920-30.

Fleissner A, L. A., Roca Mg, Read Nd, Glass N. L. 2009. Oscillatory recruitment of signaling proteins to cell tips promotes coordinated behaviour during cell fusion. *Proc Natl Acad Sci U S A,* 17**,** 19387-92.

Forche, A., Alby, K., Schaefer, D., Johnson, A. D., Berman, J. & Bennet, R. J. 2008. The parasexual cycle in *Candida albicans* provides an alternative pathway to meiosis for the formation of recombinant strains *PLoS Biol. ,* 6**,** e110.

Fu, C., Ao, J., Dettmann, A., Seiler, S. & Free, S. J. 2014. Characterization of the Neurospora crassa cell fusion proteins, HAM-6, HAM-7, HAM-8, HAM-9, HAM-10, AMPH-1 and WHI-2. *PLoS One,* 9**,** e107773.

Fungal tree of life project. 2016. Available at: http://tolweb.org/fungi (Accessed: 15 Jan 2013).

Global Action Fund for Fungal Infections (GAFFI). 2016. Available at: www.gaffi.org (Accessed: 20 Jan 2016).

Gajjar, D. U., Pal, A. K., Ghodadra, B. K. & Vasavada, A. R. 2013. Microscopic evaluation, molecular identification, antifungal susceptibility, and clinical outcomes in *Fusarium*, *Aspergillus* and, dematiaceous keratitis. *Biomed Res Int,* 2013**,** 605308.

Galagan, J. E., Calvo, S.E., Borkovich, K.A., Selker, E.U., Read, N.D., Jaffe, D., *et al*., 2003. The genome sequence of the filamentous fungus *Neurospora crassa*. *Nature,* 422**,** 859-868.

Garcia, R. R., Min, Z., Narasimhan, S. & Bhanot, N. 2015. *Fusarium* brain abscess: case report and literature review. *Mycoses,* 58**,** 22-6.

Garrett, M. K., Robinson, P.M. 1969. A stable inhibitor of spore germination produced by fungi. *Arch. Microbiol,* 67**,** 370-377.

Gaujoux, T., Chatel, M.A., Chaumeil, C., Laroche, L., Borderie, V.M. 2008. Outbreak of contact lens-related *Fusarium* keratitis in France. *Cornea,* 27**,** 1018-1021.

Georgiadou, S. P., Velegraki, A., Arabatzis, M., Neonakis, I., Chatzipanagiotou, S., Dalekos, G. N. & Petinaki, E. 2014. Cluster of *Fusarium verticillioides* bloodstream infections among immunocompetent patients in an internal medicine department after reconstruction works in Larissa, Central Greece. *J Hosp Infect,* 86**,** 267-71.

Gietzen, K., Mansard, A., Bader, H. 1980. Inhibition of human erythrocyte Ca++ - transport ATPase by phenothiazine and butyrophenones. *Biochemical and Biophysical Research Communications,* 94**,** 674-681.

Gietzen, K., Wuthrich, A., Bader, H. 1981. R 24571: A new powerful inhibitor of red blood cell Ca++ -transport ATPase and of calmodulin-regulated functions. *Biochemical and Biophysical Research Communications,* 101**,** 418-425.

Glass, N. L. & Dementhon, K. 2006. Non-self recognition and programmed cell death in filamentous fungi. *Curr Opin Microbiol,* 9**,** 553-8.

Glass, N. L., Jacobson, D. J. & Shiu, P. K. 2000. The genetics of hyphal fusion and vegetative incompatibility in filamentous ascomycete fungi. *Annu Rev Genet,* 34**,** 165-186.

Goncalves, A. P., Cordeiro, J. M., Monteiro, J., Munoz, A., Correia-De-Sa, P., Read, N. D. & Videira, A. 2014. Activation of a TRP-like channel and intracellular Ca2+ dynamics during phospholipase-C-mediated cell death. *J Cell Sci,* 127**,** 3817-29.

Gonzalez, G. M., Marquez, J., Trevino-Rangel Rde, J., Palma-Nicolas, J. P., Garza-Gonzalez, E., Cecenas, L. A. & Gerardo Gonzalez, J. 2013. Murine model of disseminated fusariosis: evaluation of the fungal burden by traditional CFU and quantitative PCR. *Mycopathologia,* 176**,** 219-24.

Gooday, G. W. 1974. Fungal sex hormones. *Annu Rev Biochem,* 43**,** 35-87.

Gopinath, V. & Velusamy, P. 2013. Extracellular biosynthesis of silver nanoparticles using Bacillus sp. GP-23 and evaluation of their antifungal activity towards *Fusarium oxysporum. Spectrochim Acta A Mol Biomol Spectrosc,* 106**,** 170-4.

Gorscak, J. J., Ayres, B,D,, Bhagat, N., Hammersmith, K.M., Rapuano, C.J., Cohen, E.J., Burday, M., Mirani, N., Jungkind, D., Chu, D.S. 2007. An outbreak of *Fusarium* keratitis associated with contact lens use in the Northeastern United States. *Cornea,* 26**,** 1187-1194.

Goryachev, A. B, Lichius, A., Wright, G. D., Read, N. D. 2012. Excitable behavior can explain the "ping-pong" mode of communication between cells using the same chemoattractant. *Bioessays,* 34**,** 259-66.

Graphpad Prism. 2016. Accessed at: http://www.graphpad.com/scientific-software/prism/ (Accessed: 20 Dec 2015).

Gu, Z., Buelow, D. R., Petraitiene, R., Petraitis, V., Walsh, T. J. & Hayden, R. T. 2014. Quantitative multiplexed detection of common pulmonary fungal pathogens by labeled primer polymerase chain reaction. *Arch Pathol Lab Med,* 138**,** 1474-80.

Guarner, J. & Brandt, M. E. 2011. Histopathologic diagnosis of fungal infections in the 21st century. *Clin Microbiol Rev,* 24**,** 247-80.

Guarro, J. 2013. Fusariosis, a complex infection caused by a high diversity of fungal species refractory to treatment. *Eur J Clin Microbiol Infect Dis,* 32**,** 1491-500.

Gullino, M.L., Katan, J., Garibaldi, A. (eds) 2012. *Fusarium* wilts of greenhouse vegetable and ornamental crops, St Paul, MN American Phytopathological Society, 1-15.

Gungel, H., Eren, M. H., Pinarci, E. Y., Altan, C., Baylancicek, D. O., Kara, N., Gursel, T., Yegenoglu, Y. & Susever, S. 2011. An outbreak of *Fusarium solani* endophthalmitis after cataract surgery in an eye training and research hospital in Istanbul. *Mycoses,* 54**,** e767-74.

Gupta, A. K., Baran, R., Summerbell, C. 2000. *Fusarium* infections of the skin. *Curr Opin Infect Dis,* 13**,** 121-128.

Gupta, V. K., Misra, A. K. & Gaur, R. K. 2010. Growth characteristics of *Fusarium* SPP. causing wilt disease in *Psidium guajava* L. in India. . *Journal of plant protection research,* 50**,** 452 - 462.

Hallen, H. E. & Trail, F. 2008. The L-type calcium ion channel cch1 affects ascospore discharge and mycelial growth in the filamentous fungus *Gibberella zeae* (anamorph *Fusarium graminearum*). *Eukaryot Cell,* 7**,** 415-24.

Harris, S. D. 2005. Morphogenesis in germinating *Fusarium graminearum* macroconidia. *Mycologia,* 97**,** 880-7.

Hayes, S., Boote, C., Lewis, J., Sheppard, J., Abahussin, M., Quantock, A. J., Purslow,

C., Votruba, M. & Meek, K. M. 2007. Comparative study of fibrillar collagen arrangement in the corneas of primates and other mammals. *Anat Rec (Hoboken),* 290**,** 1542-50.

He, D., Hao, J., Gao, S., Wan, X., Wang, W., Shan, Q. & Wang, L. 2016. Etiological analysis of fungal keratitis and rapid identification of predominant fungal pathogens. *Mycopathologia,* 181**,** 75-82.

HRT Rostock Cornea Module. 2016. Available at: https://www.heidelbergengineering.com/us/products/hrt-glaucoma-module/cornea-module/ (Accessed: 15 Dec 2015).

Hepler, P. K. 2005. Calcium: A central regulator of plant growth and development. *Plant Cell,* 17**,** 2142-2155.

Herbrecht, R., Sabou, M. & Ledoux, M. P. 2013. [Clinical and radiological aspects of mucormycosis]. *Med Sci (Paris),* 29 Spec No 1**,** 19-24.

Hernandez-Ortiz, P., Chang, C.-C., Chu, M. and Read, N.D. Calcium signaling during CAT formation and chemotropism in *Neurospora crassa*. In preparation

Herzog, S., Schumann, M. R. & Fleissner, A. 2015. Cell fusion in *Neurospora crassa. Curr Opin Microbiol,* 28**,** 53-9.

Hickey, P. C., Jacobson, D., Read, N. D. & Glass, N. L. 2002. Live-cell imaging of vegetative hyphal fusion in *Neurospora crassa. Fungal Genet Biol,* 37**,** 109-19.

Hickey, P. C., Swift, S. R., Roca, M. G. & Read, N. D. 2005. Live-cell imaging of filamentous fungi using vital fluorescent dyes and confocal microscopy. 34**,** 63-87.

Hogan, D. & Wheeler, R. T. 2014. The complex roles of NADPH oxidases in fungal infection. *Cell Microbiol,* 16**,** 1156-67.

Hol, J. A., Wolfs, T. F., Bierings, M. B., Lindemans, C. A., Versluys, A. B., Wildt De, A., Gerhardt, C. E. & Boelens, J. J. 2014. Predictors of invasive fungal infection in pediatric allogeneic hematopoietic SCT recipients. *Bone Marrow Transplant,* 49**,** 95-101.

Homa, M., Shobana, C. S., Singh, Y. R., Manikandan, P., Selvam, K. P., Kredics, L., Narendran, V., Vagvolgyi, C. & Galgoczy, L. 2013. *Fusarium* keratitis in South India: causative agents, their antifungal susceptibilities and a rapid identification method for the *Fusarium solani* species complex. *Mycoses,* 56**,** 501-11.

Horn, D. L., Freifeld, A. G., Schuster, M. G., Azie, N. E., Franks, B. & Kauffman, C. A. 2014. Treatment and outcomes of invasive fusariosis: review of 65 cases from the PATH Alliance((R)) registry. *Mycoses,* 57**,** 652-8.

Hu, J., Hu, Y., Chen, S., Dong, C., Zhang, J., Li, Y., Yang, J., Han, X., Zhu, X. & Xu, G. 2014. Role of activated macrophages in experimental *Fusarium solani* keratitis. *Exp Eye Res,* 129**,** 57-65.

Hua, X., Yuan, X., Di Pietro, A., Wilhelmus, K.R. 2010. The molecular pathogenicity of *Fusarium* keratitis. *Cornea,* 29**,** 1440-1444.

Iida, Y., Fujiwara, K., Yoshioka, Y. & Tsuge, T. 2014. Mutation of FVS1, encoding a protein with a sterile alpha motif domain, affects asexual reproduction in the fungal plant pathogen *Fusarium oxysporum. FEMS Microbiol Lett,* 351**,** 104-112.

Ikeda, I., Ohno, T., Ohno, H., Miyazaki, Y., Nishimoto, K., Fukushima, S., Makino, T.

& Ihn, H. 2014. Case of *Fusarium* paronychia successfully treated with occlusive dressing of antifungal cream. *J Dermatol,* 41**,** 340-2.

Image J. 2016. Available at: https://imagej.nih.gov/ij/ (Accessed: 20 Sep 2012).

Imaris. 2016. Available at: http://www.bitplane.com/ (Accessed: 15 Jan 2015).

Inano, S., Kimura, M., Iida, J. & Arima, N. 2013. Combination therapy of voriconazole and terbinafine for disseminated fusariosis: case report and literature review. *J Infect Chemother,* 19**,** 1173-80.

Ishikawa, F. H., Souza, E. A., Read, N. D. & Roca, M. G. 2010. Live-cell imaging of conidial fusion in the bean pathogen, *Colletotrichum lindemuthianum. Fungal Biol,* 114**,** 2-9.

Ishikawa, F. H., Souza, E. A., Shoji, J. Y., Connolly, L., Freitag, M., Read, N. D. & Roca, M. G. 2012. Heterokaryon incompatibility is suppressed following conidial anastomosis tube fusion in a fungal plant pathogen. *PLoS One,* 7**,** e31175.

Jiang, K., Brownstein, S., Baig, K., Lam, K., Toye, B. 2013. Clinicopathologic case reports of *Alternaria* and *Fusarium* keratitis in Canada. *Can J Ophthalmol,* 48**,** e151-e153.

Jones & Epstein, L. 1989. Adhesion of *Nectria haematococca* macroconidia. *Plant and Molecular Plant Pathology,* 35**,** 453-461.

Jonkers, W., Leeder, A. C., Ansong, C., Wang, Y., Yang, F., Starr, T. L., Camp, D. G., 2nd, Smith, R. D. & Glass, N. L. 2014. HAM-5 functions as a MAP kinase scaffold during cell fusion in *Neurospora crassa*. *PLoS Genet,* 10**,** e1004783.

Joseph, R., Srivastava, O.P., Pfister, R.R. 2014. Downregulation of β-actin and its regulator gene HuR affect cell migration of human corneal fibroblasts. *Molecular Vision*, 20, 593-605.

Joshi, M., Srivastava, R., Sharma, A. K. & Prakash, A. 2013. Isolation and characterization of *Fusarium oxysporum*, a wilt causing fungus, for its pathogenic and non-pathogenic nature in tomato (*Solanum lycopersicum*). *Journal of Applied and Natural Science,* 5**,** 108 - 117.

Jullienne, R., He, Z., Manoli, P., Grivet, D., Cinotti, E., Perrot, J.L., Labeile, B., Cambazard, F., Gain, P., Thuret, G. 2015. *In vivo* confocal microscopy of pine processionary caterpillar hair-induced keratitis. *Cornea,* 34**,** 350-352.

Kadri, S. S., Remy, K. E., Strich, J. R., Gea-Banacloche, J. & Leitman, S. F. 2015. Role of granulocyte transfusions in invasive fusariosis: systematic review and single-center experience. *Transfusion,* 55**,** 2076-85.

Kah, T. A., Yong, K. C. & Rahman, R. A. 2011. Disseminated fusariosis and endogenous fungal endophthalmitis in acute lymphoblastic leukemia following platelet transfusion possibly due to transfusion-related immunomodulation. *BMC Ophthalmol,* 11**,** 30.

Kalaiselvi, G., Narayana, S., Krishnan, T. & Sengupta, S. 2015. Intrastromal voriconazole for deep recalcitrant fungal keratitis: a case series. *Br J Ophthalmol,* 99**,** 195-8.

Kang, Y., Li, L., Zhu, J., Zhao, Y. & Zhang, Q. 2013. Identification of *Fusarium* from a patient with fungemia after multiple organ injury. *Mycopathologia,* 176**,** 151-5.

Kapp, M., Schargus, M., Deuchert, T., Springer, J., Wendel, F., Loeffler, J., Grigoleit,

G. U., Kurzai, O., Heinz, W., Einsele, H. & Stuhler, G. 2011. Endophthalmitis as primary clinical manifestation of fatal fusariosis in an allogeneic stem cell recipient. *Transpl Infect Dis,* 13**,** 374-9.

Karthikeyan, R. S., Leal, S. M., Jr., Prajna, N. V., Dharmalingam, K., Geiser, D. M., Pearlman, E. & Lalitha, P. 2011. Expression of innate and adaptive immune mediators in human corneal tissue infected with *Aspergillus* or *Fusarium. J Infect Dis,* 204**,** 942-50.

Karthikeyan, R. S., Vareechon, C., Prajna, N. V., Dharmalingam, K., Pearlman, E. & Lalitha, P. 2015. Interleukin 17 expression in peripheral blood neutrophils from fungal keratitis patients and healthy cohorts in southern India. *J Infect Dis,* 211**,** 130-4.

Katz, T., Wasiak, J., Cleland, H. & Padiglione, A. 2014. Incidence of non-candidal fungal infections in severe burn injury: an Australian perspective. *Burns,* 40**,** 881-6.

Kebabci, N., Van Diepeningen, A. D., Ener, B., Ersal, T., Meijer, M., Al-Hatmi, A. M., Ozkocaman, V., Ursavas, A., Cetinoglu, E. D. & Akalin, H. 2014. Fatal breakthrough infection with *Fusarium andiyazi*: new multi-resistant aetiological agent cross-reacting with *Aspergillus* galactomannan enzyme immunoassay. *Mycoses,* 57**,** 249-55.

Keskar, V. S., Wanjare, S., Jamale, T. E., Mahajan, D., Jawale, S. Y., Fernandes, G., Suryawanshi, R. & Hase, N. K. 2014. Subcutaneous hyalohyphomycosis caused by *Fusarium* in a kidney transplant recipient. *Ren Fail,* 36**,** 1129-32.

Khor, W. B., Aung, T., Saw, S.M., Wong, T.Y., Tambyah, P.A., Tan, A.L., *et al*., 2006. An outbreak of *Fusarium* keratitis associated with contact lens wear in Singapore. *JAMA,* 295**,** 2867-2873.

Khwakhali, U. S. & Denning, D. W. 2015. Burden of serious fungal infections in Nepal. *Mycoses,* 58 Suppl 5**,** 45-50.

Kilvington, S., Lam, A., Nikolic, M. & Brady, N. 2013. Resistance and growth of *Fusarium* species in contact lens disinfectant solutions. *Optom Vis Sci,* 90**,** 430-8.

Kim, H. S., Czymmek, K. J., Patel, A., Modla, S., Nohe, A., Duncan, R., Gilroy, S. & Kang, S. 2012. Expression of the Cameleon calcium biosensor in fungi reveals distinct Ca^{2+} signatures associated with polarized growth, development, and pathogenesis. *Fungal Genet Biol,* 49**,** 589-601.

Kim, H. S., Kim, J. E., Frailey, D., Nohe, A., Duncan, R., Czymmek, K. J. & Kang, S. 2015. Roles of three *Fusarium oxysporum* calcium ion (Ca(2+)) channels in generating Ca(2+) signatures and controlling growth. *Fungal Genet Biol,* 82**,** 145-57.

Kim, M. S., Lee, H.M. 2011. Breakthrough disseminated fusariosis in an immunocompromised patient on voriconazole therapy. *International Journal of Dermatology,* 51**,** 616–628.

King, B. A., Seropian, S., Fox, L.P. 2011. Disseminated *Fusarium* infection with muscle involvement. *J Am Acad Dermatol.* 65**,** 235-237.

Kirichok, Y., Krapivinsky, G., Clapham, D.E. 2004. The mitochondrial calcium uniporter is a highly selective ion channel. *Nature,* 427**,** 360-364.

Kistler, H. C. 1997. Genetic diversity in the plant-pathogenic Fungus *Fusarium oxysporum. Phytopathology,* 87**,** 474-9.

Kistler, H. C., Alabouvette, C., Baayen, R.P., Bentley, S., Brayford, D., Coddington, A., *et al*., 1997. Systematic numbering of vegetative compatibility groups in the plant pathogenic fungus *Fusarium oxysporum. Phytopathology,* 1031**,** 30-32.

Kistler, H. C., Rep, M. & Ma, L. J. 2013. *Structural dynamics of Fusarium genomes,* USA, Caister Academic Press.

Kothari, S. G. & Kothari, R. S. 2014. Successful treatment of *Fusarium* keratitis after photo refractive keratectomy. *Indian J Ophthalmol,* 62**,** 661.

Kozel, T. R. & Wickes, B. 2014. Fungal diagnostics. *Cold Spring Harb Perspect Med,* 4**,** a019299.

Kredics, L., Narendran, V., Shobana, C. S., Vagvolgyi, C. & Manikandan, P. 2015. Filamentous fungal infections of the cornea: a global overview of epidemiology and drug sensitivity. *Mycoses,* 58**,** 243-60.

Kumar, C. P. G., Menon, T., Prabu, D., Nandhakumar, B. 2006. Chlamydosporulation of *Candida albicans* and *Candida dubliniensis* on mustard agar. *Mycoses,* 50**,** 71–73.

Kuo, K. & Hoch, H. C. 1995. Visualisation of the extracellular matrix surrounding pycnidiospores, germlings, and appressoria of *Phyllosticta ampelicida*. *Mycologia,* 87**,** 757-771.

Kuo, K. & Hoch, H. C. 1996. Germination of *Phyllosticta ampelicida* pycnidiospores: prerequisite of adhesion to the substratum and the relationship of substratum wettability. *Fungal Genet Biol,* 20**,** 18-29.

Kwon, Y. H. & Epstein, L. 1993. A 90-kDa glycoprotein associated with adhesion of *Nectria hematococca* macroconidia to substrata. *Molecular Plant- Microbe Interactions,* 6**,** 481-487.

Lai, J., Pandya, V., Mcdonald, R. & Sutton, G. 2014. Management of *Fusarium* keratitis and its associated fungal iris nodule with intracameral voriconazole and amphotericin B. *Clin Exp Optom,* 97**,** 181-3.

Lamoth, F., Alexander, B. D., Juvvadi, P. R. & Steinbach, W. J. 2015. Antifungal activity of compounds targeting the Hsp90-calcineurin pathway against various mould species. *J Antimicrob Chemother,* 70**,** 1408-11.

Landa, B. B., Navas-Cortés, J. A., Hervás, A. & Jiménez-Díaz, R. M. 2001. Influence of temperature and inoculum density of *Fusarium oxysporum* f sp *ciceris* on suppression of *Fusarium* wilt of chickpea by rhizosphere bacteria. *Phytopathology,* 91**,** 807-16.

Latgé, J.-P. (2007) The cell wall: a carbohydrate armour for the fungal cell. *Molecular Microbiology*, 66, 279-290.

Laurence, M. H., Burgess, L. W., Summerell, B. A. & Liew, E. C. 2012. High levels of diversity in *Fusarium oxysporum* from non-cultivated ecosystems in Australia. *Fungal Biol,* 116**,** 289-97.

Le Clech, L., Hutin, P., Le Gal, S. & Guillerm, G. 2014. Skin nodules in a patient with acute lymphoblastic leukaemia. *BMJ Case Rep,* 2014.

Leal, S. M., Jr., Roy, S., Vareechon, C., Carrion, S., Clark, H., Lopez-Berges, M. S., *et al*., 2013. Targeting iron acquisition blocks infection with the fungal pathogens

Aspergillus fumigatus and *Fusarium oxysporum*. *PLoS Pathog,* 9**,** e1003436.

Lee, H. S., Phat, C., Nam, W. S. & Lee, C. 2014. Optimization of culture conditions of *Fusarium solani* for the production of neo N-methylsansalvamide. *Biosci Biotechnol Biochem,* 78**,** 1421-7.

Lee, J. H., Lee, S., Yoon, C. J., Park, J. H., Tchah, H., Kim, M. J. & Kim, K. H. 2016. Comparison of reflectance confocal microscopy and two-photon second harmonic

generation microscopy in fungal keratitis rabbit model *ex vivo*. *Biomed Opt Express,* 7**,** 677-87.

Leeder, A. C., Jonkers, W., Li, J. & Glass, N. L. 2013. Early colony establishment in *Neurospora crassa* requires a MAP kinase regulatory network. *Genetics,* 195**,** 883-98.

Legrand, C., Anaissie, E., Hashem, R., Nelson, P., Bodey, G.P., Ro, J. 1991. Experimental *Fusarial* hyalohyphomycosis in a murine model. *The Journal of Infectious Diseases,* 164**,** 944-948.

Leica TCS SP8. 2016. Available at: http://www.leica-microsystems.com/products/confocal-microscopes/details/product/leica-tcs-sp8/ (Accessed: 15 Dec 2015).

Lew, R. R., Abbas, Z., Anderca, M. I. & Free, S. J. 2008. Phenotype of a mechanosensitive channel mutant, mid-1, in a filamentous fungus, *Neurospora crassa. Eukaryot Cell,* 7**,** 647-55.

Li, C., Zuo, C., Deng, G., Kuang, R., Yang, Q., Hu, C., *et al*., 2013. Contamination of bananas with beauvericin and fusaric acid produced by *Fusarium oxysporum* f. sp. *cubense*. *PLoS One,* 8**,** e70226.

Li, Z., Jhanji, V., Tao, X., Yu, H., Chen, W. & Mu, G. 2013. Riboflavin/ultravoilet light-mediated crosslinking for fungal keratitis. *Br J Ophthalmol,* 97**,** 669-71.

Lichius, A., Berepiki, A. & Read, N. D. 2011. Form follows function -- the versatile fungal cytoskeleton. *Fungal Biol,* 115**,** 518-40.

Lichius, A., Goryachev, A. B., Fricker, M. D., Obara, B., Castro-Longoria, E. & Read, N. D. 2014. CDC-42 and RAC-1 regulate opposite chemotropisms in *Neurospora crassa. J Cell Sci,* 127**,** 1953-65.

Lichius, A. & Lord, K. M. 2014. Chemoattractive mechanisms in filamentous fungi. *The Open Mycology Journal,* 8**,** 28 - 57.

Lida, Y., Fujiwara, K., Yoshioka, Y. & Tsuge, T. 2014. Mutation of FVS1, encoding a protein with a sterile alpha motif domain, affects asexual reproduction in the fungal plant pathogen *Fusarium oxysporum*. *FEMS Microbiol Lett*, 351, 104–112.

Lievens, B., Rep, M. & Thomma, B. P. 2008. Recent developments in the molecular discrimination of formae speciales of *Fusarium oxysporum*. *Pest Manag Sci.,* 64**,** 781-8.

Lievens, B., Houterman, P. M. & Rep, M. 2009. Effector gene screening allows unambiguous identification of *Fusarium oxysporum* f. sp. *lycopersici* races and discrimination from other formae speciales. *FEMS Microbiol Lett*, 300, 201-15.

Lin, X. & Heitman, J. 2005. Chlamydospore formation during hyphal growth in Cryptococcus neoformans. *Eukaryot Cell,* 4**,** 1746-54.

Linden, H., Ballario, P., Macino, G. 1997. Blue light regulation in *Neurospora crassa*. *Fungal Genetics and Biology,* 22**,** 141-150.

Lisovskaia, S. A., Glushko, N. I. & Khaldeeva, E. V. 2013. [Pathogenic properties of fungi *Fusarium* genus isolated from patients with atopic dermatitis]. *Zh Mikrobiol Epidemiol Immunobiol***,** 88-92.

Liu, S., Hou, Y., Liu, W., Lu, C., Wang, W. & Sun, S. 2015. Components of the calcium-calcineurin signaling pathway in fungal cells and their potential as antifungal targets. *Eukaryot Cell,* 14**,** 324-34.

Liu, Y., Jia, H., Shi, X., Wang, J., Ning, Y., He, B., Wang, C. & Zheng, X. 2013. Minimal trephination penetrating keratoplasty for severe fungal keratitis complicated with hypopyon. *Can J Ophthalmol,* 48**,** 529-34.

Lockwood, M. B. & Crescencio, J. C. 2016. Adventitious sporulation in *Fusarium*: The yeast that were not. *IDCases,* 3**,** 5-7.

Long, A. P., Manneschmidt, A. K., Verbrugge, B., Dortch, H. R., Minkin, S. C., Prater, K. E., Biggerstaff, J. P., Dunlap, J. R., Dalhaimer, P. 2012. Lipid droplet de novo formation and fission are linked to the cell cycle in fission yeast. *Traffic,* 13**,** 705-714.

Low, C. Y. & Rotstein, C. 2011. Emerging fungal infections in immunocompromised patients. *F1000 Med Rep,* 3**,** 14.

Ma, L., Van Der Does, H., Borkovich, K., Coleman, J., Daboussi, M., Di Pietro, A. & Al., E. 2010. Comparative genomics reveals mobile pathogenicity chromosomes in *Fusarium. Nature.,* 18**,** 367-73.

Magan, N., Aldred, D., Hope, R. & Mitchell, D. 2010. Environmental factors and interactions with mycobiota of grain and grapes: effects on growth, deoxynivalenol and ochratoxin production by *Fusarium culmorum* and *Aspergillus carbonarius. Toxins (Basel),* 2**,** 353-66.

Malek, I., Bouguila, H., Nacef, L. & Ayed, S. 2013. [Favorable outcome in a case of complicated fungal keratitis]. *J Fr Ophtalmol,* 36**,** 289-91.

Manzanilla-Loˊ Pez, R. H., Esteves, I., Finetti-Sialer, M.M., Hirsch, P.R., Ward, E., Devonshire, J., Hidalgo-DiˊAz, L. 2013. *Pochonia chlamydosporia*: Advances and challenges to improve its performance as a biological control agent of sedentary endo-parasitic nematodes. *Journal of Nematology* 45**,** 1–7.

Marinach-Patrice, C., Lethuillier, A., Marly, A., Brossas, J. Y., Gene, J., Symoens, F., Datry, A., Guarro, J., Mazier, D. & Hennequin, C. 2009. Use of mass spectrometry to identify clinical *Fusarium* isolates. *Clin Microbiol Infect,* 15**,** 634-42.

Martin, D. C., Kim, H., Mackin, N. A., Maldonado-Baez, L., Evangelista, C. C., Jr., Beaudry, V. G., Dudgeon, D. D., Naiman, D. Q., Erdman, S. E. & Cunningham, K. W. 2011. New regulators of a high affinity Ca2+ influx system revealed through a genome-wide screen in yeast. *J Biol Chem,* 286**,** 10744-54.

Mayayo, E., Pujol, I., Guarro, J. 1999. Experimental pathogenicity of four opportunist *Fusarium* species in a murine model. *J. Med. Microbiol.,* 48**,** 363-366.

Meadows, B. R. A. 2012. Live cell imaging of lipid droplet distribution and motility in the filamentous fungus *Ustilago maydis.* Unpublished MRes thesis. University of Exeter. 28-50.

Mehrabi, R., Bahkali, A. H., Abd-Elsalam, K. A., Moslem, M., Ben M'barek, S., Gohari, A. M., Jashni, M. K., Stergiopoulos, I., Kema, G. H. & De Wit, P. J. 2011. Horizontal gene and chromosome transfer in plant pathogenic fungi affecting host range. *FEMS Microbiol Rev,* 35**,** 542-54.

Mehta, A. & Bellam, N. 2014. Disseminated fusariosis during acute myelogenous leukemia induction treatment. *Blood,* 123**,** 3379.

Mela, E. K., Anastassiou, E. D., Gartaganis, S. P. & Christofidou, M. 2015. Fungal isolation from disinfectant solutions of contact lens storage cases among asymptomatic users. *Eye Contact Lens,* 41**,** 87-90.

Mesquita-Rocha, S., Godoy-Martinez, P. C., Goncalves, S. S., Urrutia, M. D., Carlesse, F., Seber, A., Silva, M. A., Petrilli, A. S. & Colombo, A. L. 2013. The water supply system as a potential source of fungal infection in paediatric haematopoietic stem cell units. *BMC Infect Dis,* 13**,** 289.

Mesterhazy, A. 1973. The morphology of an undescribed form of anastomosis in *Fusarium. Mycologia,* 65**,** 916 - 919.

Michielse, C. B. & Rep, M. 2009. Pathogen profile update: *Fusarium oxysporum. Mol Plant Pathol,* 10**,** 311-24.

Mikosz, C. A., Smith, R. M., Kim, M., Tyson, C., Lee, E. H., Adams, E., *et al.,* 2014. Fungal endophthalmitis associated with compounded products. *Emerg Infect Dis,* 20**,** 248-56.

Mochizuki, K., Shiraki, I., Murase, H., Ohkusu, K. & Nishimura, K. 2012. Identification and sensitivity of two rare fungal species isolated from two patients with *Fusarium* keratomycosis. *J Infect Chemother,* 18**,** 939-44.

Molnar, A., Sulyok, L. & Hornok, L. 1990. Parasexual recombination between vegetatively incompatible species in *Fusarium oxysporum. Myco. Res.,* 94**,** 393 - 398.

Monod, M., Lurati, M. & Baudraz-Rosselet, F. 2013. [Diagnosis of non dermatophyte onychomycosis ant its relevance for treatment]. *Rev Med Suisse,* 9**,** 730-3.

Moore, D., Robson, G.D. and Trinci, A.P.J. 2011. 21st Century Guidebook to Fungi. Cambridge University Press.

Montazeri, M. & Mojaradi, M. 2008. The effect of nutrition on conidiation and conidial germination of *Fusarium anthophilum* obtained from barnyard grass (*Echinochloa crus-galli*). *Caspian J. Env., Sci.,* 6**,** 25 - 30.

Morales-Cardona, C. A., Valbuena-Mesa, M. C., Alvarado, Z. & Solorzano-Amador, A. 2014. Non-dermatophyte mould onychomycosis: a clinical and epidemiological study at a dermatology referral centre in Bogota, Colombia. *Mycoses,* 57**,** 284-93.

Morel, L. N., Cid, P. M., De Celada, R. M., Rodriguez, M. F., Beato, M., Arias, A. G. & Laguna Rde, L. 2013. Disseminated fusariosis in a pediatric population. *Pediatr Dermatol,* 30**,** e255-6.

Human type AB serum. 2016. Available at:
http://www.mpbio.com/product.php?pid=0929309
(Accessed: 15 March 2014).

Muhammed, M., Anagnostou, T., Desalermos, A., Kourkoumpetis, T. K., Carneiro, H. A., Glavis-Bloom, J., Coleman, J. J. & Mylonakis, E. 2013. *Fusarium* infection:

report of 26 cases and review of 97 cases from the literature. *Medicine (Baltimore),* 92**,** 305-16.

Mukherjee, P. K., Chandra, J., Retuerto, M., Sikaroodi, M., Brown, R. E., Jurevic, R., *et al.*, 2014. Oral mycobiome analysis of HIV-infected patients: identification of *Pichia* as an antagonist of opportunistic fungi. *PLoS Pathog,* 10**,** e1003996.

Muller, E. M., Locke, E.G., Cunningham, K.W. 2001. Differential regulation of two Ca2+ influx systems by pheromone signalling in *Saccharomyces cerevisiae. Genetics* 159**,** 1527-1538.

Muraosa, Y., Schreiber, A. Z., Trabasso, P., Matsuzawa, T., Taguchi, H., Moretti, M. L., Mikami, Y. & Kamei, K. 2014. Development of cycling probe-based real-time PCR system to detect *Fusarium* species and *Fusarium solani* species complex (FSSC). *Int J Med Microbiol,* 304**,** 505-11.

Nagygyorgy, E. D., Kovacs, B., Leiter, E., Miskei, M., Pocsi, I., Hornok, L. & Adam, A. L. 2014. Toxicity of abiotic stressors to *Fusarium* species: differences in hydrogen peroxide and fungicide tolerance. *Acta Microbiol Immunol Hung,* 61**,** 189-208.

Neji, S., Trabelsi, H., Cheikhrouhou, F., Sellami, H., Guidara, R., Trigui, A., Feki, J., Boudaya, S., Turki, H., Makni, F. & Ayadi, A. 2013. [Fusariosis diagnosed in the laboratory of an UH in Tunisia: epidemiological, clinical and mycological study]. *J Mycol Med,* 23**,** 130-5.

Nelson, G., Kozlova-Zwinderman, O., Collis, A. J., Knight, M. R., Fincham, J. R., Stanger, C. P., *et al.*, 2004. Calcium measurement in living filamentous fungi expressing codon-optimized aequorin. *Mol Microbiol,* 52**,** 1437-50.

Nenoff, P., Bernhardt, A., Tintelnot, K., Kingreen, V., Ducker, P., Cofalka, M. & Schaller, J. 2014. [Cutaneous infection due to *Fusarium oxysporum* in a female diabetic: molecular biological detection of the mold from formalin-fixed paraffin embedded tissue using sequencing of the ITS region of the rDNA]. *Hautarzt,* 65**,** 542-7.

Nenoff, P., Kruger, C., Ginter-Hanselmayer, G. & Tietz, H. J. 2014. Mycology - an update. Part 1: Dermatomycoses: causative agents, epidemiology and pathogenesis. *J Dtsch Dermatol Ges,* 12**,** 188-209; quiz 210, 188-211; quiz 212.

Nenoff, P., Paasch, U. & Handrick, W. 2014. [Infections of finger and toe nails due to fungi and bacteria]. *Hautarzt,* 65**,** 337-48.

Ng, A. S., Lau, W. W., Yu, D. K., Wong, C. C. & Chan, C. W. 2008. Clinical features and outcomes of *Fusarium* keratitis associated with contact lens wear. *Eye Contact Lens,* 34**,** 113-6.

Nicholson, R. L. & Epstein, L. 1991. *Adhesion of fungi to the plant surface,* New York and London, Pleanum Press.

Nielsen, S. E., Nielsen, E., Julian, H. O., Lindegaard, J., Hojgaard, K., Ivarsen, A., Hjortdal, J. & Heegaard, S. 2015. Incidence and clinical characteristics of fungal keratitis in a Danish population from 2000 to 2013. *Acta Ophthalmol,* 93**,** 54-8.

Nucci, F., Nouer, S. A., Capone, D., Anaissie, E. & Nucci, M. 2015. Fusariosis. *Semin Respir Crit Care Med,* 36**,** 706-14.

Nucci, M., Anaissie, E. 2002. Cutaneous infection by *Fusarium* species in healthy and immunocompromised hosts: implications for diagnosis and management.

Clinical Infectious Diseases, 35**,** 909-920.

Nucci, M. & Anaissie, E. 2007. *Fusarium* Infections in Immunocompromised Patients. *Clin Microbiol Rev,* 20**,** 695-704.

Nucci, M., Carlesse, F., Cappellano, P., Varon, A. G., Seber, A., Garnica, M., Nouer, S. A. & Colombo, A. L. 2014. Earlier diagnosis of invasive fusariosis with *Aspergillus* serum galactomannan testing. *PLoS One,* 9**,** e87784.

Nucci, M., Garnica, M., Gloria, A. B., Lehugeur, D. S., Dias, V. C., Palma, L. C., *et al*., 2013. Invasive fungal diseases in haematopoietic cell transplant recipients and in patients with acute myeloid leukaemia or myelodysplasia in Brazil. *Clin Microbiol Infect,* 19**,** 745-51.

Nucci, M., Marr, K. A., Vehreschild, M. J., De Souza, C. A., Velasco, E., Cappellano, P., *et al*., 2014. Improvement in the outcome of invasive fusariosis in the last decade. *Clin Microbiol Infect,* 20**,** 580-5.

Nucci, M., Varon, A. G., Garnica, M., Akiti, T., Barreiros, G., Trope, B. M. & Nouer, S. A. 2013. Increased incidence of invasive fusariosis with cutaneous portal of entry, Brazil. *Emerg Infect Dis,* 19**,** 1567-72.

O'Donnell, K., Sarver, B. A., Brandt, M., Chang, D. C., Noble-Wang, J., Park, B. J., *et al*., 2007. Phylogenetic diversity and microsphere array-based genotyping of human pathogenic Fusaria, including isolates from the multistate contact lens-associated U.S. keratitis outbreaks of 2005 and 2006. *J Clin Microbiol,* 45**,** 2235-48.

Oechsler, R. A., Feilmeier, M. R., Miller, D., Shi, W., Hofling-Lima, A. L. & Alfonso, E. C. 2013. *Fusarium* keratitis: genotyping, *in vitro* susceptibility and clinical outcomes. *Cornea,* 32**,** 667-73.

O'Hanlon, K. A., Cairns, T., Stack, D., Schrettl, M., Bignell, E. M., Kavanagh, K., Miggin, S. M., O'keeffe, G., Larsen, T. O. & Doyle, S. 2011. Targeted disruption of nonribosomal peptide synthetase pes3 augments the virulence of *Aspergillus fumigatus. Infect Immun,* 79**,** 3978-92.

Ohara, T. & Tsuge, T. 2004. FoSTUA, encoding a basic helix-loop-helix protein, differentially regulates development of three kinds of asexual spores, macroconidia, microconidia, and chlamydospores, in the fungal plant pathogen *Fusarium oxysporum. Eukaryot Cell,* 3**,** 1412-22.

Okura, Y., Kawamura, N., Okano, M., Toita, N., Takezaki, S., Yamada, M., Kobayashi, I. & Ariga, T. 2015. *Fusarium falciforme* infection in a patient with chronic granulomatous disease: Unique long-term course of epidural abscess. *Pediatr Int,* 57**,** e4-6.

Old, K. M., Schippers, B. 1973. Electron microscopical studies of chlamydospores of *Fusarium solani f. cucurbitae* formed in natural soil. *Soil Biol Biochem,* 5**,** 613-620.

Ortoneda, M., Guarro, J., Madrid, M. P., Caracuel, Z., Roncero, M. I. G., Mayayo, E. & Di Pietro, A. 2004. *Fusarium oxysporum* as a multihost model for the genetic dissection of fungal virulence in plants and mammals. *Infect Immun,* 72**,** 1760-1766.

Osherov, N., Yarden, O. 2010. The cell wall of filamentous fungi. In Cellular and Molecular Biology of Filamentous Fungi (ed KA Borkovich & D Ebbole),

American Society of Microbiology, 2224-2237.

Ostrosky-Zeichner, L. 2012. Invasive mycoses: diagnostic challenges. *Am J Med,* 125**,** S14-24.

Otter, J. A., Nowakowski, E., Salkeld, J. A., Duclos, M., Passaretti, C. L., Yezli, S., Ross, T., Carroll, K. C. & Perl, T. M. 2013. Saving costs through the decontamination of the packaging of unused medical supplies using hydrogen peroxide vapor. *Infect Control Hosp Epidemiol,* 34**,** 472-8.

Palma-Guerrero, J., Hall, C. R., Kowbel, D., Welch, J., Taylor, J. W., Brem, R. B. & Glass, N. L. 2013. Genome wide association identifies novel loci involved in fungal communication. *PLoS Genet,* 9**,** e1003669.

Pandey, A., Roca, M., Read, N. & Glass, N. 2004. Role of a mitogen-activated protein kinase pathway during conidial germination and hyphal fusion in *Neurospora crassa. Eukaryot Cell,* 3**,** 348-58.

Paramythiotou, E., Frantzeskaki, F., Flevari, A., Armaganidis, A. & Dimopoulos, G. 2014. Invasive fungal infections in the ICU: how to approach, how to treat. *Molecules,* 19**,** 1085-119.

Park, J. H., Sun, W., Cu, M. 2015. High-resolution *in vivo* imaging of mouse brain through the intact skull. *PNAS,* 112**,** 9236-9241.

Pellegrino, F. & Carrasco, M. A. 2013. Argon laser phototherapy in the treatment of refractory fungal keratitis. *Cornea,* 32**,** 95-7.

Penalva, M. A., Tilburn, J., Bignell, E. & Arst, H. N., Jr. 2008. Ambient pH gene regulation in fungi: making connections. *Trends Microbiol,* 16**,** 291-300.

Peng, H. X., Sivasithamparam, K. & Turner, D. W. 1999. Chlamydospore germination and *Fusarium wilt* of banana plantlets in suppressive and conducive soils are affected by physical and chemical factors. *Soil Biology and Biochemistry,* 31**,** 1363 - 1374.

Pereira, G. H., De Angelis, D. A., Brasil, R. A., Dos Anjos Martins, M., De Matos Castro E Silva, D., Szeszs, M. W. & De Souza Carvalho Melhem, M. 2013. Disseminated amphotericin-resistant fusariosis in acute leukemia patients: report of two cases. *Mycopathologia,* 175**,** 107-14.

Perini, G. F., Camargo, L. F., Lottenberg, C. L. & Hamerschlak, N. 2013. Disseminated fusariosis with endophthalmitis in a patient with hematologic malignancy. *Einstein (Sao Paulo),* 11**,** 545-6.

Phoku, J. Z., Dutton, M. F., Barnard, T. G. & Potgieter, N. 2014. Use of a bio-wipe kit to detect fumonisin B(1) in faecal materials. *Food Addit Contam Part A Chem Anal Control Expo Risk Assess,* 31**,** 1760-8.

Pietro, A. D., Madrid, M. P., Caracuel, Z., Delgado-Jarana, J. & Roncero, M. I. 2003. *Fusarium oxysporum*: exploring the molecular arsenal of a vascular wilt fungus. *Mol Plant Pathol,* 4**,** 315-25.

Ploetz, R. C. 2015. *Fusarium* wilt of banana. *Phytopathology,* 105**,** 1512-21.

Pol, A., Gross, S. P. & Parton, R. G. 2014. Biogenesis of the multifunctional lipid droplet: lipids, proteins, and sites. *J Cell Biol,* 204**,** 635-46.

Pontecorvo, G. 1956. The parasexual cycle in fungi. *Annu Rev Microbiol,* 10**,** 393-400.

Popovski, S. & Celar, F. A. 2012. The impact of environmental factors on the infection of cereals with *Fusarium* species and mycotoxin production – a review. *Acta*

agriculturae Slovenica, 101**,** 105 - 116.

Prados Rosales, R. C. & Di Pietro, A. 2008. Vegetative hyphal fusion is not essential for plant infection by *Fusarium oxysporum. Eukaryot Cell,* 7**,** 162-71.

Prinja, A., Roberts, C., Doherty, T. & Oddy, M. J. 2014. An unusual cause of an ankle mass. *BMJ Case Rep,* 2014.

Pujol, I., Guarro, J., Gene, J., Sala, J. 1997. *In vitro* antifungal susceptibility of clinical and environmental *Fusarium* spp. strains *Journal of Antimicrobial Chemotherapy,* 39**,** 163-167.

Rajmane, V. S., Rajmane, S. T., Patil, V. C., Patil, A. B. & Mohite, S. T. 2013. Maxillary rhinosinusitis due to *Fusarium* species leading to cavernous sinus thrombosis. *J Mycol Med,* 23**,** 53-6.

Ramirez, R. M. & Jacobs, R. L. 2014. Hypersensitivity pneumonitis by *Fusarium vasinfectum* in a home environment. *J Allergy Clin Immunol Pract,* 2**,** 483-4.

Ramon, A. M., Porta, A. & Fonzi, W. A. 1999. Effect of environmental pH on morphological development of *Candida albicans* is mediated via the PacC-related transcription factor encoded by PRR2. *J Bacteriol,* 181**,** 7524-30.

Read, N., Lichius, A., Shoji, J. & Goryachev, A. 2009. Self-signalling and self-fusion in filamentous fungi. *Curr Opin Microbiol.,* 12**,** 608-15.

Read, N. D., Kellock, Lj., Collins, T.J., Gundlach, A.M. 1997. Role of topography sensing for infection-structure differentiation in cereal rust fungi. *Planta,* 202**,** 163-170.

Read, N. D., Goryachev, A. B. & Lichius, A. 2012. The mechanistic basis of self fusion between conidial anastomosis tubes during fungal colony initiation. *Fungal Biology Reviews,* 26**,** 1 -11.

Rep, M. & Kistler, H. C. 2010. The genomic organization of plant pathogenicity in *Fusarium* species. *Curr Opin Plant Biol,* 13**,** 420-6.

Riquelme, M. 2013. Tip growth in filamentous fungi: a road trip to the apex. *Annu Rev Microbiol,* 67**,** 587-609.

Rispail, N., Soanes, D. M., Ant, C., Czajkowski, R., Grunler, A., Huguet, R., *et al*., 2009. Comparative genomics of MAP kinase and calcium-calcineurin signalling components in plant and human pathogenic fungi. *Fungal Genet Biol,* 46**,** 287-98.

Roca, G. M., Read, N. D. & Wheals, A. E. 2005. Conidial anastomosis tubes in filamentous fungi. *FEMS Microbiol Lett,* 249(2)**,** 191-8.

Roca, M. G., Davide, L. C., Davide, L. M. C., Mendes-Costa, M. C., Schwan, R. F. & Wheals, A. E. 2004. Conidial anastomosis fusion between *Colletotrichum* species. *Mycological Research,* 108**,** 1320-1326.

Roca, M. G., Kuo, H. C., Lichius, A., Freitag, M. & Read, N. D. 2010. Nuclear dynamics, mitosis, and the cytoskeleton during the early stages of colony initiation in *Neurospora crassa. Eukaryot Cell,* 9**,** 1171-83.

Roca Mg, A. J., Jeffree Ce, Read N. D. 2005. Cell biology of conidial anastomosis tubes in *Neurospora crassa. Eukaryot Cell,* 4**,** 911-9.

Roca Mg, D. L., Mendes-Costa Mc, Wheals A. 2003. Conidial anastomosis tubes in *Colletotrichum. Fungal Genet Biol.,* 40**,** 138-45.

Rodriguez-Galvez, E., Mendgen, K. 1995. The infection process of *Fusarium*

oxysporum in cotton root tips. *Protoplasma, 189,* 61-72.

Rojas-Tula, D. G., Gomez-Fernandez, M., Garcia-Lopez, J. J., Cobos-Ceballos, M. J., Gil-Fuentes, A., Perez-Laya, J. M., *et al.*, 2013. Endobronchial cryotherapy for a mycetoma. *J Bronchology Interv Pulmonol, 20,* 330-2.

Romani, L. 2004. Immunity to fungal infections. *Nat Rev Immunol, 4,* 1-23.

Rose, M. D. 1991. Nuclear fusion in yeast. *Annu. Rev. Microbiol., 45,* 539-567.

Ruan, Y., Kotraiah, Straney, D.C. 1995. Flavonoids stimulate spore germination in *Fusarium solani* pathogenic on legumes in a manner sensitive to inhibitors of cAMP-Dependent protein kinase. *Molecular Plant-Microbe Interactions, 8,* 929-938.

Ruhnke, M., Groll, A. H., Mayser, P., Ullmann, A. J., Mendling, W., Hof, H. & Denning, D. W. 2015. Estimated burden of fungal infections in Germany. *Mycoses,* 58 Suppl 5, 22-8.

Ruhnke, M., Groll, A. H., Mayser, P., Ullmann, A. J., Mendling, W., Hof, H. & Denning, D. W. 2015. Estimated burden of fungal infections in Germany. *Mycoses,* 58 Suppl 5, 22-8.

Ruiz-Roldan, M. C., Kohli, M., Roncero, M. I., Philippsen, P., Di Pietro, A. & Espeso, E. A. 2010. Nuclear dynamics during germination, conidiation, and hyphal fusion of *Fusarium oxysporum. Eukaryot Cell, 9,* 1216-24.

Rusnak, F., Mertz, P. 2000. Calcineurin: form and function. *Physiological reviews, 80,* 1484-1523.

Sandberg, Y., Clahsen-Van Groningen, M. C. & Ammatuna, E. 2015. Disseminated fusariosis. *Int J Infect Dis, 30,* 154-5.

Sanders, D., Pelloux, J., Browniee, C., Harper, J.F. 2002. Calcium at the crossroads of signaling. *The Plant Cell, 14,* S401-S417.

Sanders, I. R. 2006. Rapid disease emergence through horizontal gene transfer between eukaryotes. *Trends Ecol Evol, 21,* 656-8.

Schafer, K., Di Pietro, A., Gow, N.A.R., Maccallum, D. 2014. Murine model for *Fusarium oxysporum* invasive fusariosis reveals organ-specific structures for dissemination and long-term persistence. *PLoS ONE, 9,* e89920.

Scheel, C. M., Hurst, S. F., Barreiros, G., Akiti, T., Nucci, M. & Balajee, S. A. 2013. Molecular analyses of *Fusarium* isolates recovered from a cluster of invasive mold infections in a Brazilian hospital. *BMC Infect Dis, 13,* 49.

Schoffelmeer, E. A., Klis, F. M., Sietsma, J. H. & Cornelissen, B. J. 1999. The cell wall of *Fusarium oxysporum. Fungal Genet Biol, 27,* 275-82.

Schoustra, S. E., Debets, A. J., Slakhorst, M. & Hoekstra, R. F. 2007. Mitotic recombination accelerates adaptation in the fungus *Aspergillus nidulans. PLoS Genet, 3,* e68.

Sganga, G., Bianco, G., Fiori, B., Nure, E., Spanu, T., Lirosi, M. C., Frongillo, F. & Agnes, S. 2013. Surveillance of bacterial and fungal infections in the postoperative period following liver transplantation: a series from 2005-2011. *Transplant Proc, 45,* 2718-21.

Shahi, S., Beerens, B., Manders, E. M. & Rep, M. 2015. Dynamics of the establishment of multinucleate compartments in *Fusarium oxysporum. Eukaryot Cell, 14,* 78-85.

Sharma, A. K. & Chandra, S. 2013. Synthesis, structural and fungicidal studies of hydrazone based coordination compounds. *Spectrochim Acta A Mol Biomol Spectrosc,* 103**,** 96-100.

Sharon, A. & Shlezinger, N. 2013. Fungi infecting plants and animals: killers, non-killers, and cell death. *PLoS Pathog,* 9**,** e1003517.

Sharp, P. F., Manivannan, A., Xu, H. & Forrester, J. V. 2004. The scanning laser ophthalmoscope—a review of its role in bioscience and medicine. *Physics in Medicine and Biology*, 49, 1085-1096.

Short, D. P., O'donnell, K. & Geiser, D. M. 2014. Clonality, recombination, and hybridization in the plumbing-inhabiting human pathogen *Fusarium keratoplasticum* inferred from multilocus sequence typing. *BMC Evol Biol,* 14**,** 91.

Short, D. P., O'donnell, K., Thrane, U., Nielsen, K. F., Zhang, N., Juba, J. H. & Geiser, D. M. 2013. Phylogenetic relationships among members of the *Fusarium solani* species complex in human infections and the descriptions of *F. keratoplasticum* sp. nov. and *F. petroliphilum* stat. nov. *Fungal Genet Biol,* 53**,** 59-70.

Short, G. E., Lacy, M.L. 1975. Germination of *Fusarium solani* f.sp. *pisi* chlamydospores in the spermosphere of pea. *Phytopathology,* 64**,** 558-562.

Shovlin, J. P., Argueso, P., Carnt, N., Chalmers, R. L., Efron, N., Fleiszig, S. M., *et al.*, 2013. 3. Ocular surface health with contact lens wear. *Cont Lens Anterior Eye,* 36 Suppl 1**,** S14-21.

Siatiri, H., Daneshgar, F., Siatiri, N., Khodabande, A. 2011. The effects of voriconazole injection and topical voriconazole in the treatment of recalcitrant *Fusarium* keratitis. *Cornea,* 30**,** 827-875.

Sidhu, S., Chander, J. & Singh, K. 2013. Perinephric abscess caused by *Fusarium chlamydosporum* in an immunocompetent child: case report and identification of the morphologically atypical fungal strain. *Indian J Pathol Microbiol,* 56**,** 312-4.

Siekierka, J. J., Hung, S.H.Y., Poe, M., Lin, C.S., Sigal, N.H. 1989. A cytosolic binding protein for the immunosuppressant FK506 has peptidyl-prolyl isomerase activity but is distinct from cyclophilin. *Nature,* 341**,** 755-757.

Sigmaplot. 2016. Accessed at: http://www.sigmaplot.co.uk/products/sigmaplot/sigmaplot-details.php (Accessed: 15 Sep 2012)

Silva, G. M., Silveira, A. R., Betania, C. A., Macedo, D. P. & Neves, R. P. 2013. Disseminated fusariosis secondary to neuroblastoma with fatal outcome. *Mycopathologia,* 176**,** 233-6.

Silverman-Gavrila, L. B. & Lew, R. R. 2003. Calcium gradient dependence of *Neurospora crassa* hyphal growth. *Microbiology,* 149**,** 2475-85.

Simonin, A. R., Rasmussen, C. G., Yang, M. & Glass, N. L. 2010. Genes encoding a striatin-like protein (ham-3) and a forkhead associated protein (ham-4) are required for hyphal fusion in *Neurospora crassa*. *Fungal Genet Biol,* 47**,** 855-68.

Smitha, S. L. & Gopchandran, K. G. 2013. Surface enhanced Raman scattering, antibacterial and antifungal active triangular gold nanoparticles. *Spectrochim Acta A Mol Biomol Spectrosc,* 102**,** 114-9.

Soanes, D. & Richards, T. A. 2014. Horizontal gene transfer in eukaryotic plant

pathogens. *Annu Rev Phytopathol,* 52**,** 583-614.

Son, E. T., Choi, H. J., Lee, Y. M., Kim, J. H., Nam, D. H. & Cho, H. D. 2015. Cutaneous Fusariosis in Unprotected Snake Bite Wound of Farmer's Hand. *Arch Plast Surg,* 42**,** 254-6.

Srinivasan M., 2007. Infective keratitis: A challenge to Indian ophthalmologists. *Indian J Ophthalmol*, 55, 5-6.

Staib, P. & Morschhauser, J. 2007. Chlamydospore formation in *Candida albicans* and *Candida dubliniensis. Mycoses,* 50**,** 1-12.

Steinbach, W. J., Reedy, J. L., Cramer, R. A., Perfect, J. R. & Heitman, J. 2007. Harnessing calcineurin as a novel anti-infective agent against invasive fungal infections. *Nature Reviews Microbiology,* 5**,** 418-430.

Steinkellner, S., Mammerler, R. & Vierheilig, H. 2005. Microconidia germination of the tomato pathogen *Fusarium oxysporum* in the presence of root exudates. *Journal of Plant Interactions,* 1**,** 23 - 30.

Steinkellner, S., Mammerler, R. & Vierheilig, H. 2008. Germination of *Fusarium oxysporum* in root exudates from tomato plants challenged with different *Fusarium oxysporum* strains *Eur J Plant Pathol. ,* 122**,** 395-401.

Stempel, J. M., Hammond, S. P., Sutton, D. A., Weiser, L. M. & Marty, F. M. 2015. Invasive Fusariosis in the Voriconazole Era: Single-Center 13-Year Experience. *Open Forum Infect Dis,* 2**,** ofv099.

Sun, C. Q., Prajna, N. V., Krishnan, T., Mascarenhas, J., Rajaraman, R., Srinivasan, M., Raghavan, A., O'brien, K. S., Ray, K. J., Mcleod, S. D., Porco, T. C., Acharya, N. R. & Lietman, T. M. 2013. Expert prior elicitation and Bayesian analysis of the Mycotic Ulcer Treatment Trial I. *Invest Ophthalmol Vis Sci,* 54**,** 4167-73.

Sun, S., Zhao, G., Sun, X., Wang, Q. & Yu, B. 2014. [Etiology and pathogens of fungal endophthalmitis]. *Zhonghua Yan Ke Za Zhi,* 50**,** 808-13.

Taj-Aldeen, S. J., Chandra, P. & Denning, D. W. 2015. Burden of fungal infections in Qatar. *Mycoses,* 58 Suppl 5**,** 51-7.

Takahashi, T., Kida, J., Matsumoto, K., Uemura, M., Shintani, T., Imataki, O., Nakai, H., Morikami, T., Kubota, Y., Matsuoka, Y. & Taoka, T. 2014. [Picture in clinical hematology no. 71: Case of fungemia caused by *Fusarium* complicated with intractable acute myeloid leukemia]. *Rinsho Ketsueki,* 55**,** 287.

Talbot, N. J., Ebbole, D. J. & Hamer, J. E. 1993. Identification and characterisation of MPG1, a gene involved in pathogenicity from the rice blast fungus *Magnaporthae grisea*. *The Plant Cell.,* 5**,** 1575-1590.

Tamura, T., Asahara, M., Yamamoto, M., Yamaura, M., Matsumura, M., Goto, K., Rezaei-Matehkolaei, A., Mirhendi, H., Makimura, M. & Makimura, K. 2014. *In vitro* susceptibility of dermatomycoses agents to six antifungal drugs and evaluation by fractional inhibitory concentration index of combined effects of amorolfine and itraconazole in dermatophytes. *Microbiol Immunol,* 58**,** 1-8.

Taylor, P. R., Leal, S. M., Jr., Sun, Y. & Pearlman, E. 2014. *Aspergillus* and *Fusarium* corneal infections are regulated by Th17 cells and IL-17-producing neutrophils. *J Immunol,* 192**,** 3319-27.

Terasaki, J. M., Shah, S. K., Schnadig, V. J. & Valentine, V. G. 2014. Airway complication contributing to disseminated fusariosis after lung transplantation.

Transpl Infect Dis, 16**,** 621-4.

Tessari, G., Cagalli, A. & Girolomoni, G. 2014. Opportunistic deep cutaneous mycoses in solid organ transplant recipients. *G Ital Dermatol Venereol,* 149**,** 417-22.

Thewes, S. 2014. Calcineurin-Crz1 signaling in lower eukaryotes. *Eukaryot Cell,* 13**,** 694-705.

Thomas, P. A., Jesudasan, C. A., Geraldine, P. & Kaliamurthy, J. 2011. Adventitious sporulation in *Fusarium* keratitis. *Graefes Arch Clin Exp Ophthalmol,* 249**,** 1429-31.

Thomas, P. A. & Kaliamurthy, J. 2013. Mycotic keratitis: epidemiology, diagnosis and management. *Clin Microbiol Infect,* 19**,** 210-20.

Tintelnot, K. 2013. [Differential diagnosis for detection of hyphae in tissue]. *Pathologe,* 34**,** 503-10.

Tomita-Yokotani, K., Shinozaki, S. 2003. Growth of endophyte, *Neotyphodium*, and its host plant, tall fescue (*Festuca arundinacea*), under 3D-clinorotation. *Biol Sci Space*, 17, 57-60.

Tortorano, A. M., Prigitano, A., Esposto, M. C., Arsic Arsenijevic, V., Kolarovic, J., Ivanovic, D., Paripovic, L., Klingspor, L., Nordoy, I., Hamal, P., Arikan Akdagli, S., Ossi, C., Grancini, A., Cavanna, C., Lo Cascio, G., Scarparo, C., Candoni, A., Caira, M. & Drogari Apiranthitou, M. 2014. European Confederation of Medical Mycology (ECMM) epidemiological survey on invasive infections due to *Fusarium* species in Europe. *Eur J Clin Microbiol Infect Dis,* 33**,** 1623-30.

Tortorano, A. M., Richardson, M., Roilides, E., Van Diepeningen, A., Caira, M., Munoz, P., *et al.*, 2014. ESCMID and ECMM joint guidelines on diagnosis and management of hyalohyphomycosis: *Fusarium* spp., Scedosporium spp. and others. *Clin Microbiol Infect,* 20 Suppl 3**,** 27-46.

Triest, D., Stubbe, D., De Cremer, K., Pierard, D., Detandt, M. & Hendrickx, M. 2015. Banana infecting fungus, *Fusarium musae*, is also an opportunistic human pathogen: are bananas potential carriers and source of fusariosis? *Mycologia,* 107**,** 46-53.

Trinci, A. P. J. 1974. A study of the kinetics of hyphal extension and branch initiation of fungal mycelia. *Journal of general microbiology,* 81**,** 225-236.

Troke, P., Obenga, G., Gaujoux, T., Goldschmidt, P., Bienvenu, A. L., Cornet, M., Grenouillet, F., Pons, D., Ranque, S., Sitbon, K., Chaumeil, C., Borderie, V. & Lortholary, O. 2013. The efficacy of voriconazole in 24 ocular *Fusarium* infections. *Infection,* 41**,** 15-20.

Tucker, S. L. & Talbot, N. J. 2001. Surface attachment and pre-penetration stage development by plant pathogenic fungi. *Annu Rev Phytopathol,* 39**,** 385-417.

Turra, D. & Di Pietro, A. 2015. Chemotropic sensing in fungus-plant interactions. *Curr Opin Plant Biol,* 26**,** 135-40.

Turra, D., El Ghalid, M., Rossi, F. & Di Pietro, A. 2015. Fungal pathogen uses sex pheromone receptor for chemotropic sensing of host plant signals. *Nature,* 527**,** 521-4.

Ugalde, U. & Rodriguez-Urra, A. B. 2014. The Mycelium Blueprint: insights into the cues that shape the filamentous fungal colony. *Appl Microbiol Biotechnol,* 98**,**

8809-19.

Van Der Does, H. C., Duyvesteijn, R. G., Goltstein, P. M., Van Schie, C. C., Manders, E. M., Cornelissen, B. J. & Rep, M. 2008. Expression of effector gene SIX1 of *Fusarium oxysporum* requires living plant cells. *Fungal Genet Biol,* 45**,** 1257-64.

Van Eck, W. H., Schippers, B. 1975. Ultrastructure of the developing chlamydospores of *Fusarium solani* f. *cucurbitae in vitro*. *Soil Biol. Biochem.,* 8**,** 1-6.

Varon, A. G., Nouer, S. A., Barreiros, G., Trope, B. M., Magalhaes, F., Akiti, T., Garnica, M. & Nucci, M. 2014. Superficial skin lesions positive for Fusarium are associated with subsequent development of invasive fusariosis. *J Infect,* 68**,** 85-9.

Vasudevan, B., Hazra, N., Verma, R., Srinivas, V., Vijendran, P. & Badad, A. 2013. First reported case of subcutaneous hyalohyphomycosis caused by Paecilomyces variotii. *Int J Dermatol,* 52**,** 711-3.

Vemuganti, G. K., Garg, P., Gopinathan, U., Naduvilathu, T.J., John, R.K., Buddi, R., Rao, G.N. 2002. Evaluation of agent and host factors in progression of mycotic keratitis. *Ophthalmology,* 109**,** 1538-1546.

Venkat Ram, C. S. 1952. Soil bacteria and chlamydospore formation in *Fusarium solani*. *Nature,* 4334**,** 869.

Vlaardingerbroek, I., Beerens, B., Rose, L., Fokkens, L., Cornelissen, B. J. & Rep, M. 2016. Exchange of core chromosomes and horizontal transfer of lineage-specific chromosomes in *Fusarium oxysporum*. *Environ Microbiol*.

Walsh, T. J. & Gamaletsou, M. N. 2013. Treatment of fungal disease in the setting of neutropenia. *Hematology Am Soc Hematol Educ Program,* 2013**,** 423-7.

Wan, L. Y., Allen, K. J., Turner, P. C. & El-Nezami, H. 2014. Modulation of mucin mRNA (MUC5AC and MUC5B) expression and protein production and secretion in Caco-2/HT29-MTX co-cultures following exposure to individual and combined *Fusarium* mycotoxins. *Toxicol Sci,* 139**,** 83-98.

Wang, X., Lin, Z., Gao, L., Wang, A., Wan, Z., Chen, W., Yang, Y. & Li, R. 2013. Exome sequencing reveals a signal transducer and activator of transcription 1 (STAT1) mutation in a child with recalcitrant cutaneous fusariosis. *J Allergy Clin Immunol,* 131**,** 1242-3.

Weber, R. W. & Levetin, E. 2014. Allergen of the month--*Fusarium*. *Ann Allergy Asthma Immunol,* 112**,** A11.

Weber, R. W. S. & Pitt, D. 2001. Filamentous fungi- growth and physiology *Applied Mycology and Biotechnology. Elsevier Science.*

Weichert, M. & Fleissner, A. 2015. *Anastomosis and heterokaryon formation,* Switzerland, Springer International Publishing.

Weigert, R., Porat-Shliom, N. & Amornphimoltham, P. 2013. Imaging cell biology in live animals: ready for prime time. *J Cell Biol,* 201**,** 969-79.

Wheeler, K. A., Hurdman, B. F. & Pitt, J. I. 1991. Influence of pH on the growth of some toxigenic species of *Aspergillus*, *Penicillium* and *Fusarium*. *Int J Food Microbiol,* 12**,** 141-9.

Woltz, S. S. & Jones, J. P. 1971. Effect of varied iron, manganese, zinc nutrition on the *in vitro* growth of race 2 *Fusarium oxysporum* f.sp. *lycopersici* and upon the

wilting of tomato cuttings held in filtrates from cultures of the fungus. *Florida Agricultural Experiment Stations Journal Series. ,* 4126**,** 132-135.

Woolf, R. T., Yeghen, T. & Menage Hdu, P. 2012. A rash in a patient with neutropenia. *BMJ,* 345**,** e8296.

Wosten, H. A. B., Schuran, F. H. J. & Wessels, J. G. H. 1994. Interfacial self-assembly of a hydrophobin into an amphipathic protein membrane mediates fungal attachment to hydrophobic surfaces. *The EMBO Journal.,* 13**,** 5848-5854.

Wu, C. H., Lu, P. L., Hsiao, H. H., Liu, T. C., Lin, S. F., Chang, C. S., Hsu, J. F. & Liu, Y. C. 2014. Breakthrough *Fusarium solani* infection in a patient with acute myeloid leukemia receiving posaconazole prophylaxis. *Ann Hematol,* 93**,** 1079-81.

Wu, T. G., Keasler, V.V., Mitchell, B.M., Wilhelmus, K.R. 2004. Immunosuppression affects the severity of experimental *Fusarium solani* keratitis. *The Journal of Infectious Diseases,* 190**,** 192-198.

Wu, Z., Begley, C.G., Port, N., Bradley, A., Braun, R., King-Smith, E. 2015. The effects of increasing ocular surface stimulation on blinking and tear secretion. *Cornea,* 56**,** 4211-4220.

Xiang, X., Oakley, B. 2010. The cytoskeleton in filamentous fungi. In Cellular and Molecular Biology of Filamentous Fungi (ed KA Borkovich & D Ebbole), American Society of Microbiology, 209-223.

Xu, W. M., Li, S. Z., He, M., Yang, S., Li, X. Y. & Li, P. 2013. Synthesis and bioactivities of novel thioether/sulfone derivatives containing 1,2,3-thiadiazole and 1,3,4-oxadiazole/thiadiazole moiety. *Bioorg Med Chem Lett,* 23**,** 5821-4.

Xu, Y., Gao, C., Li, X., He, Y., Zhou, L., Pang, G. & Sun, S. 2013. *In vitro* antifungal activity of silver nanoparticles against ocular pathogenic filamentous fungi. *J Ocul Pharmacol Ther,* 29**,** 270-4.

Yan, X., Yu, C., Shi, Z., Wang, S. & Zhang, F. 2013. Nasal cutaneous infection in a healthy boy caused by *Fusarium moniliforme. Pediatr Dermatol,* 30**,** e43-5.

Yoshimura, H., Tada, T. & Iida, H. 2004. Subcellular localization and oligomeric structure of the yeast putative stretch-activated Ca^{2+} channel component Mid1. *Experimental Cell Research,* 293**,** 185-195.

Zelter, A., Bencina, M., Bowman, B. J., Yarden, O. & Read, N. D. 2004. A comparative genomic analysis of the calcium signaling machinery in *Neurospora crassa, Magnaporthe grisea,* and *Saccharomyces cerevisiae. Fungal Genet Biol,* 41**,** 827-41.

Zhang, S., Ahearn, D.G., Stulting, R.D., Schwan, B.L., Simmons, R.B., Pierce, G.E., Crow, S.A. 2007. Differences among strains of the *Fusarium oxysporum-F. solani* complexes in their penetration of hydrogel contact lenses and sebsequent susceptibility to multipurpose contact lens disinfection solutions. *Cornea,* 26**,** 1249-1254.

Zhang, Y., Wang, Z. Q. & Sun, X. G. 2013. [Analysis of etiology and *in vitro* drug resistance of ocular fungal infection in period of 2009 - 2010]. *Zhonghua Yan Ke Za Zhi,* 49**,** 345-9.

Zisova, L. G., Dobrev, H. P., Tchernev, G., Semkova, K., Aliman, A. A., Chorleva, K. I., Chapanova, A. T., Vutova, N. I. & Wollina, U. 2013. *Tinea atypica*: report of

nine cases. *Wien Med Wochenschr,* 163**,** 549-55.

Note: The accompanying DVD contains three Powerpoint files for the movies cited in Chapters 3, 4 and 6.